

2013

A feasibility study of multi-functional wells for water coning control and disposal

Lu Jin

Louisiana State University and Agricultural and Mechanical College, lujin329@yahoo.com

Follow this and additional works at: https://digitalcommons.lsu.edu/gradschool_dissertations



Part of the [Petroleum Engineering Commons](#)

Recommended Citation

Jin, Lu, "A feasibility study of multi-functional wells for water coning control and disposal" (2013). *LSU Doctoral Dissertations*. 2051.
https://digitalcommons.lsu.edu/gradschool_dissertations/2051

This Dissertation is brought to you for free and open access by the Graduate School at LSU Digital Commons. It has been accepted for inclusion in LSU Doctoral Dissertations by an authorized graduate school editor of LSU Digital Commons. For more information, please contact gradetd@lsu.edu.

A FEASIBILITY STUDY OF MULTI-FUNCTIONAL WELLS FOR WATER
CONING CONTROL AND DISPOSAL

A Dissertation

Submitted to the Graduate Faculty of the
Louisiana State University and
Agricultural and Mechanical College
in partial fulfillment of the
requirements for the degree of
Doctor of Philosophy

in

The Craft & Hawkins Department of Petroleum Engineering

by

Lu Jin

B.S., Daqing Petroleum Institute, 2005

M.S., Louisiana State University, 2009

December 2013

To my parents, Weiqin Jin and Huiying Qi.

ACKNOWLEDGEMENTS

I would like to express my appreciation to my advisor, Dr. Andrew K. Wojtanowicz, for his guidance, supervision, and help provided to this study.

I would also like to thank Dr. Richard G. Hughes, Dr. Stephen O. Sears, Dr. Richard F. Keim and Dr. Christopher D. White for being my examining committee members. I appreciate their effective instruction and discussion during this study.

I wish to express my gratitude to the LSU Downhole Water Sink Technology Initiative (DWSTI) and Petroleum Engineering Department for supporting this research.

I also wish to thank Mr. Fenelon Nunes, Mr. Darryl Bourgoyne, Dr. Mileva Radonjic and Dr. Rao's research groups for their help in my lab work; my friends: Gbolahan Afonja, Venu Nagineni, Yin Feng, Yu Zheng and many others, for their help in this research.

TABLE OF CONTENTS

ACKNOWLEDGEMENTS	iii
ABSTRACT.....	vi
CHAPTER 1. FEASIBILITY OF DWL WELL - PROBLEM AND APPROACH.....	1
1.1 Water Coning Control by Ideal DWL Well.....	3
1.2 Limitations of DWL Well.....	5
1.3 Hypothesis.....	8
1.4 Objective and Methods	8
1.5 Dissertation Outline and Logic	9
CHAPTER 2. LITERATURE REVIEW	11
2.1 Downhole Oil Water Separation.....	12
2.2 Oil Water Two Phase Flow in Vertical Wells	14
2.3 Injectivity Damage with Oily Water.....	17
2.4 Simplification of a System with Dimensionless Groups	22
CHAPTER 3. DWL LIMITATION DUE DOWNHOLE OIL WATER SEPARATION.....	28
3.1 Oil Water Separation under Counter-current Flow Condition in DWL Well.....	30
3.2 Maximum Water Drainage Rate to Avoid Oil Contamination	48
3.3 Discussion and Summary.....	52
CHAPTER 4. DWL WELL LIMITATION DUE INJECTIVITY DECLINE	55
4.1 Mechanisms of Formation Damage Caused by Oily Water Injection	56
4.2 Injectivity Decline Caused by Oily Water Injection in Linear Flow	59
4.3 Injectivity Damage in Radial Flow	88
4.4 Summary	123
CHAPTER 5. SCREENING RESERVOIR AQUIFER FOR DWL WATER INJECTION	126
5.1 Representing Injectivity Decline by Skin Factor	126
5.2 Formation Assessment for Oily Water Injection	130
5.3 Including Partial Penetration Effect in Formation Assessment.....	138
5.4 Formation Screening for DWL Considering Injectivity Decline.....	141
5.5 Discussion	147
5.6 Summary	148
CHAPTER 6. DIMENSIONAL ANALYSIS OF DWL FEASIBILITY	149
6.1 DWL Performance Modeling	150
6.2 Verification of DWL Dimensionless Groups with Field Databases.....	160
6.3 Relevance of Dimensionless Groups	165
6.4 Dimensionless Model of DWL Performance.....	171

6.5 Model Simplification	176
6.6 Comparative Assessment of DWL Feasibility.....	179
6.7 Summary	183
CHAPTER 7. CONCLUSIONS AND RECOMMENDATIONS.....	185
7.1 Conclusions.....	185
7.2 Recommendations.....	189
NOMENCLATURE	191
REFERENCES	194
APPENDIX A: SOLUTION DERIVATION FOR ADA MODEL IN LINEAR FLOW	214
APPENDIX B: SOLUTION DERIVATION FOR ADA MODEL IN RADIAL FLOW	219
APPENDIX C: DERIVATION OF DIMENSIONLESS GROUPS FOR DWL.....	225
APPENDIX D: COPYRIGHT PERMISSIONS.....	236
VITA	239

ABSTRACT

Although water coning is well understood, it is difficult to control in field operations resulting in low recovery and large volumes of waste produced water. A solution - proposed here - is a multi-functional well with the in-situ bottom water drainage and injection installations - Downhole Water Loop (DWL). Theoretically, DWL greatly improves well performance (for example, a two-fold increase of DWL well's water drainage rate would increase the critical (water-free) oil rate by 80%). However, DWL has practical limitations that must be quantified for actual well design.

The objective of this work is to: (1) find maximum water drainage rate to ensure separation of a small amount of under-drained oil from the drainage water; (2) learn how the small oil contamination would impact water injection and how to set criteria for oily water disposal to the bottom aquifer; and, (3) develop a method for assessing feasibility of DWL for oil reservoirs with bottom-water coning problem.

Counter-current oil water separation experiments have been to simulate the flow of oil droplets in the downhole water looping section of DWL wells. From the results, an analytical model calculates the maximum water drainage rate that prevents carry-over of oil by the injection water.

Aquifer injectivity decline is described by a mathematical model based on mass balance of oil phase in the injected water by considering the effects of oil droplets capture due combined effect of advection, dispersion and adsorption (ADA model) coupled with the two-phase relative permeability relationship. For comparison, a two-phase flow model based on the Buckley-Leverett theory describes aquifer permeability decline during oily water injection process. The two models are in a good agreement for linear flow and excellent

agreement for radial flow. Consequently, the aquifer permeability damage is converted to time-dependent skin factor and injection pressure. A comparison of the injection and fracturing pressure gives an estimate of the well stimulation cycle and a criterion for screening reservoir-aquifer candidate for DWL.

In order to assess DWL feasibility, a dimensionless model of movable oil recovery vs. seven scaling groups has been built using the inspectional analysis method and multivariable regression technique. The model is used as a final step in the five-step procedure for finding good reservoir candidates for DWL application. Six real reservoirs were used to demonstrate the procedure with three reservoirs becoming good candidates for DWL technology.

CHAPTER 1. FEASIBILITY OF DWL WELL - PROBLEM AND APPROACH

Excessive water production has been a continuing problem for operators since the beginning of the petroleum industry (Ambrose, 1921). To date, 98% of US E&P waste volume is produced water (Veil and Clark, 2009). Khatib and Verbeek (2002) estimate that, an average of 210 million bbl of water was produced each day worldwide in 1999, which means about 77 billion bbl of produced water for the whole year. Usually, produced water volume increases over the life of a conventional petroleum well and the water/oil ratio rises with production. According to a report by Schlumberger (2000), 75 % of the total production from petroleum reservoirs is only water, equivalent to 249.3 million bbl of water per day worldwide in 2005 (Khatib, 2007). It has been also reported that oil wells produce – on average - more than 7 bbl of water for each barrel of oil (Lee, et al. 2002). When the wells mature, water may amount to as much as 98% of the fluids brought to the surface.

Seright, et al. (2003) categorized various water problems in oilfield from least to most difficult to solve, and stated that water coning and underrunning are the most difficult ones with no easy, low-cost solutions. Countless efforts have been done to understand and control water coning since Muskat and Wyckoff discussed the coning mechanisms in 1935. Various methods have been used in the field to control this problem: perforating high above the original OWC, keeping production rate below the critical value, creating a permeability barrier between the oil and water zones by injecting resins, polymers, foam or gels, using horizontal well to reduce and delay water cresting, changing the fluids mobility ratio in-situ, injecting the produced water back to the reservoir, and lifting or in-flowing oil and water

separately by downhole oil water separation (DOWS) or downhole water sink (DWS) wells, respectively.

However, most of these methods could merely either delay water coning or only partially solve the water coning problem. For example, DWS well is a relatively new and quite promising method. It can control water coning from its source and even completely eliminate it by draining water close to the oil water contact (OWC) as shown in the left side of Figure 1.1. However, a large amount of water needs to be drained by the bottom completion in order to prevent the water coning up. Such a large amount of water may cause environmental problem on the surface and the reservoir may be depleted fast when both oil and water are drained out of the formations, as a result, the final oil recovery would be reduced.

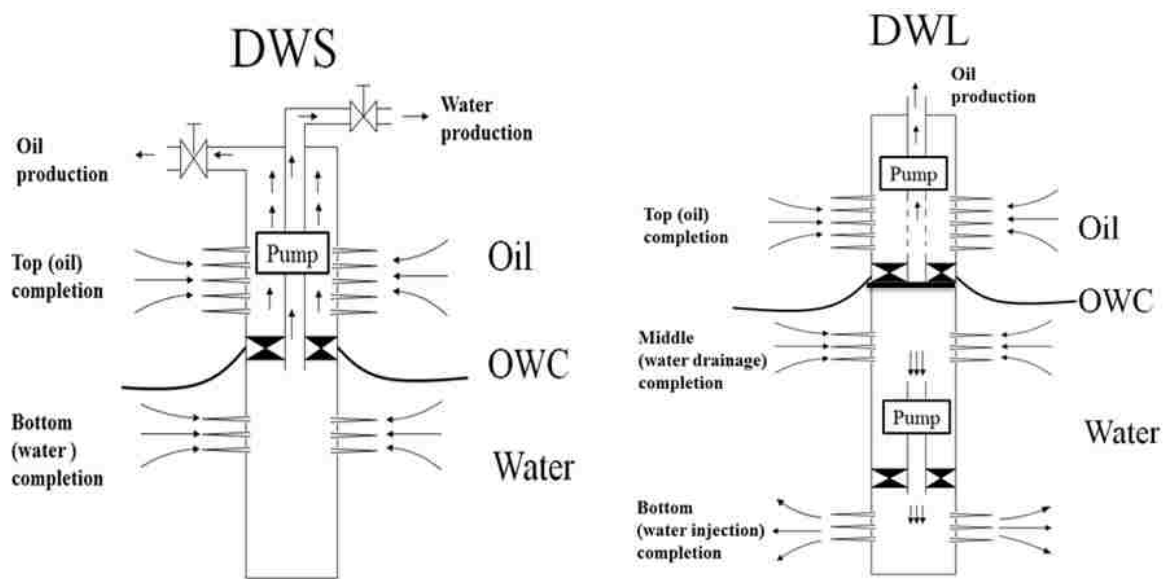


Figure 1.1. Schematic of DWS and DWL well completions

A new water coning control technology --- Downhole Water Loop (DWL, shown in the right side of Figure 1.1), was proposed based on DWS to keep its advantage while avoiding the drawbacks. As shown in the figure, DWL has a triple completion in the oil and

water zones: oil is produced from the top completion and water is drained and injected via the middle and bottom completions in the aquifer, respectively. Because DWL injects the water back into the same aquifer instead of lifting to the surface, the surface produced water would be dramatically reduced and the water drive in the reservoir could be maintained. This is important in bottom water drive reservoirs, especially when the aquifer is weak.

1.1 Water Coning Control by Ideal DWL Well

In previous work, the production performance of an ideal DWL was studied (Jin, 2009a). The objective was to model the DWL mechanisms analytically and numerically, and predict DWL well production performance. An ideal DWL well is defined here as producing oil at the top completion, with no oil contamination in the drainage/injection water. Performance of ideal DWL well is:

$$q_{oc} = f(q_w, z_{di}, \Delta p_o) \dots\dots\dots(1.1)$$

$$z_{di_min} \leq z_{di} \leq 0.8h_w \dots\dots\dots(1.2)$$

$$\Delta p_o < \Delta p_{o_max} \dots\dots\dots(1.3)$$

$$c_{oil} = 0 \dots\dots\dots(1.4)$$

Where, q_{oc} is the critical oil production rate, bpd; q_w is the water drainage/injection rate, bpd; z_{di} is the D/I spacing (distance between water drainage and injection completions), ft; h_w is the thickness of aquifer, ft; Δp_o is the pressure drawdown in the top completion caused by oil production, psi; Δp_{o_max} is the maximum pressure drawdown allowed for oil production, psi; and c_{oil} is the oil concentration in the drainage/injection water, percent.

In the thesis, the coning control mechanism of DWL was explained using flow potential theory and a simple analytical model was developed based on the theory. The model could be used to calculate the critical oil production and water drainage/injection rates

of DWL. It could also be used to confirm the principal relationships between the DWL design and operational variables, such as the oil production and water drainage/injection rates, critical rates and the D/I spacing. The results showed that the critical oil rate could be increased dramatically by using a DWL well compared to the conventional wells, and small values of D/I spacing rapidly increase the critical oil production rate. Hence, the DWL system could work even in reservoirs with small bottom water (Jin, et al. 2009c and 2010a).

A numerical simulation model was built and used to study the effects of DWL well completion variables on well system performance. Three operational parameters were selected for the simulation study: top (production) rate, drainage/injection rate (bottom rate) and the D/I spacing. It showed that DWL would work even for a small D/I spacing, which means that the DWL system does not require deep drilling or deviated wells to inject produced water. Moreover, the system would not reduce the water-drive ability of the aquifer (reservoir pressure) while giving a low water-cut oil production (Jin and Wojtanowicz, 2010b).

A well performance (nodal) analysis model was also developed for a DWL well completed in an oil reservoir underlain by a water layer of known thickness. In the model, the positions (depths) of the three well completions and the rates of production and drainage/injection are design parameters, while all other properties are reservoir system properties. The model could be used to find the operational range of DWL for a given reservoir system and to compare DWL wells with conventional wells, single-completed at the top of the oil layer (Jin and Wojtanowicz, 2010b).

The results showed that for each DWL system, there is such a combination of the top production rate, bottom drainage-injection rate and drainage-injection distance (D/I spacing)

that would result in water-free oil production. There is a minimum D/I spacing above which the detrimental effect of pressure interference between the two water completions is practically eliminated and the beneficial effect of water drainage on well performance is strong: a two-fold increase of water drainage rate would increase the critical oil rate by 80%. Also, because the minimum D/I spacing is relatively small, DWL wells may be installed in reservoirs with thin layers of bottom water (Jin, 2009a).

The advantage of DWL can be summarized as follows:

1. It improves oil production by controlling water coning from bottom aquifer;
2. It does not lift huge amount of water to the surface and reduces production cost;
3. It saves water treatment cost and increases net present value in areas with high water disposal cost;
4. It does not require the separated injection zone;
5. It does not drain out the water in the aquifer, which can maintain the oil production;
6. It protects environment by reducing produced water.

1.2 Limitations of DWL Well

Although the results in my MS thesis (Jin, 2009a) show high production performance of an ideal DWL well, realistic limitations of such well have not been addressed in the model.

Firstly, oil contamination in the drainage water was ignored. It simply assumed the drainage water was clean as no oil enters the water drainage completion. This is not always the case especially when the drainage rate is high, and a trace of oil might flow to the drainage completion with water as shown in Figure 1.2: top and bottom rates are fixed then oil cut in the drainage water is observed. It may cause water injectivity damage if this oil is

injected to the aquifer, regardless of its small quantity. Thus, it is important to determine the maximum water drainage rate that can prevent the oil entering to the aquifer.

Secondly, the D/I spacing is a critical factor in the design of DWL and it is a key parameter for the performance of ideal DWL due to the pressure interference between water drainage and injection completions. In a real DWL, it has another important function that it provides space for oil separating from the drainage water. If the spacing is too short, oil droplets may not have enough time to separate from the drainage water. Thus, it is necessary to know the minimum spacing needed for oil/water separation in the looping section.

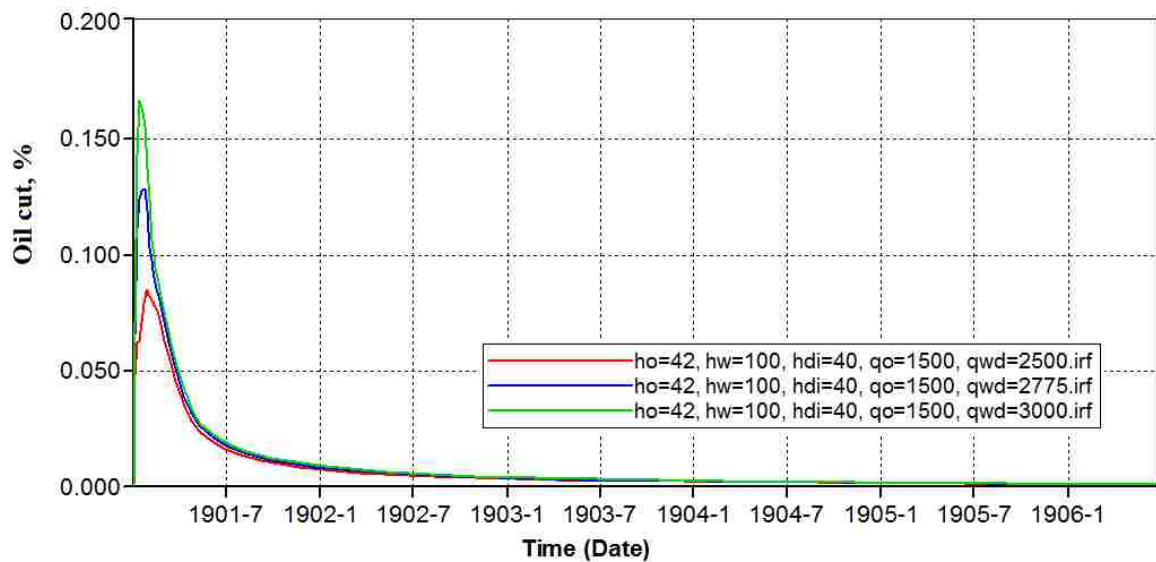


Figure 1.2. Oil contamination in the DWL drainage water

Thirdly, ideal DWL did not consider injectivity decline caused by oil contamination as it assumed clean water injection. However, it might be unavoidable to have a little oil in the injection water in practice which could affect the DWL performance quite significantly (Jin and Wojtanowicz, 2011b). Certain water looping rates are needed to keep the water control effect of DWL, however, the injection pressure will increase with injectivity decline if the injection rate is constant. When the injection pressure approaches the formation

fracturing pressure, the injection rate has to be reduced or the formation has to be stimulated to avoid formation fracture, which reduces the performance of DWL and adds to the cost of production. Jin and Wojtanowicz (2011b) found that stimulation treatment to restore well's injectivity is the main component of the cost for DWL wells as shown in Figure 1.3, which indicates that injectivity damage is the most significant control factor in the process especially when a DWL well is installed in an offshore platform. Thus, the injectivity decline effect caused by oily water injection has to be evaluated and it should be minimized in the design of actual DWL systems.

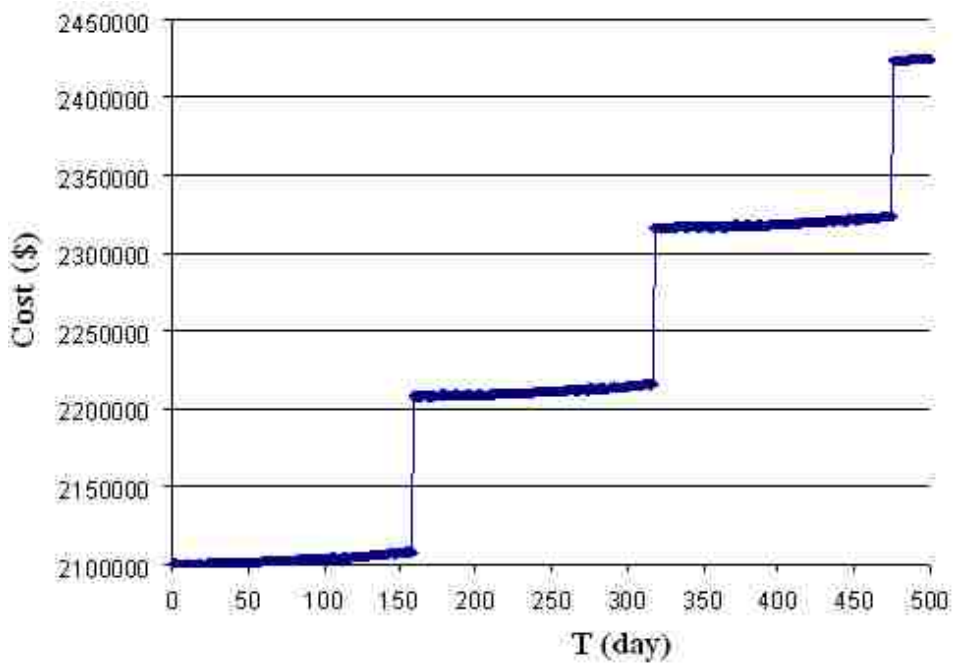


Figure 1.3. DWL cost and formation stimulation relationship (Jin and Wojtanowicz, 2011b)

Last, the model considered in the thesis is dimensional. However, when assessing DWL feasibility for a specific field, a large number of variables (20+) are involved in the problem due to the variety of bottom-water reservoirs, geometry of well configurations, and operational parameters. The above model does not identify the level of significance for each

parameter. It could be very time consuming to consider these parameters individually, so a dimensionless model is needed.

1.3 Hypothesis

Based on the work done in the thesis and limitations for a real DWL well listed above, it is presumed in this work that water coning can be controlled by DWL because it has a water drainage completion to counter balance the pressure drawdown caused by oil production in the pay zone. However, the performance of DWL such as critical oil rate, water cut in the top completion and oil recovery speed are limited by the maximum water drainage rate to prevent oil contamination in the injection water. Water injectivity will decline if oil enters the aquifer with injection water, which will reduce the half-life of the injection completion and affect the operation of DWL. Not all the parameters related to DWL are in equal importance level, some of them are negligible when screening reservoir candidates for the installation. Scaling groups can be defined to describe the DWL system in dimensionless space with fewer variables involved in the analysis process, and these groups can be used to select the proper reservoirs that are suitable to install DWL. Also, the movable oil recovery performance of DWL can be expressed by correlations using these dimensionless groups.

1.4 Objective and Methods

The main objectives of this work are:

1. Quantify limitations for DWL including determine the maximum water drainage rate for DWL without oil contamination in injection water and evaluate the water injectivity decline with oily water injection;

2. Define criteria for reservoir-aquifer system screening based on the aquifer thickness and injectivity;
3. Formulate algorithm for DWL feasibility assessment using dimensionless groups.

The following methods are used in this research to achieve the above objective:

1. Physical experiment to identify the maximum water rate to prevent oil droplet entering the injection completion;
2. Analytically modeling the oil water separation in counter-current flow conditions;
3. Analytically modeling the water injectivity damage caused by oil contamination in the injection water;
4. Design simulation experiments for parametric analysis to identify the most important dimensionless groups in the oil recovery process of DWL and develop an empirical formula to predict the movable oil recovery based on the simulation results.

1.5 Dissertation Outline and Logic

According to the objective of the research, the dissertation will be organized in the following chapters:

Chapter 1 briefly states the water problem in field and the origin of DWL, work done to ideal DWL so far and the realistic limitations for its application. As the first chapter, it explains the reason of undertaking this study, its objective and methods used in the research.

Chapter 2 presents a literature review based on the phenomenon involved in DWL design and operations: the success and failure of downhole oil water separation technology,

oil water two phase flow in vertical wells, formation damage during produced water re-injection process and how to simplify a complicated system using dimensionless groups.

Chapter 3 introduces a physical model to observe oil water separation in counter-current flow conditions. The separation mechanisms will be explained and analytical models will be developed to determine the maximum water drainage rate to avoid oil contamination in the injection water.

Chapter 4 derives analytical models for water injectivity decline caused by oil contamination in both linear and radial flows. The first model considers the effect of advection, dispersion and adsorption of oil droplets flowing through the porous media, and the second model is derived based on the Buckley-Leverett theory. The models are verified by both published experimental data and numerical simulation results.

Chapter 5 converts the growing formation damage to a dynamic skin factor model. The model could be used to predict the injection pressure and assess formations for oily water injection, as well as screen candidates for DWL.

Chapter 6 defines a complete set of dimensionless groups for DWL using inspectional analysis. Two databases with more than 700 reservoirs will be used to test the completeness and independence of the scaling groups. DWL performance model will be developed using these dimensionless groups. A general algorithm including all practical limitations will be developed to assess the feasibility of DWL for various reservoirs.

Chapter 7 summarizes the main conclusions of the study and provides recommendations for future research.

CHAPTER 2. LITERATURE REVIEW

Although DWL is a new technology that has not been used in field yet, similar devices such DWS and downhole oil water separation (DOWS, shown in Figure 2.1), have already been used in practice for many years (Stuebinger, et al., 1997; Verbeek, et al., 1998; Alhoni, et al., 2003; Rivera, et al., 2008). Produced water re-injection (PWRI) has been applied in field to reduce surface produced water and improve oil production for a long time (Barkman and Davidson, 1972; Pang and Sharma, 1997; Palsson, et al., 2003; Abou-Sayed, et al., 2007). Since DWL is a combination of these technologies, their success and failure serve as guidelines for DWL in design, operation and improvement. Due to the similarity between DOWS and DWL, as both of them have an injection completion and need to separate oil and water downhole, the DOWS technology will be reviewed in the next section followed by oil water two phase flow in vertical wells and formation damage during produced water re-injection.

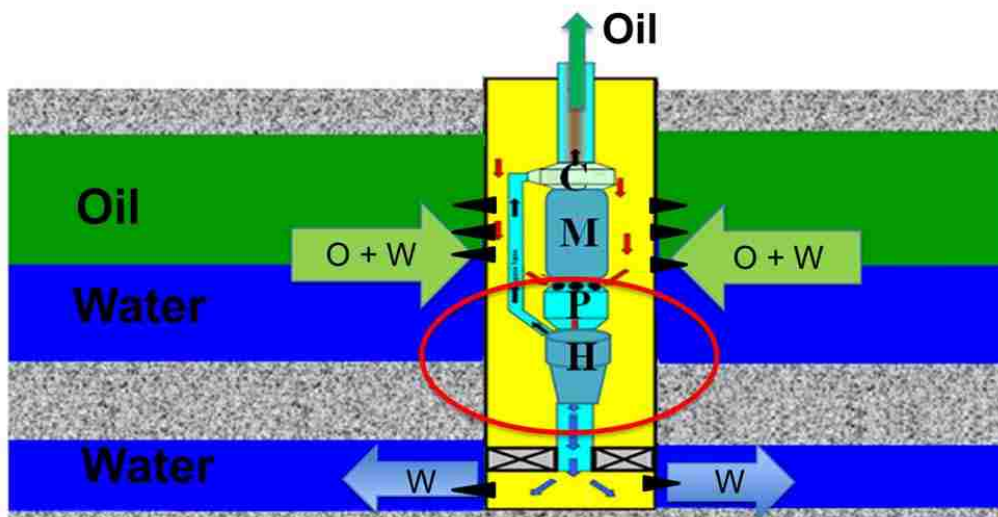


Figure 2.1. Schematic of DOWS installation

2.1 Downhole Oil Water Separation

Based on the mechanism of oil water separation, currently applied DOWS can be divided to two types: gravity separation and hydrocyclone separation. Most installed DOWS belong to hydrocyclone type as it can handle high fluid rate downhole (Veil, et al., 1999; Ogunsina and Wiggins, 2005).

The gravity type of DOWS takes advantage of the gravity separation of oil and water that occurs in the tubing/casing annulus where oil rises upward due to density differences with the water (Stuebinger, et al., 1997; Stuebinger and Elphingstone, 2000). The separation process is controlled by Stoke's Law. The main limitation for this type of DOWS is the maximum fluid capacity handled downhole, because it requires sufficient vertical space between the injection and production completions to allow for sufficient gravity separation, i.e. the system must provide sufficient wellbore volume that allowing the oil droplets to rise and separate from the water stream.

Hydrocyclone type of DOWS separates oil and water using the force difference between centrifugal force generated by the spinning fluid and the drag force on the moving oil droplets (Kjos, et al., 1995; Matthews, et al., 1996; Peachey, et al., 1998; Bowers, et al., 2000; Alhoni, et al., 2003). In operation, fluids mixture is first introduced into the hydrocyclone from the top cylindrical portion, then the swirling of the mixture makes the water, the heavier fluid, to spin to the outside of the hydrocyclone and move toward the lower outlet while the lighter phase, oil, remains in the center of the hydrocyclone where it is drawn through a vortex finder into the upper outlet and produced by the pump to the surface. Comparing to the gravity type of DOWS, hydrocyclone DOWS can handle large amount of

fluids in a limited space and provide very effective separation of oil from high water cut fluids, the water disposal stream usually containing less than 200 ppm residual oil.

Usually, DOWS is used in wells with high water cut and involving large amount of oil/water separation, 100% separation is difficult to achieve which means a small part of oil would be left in the water and injected to the disposal zone despite the high separation efficiency (Veil, et al., 1999; Ogunsina and Wiggins, 2005).

The number of installations peaked around 1998 due to its water control and oil enhancement effect in the beginning of production as shown in Figure 2.2, and more than 40 devices were installed worldwide. However, the trend did not last long, seldom new installations were reported in recent years (Veil and Quinn, 2004).

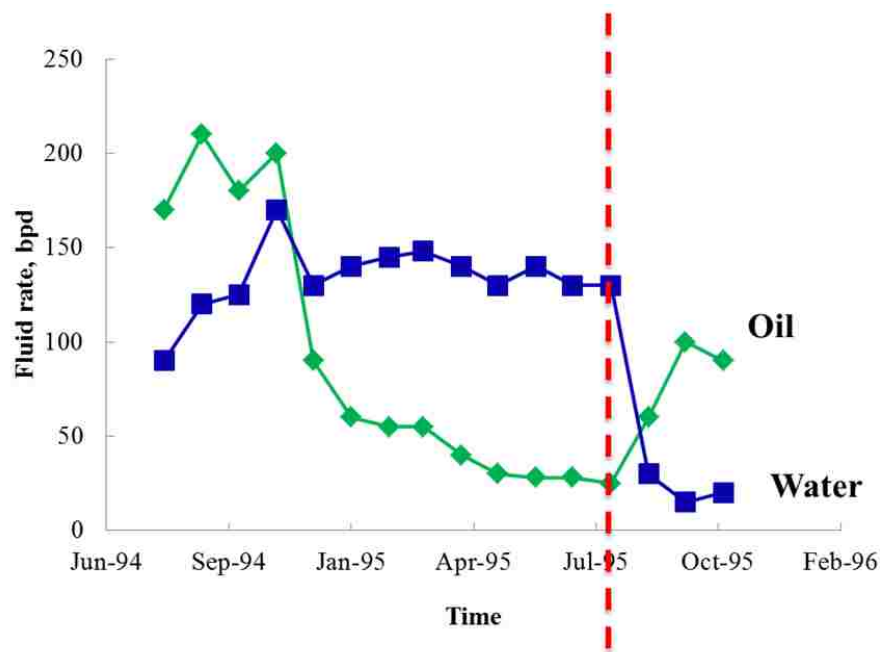


Figure 2.2. DOWS performance in Alliance Field (Matthews, et al. 1996)

High failure ratio is the most important reason for the languishment of this technology, and about 50% of the failure is caused by water injectivity damage in the receiving formation. A field test in East Texas showed that water injectivity lost about 60%

of its original value in merely 5 days (Argonne National Laboratory and Arthur Langhus Layne – LLC, 2001).

The experience of DOWS indicates that, separating oil and water downhole could be a way to reduce surface produced water and improve oil production rate, however, the injectivity decline effect should be carefully evaluated before installing such devices.

2.2 Oil Water Two Phase Flow in Vertical Wells

It is obvious that, DOWS separates fluids with relatively high oil content as all oil and water are produced to the same completion for separation. In contrast, the main oil and water streams flow to different completions individually in DWL, only very small oil content appears in the drainage water as shown in Figure 1.2. Both downhole videos and lab experiments showed that, oil phase at such a low concentration usually dispersed in water when it entered a vertical well with a high rate water stream (Flores, et al., 1999; Janssen, et al., 2001). Flores, et al., (1999) observed the phase distribution profiles in vertical pipes and identified six flow patterns with three being water dominated as shown in Figure 2.3: dispersion of oil in water (D O/W), very fine dispersion of oil in water (VFD O/W) and oil in water churn flow (O/W CF) are water-dominated flow patterns; water in oil churn flow (W/O CF), dispersion of water in oil (D W/O) and very fine dispersion of water in oil (VFD W/O) are oil-dominated flow patterns. D O/W and VFD O/W might be suitable to describe the flow in the looping section of DWL for the low oil concentration in the drainage water.

Brauner (1998, 2002) carried out a series of experimental and theoretical work to model the liquid-liquid two-phase flow systems including flow pattern determination, water holdup estimation and pressure gradient prediction. It was found that the flow behavior of the mixture strongly depends on the dominated phase: most water-dominated flow patterns show

significant slippage but relatively low frictional pressure gradients; in contrast, the oil-dominated flow patterns exhibit negligible slippage but significantly larger frictional pressure gradients. The inclined angle of the pipe also has important effect on the phase distribution profiles in the mixture. The results indicate that, conclusions from one fluids' system may not be applied to the other one if they have very different properties. Thus, the various concepts and results experienced in gas-liquid flow could not be applied to oil-water flow directly due to the property differences between oil and gas, and rules developed from flow in horizontal or inclined pipes could not be used in vertical flow without modification.

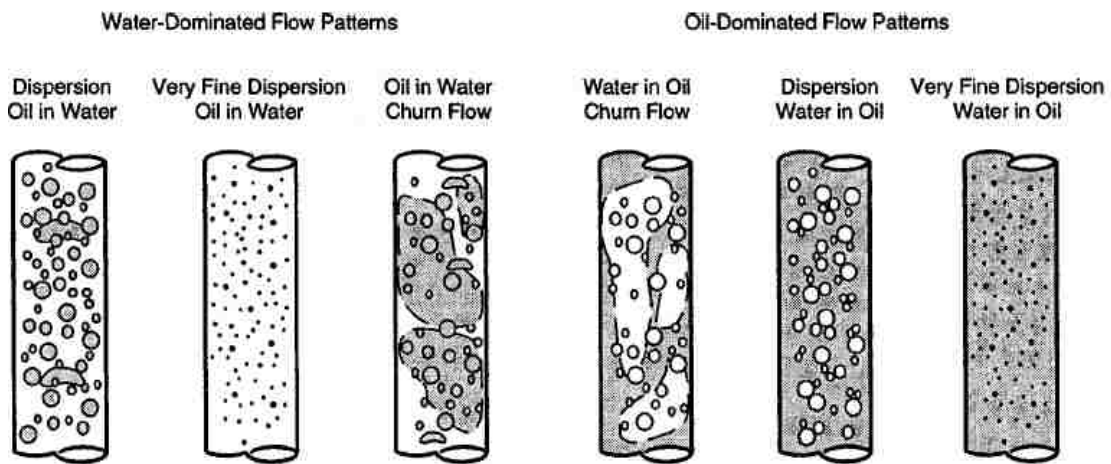


Figure 2.3. Oil water flow patterns in vertical pipes (Flores, et al., 1999)

When oil dispersed in water, the mixture is immiscible and relative movement between the phases occurs due to their density difference, which is traditionally described by force balances (Wallis, 1969; Geankoplis, 1993). According to the flotation theory, the heavier phase has the tendency to separate from the lighter one by settling, while the lighter phase tries to separate from the heavier one by creaming, as a result, the lighter fluid is on top of the heavier one. Generally, four forces are acting on a droplet dispersed in a medium: gravity, buoyancy, viscous resistance (drag force) and Brownian (thermally induced) motion.

Arntzen (2001) found that the thermally-induced motion is important only in the lower range of droplet sizes $< 1\mu m$, and is usually disregarded for gravity separation applications.

Wallis (1969) generalized about the drift flux model which was proposed by Zuber and Findlay in 1965, to estimate the slip between phases leading to estimation of in-situ volume fractions of each phase in gas-liquid two-phase flow. Hasan and Kabir (1990, 1999) modified the model for oil water flow, which can be expressed as:

$$u_o = C_0 u_m + u_d \dots\dots\dots(2.1)$$

$$u_d = 1.53(1 - f_o)^n \left[\frac{\sigma_{ow}g(\rho_w - \rho_o)}{\rho_w^2} \right]^{0.25} \dots\dots\dots(2.2)$$

Where u_o , u_m and u_d are the oil velocity, total mixture velocity and the drift velocity, respectively, m/s; and C_0 is the distribution coefficient that accounts for the effect of velocity and concentration, dimensionless; f_o is the oil volume fraction; σ_{ow} is the oil-water interfacial tension, dyne/cm; ρ_w and ρ_o are densities of water and oil, respectively, kg/m^3 . This model was then extended to model three phase steady-state flow by Shi, et al., (2005b) and oil water separation in inclined tube by Rivera, et al., (2008).

In most production wells, oil and water are produced to surface together so they both flow in the same direction (co-current flow). Due to the slip effect, oil rises up faster and separates from water, called co-current separation, has been widely studied (Stuebinger and Elphingstone, 2000; Ouyang, 2000; Shi, et al., 2005a,b; Rivera, et al., 2008; Fitnawan, et al., 2009). Comparing to co-current flow, counter-current flow where two phase flow in the opposite directions, has not been investigated so widely (Ouyang, 2000). Most of the experimental and theoretical works in this area focused on gas-liquid flow (Johnston, 1988a,b; Ghiaasiaan, et al., 1997; Kim, et al., 2001).

However, for the water injection in-situ such as in DWL, the oil rises in opposite direction, called counter-current separation. The phenomenon has not received much attention yet (Ouyang, 2003a, b). In Ouyang's work, he successfully modeled the water separation behavior in the continuous oil stream. However, how the oil droplets motion in the continuous water stream was not mentioned. As indicated by Flores, et al., (1999) and Brauner (2002), flow behavior of the mixture strongly depends on the dominated phase, which means models from oil-dominated flow may not be used to water-dominated flow directly. Thus, the oil flow behavior under counter-current flow conditions (when water is the continuous phase and oil is the dispersed phase in DWL) needs to be experimentally investigated.

2.3 Injectivity Damage with Oily Water

Field evidence shows that almost all water injection wells suffer more or less injectivity decline problems no matter how clean the injection water is, and the injectivity maintenance using untreated produced water is possible (Barkman and Davidson, 1972; Pang and Sharma, 1997; Palsson, et al., 2003; Abou-Sayed, et al., 2007). Due to the complexity of the injectivity decline process, different situations often need to be considered separately and injectivity decline models are also required to predict the performance of injection wells under various conditions (Bennion, et al., 1998; Furtado, et al. 2007). Injectivity issues are even more important to technologies depending heavily on water injection, such as DWL and DOWS.

Bennion, et al., (1998) found that poor injection water quality is a prime reason for injectivity decline. Almost all problems associated with impaired injectivity can ultimately be

related back to problems associated with water quality. They summarized that the potential damage mechanisms can be divided to the following categories:

1. Mechanically induced damage, including:
 - a) Injection of solids,
 - b) Velocity induced damage (fines migration) and settling, where fines are present
2. Injection water/formation rock interactions, including:
 - a) Clay swelling,
 - b) Clay deflocculation,
 - c) Formation dissolution,
 - d) Chemical adsorption/wettability alterations.
3. Relative permeability effects, including:
 - a) Skim oil entrainment,
 - b) Free gas entrainment.
4. Biologically induced impairment, including:
 - a) Bacterial entrainment and growth.
5. Injection water/in situ fluid interactions, including:
 - a) Formation of insoluble scales,
 - b) Emulsification and emulsion blocks,
 - c) Precipitation,
 - d) Wax/asphaltene deposition.

For injectivity decline in DWL, emulsion blocks and skim oil entrainment seem to be the most important reason as oil contamination is difficult to avoid in the injection water.

Civan (2007) stated that, the formation damage mechanisms are different in single phase and multiphase systems. In single phase system, since absolute permeability is a property of porous media, any change of pore morphology and texture in the formation will affect the permeability. The important factors for formation damage are invasion, generation, and migration of fine particles, clay swelling, chemical precipitation, asphaltene, paraffin, and gel deposition, and mechanical deformation of the rock. Formation damage in multiphase systems involves factors that are not considered in single phase cases: wettability of the formation, capillary pressure and relative permeabilities come into play with the presence of crude oil or emulsion in the injection water.

Soo and his partners carried out a series of experimental and theoretical work to study emulsion flow behavior in porous media (Schmidt, et al., 1984; Soo and Radke, 1984a, b, 1986; Soo, et al., 1986). They focused on dilute oil-in-water emulsions (5000 ppm oil concentration) with average oil droplet from 2 to 10 μm . Ottawa sand packs with permeabilities of 580 md and 1170 md were used in the oily water flooding. Severe water permeability decline was observed in the experiments: more than 40% of the injectivity was lost after injecting 20 pore volumes (PV) of emulsion with 3.1 μm oil droplets to the 1170 md sand pack. Their experiments demonstrated that the degree of injectivity damage increases with the oil droplet size. In an 1170 md sand pack, the injectivity damage with 4.5 μm oil droplets is three to four times more than that of 2 μm oil droplets. Also, the degree of damage increases with decreasing of permeability or pore size of the porous medium for a given oil droplet size. Similar observations were reported by McAuliffe (1973 a, b) and Spielman and Su (1977). For example, McAuliffe (1973 a) observed a 44% water

permeability loss using 1 μm oil droplets and a 98 % loss using 12 μm oil droplets after injecting 9 PV of 5000 ppm emulsion into a 1600-md Boise sandstone core.

Buret, et al., (2010) carried out considerable experimental work on dilute oil emulsion (from 47 to 300 ppm) flowing through porous media to simulate the impact of oil contamination in injection water on well injectivity. They built various SiC packs to simulate different formations with permeabilities from 109 md to 2490 md. The oil droplet sizes used in the experiments were from 0.32 to 11.4 μm . By installing multiple pressure gauges along the core holder, they observed that rapid permeability loss (up to 90%) occurred in the vicinity of the injection face and then propagated deeply inside the porous medium. They also confirmed the observations made by previous researchers described above.

Although, numerous works have been done and many models are available to predict the injectivity decline caused by solid particles, there is a lack of easy to use models to predict the injectivity damage caused by oil contamination in the injection water (Al-Riyami and Sharma, 2002; Vaz, et al., 2006; Buret, et al., 2010). Alvarado and Marsden proposed a bulk viscosity model to study the emulsion flow through porous media in 1979, which treats the emulsion as a continuum, single phase fluid, no interaction between oil droplet and pore wall is allowed. This treatment is valid when the oil concentration is high, however, it is not suitable for dilute oily water flow through porous media (Soo and Radke, 1984a).

Soo and his co-workers (1984a, b; 1986) found that the capture of oil droplets in rock is similar to that of solid colloids during a deep bed filtration process. Thus, the modeling of droplet capture, that is, mass transfer between the liquid globule and the solid matrix, is analogous to the traditional solid particle filtration theory. Two main capture mechanisms are thought to be operative: straining, in which droplets clog the pore throats, and interception,

with droplets captured by van der Waals colloidal forces. For emulsions, there is usually a range of droplet sizes, and straining dominates large droplet capture while interception contributes primarily to small droplet capture. They use three empirical parameters to characterize the filtration process:

Average filter coefficient of a clean bed: λ

Average flow redistribution parameter: α

Average flow restriction parameter: β

The filtration process is mathematically expressed by these parameters as:

$$\frac{\partial \sigma}{\partial t} = \lambda \left(1 - \frac{\alpha \sigma}{\phi_0} \right) u c \dots\dots\dots(2.3)$$

$$\frac{K_x}{K_0} = 1 - \frac{\beta \sigma}{\phi_0} \dots\dots\dots(2.4)$$

Where, σ is the local retention, fraction; ϕ_0 is the initial porosity, fraction; u is the interstitial flow velocity, m/s; c is the emulsion volume concentration, fraction; K_x is the local permeability at time t and K_0 is the initial permeability, md. The values of the three parameters λ , α and β are determined by fitting the experimental data from effluent concentration profiles and permeability response. The authors tried to estimate these parameters a priori, however, it involves the use of some empirical relationships and three other parameters. Thus, it needs to evaluate six parameters in order to use this model. As noted by the authors, several of these parameters are not unique although the range over which they can vary is small.

Similar to Soo, et al., Buret, et al., (2010) noticed the similarity between formation damage caused by solid particles and oil droplets. Aimed at reducing the number of parameters in the injectivity decline prediction through a better understanding of the actual physics process, they use the colloidal approach to explain injectivity decline via dimensional

analysis. The maximum permeability reduction for each droplet to pore throat-size ratio is determined by random sequential adsorption theory.

Rege and Fogler (1988) presented a network model that is suitable for both solid particles and emulsion drops transport in porous media. The model utilized the concept of flow-biased probability for the movement of particles and drops through different flow paths. The model can predict the effluent concentration profiles and permeability changes occurring during the filtration process and match various experimental data by parameter adjustments. Although it provides a useful insight into microscopic details, the network model is highly computational with the utilization of supercomputers and turns to be impractical in routine design.

Romero, et al., (2011) studied the capture rate of oil droplets by rocks with variation of capillary number, which represents the ratio of viscous force to capillary force on an oil droplet when it flows through the formation. They also found it is difficult to measure the parameters that used in Soo, et al.'s model, which is described above. To overcome the limitations of the filtration model, they proposed another network model to study the transient permeability reduction caused by presence of oil in the water. The model contains a set of nonlinear equations for each pore element and need to be solved numerically. Their results show that there is a critical capillary number to divide the regions of oil droplet capture.

2.4 Simplification of a System with Dimensionless Groups

It is usually difficult to determine all the essential factors for fluids flowing through pipes or porous media by pure theory, and hence dependence must often be placed upon experimental (either physical or numerical) investigations (Bird, et al., 2007; Munson, et al.,

2009). The number of tests to be made directly relates to the variables involved in process under investigation, the more parameters considered the more tests are needed, which might be unrealistic to carry out in a limited time. For example, there are more than 20 dimensional parameters related to bottom-water reservoirs, geometry of well configurations and well operations for DWL, which means there are more than $2^{20}=1,048,576$ combinations to test if we only consider two values of each parameter. The test number can be greatly reduced by a systematic program based on dimensional analysis and specifically on the laws of similitude or similarity, which permit the application of certain relations by which test data can be applied to other cases with proper calibration.

The similarity laws enable us to make experiments with a convenient fluid such as water or air, and then apply certain results to a fluid which is less convenient to work with, such as gas, steam or oil. Also, valuable results can be obtained as a minimum cost by tests made with small-scale models of the full-sized apparatus. The laws of similitude make it possible to determine the performance of the real system from tests made with mathematical (analytical or numerical) models as shown in Figure 2.4 (Mousaviraad, 2010).

There are three similarities exist between prototype and model: geometric similarity, kinematic similarity and dynamic similarity. Geometric similarity means that the model and its prototype be identical in shape but differ only in size. Kinematic similarity implies geometric similarity and in addition it implies that the ratio of the velocities at all corresponding points in the flow is the same. Dynamic similarity represents the force relationship between prototype and mode, i.e. if two systems are dynamically similar, corresponding forces must be in the same ratio in the two. Forces that may act on a fluid element include those due to gravity, pressure, viscosity, elasticity and surface (or interfacial)

tension. Mathematically, these similarities are expressed by dimensionless groups, which are the combinations of dimensional parameters involved in the process under consideration (Sonin, 1997).

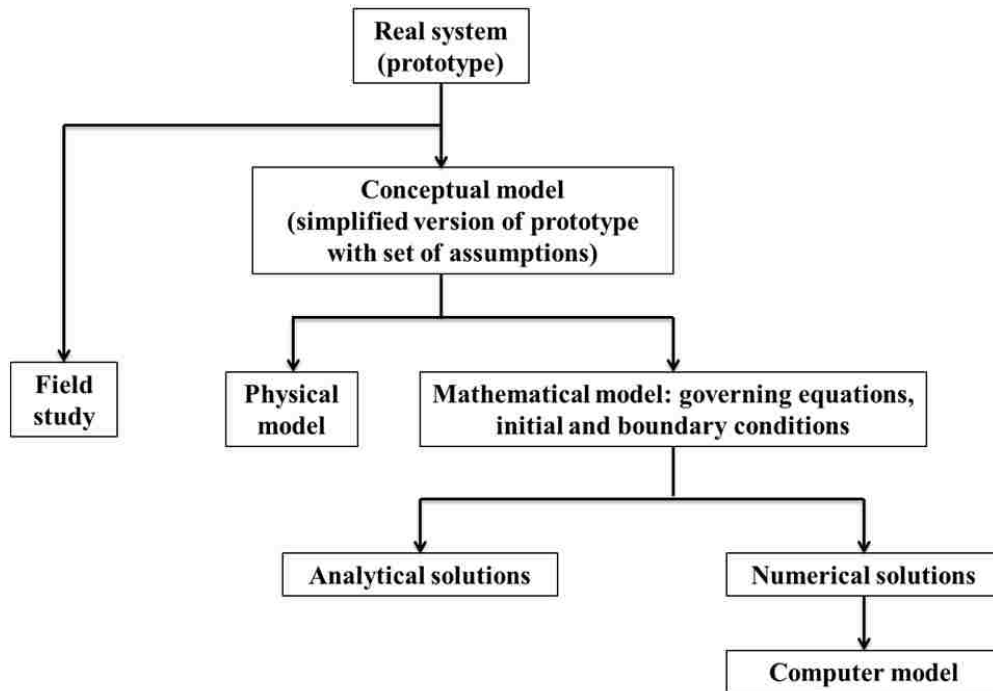


Figure 2.4. Simplification of real system by similarity laws (Mousaviraad, 2010)

Two different methods, dimensional analysis (DA) and inspectional analysis (IA), have been developed to obtain dimensionless groups and both of them are widely used. DA is used more in general fluid dynamics research such as pipe flow, heat transfer and so on (Mendez and Ordóñez, 2005; Gibbings, 2011), while petroleum engineers, especially in reservoir engineering areas, rely more on IA (Shook, et al., 1992; Peters and Ham, 1993; Gharbi, et al., 1998; Novakovic, 2002).

DA is widely used in experimental design and analysis because it only needs the pertinent variables. The dimensionless groups are derived by requiring that the power products of the variables be dimensionless. This requirement gives a homogeneous system of

linear algebraic equations with solutions yielding a set of dimensionless groups. Buckingham's π theorem is a classic method to form the dimensionless groups in this way as shown in Figure 2.5.

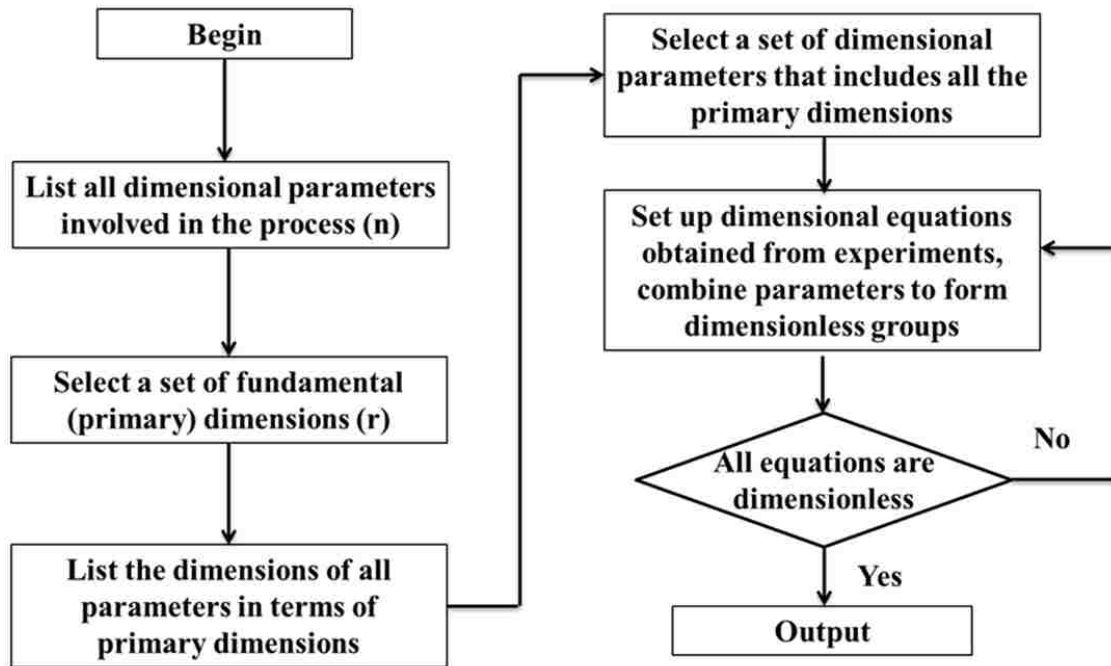


Figure 2.5. Procedure of dimensional analysis (DA, Novakovic, 2002)

Groups from dimensional analysis can be combined to form global dimensionless groups, which can be more easily interpreted physically (Rapoport, et al., 1955). Some researchers recommend determining the final form of physically meaningful dimensionless groups through experiments (Offeringa, et al, 1954; Croes and Schwarz, 1955; Carpenter, 1962; Bear, 1972; Grattoni, et al., 2001). Many famous dimensionless groups are obtained by DA and give useful insight to the principles of different problems. For example, Reynolds number stands for the ratio of inertia forces to viscous forces when a fluid flows through a completely filled pipe where gravity does not affect the flow pattern and capillarity is of no practical importance, hence the significant forces are inertia and fluid friction due to viscosity.

IA shares a similar logic with DA, however, it transforms the dimensional space to dimensionless space variable-by-variable instead of making decision based on the primary dimensions of variables (Ruark, 1935; Bear, 1972; Shook, et al, 1992; Novakovic, 2002; Trivedi and Babadagli, 2008). Inspectional analysis couples differential equations of the physical process together with initial and boundary conditions and then transforms the whole system into dimensionless form. This can be done through the following steps:

1. Formulation of all governing equations together with the initial and boundary conditions;
2. Transformation to dimensionless space by defining scale and transformation factors;
3. Primary elimination and secondary substitution;
4. Redundancy elimination;
5. Completeness validation.

Both methods have their own advantages and limitations. Inspectional analysis usually gives scaling groups whose physical meanings are readily apparent, whereas the physical meanings of groups from dimensional analysis may be quite obscure (Ruark, 1935; Bear, 1972; Sonin, 1997; Gharbi et al, 1998; Novakovic, 2002; Hernandez and Wojtanowicz, 2007). For example, without knowing a differential equation, it is easy to define intuitively a similarity group as a ratio of the capillary-to-viscous forces, or the viscous-to-gravity forces. On the other hand, IA requires mathematical equations for the process under study. If such equations are unavailable, inspectional analysis cannot begin.

Dimensional analysis is useful in providing some guidance for setting up experiments to initiate the study and it is especially useful when people face new research objectives,

whose physical characters have not been well studied, yet. Moreover, the dimensional analysis method is more universal than the inspectional analysis. When very little theory is available, dimensional analysis can be relied upon to provide initial guidance in setting up experiments (Christophe, et al., 2008).

The inspectional analysis method is used more frequently in reservoir engineering because the underlying physical laws are known and expressed in the form of partial differential equations and boundary conditions (Shook, et al., 1992). Principles of scaling in petroleum studies were outlined by Rapoport (1955) for the immiscible displacement of oil by water. These principles were extended to miscible flow later (Gharbi, et al., 1998; Wood, et al., 2008; Trivedi and Babadagli, 2008). Interestingly, different dimensionless groups have been derived by various authors, to describe the same phenomenon, for example, the formats of gravity number vary from different authors (Croes and Schwarz, 1955; Rapoport, 1955; Lake, 1989; Shook, et al, 1992; Novakovic, 2002; Wood, et al., 2008). The reason of such a difference may stem from the derivation process of IA: as the defining of scale factors and transformation factors is arbitrary, the re-arrangement process and elementary matrix operations can also be carried out in different ways by different authors. Moreover, the choice of different coordinates system could also lead to different scaling groups.

CHAPTER 3. DWL LIMITATION DUE DOWNHOLE OIL WATER SEPARATION

Although oil droplets would inevitably enter the drainage water as shown in Figure 1.2, they would also separate from the water by gravity, before being injected to the formation. The gravity separation that has been used in downhole oil water separation wells which make use of the gravity difference between oil and water and achieves natural separation of oil and water in the tubing/casing annulus (Stuebinger, et al., 1997; Stuebinger and Elphingstone, 2000). After oil and water enter the water drainage completion of DWL, oil would rise and accumulate a layer below the packer at the top of the separation section. Then, the accumulated oil would be produced or lifted as shown in three variants of DWL in Figure 3.1 to Figure 3.3.

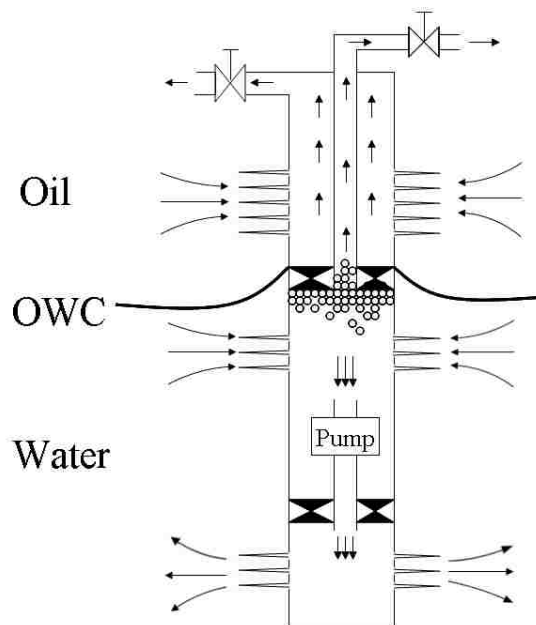


Figure 3.1. DWL design in reservoir with thick and strong bottom water

This chapter previously appeared as “Jin, L. and Wojtanowicz, A. K. Experimental and Theoretical Study of Counter-current Oil–water Separation in Wells with in-situ Water Injection. *Journal of Petroleum Science and Engineering*, Vol. 109, Sept. 2013.” It is reprinted by permission of Elsevier provided by Copyright Clearance Center.

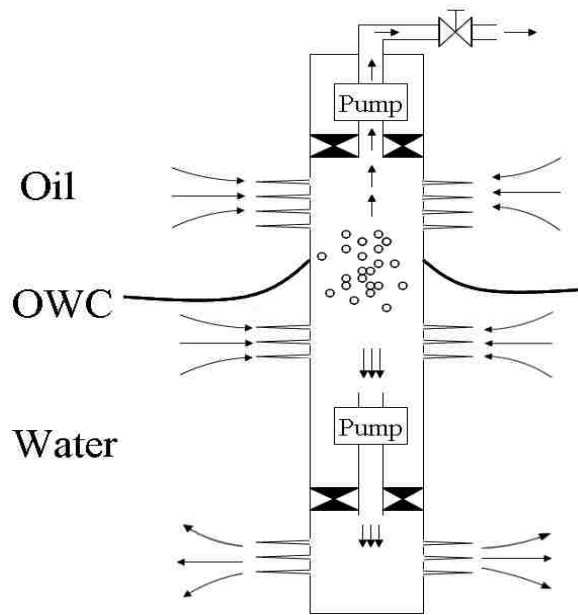


Figure 3.2. DWL design in reservoir with thick and weak bottom water

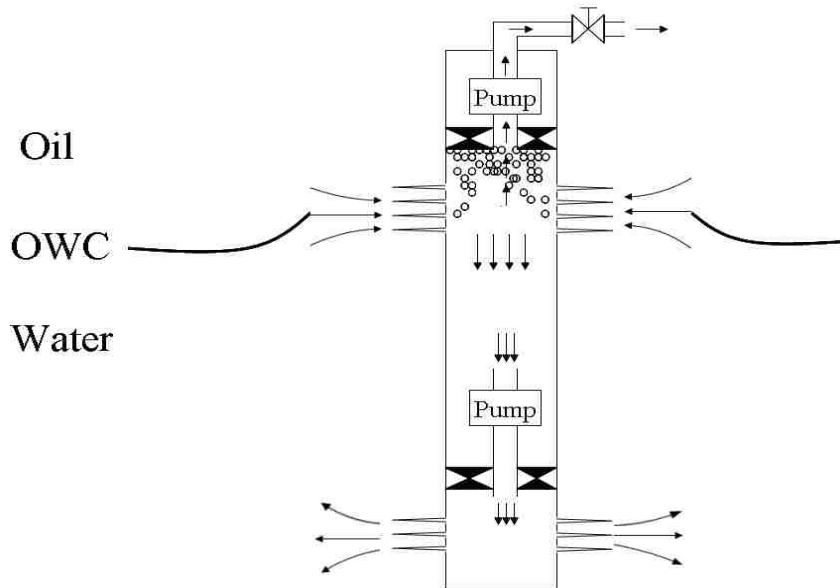


Figure 3.3. DWL design in reservoir with thin and weak bottom water

Figure 3.1 depicts the DWL installation in reservoir with thick and strong bottom water where the reservoir pressure is high enough to lift oil to the surface. Three completions with two packers are used: the top completion is perforated in the oil zone and produces oil via the annulus to the surface without a pump. A packer is set in the oil water contact (OWC)

to support the tubing. The water drainage completion is penetrated below the OWC to drain water for water coning control. A large amount of water and a trace of oil flow into the well via this completion. Due to the density difference, oil tends to stay in the top of water and accumulates a layer below the packer. This layer of oil could be produced to the surface via the tubing by opening the valve on the ground. The drainage water is injected back to the deeper aquifer by a pump via the water injection completion where the second packer is used to fix the tubing and pump.

Figure 3.2 shows the design of DWL in reservoir with thick but weak aquifer where the reservoir pressure is not high enough to lift oil to the surface. Thus, two pumps are needed in the design: the first pump is installed in the top of reservoir to lift fluids produced by the top completion to the surface. The water drainage completion is penetrated below the OWC for coning control, similar to the first design, water and a little oil flow to the completion and separated in the well, while the separated oil rises to the pump and produced to the surface with fluids entering via the top completion. The water injection pump and completion are the same to the first design.

For reservoir with thin and weak aquifer, only two completions are needed as shown in Figure 3.3. The long top completion is perforated at the OWC, both oil and water are produced via this completion and then separated in the well. The separated oil is lifted to the surface by the pump installed in the top of the reservoir while the separated water is injected to the aquifer by the second pump via the bottom completion.

3.1 Oil Water Separation under Counter-current Flow Condition in DWL Well

Downhole videos from wells producing at very high water cut have shown that the dispersed oil droplets could be quite big and moving up fast. When an oil droplet enters a

stagnant water column, it suffers three forces: upward buoyancy (F_B), downward gravity (F_G) and downward drag force (F_D). The velocity of the droplet and force development acting on it can be divided to three stages illustrated in Figure 3.4.

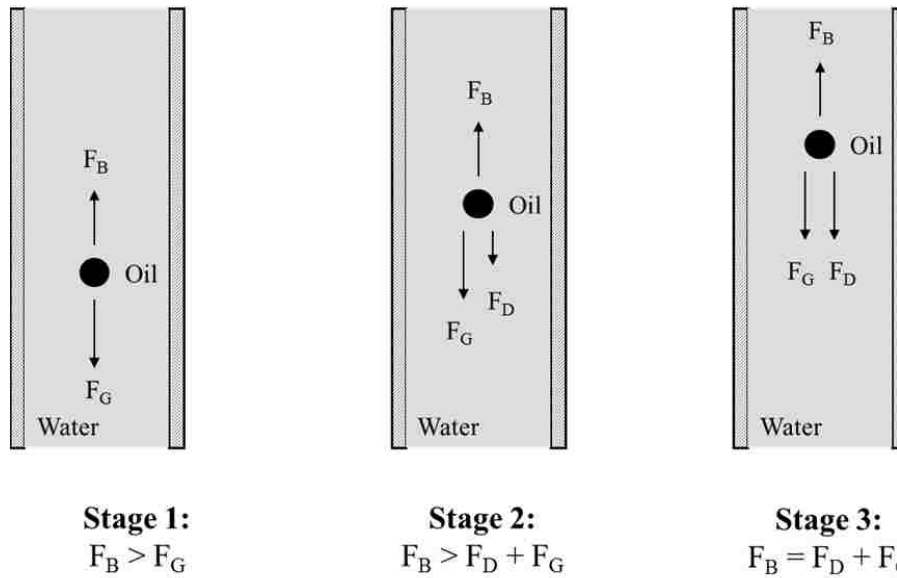


Figure 3.4. Forces acting on an oil droplet rising in a stagnant water column

In the first stage, the buoyancy is greater than the gravity because oil is lighter than water, as the total force is upward which makes the oil droplet rise up with acceleration. In the second stage, with the increase of rising velocity of the oil droplet, the water exerts a downward drag force on the oil droplet due to the friction between them. As the buoyancy is greater than the sum of gravity and drag force, the oil droplet still rises up with acceleration, however, the acceleration becomes smaller. In the third stage, the acceleration of the droplet stops as the buoyancy is equal to the sum of gravity and drag force, and the velocity of the oil droplet reaches to its terminal value.

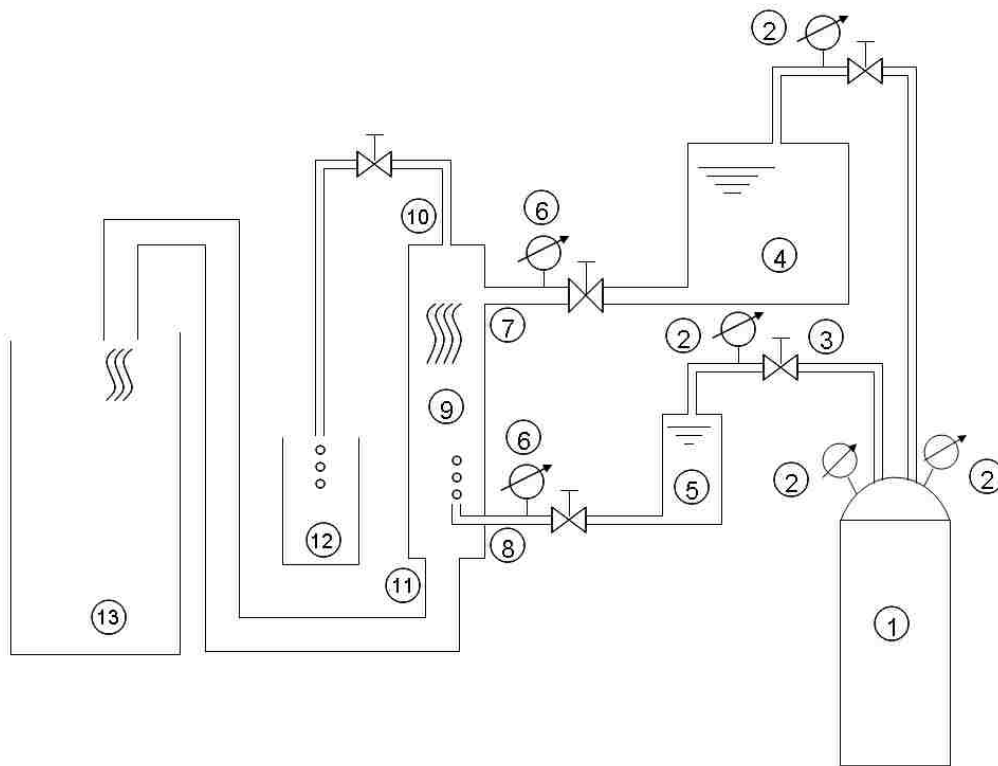
Based on large amount of experimental observations, recent researchers found that, the terminal velocity of oil droplets rising in stagnant water falls between 4 to 18 cm/s and the time to reach this velocity is about 0.33 to 1 s, which means the oil droplets can reach the

terminal velocity after traveling 2 to 18 cm in a vertical pipe (Augier, et al., 2003; Wegener, et al., 2010; Kurimoto, et al., 2010; Friedman and Friedman, 2011). For oil droplets rising in the looping section of DWL, the time for them to reach the terminal velocity would be less than that in stagnant water as the flowing water helps the oil droplets reach the equilibrium condition faster by exerting higher drag force on the droplets.

3.1.1 Experimental Setup

To simulate oil droplets moving in the looping section of DWL, a physical model built as shown in Figure 3.5. In the figure, a separation process takes place in a clear PVC chamber marked 9, with water inlet 7 and oil inlet 8. The inner diameter of the chamber is 5.715 cm and the distance between oil/water inlets is 22.9 cm which is long enough for oil droplets to reach the equilibrium condition. The flow rates of oil and water could be adjusted individually with two separated valves, and the rates are measured by two flow meters. The maximum water and oil flow rates are 26.5 L/min and 0.12 L/min, respectively. The water velocity is calculated from the water flow rate and chamber diameter, while the oil droplet velocity is measured by recording the time when it travels from the oil inlet to the water inlet. At each combination of oil/water flow rates, the velocity of 10 different oil droplets is recorded and the average value is used to analyze. The separated oil is removed from the chamber via oil outlet 10 and the water flows to the water collector 13 via water outlet 11. 7 oils with wide range of density, viscosity and interfacial tension values are used in the experiments as shown in Table 3.1, all of the properties are measured at 20 °C. The general purpose of the experiments is to observe the oil droplet flow behavior in the stagnant and moving water stream, relate oil and water velocities and determine the maximum water

velocity for the oil/water separation. A series of tests were made which covered a wide range of water flow velocities for each oil as shown in Table 3.2.



1: Pressure source; 2: Pressure gauge; 3: Valve; 4: Water reservoir; 5: Oil reservoir; 6: Flow meter; 7: Water inlet; 8: Oil inlet; 9: Counter-current flow chamber; 10: Oil outlet; 11: Water outlet; 12: Oil collector; 13: Water collector.

Figure 3.5. Experimental setup of oil water counter-current oil water separation

Table 3.1. Oils used in experiments

Property Sample	Density, ρ kg/m^3	Dynamic viscosity, μ cp	Oil and water interfacial tension, σ_{ow} , $dyne/cm$
Soltrol	775.7	4.5	30.5
Light mineral oil	836.5	53.3	53.0
Heavy mineral oil	876.3	155	65.0
#11 oil	905.7	373.4	36.9
#21 oil	839.2	12.5	26.9
#22 oil	830.9	15.4	30.0
#44 oil	878.9	180.7	61.5

Table 3.2. Experimental matrix for oil water counter-current separation

Oil Oil rate, cm^3/min	Water rate, cm^3/min	Soltrol	Light mineral oil	Heavy mineral oil	#11 oil	#21 oil	#22 oil	#44 oil
0		5.0	120.0	120.0	120.0	50.0	40.0	100.0
1,847		5.0	120.0	120.0	120.0	50.0	40.0	100.0
3,848		5.0	120.0	120.0	120.0	50.0	40.0	100.0
5,695		5.0	120.0	120.0	120.0	50.0	40.0	100.0
7,542		5.0	120.0	120.0	120.0	50.0	40.0	100.0
9,543		5.0	120.0	120.0	120.0	50.0	40.0	100.0
11,390		5.0	120.0	120.0	120.0	50.0	40.0	100.0
13,236		5.0	120.0	120.0	120.0	50.0	40.0	100.0
15,083		5.0	120.0	120.0	120.0	50.0	40.0	100.0
17,084		5.0	120.0	120.0	120.0	50.0	40.0	100.0
18,931		5.0	120.0	120.0	120.0	50.0	40.0	100.0

3.1.2 Mechanistic Model

As shown in Figure 3.6, three forces control the oil droplet moves in the flowing water stream. When the buoyancy is greater than the summation of gravity and drag force, oil droplet will separate from water in a counter-current flow pattern, otherwise, it will move down co-currently with water. Mechanistic model describes the phenomena as follows:

Buoyancy force:

$$F_B = \frac{1}{6} \rho_w g \pi d_o^3 \dots\dots\dots(3.1)$$

Gravity force:

$$F_G = \frac{1}{6} \rho_o g \pi d_o^3 \dots\dots\dots(3.2)$$

Drag force (Levich, 1962; Ouyang, 2003b):

$$F_D = \frac{1}{8} \mu_D C_D \rho_w (u_w - u_o)^2 \pi d_o^2 \dots\dots\dots(3.3)$$

$$C_D = \begin{cases} 24 \text{Re}_d^{-1}, & \text{Re}_d < 1 \\ 30 \text{Re}_d^{-0.625}, & 1 \leq \text{Re}_d \leq 1000 \\ 0.44, & \text{Re}_d > 1000 \end{cases} \dots\dots\dots(3.4)$$

$$\text{Re}_d = \frac{\rho_w |u_{wr}| d_o}{\mu_w} \dots\dots\dots(3.5)$$

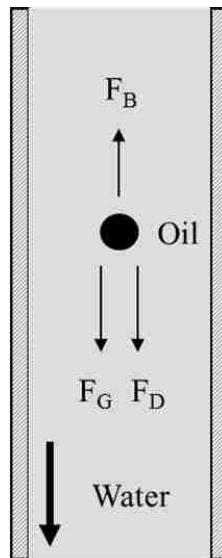


Figure 3.6. Oil droplet moving in a moving water stream

If we assume the oil velocity direction is positive, then:

$$|u_{wr}| = ||u_o| - |u_w|| \dots\dots\dots(3.6)$$

Counter-current separation:

$$F_B > F_G + F_D \dots\dots\dots(3.7)$$

Oil droplet reaches equilibrium:

$$F_B = F_G + F_D \dots\dots\dots(3.8)$$

Co-current flow:

$$F_B < F_G + F_D \dots\dots\dots(3.9)$$

Where, F_B is the buoyancy force, N; ρ_w and ρ_o are the densities of water and oil, respectively, kg/m^3 ; g is the gravitational constant, 9.8 m/s^2 ; d_o is the oil droplet diameter, m; F_G is the gravity force, N; F_D is the gravity force, N; μ_D is the dimensionless viscosity which represents the effect of fluids' viscosities on drag force; C_D is the drag coefficient, dimensionless; u_w and u_o superficial velocities of water and oil, m/s; μ_w is the viscosity of water, cp; Re_d is the droplet Reynolds number, dimensionless.

From Equation 3.3, it is clear that, the drag force increases with water velocity. To assure separation, Equation 3.7 should be satisfied. Also, the maximum critical water velocity can be derived from Equation 3.8. By combining Equations 3.1 to 3.8, we find the critical water velocity as:

$$u_{wC} = u_{wrC} = \sqrt{\frac{4(\rho_w - \rho_o)gd_o}{3\mu_D C_D \rho_w}} \dots\dots\dots(3.10)$$

Despite the simple format, Equation 3.10 is not so easy to use, as the oil droplet size depends on water velocity. Moreover, there is a controversy about the dimensionless viscosity group, μ_D , which will be discussed later.

When oil droplets flow in water stream, it is necessary to consider the interaction between the two phases such as oil droplet break up. The mechanism of break up mainly depends on two forces: an external disturbing force (inertial or viscous force) induced by the flow field that tries to deform the droplet and an internal restoring force (interfacial tension) that tries to maintain the droplet size and initial shape. The droplet breaks up when the deformation becomes excessive (Hinze, 1955; Van den Broek, et al., 2001; Van der Zande, et al., 2001). Thus, interfacial tension is important in determining droplet size.

Moreover, Weber number and Capillary number, shown in Equations 3.11 and 3.12, respectively, both use interfacial tension to characterize the flowing behavior of an individual

oil droplet in water stream (Janssen and Meijer, 1993; Eastwood, et al. 2004; Saylor and Bounds, 2012.). Weber number measures the relative importance of inertia and interfacial tension on a droplet while Capillary number represents the ratio of viscous force to interfacial tension acting across an interface between oil and water.

$$W_e = \frac{\rho_w u_{wr}^2 d_o}{\sigma_{ow}} \dots\dots\dots(3.11)$$

$$C_a = \frac{\mu_w u_{wr}}{\sigma_{ow}} \dots\dots\dots(3.12)$$

Usually, the critical Weber number is used to determine oil droplet size, d_o , in high rate co-current flow, where the flow is in turbulent condition and inertial effects control droplet size (Karabelas, 1978; Barton, 1990; Angeli and Hewitt, 2000). The approach, however, has been found not accurate in some cases - especially for the counter-current flow condition. The discrepancy could result in up to 80-fold overestimation of the critical oil droplet size (Clift, et al., 1978; Ouyang, 2003b). The reason is that, for high water velocity in co-current flow, Weber number controls the size of oil droplets, i.e. the break up occurs mainly due to inertia (Eastwood, et al. 2004). However, in the counter-current flow case, discussed above, the maximum water velocity is limited, so the capillary number mainly controls droplets break up.

Ouyang used an adjustment factor 0.015 in his correlation as shown in Equation 3.13, to improve the prediction but he also suggested more experimental data should be used to validate the correlation.

$$d_o = 0.015 \frac{\sigma_{ow} W_{e,cr}}{\rho_o u_o^2} \dots\dots\dots(3.13)$$

Where, σ_{ow} is the interfacial tension, dyne/cm; $W_{e,cr}$ is the critical Weber number, dimensionless. Sleicher (1962) found that, when the viscosity of dispersed phase is much higher than that of the continuous phase, the Ohnesorge number ($On = \mu_o / \sqrt{\rho_o d_o \sigma_{ow}}$), should be included in the Weber number to consider the viscous force from the dispersed phase. He proposed a correlation to determine the droplet size as:

$$d_o = \frac{C \left[1 + 0.7 \left(\frac{\mu_o u_{wr}}{\sigma_{ow}} \right)^{0.7} \right]}{\frac{\rho_w u_{wr}^2}{\sigma_{ow}} \left(\frac{\mu_w u_{wr}}{\sigma_{ow}} \right)^{0.5}} \dots\dots\dots (3.14)$$

Where C is a coefficient depending on oil properties and should be determined from a calibration experiment, i.e. measuring the maximum droplet size for a certain water velocity, then substituting the droplet size and water velocity into Equation 3.14 and calculating the C value.

In addition to the oil droplet size estimation, the effect of viscosity on drag force is a controversial issue. In the Levich's work, this effect was simply ignored in co-current flow (1962). However, Ouyang (2003a, b) found that, viscosity had a significant effect on the flow pattern in counter-current flow. He proposed a dimensionless group $\mu_{D1} = (3\mu_w + 2\mu_o) / (3\mu_w + 3\mu_o)$, to consider this effect as shown in Equation 3.3. Unfortunately, he did not use water as continuous phase in the experiments, so his dimensionless group may not apply in this study. Brauner (1998) presented another dimensionless group $\mu_{D2} = 3(2\mu_w + 3\mu_o) / (\mu_w + \mu_o)$, to consider the viscosity effect based on large amount of literature survey. The formulation is found to be useful in this study.

After getting the values of oil droplet size and dimensionless viscosity group, Equation 3.10 could be solved iteratively to get the critical water velocity, as the oil droplet

size relates to the water velocity. Comparing the results with experimental data, we found that the coefficient in Brauner's viscosity group could be reduced from 3 to 2 as shown in Equation 3.15:

$$\mu_D = \frac{2(2\mu_w + 3\mu_o)}{\mu_w + \mu_o} \dots\dots\dots(3.15)$$

With this viscosity group, the critical water velocity can be predicted more accurately as shown in Figure 3.7. Sensitivity analysis showed that, oil/water viscosity ratio (μ_o/μ_w) contributed more than 10% to both oil droplet moving velocity and critical water velocity, which will be discussed later.

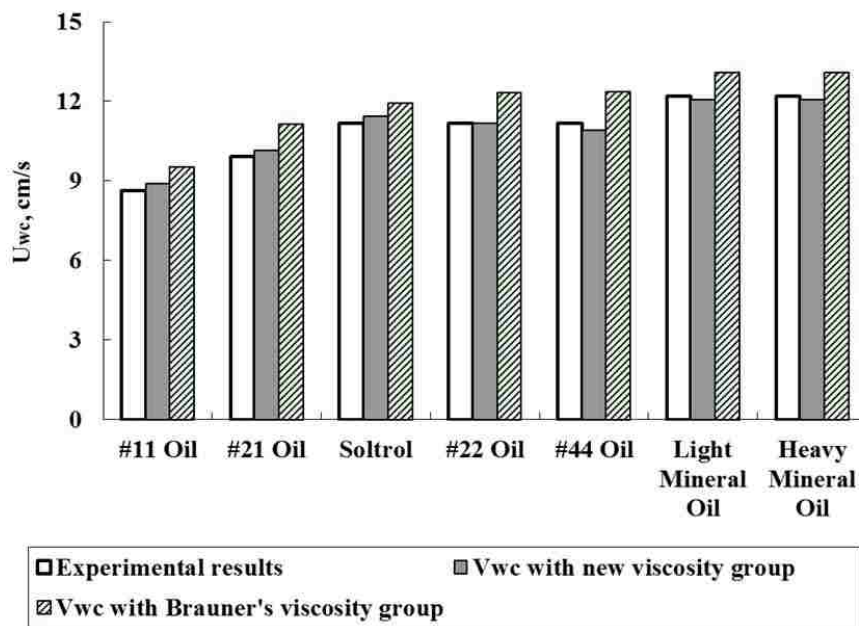


Figure 3.7. Comparison of critical water velocity using new and Brauner's viscosity groups

3.1.3 Drift-Flux Model

The mechanistic model, although has sound theoretical basis, it has its intrinsic limitations: needs experiments to determine oil droplet size, could only be used to determine

the critical water velocity, could not predict oil droplet moving speed at any water velocity. Thus, a simple, continuous and smooth model is needed to fully describe the oil droplet flow behavior under counter-current conditions.

Drift-flux technique is well-suited for modeling multiphase flow in pipes and wells, which has been widely used in reservoir simulators for its simple, accurate, continuous and differentiable characters. The method has been proved to be useful in calculating phase velocity and predicting pressure drop in co-current flows (Hasan and Kabir, 1990, 1999; Alkaya, 2002; Shi, et al., 2005a, b). Ouyang extended the model to two-phase counter-current flow, where oil was the continuous phase and water dispersed as droplets in oil stream (2003a). Here, we intend to use this method for water being a continuous phase so the drift-flux model must be modified to calculate the oil droplet rise velocity for various water flow rates.

Zuber and Findlay developed the drift-flux model to account for the effects of non-uniform flow, phase concentration profiles and the local relative velocity between phases for gas-liquid flow in 1965. Ishii further found this model was good for various gas-liquid flow regimes in 1977. Hasan and Kabir (1990) and Shi, et al. (2005a) extended the method to oil-water co-current flow to model the in-situ oil velocity considering the slip effect between phases as:

$$u_o = C_o u_m + u_d \dots\dots\dots(3.16)$$

Where u_o is the in-situ oil velocity, m/s, u_m is the average superficial mixture velocity, m/s, u_d is the drift velocity of oil describing the buoyancy effect and C_o is the profile parameter (or oil distribution coefficient), dimensionless, which can be shown in the following equation summarized by Shi, et al. (2005a):

$$C_o = \begin{cases} 1.2, & f_o \leq 0.4 \\ 1.2 - \frac{2(f_o - 0.4)}{3}, & 0.4 < f_o < 0.7 \\ 1.0, & f_o \geq 0.7 \end{cases} \dots\dots\dots(3.17)$$

Where f_o is the in-situ oil volume fraction, and the drift velocity u_d which accounts for the maximum oil droplet velocity in stagnant water, could be expressed as Equation 3.18 developed by Harmathy in 1960 and recommended by many authors (Hasan and Kabir, 1990; Brauner, 1998; Shi, et al., 2005a, b):

$$u_d = 1.53(1 - f_o)^n \left[\frac{1000\sigma_{ow}g(\rho_w - \rho_o)}{\rho_w^2} \right]^{0.25} \dots\dots\dots(3.18)$$

Where the exponent n varies from 1 to 2.5 based on oil properties, and f_o is the in-situ oil volume fraction, which could be determined by the following correlation for low oil concentration developed by Hasan and Kabir (1999):

$$f_o = \frac{q_o}{A \left\{ 1.2u_m + 1.53 \left[\frac{\sigma_{ow}g(\rho_w - \rho_o)}{\rho_w^2} \right]^{0.25} \right\}} \dots\dots\dots(3.19)$$

Where q_o is the oil rate. m³/s; A is the cross-section area of the pipe, m².

In counter-current flow, the water stream flows downwards and the oil droplets move upwards. As we assumed the oil velocity direction is positive, Equation 3.16 could be rearranged to:

$$u_o = u_d - C_o u_m \dots\dots\dots(3.20)$$

As the oil fraction in this study is extremely small, the mixture velocity could be simplified to water velocity, $u_m \approx u_w$, so Equation 3.20 becomes:

$$u_o = u_d - C_o u_w \dots\dots\dots(3.21)$$

Close observation of the above equations, it is found that, there is no viscosity items in the model. Hasan and Kabir used several different oils in co-current flow experiments and concluded that viscosity was not important in flow behavior prediction (1990). However, other studies showed that, viscosity played an important role in determining the velocity of the dispersed bubbles or droplets, especially when there was a significant difference between the viscosities of dispersed and continuous phases (Zukoski, 1966; Shosho and Ryan, 2001; Joseph, 2003; Perron, et al., 2006a, b; Gokcal, et al., 2008; Mandal, et al., 2008). Gokcal, et al. (2009) performed a series of experiments to investigate the impact of inclination angle and viscosity on drift velocity. Their experiments covered a wide range of oil viscosity, from 1 to 1287 cp. Results showed that, the average deviation in drift velocity without considering the oil viscous effect was around 20%, while it could reach as much as 40% to high viscosity oil. Gokcal, et al. (2009) used the best fit line to regress the drift velocity model and got a good agreement to the experimental data. However, they did not consider the viscosity of continuous phase, i.e. water viscosity, in their model, while it was showed to be important for bubbles or droplets moving in another media with different viscosity by other authors (Brauner, 1998; Shosho and Ryan, 2001; Mandal, et al., 2008). Different dimensionless numbers were used to consider phase viscosities, here we used the same dimensionless viscosity number as in the mechanistic model, which is shown in Equation 3.15, modified from Brauner’s dimensionless viscosity number. Similar to Gokcal, et al. (2009), we used the data fitting method to include the dimensionless viscosity number in the drift velocity based on the current drift velocity equation in the following format:

$$u_d = 1.53(1 - f_o)^n \left[\frac{\sigma_{ow} g(\rho_w - \rho_o)}{\rho_w^2} \right]^{0.25} \mu_D^m \dots\dots\dots(3.22)$$

Where m is the exponent to be adjusted to make the Equation 3.22 fit the experimental data and reach the maximum R-squared value (i.e. the coefficient of determination) for all 7 oils, and m is determined by linear regression as follows:

First, changing the Equation 3.22 into logarithmic format as:

$$\ln u_d - \ln \left\{ 1.53(1 - f_o)^n \left[\frac{\sigma_{ow} g(\rho_w - \rho_o)}{\rho_w^2} \right]^{0.25} \right\} = m * \ln \mu_D \dots\dots\dots(3.23)$$

Second, linear regressing left hand side (LHS) of Equation 3.23 versus $\ln \mu_D$ to get the m and R-squared value as shown in Figure 3.8. It is clear in the figure that, R-squared value reached the maximum value of 0.875 when $m = -0.977$, which indicated Equation 3.22 could be written as:

$$u_d = 1.53 \frac{(1 - f_o)^n}{\mu_D^{0.977}} \left[\frac{\sigma_{ow} g(\rho_w - \rho_o)}{\rho_w^2} \right]^{0.25} \dots\dots\dots(3.24)$$

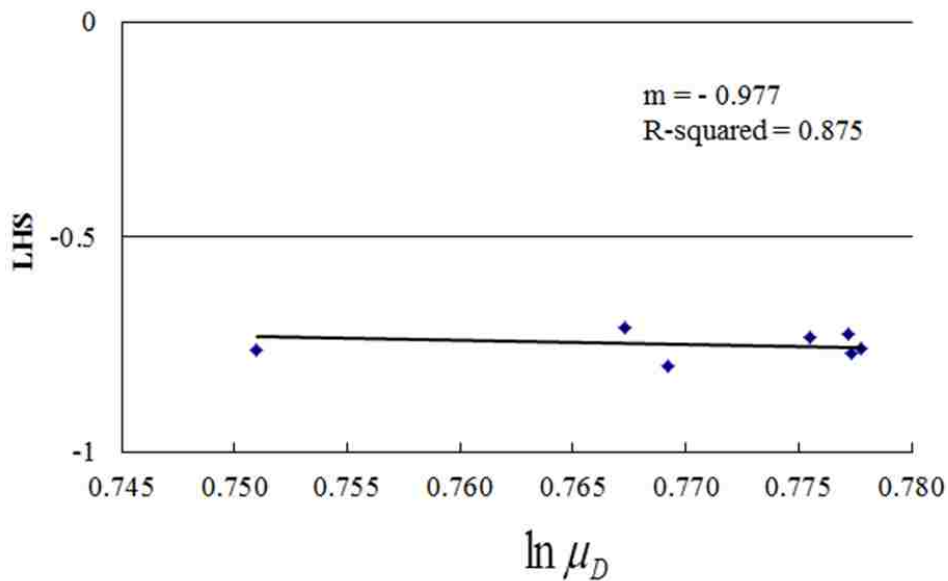


Figure 3.8. Linear regression of viscosity group coefficient m

Combine Equations 3.21 and 3.24, we could get the drift-flux model for oil-water counter-current flow, which could be used to predict the oil velocity at any water rate as:

$$u_o = 1.53 \frac{(1-f_o)^n}{\mu_D^{0.977}} \left[\frac{\sigma_{ow} g (\rho_w - \rho_o)}{\rho_w^2} \right]^{0.25} - C_o u_w \dots\dots\dots (3.25)$$

The critical water velocity could be determined when set the oil velocity to zero as:

$$u_{wC} = \frac{1.53(1-f_o)^n}{C_o \mu_D^{0.977}} \left[\frac{\sigma_{ow} g (\rho_w - \rho_o)}{\rho_w^2} \right]^{0.25} \dots\dots\dots (3.26)$$

3.1.4 Experimental Results and Model Validation

As shown in Table 3.2, oil droplet velocity is recorded at each gradually increased water velocity, and Equation 3.21 shows that, the relation between oil velocity u_o and water velocity group $C_o u_w$ is expected to be nearly linear when the oil fraction is small. As the oil fraction in the experiments is very small, the exponent n is set to be 1 in our calculations. Notice that, the value of C_o is fixed at 1.2 for oil fraction less than 40%, which might need a modification in our experiments due to the extremely low oil concentration. As the same to linear regression of Equation 3.22, we could apply the same method to Equation 3.21 to find the best value of C_o . First, changing the format of Equation 3.21 as:

$$1 - \frac{u_o}{u_d} = C_o \frac{u_w}{u_d} \dots\dots\dots (3.27)$$

Then, linear regressing $(1-u_o/u_d)$ versus u_w/u_d to find out C_o for the maximum R-squared value as shown in Figure 3.9, which clear shows R-squared value reached 0.9125 when $C_o = 1.235$.

Figure 3.10 shows the comparison of oil droplet velocity between experiments and drift-flux model. As shown in the figure, a good agreement is obtained which meets the expectation for all of the 7 oils. The drift-flux model successfully predicts the oil droplet

velocity at various water velocities in counter-current flow condition, which indicates that the model can be used in counter-current flow where water is the continuous phase.

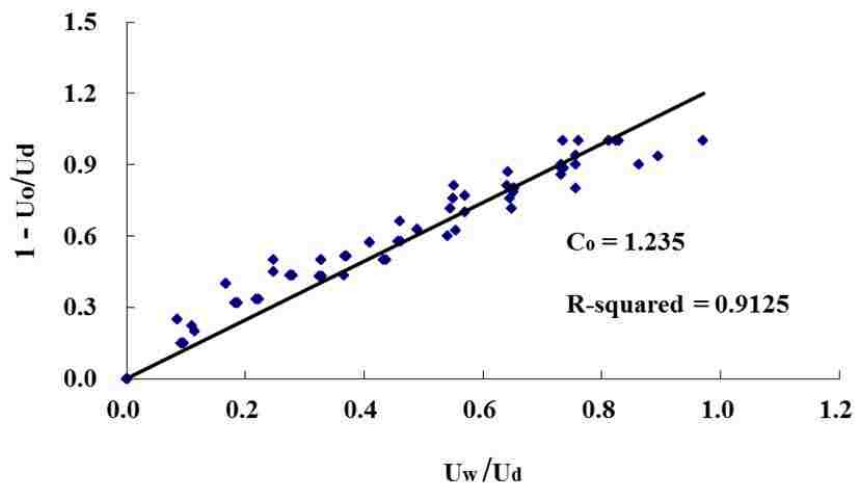


Figure 3.9. Linear regression of drift-flux coefficient C_o

Figure 3.11 shows the comparison of critical water velocity between experiments, drift-flux model and mechanistic models. The average deviation between mechanistic model and experimental results is about 3.5%, while it is about 5% for drift-flux model and experiments. This comparison shows that, both mechanistic and drift-flux model give accurate estimation of critical water velocity for possible oil/water separation under counter-current flow conditions.

When oil droplets moving through the water column, oil and water properties such as density, viscosity and interfacial tension should have some effects on the droplet velocity, however, we did not find quantitatively study of their significance level in literature. In order to make this problem clear, we use a statistical analysis of variance (ANOVA) to investigate the significance level of the control parameters using experimental data from our experiments and other published results.

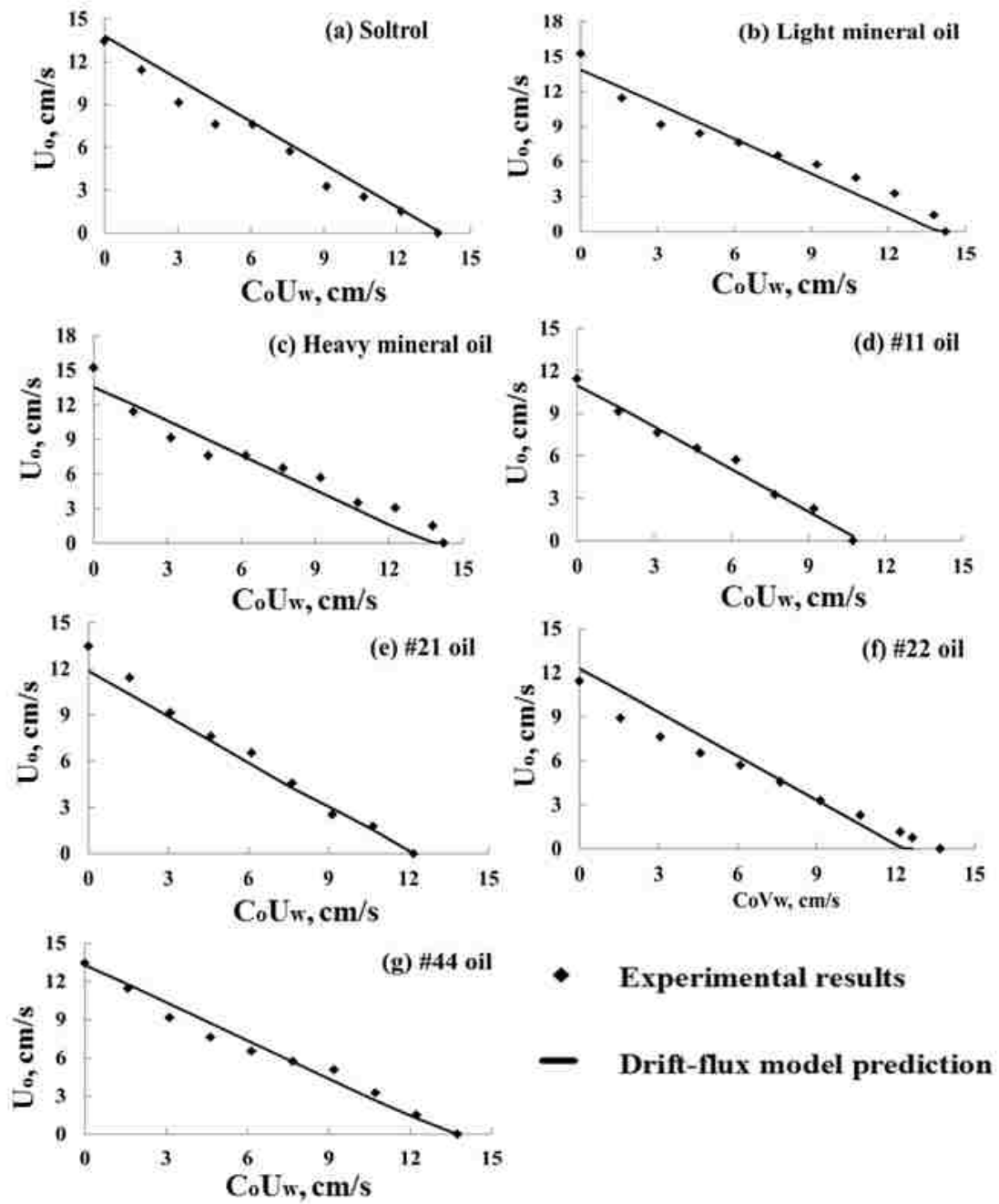


Figure 3.10. Comparison of droplet velocity between experiments and drift-flux model

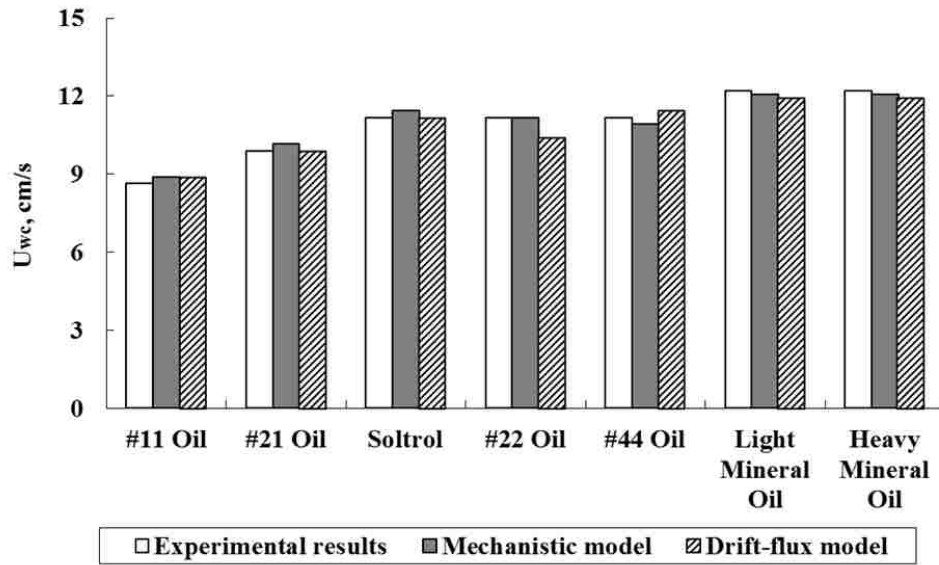


Figure 3.11. Comparison of critical water velocity for experiments and models

ANOVA is particularly useful for studying statistical relationship between a dependent variable and individual or groups of independent variables (Montgomery and Runger, 2010). We use this method to determine the significance level of oil/water interfacial tension, density ratio and viscosity ratio on the critical water velocity. Figure 3.12 and Figure 3.13 show that, the most important parameter is the oil/water interfacial tension. The reason is that, it is the main force to keep the droplet in its original shape when both inertia and viscous force try to deform the droplet. When scaling the flow, for example, interfacial tension appears in all Weber, Capillary and Ohnesorge numbers. Another important parameter is viscosity ratio with more than 10% contribution to variation of critical velocity, which indicates that oil/water viscosity contrast should not be ignored.

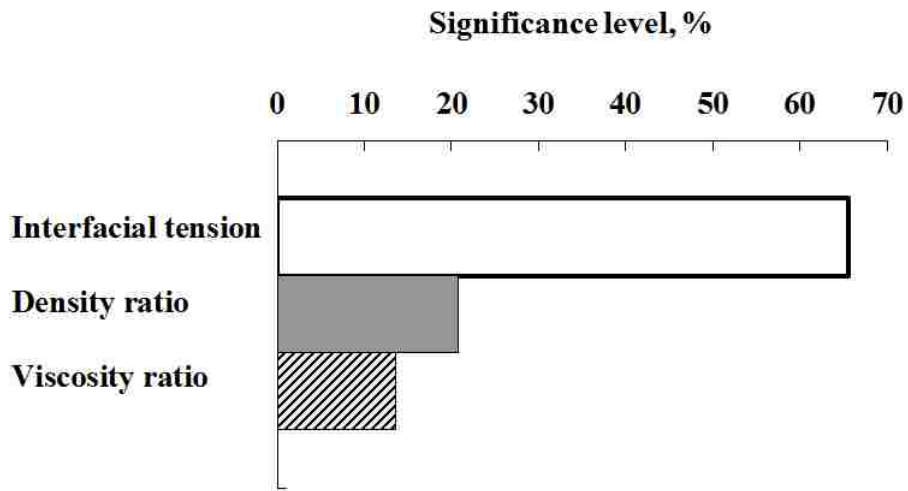


Figure 3.12. Significance level of each parameter for the critical water velocity

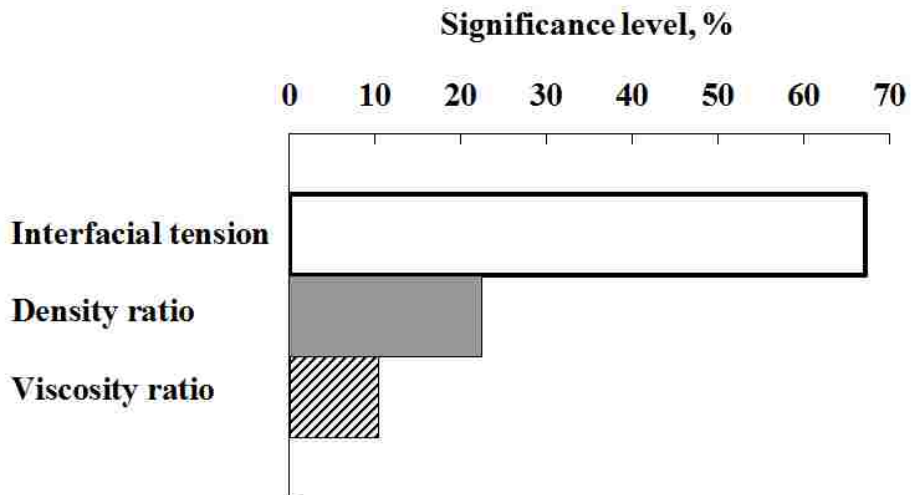


Figure 3.13. Significance level of each parameter for oil droplet moving velocity (data from Licht and Narasimhamurty, 1955 and Klee and Treybal, 1956)

3.2 Maximum Water Drainage Rate to Avoid Oil Contamination

As shown in Figure 3.11, the critical water velocity for possible counter-current oil separation is around $u_{wC} = 0.1 \text{ m/s}$ (0.33 ft/s) for most oils. In a real DWL well, this value corresponds to a point in the perforated well section above which separation takes place, and oil droplets below this section will enter the injection completion due to the high water

velocity. If we assume the water rate is linearly distributed along the completion, then the oil separation section could be determined as follows:

Assume the water drainage completion length is h_{wd} , drains water at rate q_w and the well diameter is d as shown in Figure 3.14, the water rate at the bottom of separation section h_{sep} is:

$$q_{sep} = \frac{q_{wd} * h_{sep}}{h_{wd}} \dots\dots\dots (3.28)$$

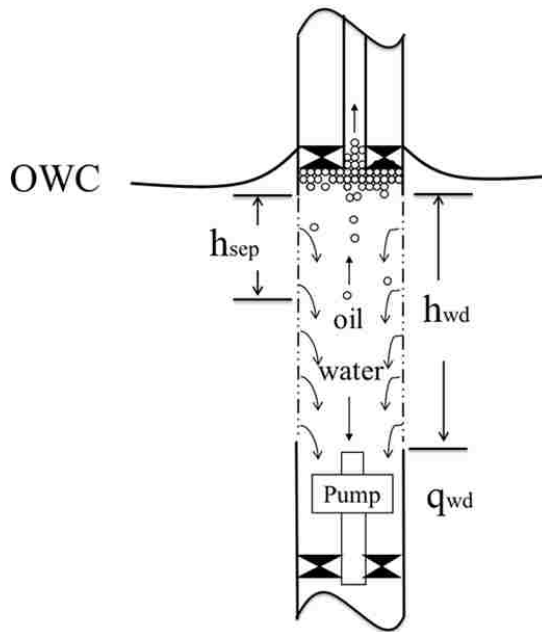


Figure 3.14. Schematic of oil water separation in DWL

The water velocity at the bottom of separation section should be less than the critical velocity to ensure the separation:

$$u_{sep} = \frac{4q_{sep}}{\pi d^2} \leq u_{wC} \dots\dots\dots (3.29)$$

Combine Equations 3.26, 3.28 and 3.29, we can get the point where all oil could be separated:

$$h_{sep} = \frac{\pi d^2 h_{wd}}{4q_{wd}} * \frac{1.53(1-f_o)^n}{C_o \mu_D^{0.977}} \left[\frac{\sigma_{ow} g (\rho_w - \rho_o)}{\rho_w^2} \right]^{0.25} \dots\dots\dots (3.30)$$

It is also shown how oil separation could be predicted from a given water sink completion length and drainage-injection rate. A simulation model with strong water coning was designed using #22 oil as shown in Table 3.3. The critical oil rate for conventional well is only about 3 bopd in this reservoir, while DWL improves the value to 15 bopd with 1500 bwpd water drainage-injection rate. Figure 3.15 shows the water rate and oil cut in the drainage water change with the water drainage completion depth. It is clear that, the main oil contamination happens in the top 3 ft of the completion and the maximum water velocity in this oil contaminated section is about 0.11 ft/s < 0.33 ft/s, which indicates all the oil droplets could be separated before entering the injection completion.

Table 3.3. Parameters used in DWL simulation model

Parameter	Value	Unit	Parameter	Value	Unit
Horizontal permeability (K_h)	3500	md	Length of water drainage completion (h_{wd})	10	ft
Vertical permeability (K_v)	3150	md	Length of water injection completion (h_{wi})	10	ft
Water relative perm (K_{rw}^*)	0.095		Length of oil water separation (h_{sep})	8	ft
Oil relative perm (K_{ro}^*)	0.125		Water specific gravity (γ_w)	1.05	
Well radius (r_w)	0.292	ft	Oil specific gravity (γ_o)	0.83	
Drainage radius (r_e)	850	ft	Water viscosity (μ_w)	1	cp
Oil zone thickness (h_o)	18	ft	Oil viscosity (μ_o)	1.54	cp
Water zone thickness (h_w)	64	ft	Water volume factor (B_w)	1.02	bbl/stb
Distance from top perforation to OWC (Z_{op})	15	ft	Oil volume factor (B_o)	1.1	bbl/stb
Distance from water drainage perforation to OWC (Z_{wd})	15	ft	Oil production rate (q_o)	15	bpd
D/I spacing (h_{DI})	20	ft	Water drainage rate (q_w)	1500	bpd

From Figure 3.10, we can see that, oil droplet rises fast when the water velocity is low, which indicates that, the oil/water separation could be accelerated by reducing the water

velocity. However, water velocity relates to water rate, which is always required to be high in DWL wells. One way to reduce water velocity without sacrificing the water rate is increasing the well diameter. If the well size increases from 3 in to 7 in, the water velocity would decrease about 81.5% with the same water rate, or the water drainage rate could be improved more than 400% with the same oil separation effect.

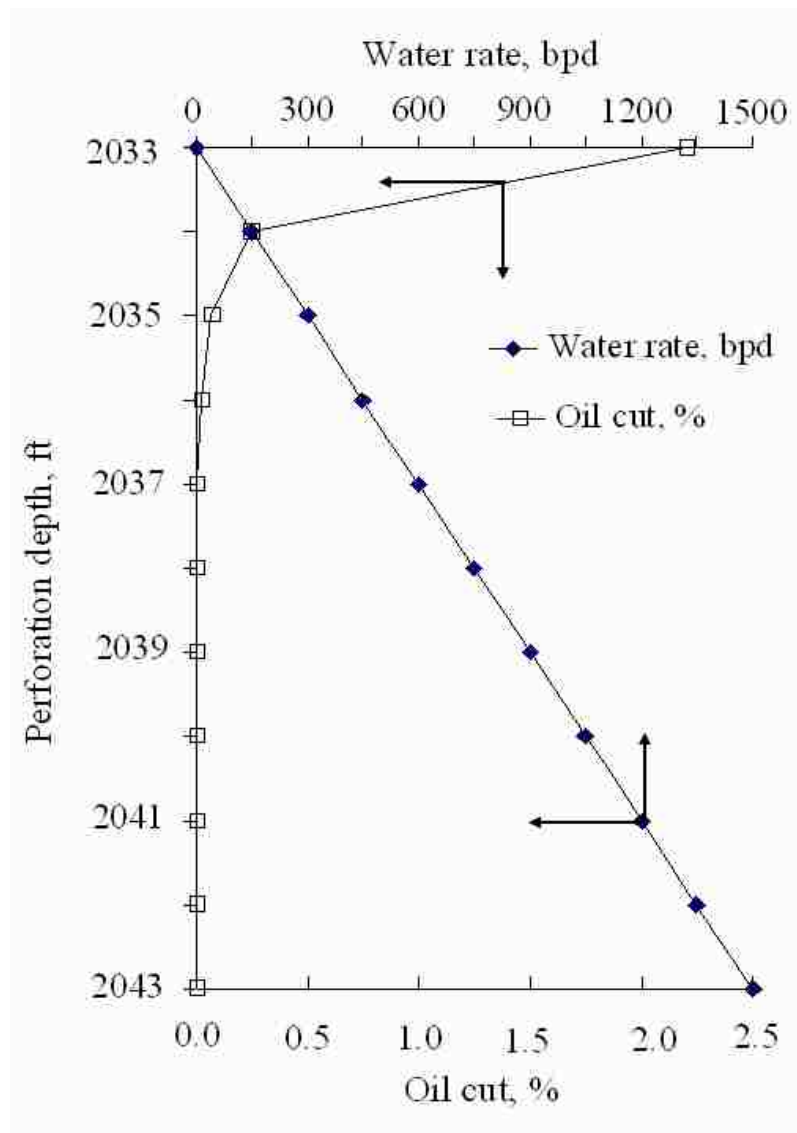


Figure 3.15. Water rate and oil cut change with perforation depth

3.3 Discussion and Summary

The dimensionless viscosity group μ_D varies from 5.65 to 6.0 for the oils used in the experiments. From Equations 3.10 and 3.26, we can see that, the prediction would significantly miss the true value if we don't account for the viscosity effect in counter-current flow conditions. The observation made by Ouyang (2003a, b) and Gokcal, et al. (2009) showed that, ignorance of fluid viscosities would lead to as much as 40% deviation in oil droplet drift velocity prediction, which is confirmed in our experiments. Table 3.4 shows the comparison of drift velocity observed in experiments and calculated from different correlations. It is clear that, Harmathy's correlation overestimates the drift velocity when oil fraction is extremely low and it could be improved by including a dimensionless viscosity group as shown in Equation 3.24. However, Harmathy's correlation could work well without considering viscosity effect when the oil fraction was high as it is proportional to $(1-f_o)^n$, this might be the reason why many authors recommended it for high oil fraction circumstances such as slug and chum flows (Hasan and Kabir, 1990, 1999; Brauner, 1998; Shi, et al., 2005a, b).

Table 3.4. Drift velocity for different oil droplets

Oil	Drift velocity, cm/s						
	Experimental run	Equation 20	Deviation, %	Klee and Treybal, 1956	Deviation, %	Harmathy, 1960	Deviation, %
Soltrol	13.45	13.81	2.72	13.52	0.53	72.15	436.52
Light min. oil	15.24	14.25	6.50	13.67	10.32	76.54	402.22
Heavy Min. oil	15.24	13.54	11.16	13.11	13.96	75.12	392.90
#11 oil	11.43	10.97	4.02	10.98	3.97	60.93	433.05
#21 oil	13.45	11.86	11.79	12.04	10.46	64.33	378.42
#22 oil	11.43	12.29	7.53	12.45	8.95	66.95	485.73
#44 oil	13.45	13.28	1.25	12.91	4.02	73.69	448.03
Average	13.4	12.86	6.42	12.67	7.46	69.96	425.27

Based on the experimental observation and theoretical analysis of the oil-water counter-current flow, we can get conclusions from the study as follows:

1. Oil/water separation in wellbore is possible under counter-current flow condition in wells with water re-injection in-situ such as DOWS and DWL, where water is the continuous phase flows downward while the dispersed oil droplets moving upward due to the slip effect;
2. Both mechanistic and drift-flux models were developed to predict the oil droplet velocity and critical water velocity for oil/water counter-current separation. Both models yield accurate results which were validated by experimental results;
3. Oil-water interfacial tension is the most important factor in the separation process, as it controls the oil droplet size, which significantly simplifies the model by replacing the droplet size (most difficult to measure) with a correlation based on interfacial tension developed using the experimental results;
4. Oil and water viscosities are important factors in counter-current flow, which contributes more than 10% in determining the critical water velocity, although they are usually ignored in co-current flow conditions;
5. A 0.33 ft/s (0.1 m/s) value of critical maximum water velocity for counter-current oil separation is found in this study, which corresponds to a point in the perforated well section above where separation takes place, and a simple model is developed to predict this point from a given water sink completion length and drainage-injection rate;
6. Simulation shows that, the main oil contamination happens in the top section of the water drainage completion where water velocity is low. Thus, longer

completion length is helpful to the oil separation as it reduces the water velocity in the top section;

7. Increasing the well size could also significantly reduce the water velocity and accelerate the oil separation while keep the water rate constant.

CHAPTER 4. DWL WELL LIMITATION DUE INJECTIVITY DECLINE

To control water coning effectively, DWL has to drain and inject large amount of water in-situ. As discussed in Chapter 2, DWL well's injectivity may decline due oil content in the drainage water. Theoretically, oil contamination could be eliminated in the following ways:

1. Raise the oil production rate to increase the pressure drawdown in the top completion while keeping the water drainage rate constant;
2. Reduce the water drainage rate to decrease the pressure drawdown in the aquifer while keep the oil production rate constant;
3. Keep the water drainage rate below the maximum limit to ensure oil separating from the counter-current flowing water.

However, all methods sacrifice the merit of DWL for water coning control, as DWL tries to balance the pressure drawdown caused by oil production. If the pressure drawdown in the pay zone is greater than the pressure drawdown in the aquifer, then water will cone up to the top completion and soon breakthrough, which will quickly increase the water cut and reduce the oil production rate. And the critical rate for a small oil-free water drainage rate is usually too low to be economical (Jin and Wojtanowicz, 2011b). The water drainage completion is usually placed below and close to the oil water contact (OWC) to minimize water drainage needed to balance the oil production pressure drawdown. This makes oil droplets enter the drainage water easily due to the pressure interference effect. Although oil can separate from the drainage water in the looping section when there is enough spacing between the water drainage and injection completions, if the distance is small, oil would not

be separated. Thus, DWL without oil contamination in the drainage water is practically difficult to achieve, especially at the beginning of production as shown in most of our simulations (Jin and Wojtanowicz, 2011b).

Injectivity issues are the most serious problems for almost all the injection wells (Pang and Sharma, 1997), and they are even more important to DOWS and DWL technologies, which depend heavily on water injection. DOWS field practices have shown that it would take most effort to maintain injectivity (Veil and Quinn, 2004; Abou-Sayed, et al. 2007). Veil and Quinn (2004) pointed out that the most important factor for the success of DOWS is that the injection formation has good injectivity. Numerous laboratory experiments show that even very small amount (below 100 ppm) of oil in injected water can cause severe injectivity damage (Buret, et al., 2010). Therefore, the understanding of injectivity decline mechanisms around DWL well is essential to predict the behavior of DWL and set up guidelines for the real practice. In case of DWL, the main problem appears to be resulting from oil contamination in the injection water. Therefore, prediction of injectivity decline resulting from low oil content in the drainage water will be addressed in this chapter.

4.1 Mechanisms of Formation Damage Caused by Oily Water Injection

Soo and his partners carried out experimental and theoretical work to study the emulsion flow behavior in porous media. They found that the capture of oil droplets in rock is similar to that of solid colloids during a deep bed filtration process (Schmidt, et al., 1984; Soo and Radke, 1984a, b, 1986; Soo, et al., 1986). Thus, droplet capture, that is, mass transfer between the liquid globule and the solid matrix, is analogous to the traditional solid particle filtration theory. The two main capture mechanisms at work are: straining, where oil droplets clog the pore throats, and interception - with droplets captured by van der Waals

colloidal forces. For emulsions, there is usually a distribution of droplet sizes, so straining would dominate the large droplet capture while interception would contribute primarily to small droplet capture. Usually, it is probably sufficient to assume a uniform droplet size distribution, and the capture parameters employed would then reflect combined straining and interception modes (Soo and Radke, 1984a, b, 1986; Auset and Keller, 2006; Buret, et al., 2010).

A more detailed description of the two oil droplet capture mechanisms proposed by Soo and his partners as a filtration process, are summarized below. Straining capture: while flowing through porous media, oil droplets block the pore throats having sizes smaller than their own by lodging between sand grains as shown in Figure 4.1. Certain pressure gradients are required to make the oil droplets pass the throats based on the diameters of droplets and pore throats (Ng, et al., 1978; Krummel, et al., 2013). This phenomenon is known as Jamin effect: when a droplet encounters a pore throat smaller than its own diameter as shown in Figure 4.2, it blocks the pore throat unless the pressure difference on it can overcome the capillary resistance force and makes the droplet deform and squeeze through the pore throat (McAuliffe, 1973a; Cosse, 1993). However, some throats may need very high pressure gradients, if they are insufficient, the oil droplets will remain trapped and the immobilized oil becomes residual oil as shown in Figure 4.3 (Krummel, et al., 2013).

Interception capture: when oil droplets are smaller than the pore throats, they are trapped in recirculation eddies, wedge in the crevices, or sometimes attach to the pore walls due to van der Waals, electrical, gravitational and hydrodynamic forces. These small droplets will accumulate in the pore space and reduce the flow path for water as shown in Figure 4.4

(Auset and Keller, 2006). With the increase of droplet size, some droplets may coalesce to bigger ones that can block the pore throats which becomes straining capture.

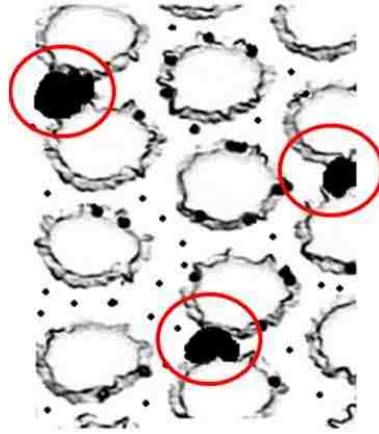


Figure 4.1. Straining capture of big oil droplet

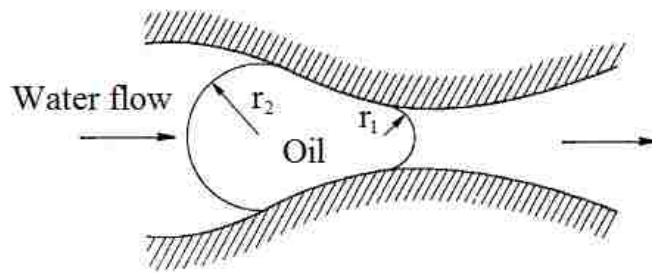


Figure 4.2. Oil droplet flows through restricted pore throat



Figure 4.3. Shape of oil blobs or ganglia trapped in porous media

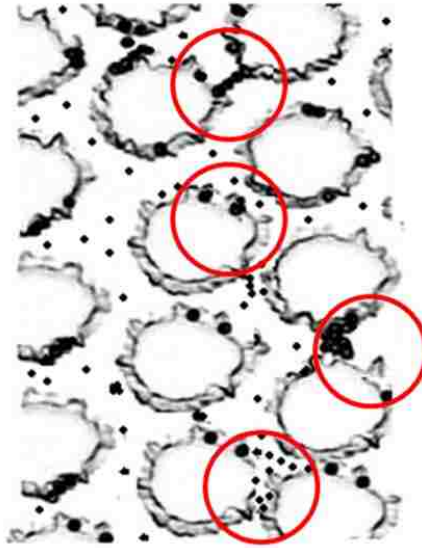


Figure 4.4. Interception capture of small oil droplet

With oil droplets captured in the rock, the flow path for water is blocked which leads to injectivity decline. To characterize the filtration process, Soo and his partners used three empirical parameters: average filter coefficient of a clean bed, average flow redistribution parameter and average flow restriction parameter. The values of the three parameters are determined by fitting the experimental data for effluent concentration profiles and permeability response. However, the values are not easy to determine as they were found to vary from run to run (Rege and Fogler, 1988; Romero, et al., 2011).

4.2 Injectivity Decline Caused by Oily Water Injection in Linear Flow

Although, numerous works have been done and many models are available to predict the injectivity decline caused by solid particles, there is a lack of easy to use models to predict the injectivity damage caused by oil contamination in the injection water (Pang and Sharma, 1997; Al-Riyami and Sharma, 2002; Vaz, et al., 2006; Buret, et al., 2010).

One purpose of this study is to build a simple analytical model for injectivity decline caused by invasion of oil droplets and their adsorption in porous media. By using the mass

balance principle we can derive governing equations for oil mass transfer from oily water to the rock matrix, resulting from various droplet capture mechanisms. The model shall describe oil saturation increase in the rock space, and define the maximum (equilibrium) oil saturation based on droplet to pore throat size ratio and the capillary number. The oil saturation change should give permeability reduction described by the relative permeability relationship.

4.2.1 Basic Assumptions

Similar to Moghadasi, Soo and their coworkers' study, the mathematical expressions derived in this work are based on the following assumptions (Soo and Radke, 1984a, b, 1986; Soo, et al., 1986; Moghadasi, et al., 2004):

1. The rock is homogeneous and no fine migration happens in the injection process;
2. The oil droplets and pore throats are log-normally distributed;
3. Oil droplet is the only contaminant, there is no solid particles in the injection water;
4. Oil droplets are stable and their sizes are constant in the water before being injected into the core;
5. The oily water is injected into the core at a constant flow rate;
6. No oil is generated or disappeared in the process.

4.2.2 Mathematical Model of Oil Droplet Transport and Adsorption in Porous Media

To establish the mathematical model of oil droplet transport and capture in porous media, three mechanisms are considered: advection due velocity, dispersion caused by the molecular transport, concentration gradient and external force fields (mechanical mixing, turbulent diffusion and so on) - described by Fick's Law and adsorption induced by straining

and interception captures as described above. In one-dimensional flow, the oil transport to the porous media can be expressed as:

$$\text{Advective mass flux rate} = u_x C A_x$$

$$\text{Dispersive mass flux rate (Fick's Law)} = - D_x (\partial C / \partial x) A_x$$

$$\text{Rate of capturing by adsorption (Langmuir Adsorption): } \frac{\partial S_{o,m}}{\partial t} = \alpha \left(1 - \frac{S_{o,m}}{S_{oe,m}} \right) C$$

Where, u_x is the interstitial water velocity in x direction, which equals to the Darcy velocity divided by the porosity, m/s; C is the mass concentration of oil in the water, kg/m³; A_x is the cross-section area in x direction, m²; D_x is the overall dispersive coefficient which including effects of molecular transport, concentration gradient, mechanical aspects an so on, m²/s; $S_{o,m}$ is the mass saturation of oil trapped in the rock, which can be easily transferred to volume saturation by dividing the oil density, kg/m³; α is the adsorptive coefficient which represents the oil droplet trapping ability of a rock, 1/s; $S_{oe,m}$ is the equilibrium mass oil saturation in the rock, kg/m³.

The oil adsorption rate relates to oil concentration in the water and equilibrium oil saturation in the rock. Higher oil concentration means more oil in the water and the matrix has higher probability to capture oil droplets, thus the oil saturation increases faster. The equilibrium oil saturation is a function of velocity, which will be discussed in detail later. Usually, higher velocity leads to lower equilibrium oil saturation which reduces the oil adsorption rate. The adsorption stops when the oil saturation in the rock reaches the equilibrium value.

The total amount of oil transported parallel to the flow direction is obtained by summing the mass transported by advection and dispersion. Thus, the total amount of mass transported to a unit control volume is:

$$m_x = \phi u_x C - \phi D_x \frac{\partial C}{\partial x} \dots\dots\dots(4.1)$$

Mass change in the control volume is:

$$\Delta m = -\frac{\partial m_x}{\partial x} d_x \dots\dots\dots(4.2)$$

Because there is no loss of oil in the process, the difference between the amount of oil entering and leaving the controlled volume must be equal to the amount of oil accumulated in the element, part of it is trapped in the rock matrix and part of it is remaining in the water in the controlled volume. So, the rate of mass change can be expressed as:

$$\Delta m = [\phi \frac{\partial C}{\partial t} + (1 - \phi) \frac{\partial S_{o,m}}{\partial t}] d_x \dots\dots\dots(4.3)$$

Where, ϕ is the porosity of the porous media, fraction. Combining Equations 4.1, 4.2 and 4.3 gives one dimensional continuity equation for oily water flow through porous media as:

$$D \frac{\partial^2 C}{\partial x^2} - u \frac{\partial C}{\partial x} = \frac{\partial C}{\partial t} + \frac{(1-\phi)}{\phi} \frac{\partial S_{o,m}}{\partial t} \dots\dots\dots(4.4)$$

Since most experiments are carried out under flow conditions, where the velocity effect is much stronger than the dispersion effect, i.e. the flow is in advection dominated region. In this region, the mechanism of immiscible fluids is similar to that of miscible fluids (Perkins and Johnston, 1963, 1969; Duan, 2009).

To solve Equation 4.4, $\frac{\partial S_{o,m}}{\partial t}$ should be transformed to an expression of $\frac{\partial C}{\partial t}$ to get an analytical solution. Based on the Langmuir Adsorption Equation, the adsorbed oil saturation $S_{o,m}$ can be solved as shown in the following equation (Satter, et al., 1980):

$$S_{o,m} = [1 - \exp(-\frac{\alpha t C}{S_{oe,m}})] S_{oe,m} \dots\dots\dots(4.5)$$

Notice that, both time and oil concentration are variables in Equation 4.5, usually it is helpful to reduce the number of variables to make the process analysis more clear. Studies of

the kinetics of adsorption often assume simple relationship between oil saturation “ $S_{o,m}$ ” and oil concentration “ C ” at low oil concentration, as the adsorption process mainly depends on concentration rather than time, and concentration is a function of time itself which includes the time effect already. The reason is that, when the oil concentration is low, the number of oil droplets is much less than that of pores in the rock. Oil droplets are caught quickly by pores with similar or smaller sizes in the clean aquifer until all the available capturing sites are filled, i.e. the equilibrium oil saturation is reached (Schmidt, et al., 1984). Thus, Equation 4.5 can be simplified as Equation 4.6, which is also adopted by some commercial reservoir simulators such as CMG[®] (McKee and Swailes, 1991; CMG, 2011; Xu, et al., 2013).

$$S_{o,m} = \frac{\alpha S_{oe,m} C}{1 + \alpha C} \dots\dots\dots (4.6)$$

However, Equation 4.6 contains strong non-linear items after transformation as shown in Equation 4.7, which is difficult to solve analytically when substitute into Equation 4.4:

$$\frac{\partial S_{o,m}}{\partial t} = \left[\frac{\alpha S_{oe,m}}{1 + \alpha C} - \frac{\alpha^2 S_{oe,m} C}{(1 + \alpha C)^2} \right] \frac{\partial C}{\partial t} \dots\dots\dots (4.7)$$

When the oil concentration is low, i.e. the value of C is small, the oil adsorption rate in the matrix is proportional to the oil concentration change rate in the water. Thus, the following relationship is valid and could be used to solve Equation 4.4 analytically (Marino, 1974; Satter, et al., 1980; Yadava, et al., 1990):

$$\frac{\partial S_{o,m}}{\partial t} = \beta \frac{\partial C}{\partial t} \dots\dots\dots (4.8)$$

Where, β is a parameter related to oil adsorption process, dimensionless. Using Equation 4.8, $\frac{\partial S_{o,m}}{\partial t}$ is eliminated from Equation 4.4 and the distributed oil concentration vs. time and distance can be determined by solving Equation 4.4 with one initial and two

boundary conditions. We assume an infinite linear injection zone and define the following initial and boundary conditions:

Initial condition, there is no oil in the core before injection:

$$S_{o_m} = C = 0 \quad \text{at } t = 0, x > 0 \quad \dots\dots\dots(4.9)$$

Inner boundary condition, oil concentration is constant in the injection water before entering the core:

$$C = C_0 \quad \text{at } t > 0, x = 0 \quad \dots\dots\dots(4.10)$$

Outer boundary condition, there is no oil in the core at infinite length:

$$S_{o_m} = C = 0 \quad \text{at } t > 0, x \rightarrow \infty \dots\dots\dots(4.11)$$

Solution to Equation 4.4 gives oil concentration distribution profile in the water as shown in Equation 4.12. The detailed solution derivation process can be found in Appendix A.

$$C = \frac{C_0}{2} \left\{ \operatorname{erfc} \left[\frac{Rx-ut}{\sqrt{4DRt}} \right] + \exp \left(\frac{ux}{D} \right) \operatorname{erfc} \left[\frac{Rx+ut}{\sqrt{4DRt}} \right] \right\} \dots\dots\dots(4.12)$$

Where, $\operatorname{erfc} ()$ is the complementary error function, and R is:

$$R = 1 + \frac{\beta(1-\phi)}{\phi} \dots\dots\dots(4.13)$$

The dimensionless parameter “ R ” – also called retention factor - represents the interaction between oil droplets and rock. Its higher value means more oil droplets contact to the grains and are captured faster, which leads to higher oil saturation in the rock (Gupta and Greenkorn, 1974; Rege and Fogler, 1988).

In the actual evaluation of Equation 4.12, the term “ $\exp \left(\frac{ux}{D} \right)$ ” is large while the term “ $\operatorname{erfc} \left[\frac{Rx+ut}{\sqrt{4DRt}} \right]$ ” becomes very small for large values of argument – tens orders of magnitude smaller than the term “ $\exp \left(\frac{ux}{D} \right)$ ”, so their product can be ignored. For example, only the first and second

terms were considered in Equation 4.12 to match laboratory results under various conditions (Brigham, 1974).

When the oil concentration distribution profile is known, the oil saturation change in the rock can be determined using Equation 4.6. Following this approach and by substituting Equations 4.12 and 4.13 into Equation 4.6, we get the volume oil saturation distribution in the rock and mass oil concentration in the water as:

$$\left\{ \begin{array}{l} C = \frac{C_0}{2} \operatorname{erfc} \left(\frac{Rx-ut}{\sqrt{4DRt}} \right) \\ S_o = \frac{S_{o_m}}{\rho_o} = \frac{\alpha S_{oe_m} C_0 \operatorname{erfc} \left(\frac{Rx-ut}{\sqrt{4DRt}} \right)}{\rho_o [2 + \alpha C_0 \operatorname{erfc} \left(\frac{Rx-ut}{\sqrt{4DRt}} \right)]} \dots\dots\dots (4.14) \\ R = 1 + \frac{\beta(1-\phi)}{\phi} \end{array} \right.$$

4.2.3 Equilibrium Oil Saturation

Equilibrium volume oil saturation, S_{oe} , is defined here as the asymptotic maximum value of oil saturation in the core that would not increase with continuing injection of the same oily water at a constant rate. The equilibrium mass oil saturation, S_{oe_m} , can be determined by multiplying equilibrium volume oil saturation with oil density. It is a function of droplet to pore throat size ratio and capillary number as shown in Equations 4.15 and 4.16, respectively:

$$N_d = \frac{d_o}{d_{pt}} \dots\dots\dots (4.15)$$

$$N_{Ca} = \frac{\mu_w u}{\sigma_{ow}} = \frac{\mu_w q}{A \phi \sigma_{ow}} \dots\dots\dots (4.16)$$

Where, N_d is the droplet to pore throat size ratio (we will call it “size ratio” for short in the following text), dimensionless; d_o is the average oil droplet diameter, μm ; d_{pt} is the

average pore throat diameter, μm ; N_{Ca} is the capillary number - the ratio of viscous to capillary force, dimensionless; μ_w is water viscosity, cp; u is interstitial velocity, m/s; q is injection rate, m^3/s ; A is rock cross section area, m^2 ; ϕ is porosity of the porous media, fraction; σ_{ow} is oil water interfacial tension, dyne/cm.

Oil droplet size distributions are controlled by blender speed and are determined from photomicrographs by a particle counter, and then the average oil droplet size is used in calculation. Pore throat size distributions can be determined either from water drainage curves measured with a simple centrifuge or photomicrographs of rock slice, and similar to oil droplet size, the average pore throat size is used in calculation (Soo and Radke, 1984a). Thus, the statistics of oil droplet and pore throat sizes are already included in their average values. The detailed mechanisms of measuring pore size distributions using capillary pressure curves were described by Mishra and Sharma (1988).

There are many different definitions of the capillary number in the literature. For example, some authors define N_{Ca} using superficial (filtration or Darcy) velocity while others use interstitial velocity to represent the viscous effect. Although these capillary numbers have the same physical meaning, one should be careful to use them as their effective validity regions are different (Hilfer and Øren, 1996). For example, for a core sample with porosity 0.1, the value of “critical” capillary number defined below using superficial velocity is 10^{-5} but the one with interstitial velocity gives 10^{-4} . As capillary number plays an important role in this study, we discuss it further in the following sections.

$$N_{Ca}^* = \frac{\mu_w u_c}{\sigma_{ow}} \dots\dots\dots (4.17)$$

Where u_c is the critical velocity to move the residual oil saturation in the rock, m/s. Currently, there is no widely accepted formula to calculate the equilibrium oil saturation

from oil droplet size (Schmidt, et al., 1984; Soo and Radke, 1984a, b; Rege and Fogler, 1988; Buret, et al., 2010; Romero, et al., 2011). Based on the experimental results and discussions in various publications, we can develop a correlation to estimate the value of equilibrium volume oil saturation.

Most of laboratory experiments have been carried out under low-velocity condition with small value of the capillary number ($N_{Ca} \leq 10^{-4}$) representing the actual field injection scenario. For example, if an injection well with 0.3 ft radius, 20 ft completion length is injecting water at 5000 bpd with 0.5 cp viscosity and 50 dyne/cm oil water interfacial tension to a disposal formation with 0.3 porosity, the capillary number is 8.76×10^{-5} . Experiments conducted within this range of capillary number for different cores and fluids have shown that the equilibrium oil saturation mainly depends on the oil droplet to pore throat size ratio with little effect of velocity (Schmidt, et al., 1984; Soo and Radke, 1984a, b, 1986; Soo, et al., 1986; Buret, et al., 2008, 2010). Using data from these experiments, we make a semi-log plot shown in Figure 4.5. The plot comprises two regions of the relationship between So_e^* (equilibrium oil saturation at low capillary number region) vs. the size ratio: the “interception” capture ($N_d \leq 0.25$) and “straining” capture ($N_d > 0.25$) regions – described above.

In the interception capture region, oil saturation increases fast with the size ratio. This is because, initially, oil droplets move freely in large pores and are preferentially captured in the small size pores. As the injection proceeds, more and more of the small pores become blocked. This blockage leads to a flow diversion toward even larger pores and the rate of small oil droplet capture decreases until an equilibrium saturation is reached and no more capture occurs.

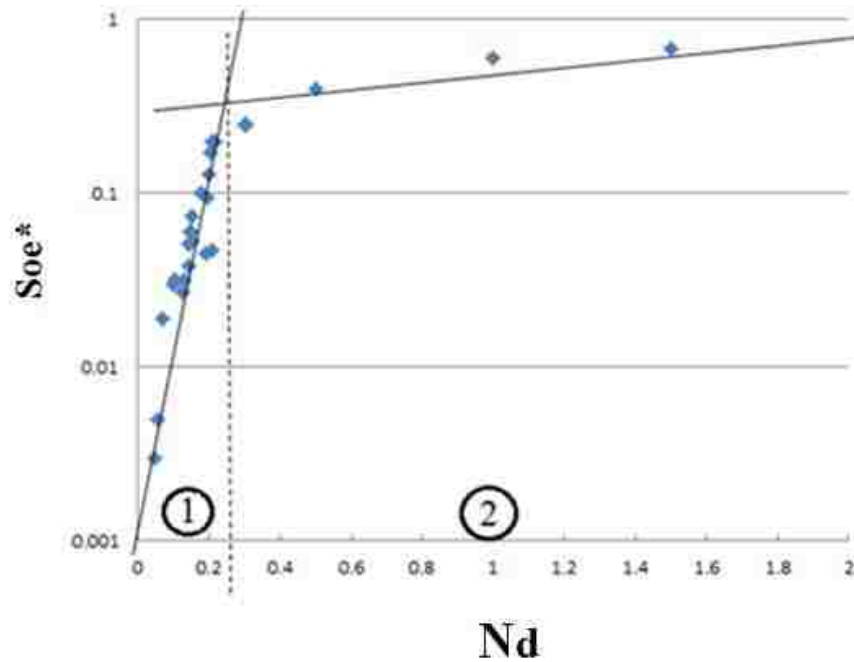


Figure 4.5. Equilibrium oil saturation changes with droplet to pore throat size ratio in low capillary number region

In the straining capture region, equilibrium oil saturation is always high and changes slowly with respect to the size ratio. One explanation is that, the big oil droplets block the pore throats by lodging between sand grains by a single droplet or several droplets bridged together, if the pressure gradient is not enough to overcome the capillary resistance between the grains and droplets, the flow path is plugged and no other droplets can pass it.

When the flow velocity is high (typically $N_{Ca} > 10^{-4}$), equilibrium oil saturation decreases rapidly with respect to capillary number as shown in Figure 4.6 using data from Soo and Radke (1984b). In this region, the viscous force is much greater than the capillary force, which makes the strained droplets squeeze through or break up and pass the pore throats. This phenomenon has been confirmed by other researchers who also suggested exponential decrease of equilibrium oil saturation in this region (Rege and Fogler, 1988; Romero, et al., 2011).

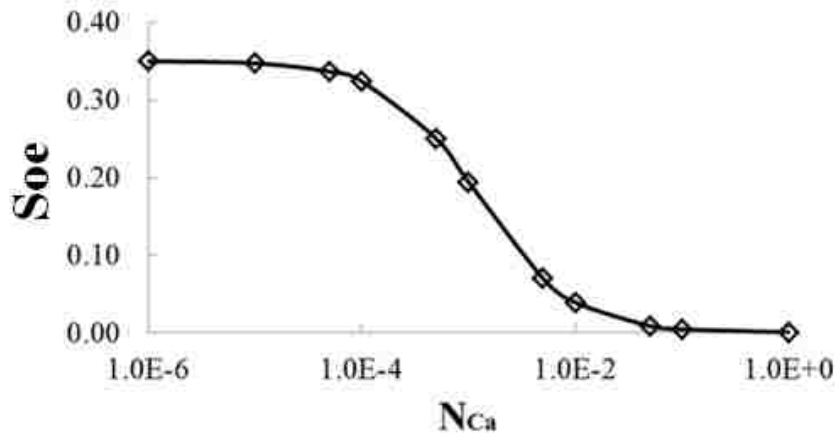


Figure 4.6. Equilibrium oil saturation changes with capillary number

Various correlations have been developed to predict the residual oil saturation based on capillary number for routine core analysis, which is known as capillary desaturation process. Due to physical analogy between residual oil saturation and the equilibrium oil saturation postulated in this study, we use the residual oil saturation correlation to relate the equilibrium oil saturation change to capillary number. Equation 4.18 is such a relationship used in a commercial numerical simulator for $N_{ca} < 1$, to predict residual oil saturation when the “bump rate” test data is not available (Schlumberger, 2007):

$$S_{oe} = S_{oe}^* \left[1 - \exp \left(-\lambda \frac{N_{ca}^*}{N_{ca}} \right) \right] \dots \dots \dots (4.18)$$

Where, S_{oe}^* is the maximum equilibrium volume oil saturation under low capillary number condition, which is determined by routine core analysis, fraction; λ is empirical constant experimentally determined from the bump rate tests, dimensionless; N_{ca}^* is the critical capillary number that the equilibrium oil saturation begins to decrease, dimensionless. Substantially different capillary desaturation curves are obtained for different types of rock in the literature. The shape of the curve depends largely on the pore size distribution in the porous medium and fluids properties (Foster, 1973; Morrow, et al., 1981; Lake, 1989; Sheng,

2011). In most cases, there is no clarity on the values of critical capillary number from laboratory data and it may vary from 10^{-6} to 10^{-4} for different rocks. The precise value needs to be determined experimentally for each rock and fluids combination (Morrow, et al., 1988; Lake, 1989; Hilfer and Øren, 1996; Hirasaki, et al., 2006; Sheng, 2011).

4.2.4 Bump Rate Test for Trapped Oil Mobilization

Usually, the trapped oil mobilization in a core can be determined from a “bump rate” test, which directly shows the oil saturation and water relative permeability change with respect to the capillary number. We use the following example to show the typical “bump rate” test procedure used in the core lab for a core from Entrada Formation with 2.47 cm in diameter and 5.11 cm in length:

1. Cleaning the core and establish initial (or connate) water saturation using a centrifuge in an air-displacing-brine configuration, $S_{wc} = 0.068$;
2. Aging the core sample with crude oil to the initial reservoir conditions;
3. Measuring the effective permeability to oil with corresponding initial water saturation, $k_{oe}^* = 200 \text{ md}$, $k_{ro}^* = 1$;
4. Injecting brine into the sample at $3 \text{ cm}^3/\text{min}$ ($N_{Ca}^* \approx 10^{-5}$) to a 99.95 water-cut, the oil recovery is 69.2% of the original oil-in-place (OOIP);
5. Measuring the residual oil saturation and effective permeability to water correspondingly at the low capillary number, $S_{oe}^* = 0.287$, $k_{we}^* = 41.2 \text{ md}$, $k_{rw}^* = 0.206$;
6. Raising the brine injection rate to the “bump rate” at $6 \text{ cm}^3/\text{min}$ ($N_{Ca}^* \approx 2 * 10^{-5}$) to a 99.95 water-cut, the oil recovery is 76.9% of the OOIP;

7. Measuring the residual oil saturation and effective permeability to water correspondingly at the high capillary number, $S_{oe} = 0.215$, $k_{we} = 73.5 \text{ md}$, $k_{rw} = 0.368$;

When the water injection rate increases from $3 \text{ cm}^3/\text{min}$ to the bump rate, $6 \text{ cm}^3/\text{min}$, more oil (7.7%) is produced and water relative permeability increases significantly, from 0.206 to 0.368 as shown in Figure 4.7. The $S_{oe} = 0.215$ obtained from the bump rate seems to be useful as an increment of oil production is observed. Under high speed centrifuge condition where the viscous force is much greater than the capillary force, the residual oil saturation can be lowered to 0.15 which means the trapped oil is displaced with the increase of capillary number.

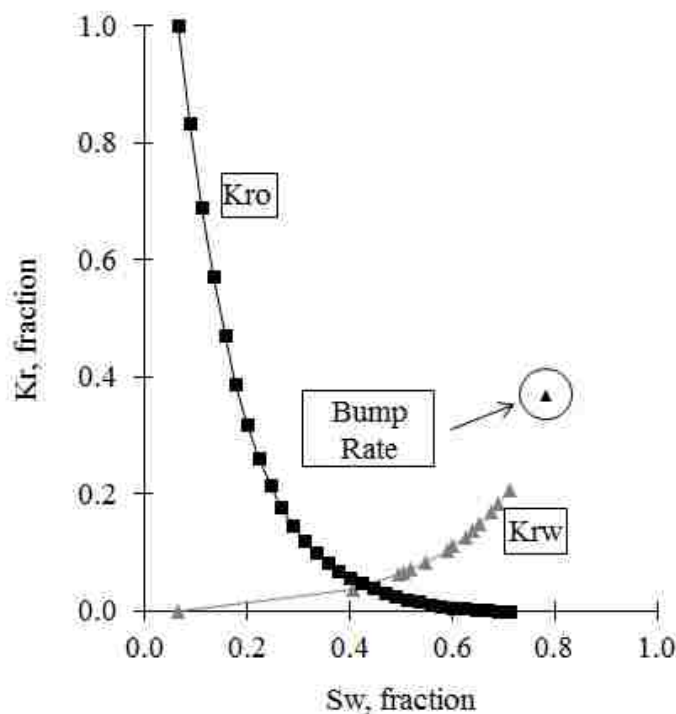


Figure 4.7. Relative permeability curves from “bump rate” test

Based on oil droplet trapping and the equilibrium oil saturation change mechanisms we can divide different oil droplet capture regions for different combinations of capillary

number and size ratio values as shown in Figure 4.8. To find the equilibrium oil saturation in Equation 4.5, we need to know the size ratio to determine S_{oe}^* from Figure 4.5. Then, we use Equations 4.16 and 4.18 to calculate S_{oe} for known injection rate and interstitial velocity.

4.2.5 Injectivity Decline Prediction in Linear Flow

Distributed values of oil saturation with distance can be used to determine the degree of damage to water injectivity caused by the oil content. For two-phase (oil and water) flow through porous media, we can use relative permeability theory to estimate the injectivity decline (Devereux, 1974a, b; Spielman and Su, 1977; Ohen, et al., 1996; Bennion, et al., 1998; Civan, 2007).

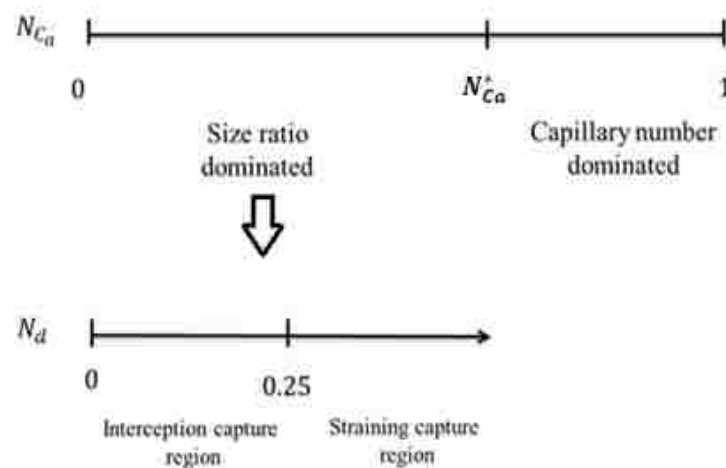


Figure 4.8. Oil droplet capture regions for combinations of capillary number and size ratio

Using the relative permeability concept (Schramm, 1992), the water injectivity in linear flow can be expressed as:

$$I_w = \frac{q_w}{\Delta p} = \frac{10^{-6} K_w A}{\mu_w \Delta L} = \frac{10^{-6} K K_{rw} A}{\mu_w \Delta L} \dots \dots \dots (4.19)$$

Where, I_w is the water injectivity index, m³/s/kpa; q_w is the water injection rate, m³/s; Δp is the pressure drop through the core, kpa; K_w is the effective water permeability, D; K is

the absolute permeability of the core, D; K_{rw} is the relative permeability to water, fraction; A is the cross section area of the core, m^2 ; ΔL is the length of the core, m. As only K_{rw} changes during the injection process, the water injectivity decline as a function of time can be calculated from Equation 4.20 (Saripalli, et al., 2000):

$$I_D = \frac{I_{w,t}}{I_{w,0}} = \frac{K_{w,t}}{K_{w,0}} = \frac{K_{rw,t}}{K_{rw,0}} \dots\dots\dots(4.20)$$

Where, I_D is the dimensionless injectivity decline index, and subscripts 0 and t denote initial and instant values, respectively. Relative permeability values can be obtained in various ways. If core data is not available, Corey's function might approximate the relative permeability to water at different oil saturations (Brooks and Corey, 1966) as:

$$K_{rw} = K_{rw}^* \left(\frac{1-S_o-S_{wc}}{1-S_{wc}-S_{or}} \right)^{n_w} \dots\dots\dots(4.21)$$

Where, K_{rw}^* is the water relative permeability at residual oil saturation, fraction; S_{wc} is the connate water saturation, fraction; S_{or} is the residual oil saturation, fraction; n_w is the exponent for water relative permeability, dimensionless.

For injection of oily water injecting to an aquifer, $K_{rw}^* \equiv 1$ and $S_{or} \equiv 0$, so the water relative permeability becomes:

$$K_{rw} = \left(\frac{1-S_o-S_{wc}}{1-S_{wc}} \right)^{n_w} \dots\dots\dots(4.22)$$

Equation 4.22 is valid for $0 \leq S_o \leq S_{oe}$. As shown in Figure 4.9, the effect of oil capture on injecting damage changes considerably for different rock and fluid properties. Oil would not flow for oil saturation below equilibrium oil saturation, S_{oe} . Since the S_{oe} value depends on flow velocity, it could be much smaller than the typical value of residual oil saturation from standard core testing (Brooks and Corey, 1966; Ramakrishnan and Wasan, 1984; Huang, et al., 1997). Moreover, water injectivity would decline at different rates

(exponent n_w) in different formations. Usually n_w has smaller value in oil wet rock than that in water wet rock (Schramm, 1992). It follows that, water injectivity would decline slower in oil wet aquifers that are not very common. If core testing data is available, the water drainage relative permeability curve should be used, as the oil droplets invasion process is a water drainage process (Huang, et al., 1997).

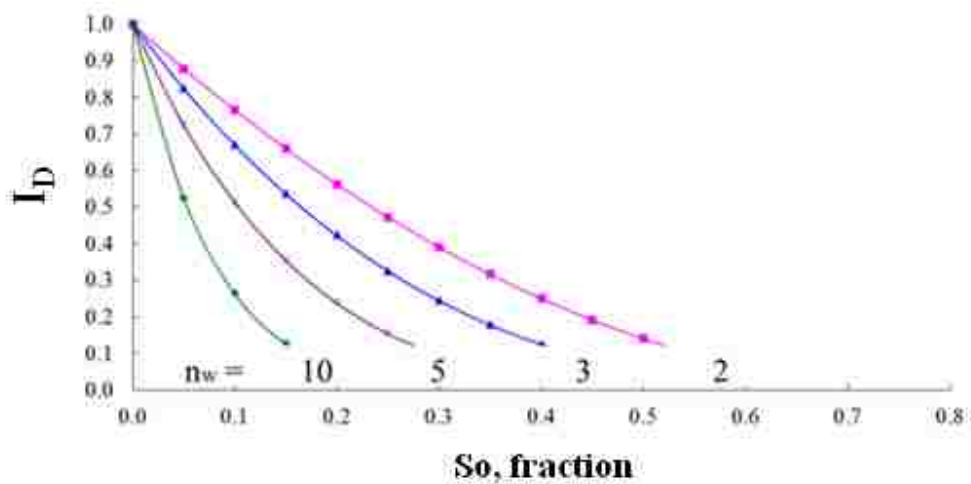


Figure 4.9. Shape of water injectivity decline curves

4.2.6 Results and Discussion

From the mathematical model derived above, we are able to predict the change of oil concentration in the water, oil saturation in the pore space and water permeability with time and distance during the injection process. In the following sections, we use published data to verify the model's prediction of these three parameters. If the model is valid for all of them, then we can use it to predict the phenomena that are difficult to measure experimentally, such as oil concentration in the water at a certain location of the core, oil saturation distribution profile in the core during the injection process.

Oil Concentration Change with Time and Distance

Table 4.1 shows the experimental data reported from injection experiments and parameters used to match the effluent oil concentration. Soo and Radke (1984a) carried out experiments using Ottawa sand packs to investigate the emulsion flow behavior in porous media. They kept the oil concentration in the injection water at 5000 ppm while changing droplet size to evaluate the effect of size ratio on permeability decline. They measured the effluent oil concentration as shown in Figure 4.10. It is clear that, the size ratio plays an important role when the emulsion flows through the sand pack. Higher size ratio delays the oil breakthrough time which indicates that big oil droplets are more captured in the rock than the small ones. Buret, et al., (2010) confirmed this phenomenon by varying both size ratio and inflow oil concentration as shown in Figure 4.11. Again, the model matches the results very well for different cases.

Table 4.1. Experimental runs for effluent concentration measurement

Parameter	Soo and Radke, 1984a			Buret, et al., 2010		Unit
	Case 1	Case 2	Case 3	Case 1	Case 2	
Core	Ottawa sand pack	Ottawa sand pack	Ottawa sand pack	SiC pack	SiC pack	
Core length (L)	0.05	0.05	0.05	0.1	0.1	m
Core diameter (d)	0.025	0.025	0.025	0.0152	0.0152	m
Porosity (ϕ)	0.34	0.34	0.34	0.4	0.45	<i>fraction</i>
Flow velocity (u)	$4 \cdot 10^{-5}$	$4 \cdot 10^{-5}$	$4 \cdot 10^{-5}$	$3.77 \cdot 10^{-5}$	$3.77 \cdot 10^{-5}$	m/s
Size ratio (N_d)	0.071	0.105	0.152	0.02	0.1	<i>dimensionless</i>
Oil concentration (c_o)	5000	5000	5000	82	129	ppm
Dispersive coefficient (D)	$1.0 \cdot 10^{-6}$	$2.0 \cdot 10^{-7}$	$1.5 \cdot 10^{-7}$	$5.0 \cdot 10^{-7}$	$3 \cdot 10^{-7}$	m^2/s
Adsorptive constant (β)	1.3	3	7	100	400	<i>dimensionless</i>

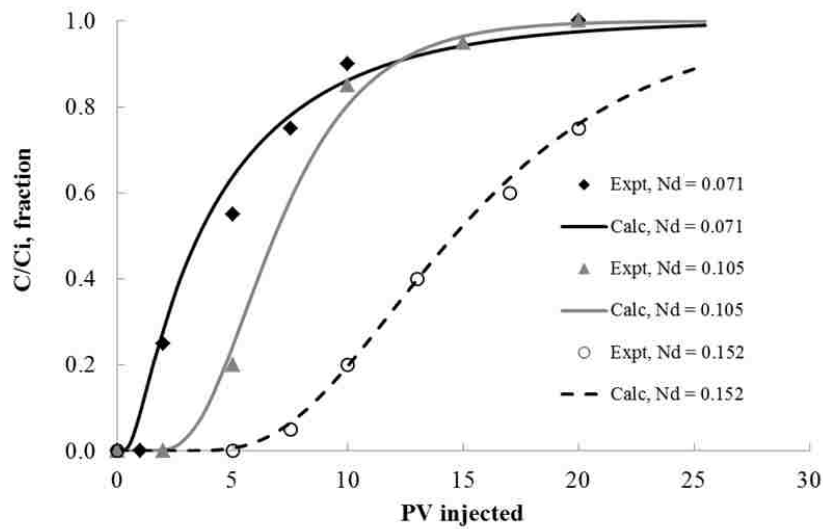


Figure 4.10. Comparison of calculated and measured effluent oil concentration for Soo and Radke experiments for different size ratios (1984a)

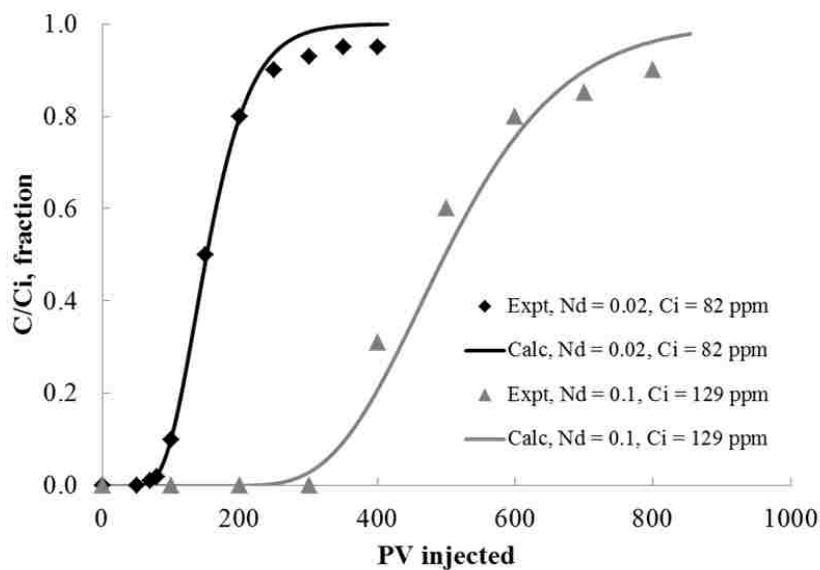


Figure 4.11. Comparison of calculated and measured effluent oil concentration for various size ratio and influent oil concentrations for Buret, et al., experiments (2010)

Only the effluent oil concentration change with time was measured in the experiments. It was difficult to determine spatial distribution of oil concentration in water throughout the core, so no concentration distribution was reported in the references. However, using the model, it is possible to find oil concentration and saturation change with location in the rock.

Calculated spatial distribution of oil concentration in water at any time is shown in Figure 4.12 and Figure 4.13. The fast decrease of oil concentration with distance shown in the figures indicates that significant amount of oil is retained in the rock when the oily water flows through it, which is to be discussed in the next section.

Oil Saturation Change with Time and Distance

Oil saturation development and distribution in the rock sample are the key factors to understand injectivity impairment process during oily water injection (Devereux, 1974a, b; Spielman and Su, 1977; Schramm, 1992; Ohen, et al., 1996; Bennion, et al., 1998; Civan, 2007). However, similar to the oil concentration in water, no oil saturation change along the core samples have been reported from oily water injection experiments. Using the model developed in this study, we are able to predict oil saturation distribution profile in the core at any location and time as shown in Figure 4.14 and Figure 4.15, respectively. From the figures, it is clear that oil captured in the rock reduces with distance from the rock face. The trend clearly corresponds to the predicted oil concentration change with distance in Figure 4.12 and Figure 4.13. However, all these predictions are merely theoretical and require some verification.

As there was no experimental data available for the oil saturation distribution in the core, we build a one-dimensional simulation model using the commercial reservoir simulator STARS of CMG[®], to verify and visually observe the dilute oily water flowing through the core. We used Buret, et al.'s data and built the model as shown in Figure 4.16. In the model, each grid has length of 0.5 cm in horizontal direction, 0.27 cm in vertical direction with 1.345 cm width. Initial oil saturation in the core was set equal to zero and the oily water was injected from left to right. Figure 4.17 shows advancement of the oil front with saturation

distribution matching that in Figure 4.15. The distribution shows expansion of the maximum-damage zone ($S_o = S_{oe}$) proceeded with a relatively short frontal zone (from x_1 to x_2) with oil saturation dropping from S_{oe} to zero.

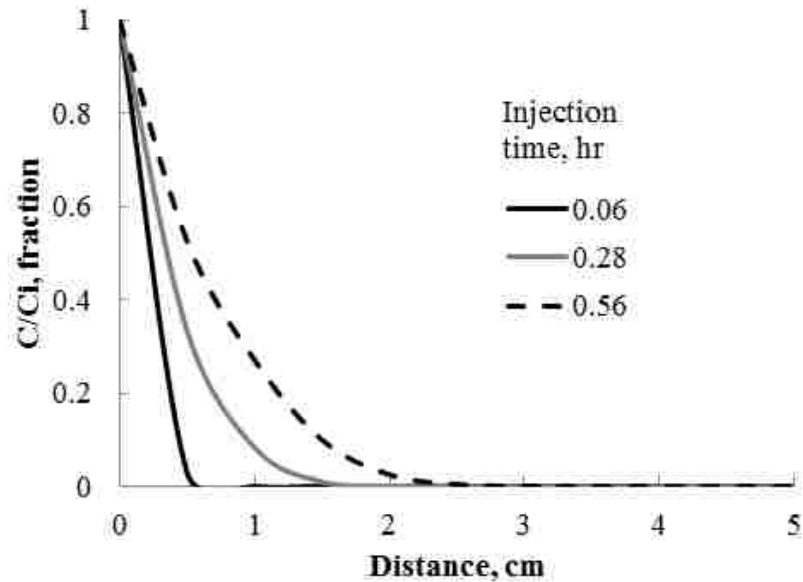


Figure 4.12. Predicted oil concentration vs. distance after matching Soo and Radke experiments (1984a)

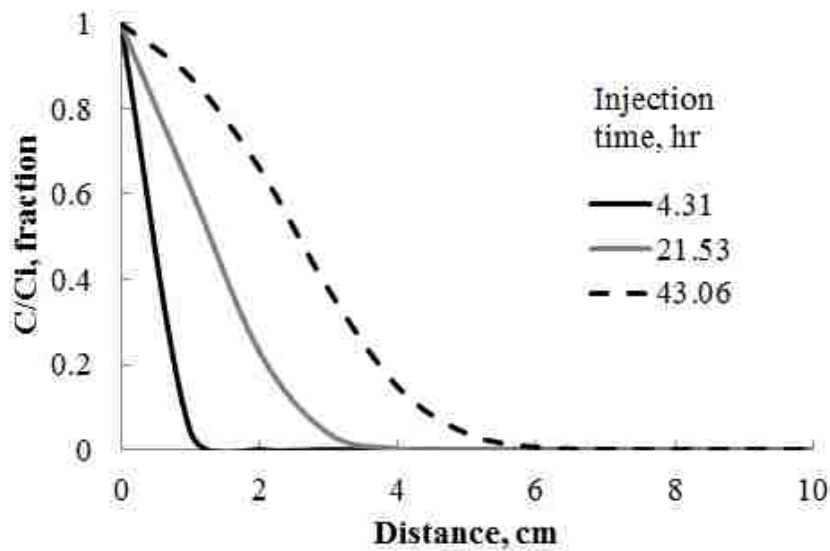


Figure 4.13. Predicted oil concentration vs. distance after matching Buret, et al., experiments (2010)

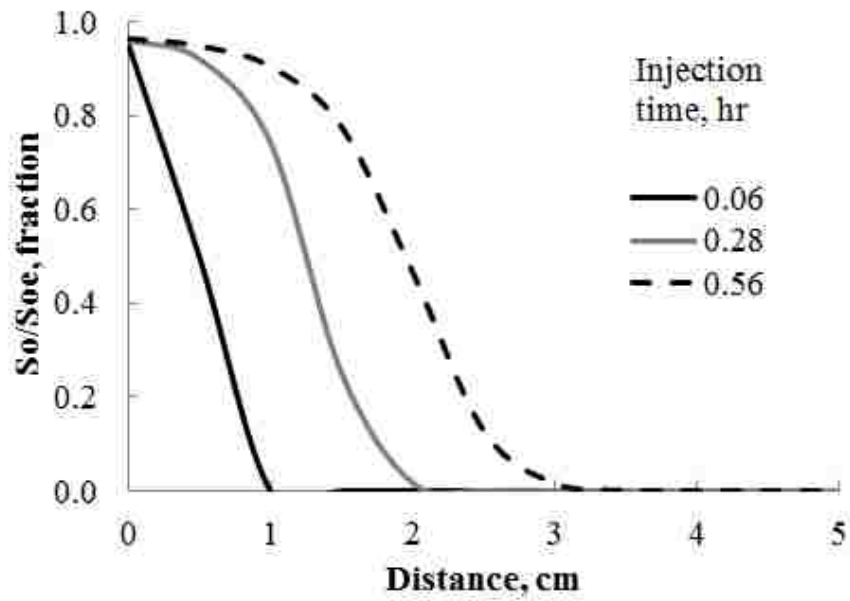


Figure 4.14. Predicted distribution of oil saturation in the core at different times after matching Soo and Radke experiments (1984a)

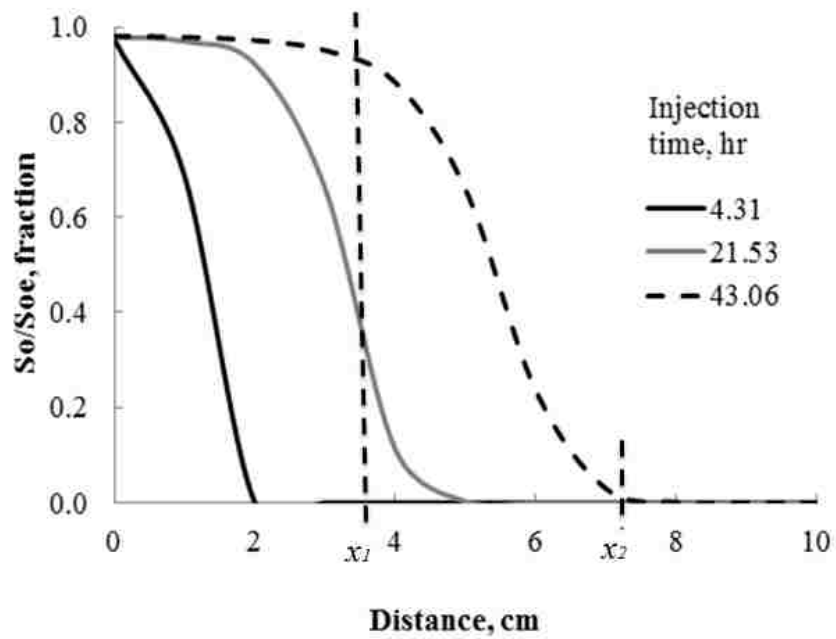


Figure 4.15. Predicted distribution of oil saturation in the core at different times after matching Buret, et al. experiments (2010)

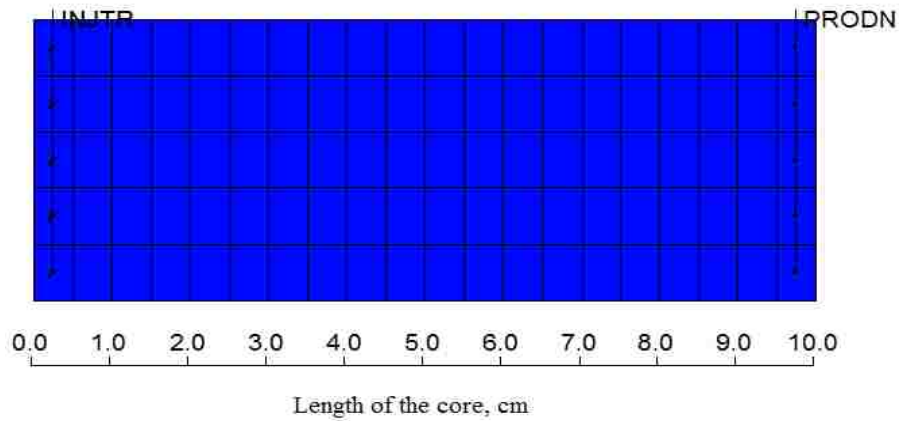


Figure 4.16. Cross-section view of simulation model for oily water injection to a core

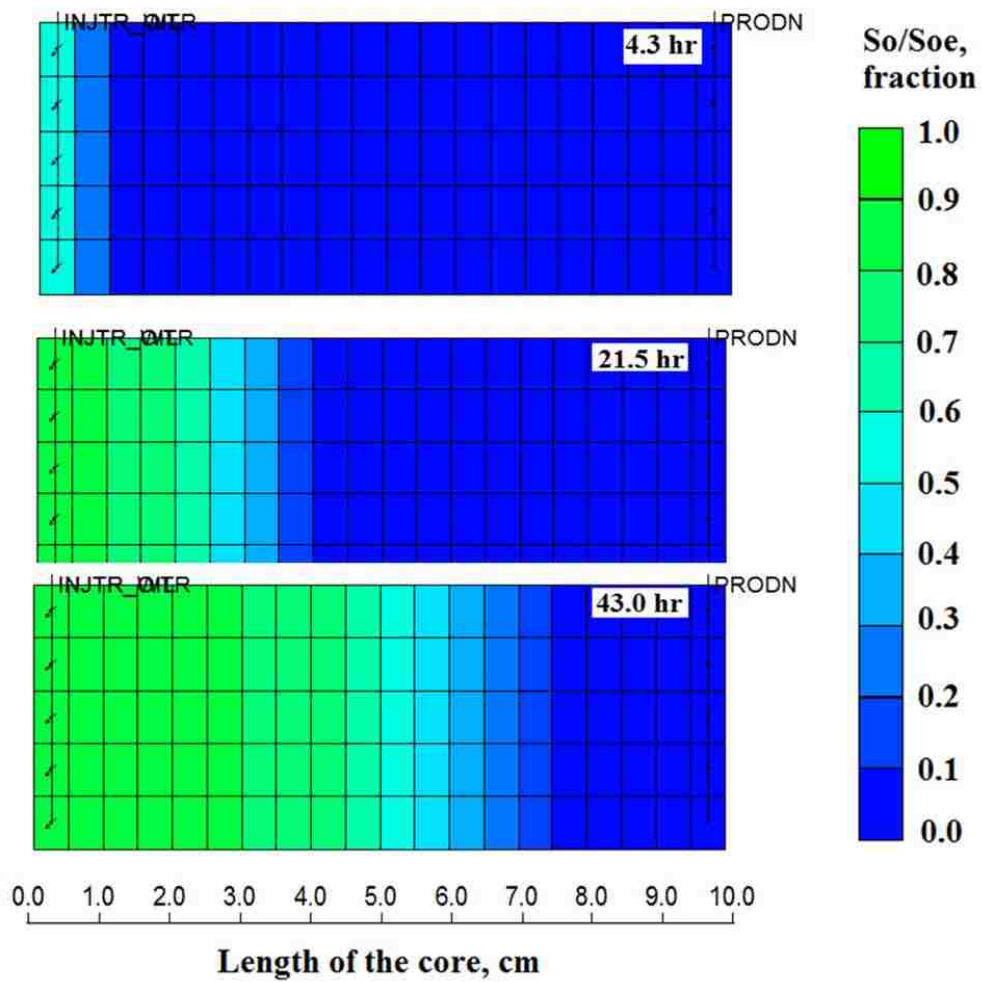


Figure 4.17. Simulated advancement of oil front during oily water injection in Buret, et al. experiments (2010)

Water Permeability Damage

In core flooding experiments, the expanding oil saturation might be expressed as distributed permeability damage in the core (Soo and Radke, 1984b; Soo, et al., 1986; Zhang, et al., 1993; Ohen, et al., 1996; Buret, et al., 2010). The conversion is made using the fractional flow concept and the relative permeability relationship. For the oil front zone, the average oil saturation is:

$$S_{o_avg} = \frac{\int_{x_1}^{x_2} S_o(x) dx}{\Delta x} \dots\dots\dots(4.23)$$

Where, $\Delta x = x_2 - x_1$, is the size of oil front zone, m; S_{o_avg} is the average oil saturation in the zone, fraction; and $S_o(x)$ is the function of oil saturation distribution. By considering relative permeability relationship, $K_{rw} = \varphi(S_o)$, similar to Equation 4.22, we can compute average relative permeability of the oil advancement front (from x_1 to x_2) as:

$$K_{rw_avg} = \frac{\Delta x}{\int_{x_1}^{x_2} \frac{dx}{K_{rw}(x)}} \dots\dots\dots(4.24)$$

Where,

$$K_{rw}(x) = \varphi[S_o(x)] \dots\dots\dots(4.25)$$

For the core injection experiments we may have discrete measurements of pressure drop over the length of the core as shown in Figure 4.18. In such case, we may compute a series of permeabilities in the core sections as:

$$K_{wi} = \frac{10^6 q \mu_w L_i}{A \Delta p_i} \dots\dots\dots(4.26)$$

Or the average permeability as:

$$K_{w_avg} = \frac{10^6 q \mu_w L_t}{A \sum_{i=1}^n \Delta p_i} \dots\dots\dots(4.27)$$

Where, L_i is the length of each section, m; L_t is the total length of the core, m; A is the cross-section area of the core, m²; q is the flow rate through the core, m³/s; Δp_i is the

pressure drop in a subsection, kpa; K_{wi} is the water permeability of a subsection, D; K_{w_avg} is the average water permeability over the core section, D; i is the subsection number and n the total subsection number over the core. The above equations show that a thin section with small permeability could significantly reduce the average core permeability.

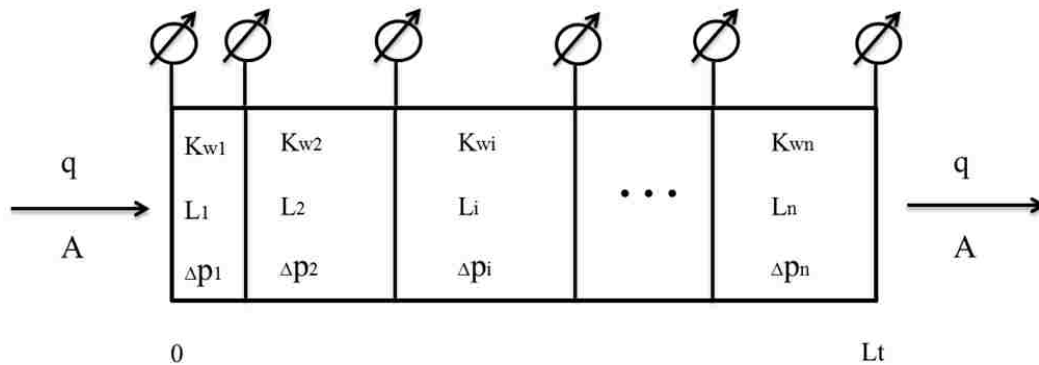


Figure 4.18. Local and average water permeability over a core

In order to use the theoretical model and verify results from the published core floods, some input data must be inferred from the results. Typically, relative permeability data are not reported from experiments and it can be estimated using the core permeability and oil saturation data. This approach becomes also useful for reducing the number of experiments as we only need to carry out part of the experimental work to get several data points and predict the whole set of injectivity curves based on these data.

Generally, for a given rock and fluid, the dispersion coefficient value, D , is small and could be treated as a constant in some cases, especially when the flow is in low capillary number region. Adsorption coefficients, α or β increase with size ratio and oil concentration as oil droplets have higher probability to be captured, and it decreases with capillary number as oil droplets may deform and squeeze through the pore throats when the viscous force is high, also they have less time to contact to a rock section and its probability to be captured

becomes lower (Coats and Smith, 1964; Gupta and Greenkorn, 1974; Rege and Fogler, 1988).

Figure 4.19 shows the water injectivity reduction in different sections of the core measured and calculated with the model. For the model input, we used values of model constants from Table 4.1 and the fractional flow function shown in the following equation for Case 1 reported by Buret, et al. (2010):

$$K_w(S_o) = 2490(1 - S_o)^{12.5} \dots\dots\dots(4.28)$$

Where, $K_{rw}^* = 1$, $S_{wc} = 0$, $S_{or} = 0$ as the sand pack is made with clean S_iC without connate water and residual oil.

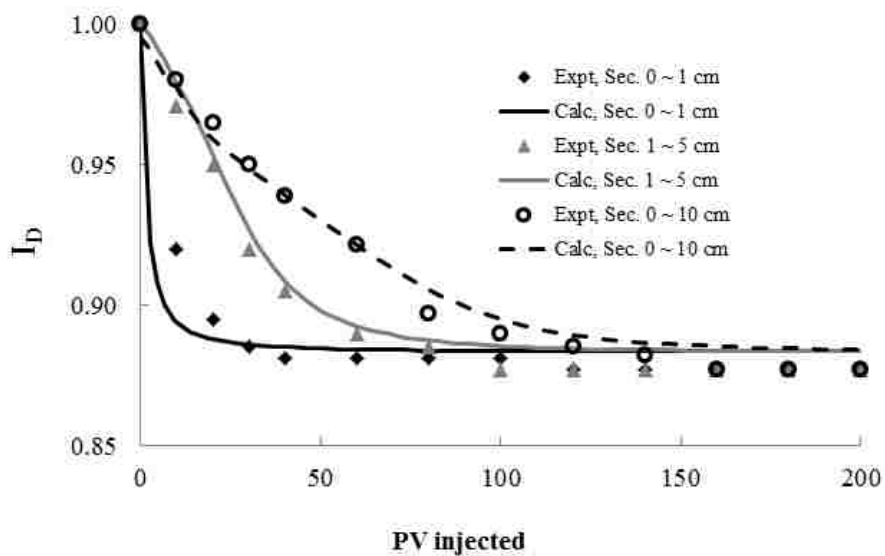


Figure 4.19. Calculated and measured water injectivity damage in different core sections – data from Buret, et al. (2010)

Since the fractional flow relationship was not reported, we estimate it by the following steps:

First, we used the model to fit the reported values of oil concentration change vs. time at the core exit to find parameters D and β ;

Next, we predicted the oil concentration change vs. time for each section of the core;

Then, we inferred the fractional flow relationship using the reported K_w and calculated S_o change in the first section of the core at different times. The adsorptive coefficient (α) and exponent for water relative permeability (n_w) could be determined;

Finally, we used the fractional flow relationship to predict the K_w change in other sections based on the previously computed D , β , α and n_w , and verified the predictions with reported data.

A very good match indicates the validation of the model. From the figure we can see that, even for the small size ratio (0.02) and oil concentration (82 ppm), there is still about 13% permeability loss of the core. The most severe damage happens in the first section (0~1 cm) of the core at the beginning of injection. However, if the injection continues, the whole core will be damaged. This observation confirms the situation discussed in Figure 4.15 and Figure 4.17. If the core flooding does not last long enough to reach the final equilibrium condition, then the first section will be found damaged severely while the other sections are less or no damage as shown in Figure 4.20, which was also experimentally confirmed by other researchers (Zhang, et al., 1993; Ohen, et al., 1996). This effect is more obvious for higher size ratio as shown in Figure 4.21. The water permeability in the first section reduces to 0.2 and 0.1 of the original value when oily water with size ratio at 1 and 1.67 is injected, respectively (Buret, et al., 2010).

Figure 4.22 clearly shows the effect of size ratio on injectivity decline for the same core: size ratio at 0.071 causes about 20% injectivity decline while 0.152 size ratio makes the core lose 75% of its water permeability. It also indicates that higher oil concentration gives sooner equilibrium: 5000 ppm oily water injection only needs 20 pore volumes while

hundreds to thousands of PV needed for low oil concentration from 100 to 500 ppm (Zhang, et al., 1993).

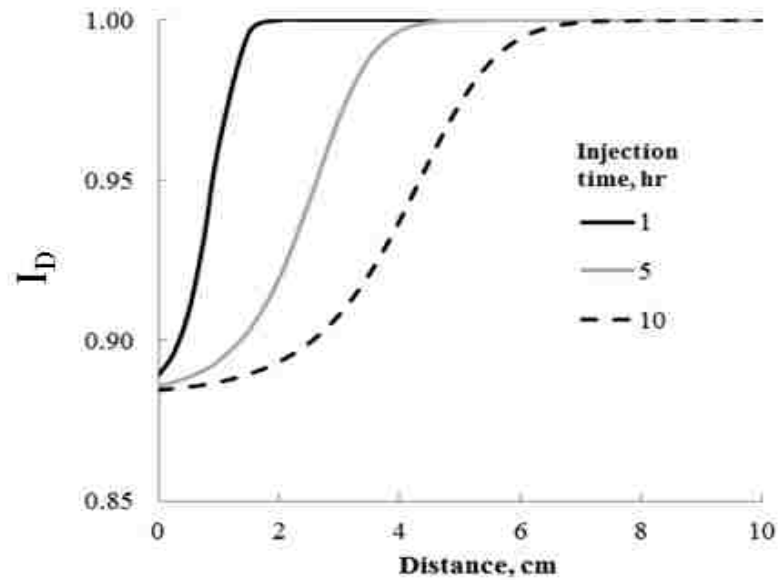


Figure 4.20. Calculated spatial distribution of water injectivity damage in core at different time – data from Buret, et al. (2010)

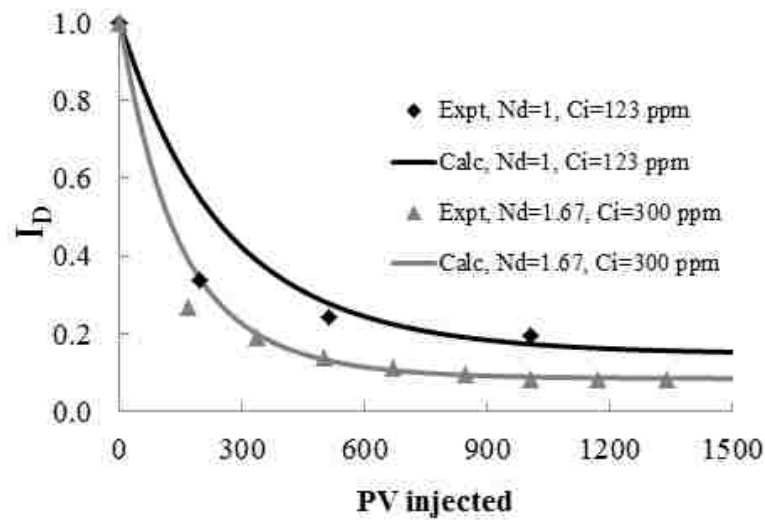


Figure 4.21. Calculated and measured water injectivity reduction in first (1 cm) section of core – data from Buret, et al. (2010)

Notice that, the size ratios in Figure 4.22 are quite small, from 0.071 to 0.152, but the water permeability is reduced faster than other cases. The reason might be that the core used

in Figure 4.22 is highly water wet, as we use higher value of n_w ($= 15$) to match the results, which indicates the core is strong water wet while other cores likely to be neutral or slightly oil wet. This indicates that oil wet formations are better candidates to carry out water injection than water wet ones, which has been confirmed by both the laboratory research and field tests (Wang, et al., 2010; Ju, et al., 2012).

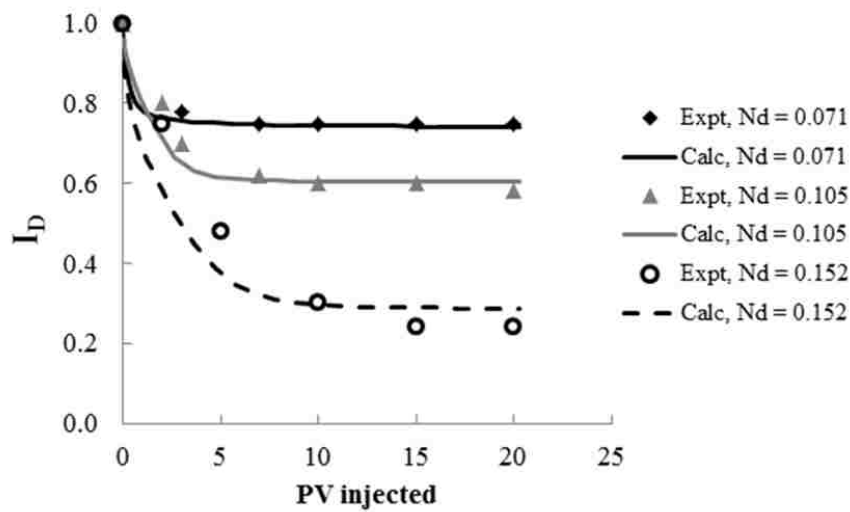


Figure 4.22. Size ratio effect on water injectivity reduction from model and experiments with constant oil concentration – data from Soo and Radke (1984a)

Most of the publications in oily water injection area address the flow in the low capillary number region, where velocity effect is small. However, the effect of velocity could not be ignored for water flow at high capillary number where viscous force effects becomes significant as shown in Figure 4.23(A) (Soo and Radke, 1984b; Rege and Fogler, 1988; Romero, et al., 2011). However, the full set of experimental data including basic core parameters is not available in the references and the velocity effect is just simply mentioned. Thus, we are unable to quantitatively match the model to the experimental results as we do for the low capillary number region. We only compare our results qualitatively with similar work done by Soo and Radke in 1984 as shown in Figure 4.23(B), where 10,000 ppm oily

water with size ratio 1.5 was injected to a core at capillary number from 10^{-5} to 10^{-2} . The model's output confirms the injectivity damage for capillary number greater than 10^{-4} , while there is almost no damage when the N_{Ca} value approaches 10^{-2} . Thus, qualitatively, the model correctly simulates the physical effect observed in experiments.

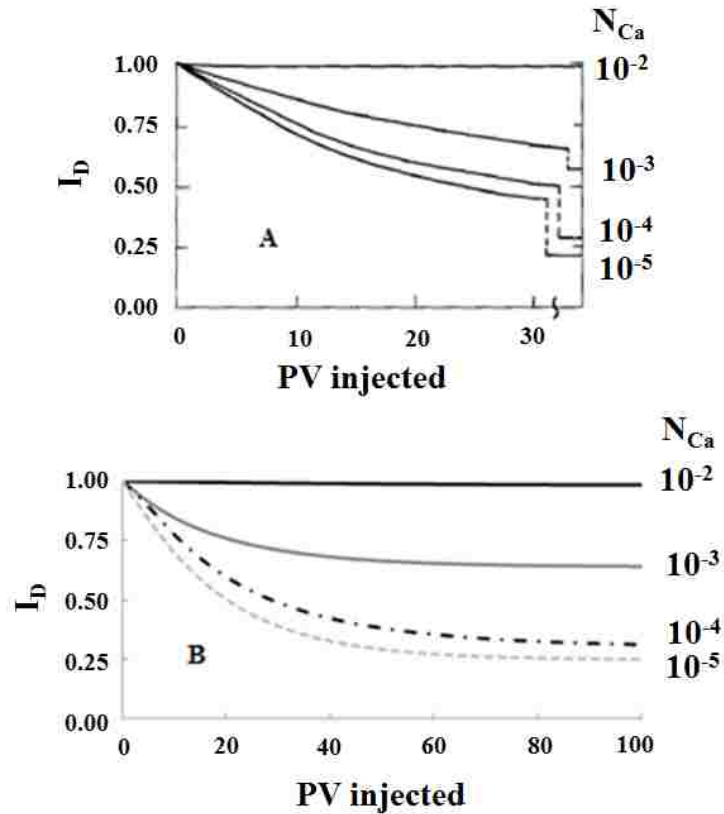


Figure 4.23. Effect of capillary number on water injectivity decline: (A) Soo and Radke, 1984b; (B) Model predictions

In the model, we consider the N_{Ca} effect by including it in S_{oe} as shown in Equation 4.18. S_{oe} decreases rapidly with N_{Ca} at high capillary number region as shown in Figure 4.6 (Soo and Radke, 1984b). From the relative permeability relationship shown in Equation 4.21, it is clear that low equilibrium oil saturation gives high water relative permeability, which means small water injectivity damage.

4.3 Injectivity Damage in Radial Flow

For real injection wells, water flows radially out from well to aquifer for homogeneous systems where the interstitial velocity changes with time. Currently, most models for two phase formation damage in radial geometry are very complex and need to be solved numerically (Civan, 2007; Idowu, 2009). Thus, the purpose of this section is to develop analytical models which can be used to predict the oil saturation advancement and induced formation damage, as well as estimate the injection pressure increase during oily water injection process in radial geometry.

4.3.1 Radial ADA Model of Well's Injectivity Decline

Although the flow geometries are different in linear and radial flows, the formation damage mechanisms caused by oil droplets are the same: straining, where oil droplets clog the pore throats, and interception - with droplets captured by van der Waals colloidal forces etc. (Soo and Radke, 1984a, b, 1986; Soo, et al., 1986). Thus, the principle of mass transfer between the liquid globule and the solid matrix is also valid to radial flow, and the advection-dispersion-adsorption (ADA) methodology could be applied to model the injectivity decline in radial geometry.

Using the same assumptions as linear flow, the oil transport to the porous media in cylindrical coordinate shown in Figure 4.24, can be expressed as:

$$\text{Advective mass flux rate} = \frac{\partial}{\partial r} (C u_r \Delta \theta \Delta z \phi) \Delta r$$

$$\text{Dispersive mass flux rate (Fick's Law)} = - \frac{\partial}{\partial r} \left(D_r \frac{\partial C}{\partial r} \Delta \theta \Delta z \phi \right) \Delta r$$

$$\text{Rate of capturing by adsorption (Langmuir Adsorption): } \frac{\partial S_{o,m}}{\partial t} = \alpha \left(1 - \frac{S_{o,m}}{S_{oe,m}} \right) C$$

Where, u_r is the interstitial water velocity in r direction, m/s; $\Delta\theta, \Delta z, \Delta r$ are the arc length, height and radius of the controlled volume as shown in Figure 4.24, respectively, m; D_r is the overall dispersive coefficient which represents the strength of dispersion in the porous media, m^2/s .

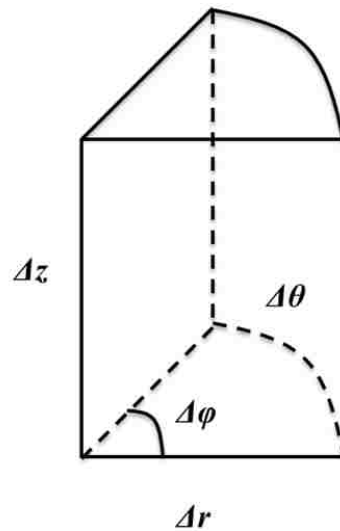


Figure 4.24. Control volume in cylindrical coordinate

Bear (1972) suggested that dispersion is the macroscopic outcome of the actual movement of an individual oil droplet through the pores where various physical and chemical phenomena take place. According to Lake (1989), dispersion is the mixing of oil and water caused by diffusion, local velocity gradients and mechanical mixing in pore bodies. The dispersive coefficient stands for how fast the oil mixes with water: the larger the coefficient, the faster the mixing, and it could be expressed as a function of velocity: $D_r = d u_r$ where d is a constant referred as dispersivity, which is a measure of heterogeneity of the porous media, m (Van Genuchten and Wierenga, 1986; Arya, et al., 1988; Tang and Peaceman, 1987; Duan, 2009). In linear flow, the dispersive coefficient is a constant because the velocity does not change with time and distance. However, in radial flow, it decreases with injection distance

following the reduction of velocity. As pointed out by Saxena (1990), the local dispersion plays a relative unimportant role comparing to the advection effect in the transport of contaminants in aquifers, which will be discussed in detail later.

As there is no oil generated or disappeared in the injection process, the mass balance equation for oil phase can be expressed as:

$$\frac{\partial C}{\partial t} \Delta r \Delta \theta \Delta z \phi + \frac{\partial S_{o,m}}{\partial t} (1 - \phi) \Delta r \Delta \theta \Delta z = \frac{\partial}{\partial r} \left(\frac{\partial C}{\partial r} du_r \Delta \theta \Delta z \phi \right) \Delta r - \frac{\partial}{\partial r} (C u_r \Delta \theta \Delta z \phi) \Delta r \dots\dots\dots(4.29)$$

As $u_r \Delta \theta$ is constant in the flow direction, thus, Equation 4.29 can be rearranged as:

$$\frac{\partial C}{\partial t} \Delta r \Delta \theta \Delta z \phi + \frac{\partial S_{o,m}}{\partial t} (1 - \phi) \Delta r \Delta \theta \Delta z = du_r \Delta \theta \Delta r \Delta z \phi \frac{\partial^2 C}{\partial r^2} - u_r \Delta \theta \Delta r \Delta z \phi \frac{\partial C}{\partial r} \dots\dots\dots(4.30)$$

Dividing $\Delta r \Delta \theta \Delta z \phi$ in both sides of Equation 4.30, the material balance equation becomes:

$$du_r \frac{\partial^2 C}{\partial r^2} - u_r \frac{\partial C}{\partial r} = \frac{\partial C}{\partial t} + \frac{(1-\phi)}{\phi} \frac{\partial S_{o,m}}{\partial t} \dots\dots\dots(4.31)$$

Notice that, the form of material balance equation in radial flow is very similar to that in linear flow - Equation 4.4. Thus, to solve Equation 4.31, $\frac{\partial S_{o,m}}{\partial t}$ should be transformed to an expression of $\frac{\partial C}{\partial t}$ first. Apply Equations 4.5 through 4.8 to $\frac{\partial S_{o,m}}{\partial t}$, Equation 4.31 could be expressed as:

$$du_r \frac{\partial^2 C}{\partial r^2} - u_r \frac{\partial C}{\partial r} = \frac{\partial C}{\partial t} + \frac{\beta(1-\phi)}{\phi} \frac{\partial C}{\partial t} \dots\dots\dots(4.32)$$

Rearrange Equation 4.32 and assuming the aquifer is fully penetrated (for the purpose of derivation simplification, the partial penetration effect will be included in the injectivity decline model later), we can simplify the governing equation as:

$$\frac{\partial C}{\partial t} + v \frac{\partial C}{\partial r} = dv \frac{\partial^2 C}{\partial r^2} \dots\dots\dots (4.33)$$

$$v = \frac{q}{2\pi h_w \phi R r} \dots\dots\dots (4.34)$$

$$R = 1 + \frac{\beta(1-\phi)}{\phi} \dots\dots\dots (4.35)$$

Where, q is the flow rate, m^3/s ; h_w is the aquifer thickness, m ; v is the interstitial velocity with retention factor, m/s ; R is the retention factor, dimensionless; When there is no adsorption, i.e. $R = 1$, Equation 4.33 becomes advective-dispersive equation which is described by Hoopes and Harleman (1967) and Kwok, et al. (1995).

Similar to linear flow, the following initial and boundary conditions can be used to solve Equation 4.33:

Initial condition, there is no oil in the aquifer before injection:

$$S_{o_m} = C = 0 \quad \text{at } t = 0, r > r_w \dots\dots\dots (4.36)$$

Inner boundary condition, oil concentration is constant in the injection water before entering the aquifer:

$$C = C_0 \quad \text{at } t > 0, r = r_w \dots\dots\dots (4.37)$$

Outer boundary condition, there is no oil in the aquifer at infinite length:

$$S_{o_m} = C = 0 \quad \text{at } t > 0, r \rightarrow \infty \dots\dots\dots (4.38)$$

Unlike linear flow, the flow velocity in radial flow changes with distance, which makes it difficult to get the exact solution of Equation 4.33 (Bear, 1972). However, an approximate solution can be derived based on the assumption that the effect of dispersion, expressed by the right-hand side term of Equation 4.33, is small comparing to the local advective effect as the fluids move away from the well (Hoopes and Harleman, 1967; Tang and Babu, 1979). Thus, the product of dispersion and rapidly reducing velocity is small so

the right hand side term in Equation 4.33 can be ignored. The assumption leads to the following approximation:

$$\frac{\partial C}{\partial t} \approx -v \frac{\partial C}{\partial r} \dots\dots\dots(4.39)$$

Physically, the assumption presents the invasion of injected oily water as a frontal displacement process with minimum mixing in the direction of flow (Schmidt, et al., 1984; Saxena, 1990). Devereux (1974) proposed that oil droplets travel as a shock front in the core with equilibrium oil saturation behind during oily water injection, which was experimentally confirmed by Schmidt, et al. (1984) later, especially when the core is long. Schmidt, et al. (1984) found that the larger oil droplets travel several hundred microns before they are captured while the smaller ones travel a few centimeters before being caught. They also concluded that most of the droplet capture occurs at the saturation front and the assumption of instantaneously droplet capture is valid in modeling.

Although the dispersion effect is neglectable small, it still can be accounted by the following transformation to make the solution smoother (Bear, 1972, pp. 635~638):

$$\frac{\partial^2 C}{\partial r^2} = \frac{\partial}{\partial r} \left(\frac{\partial C}{\partial r} \right) = \frac{\partial}{\partial r} \left(-\frac{1}{v} \frac{\partial C}{\partial t} \right) = -\frac{1}{v} \frac{\partial}{\partial t} \left(-\frac{1}{v} \frac{\partial C}{\partial t} \right) = \frac{1}{v^2} \frac{\partial^2 C}{\partial t^2} \dots\dots\dots(4.40)$$

Substitute Equations 4.40 into 4.33, the governing equation becomes:

$$\frac{\partial C}{\partial t} + v \frac{\partial C}{\partial r} = \frac{d}{v} \frac{\partial^2 C}{\partial t^2} \dots\dots\dots(4.41)$$

The resultant approximate solution, shown in section B.1 of Appendix B, is:

$$C = \frac{C_0 \operatorname{erfc} \left(\frac{r^2 - \frac{qt}{2\pi h_w \Phi R}}{\sqrt{\frac{4}{3} dr^3}} \right)}{\operatorname{erfc} \left(\frac{r_w^2 - \frac{qt}{2\pi h_w \Phi R}}{\sqrt{\frac{4}{3} dr_w^3}} \right)} \dots\dots\dots(4.42)$$

Hoopes and Harleman (1967) carried out extensive laboratory experiments in a sand box model of 180° sector to verify the validation of approximate solution shown in Equation 4.42. Based on the results, they concluded that the approximate solution could be used to predict the concentration development in radial flow. They also found that, the difference between analytical and numerical solutions caused by the approximation diminished for distances larger than 20 droplet diameters from the well. Practically, such a small difference could be ignored in field practice.

Substitute Equation 4.42 into Equation 4.6 and divide by the oil density, the oil volume saturation in the pore space can be expressed in Equation 4.43:

$$S_o = \frac{\alpha S_{oe} m C_0 \operatorname{erfc}\left(\frac{r^2 - \frac{qt}{2\pi h_W \phi R}}{\sqrt{\frac{4}{3} dr^3}}\right)}{\rho_o \left[\operatorname{erfc}\left(\frac{r_w^2 - \frac{qt}{2\pi h_W \phi R}}{\sqrt{\frac{4}{3} dr_w^3}}\right) + \alpha C_0 \operatorname{erfc}\left(\frac{r^2 - \frac{qt}{2\pi h_W \phi R}}{\sqrt{\frac{4}{3} dr^3}}\right) \right]} \dots\dots\dots (4.43)$$

Due to the dispersion effect, the oil saturation front is not exactly sharp as shown in Figure 4.25. For a given time, there are three sections of oil saturation in the aquifer which can be expressed by the following equation:

$$\begin{cases} S_o = \frac{\alpha S_{oe} C_0}{1 + \alpha C_0}, & r \leq r_{f1} \\ 0 < S_o < \frac{\alpha S_{oe} C_0}{1 + \alpha C_0}, & r_{f1} < r \leq r_{f2} \\ S_o = 0, & r > r_{f2} \end{cases} \dots\dots\dots (4.44)$$

Theoretically, the oil front position r_{f1} and r_{f2} at any given time can be calculated from Equation 4.43. However, the complementary error function and the complicated expression inside make it difficult to solve the equation directly.

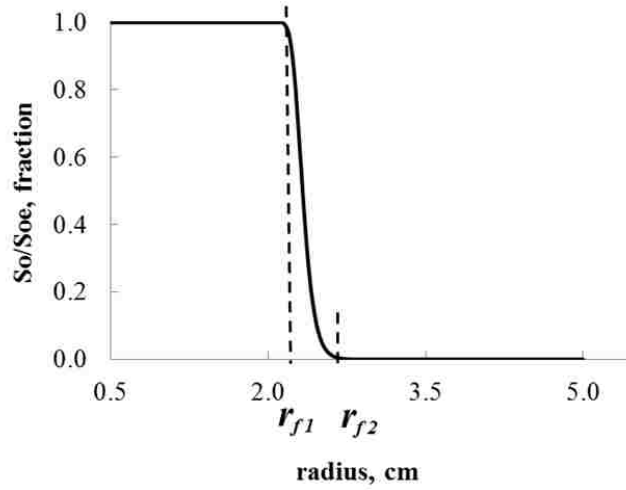


Figure 4.25. Schematic of oil saturation distribution in ADA radial model

By introducing two variables x and x_w , Equation 4.43 can be simplified to:

$$\left\{ \begin{aligned} S_o &= \frac{S_{o,m}}{\rho_o} = \frac{\alpha S_{oe,m} C_o \operatorname{erfc}(x)}{\rho_o [\operatorname{erfc}(x_w) + \alpha C_o \operatorname{erfc}(x)]} \\ x &= \frac{\frac{r^2}{2} - \frac{qt}{2\pi h_w \phi R}}{\sqrt{\frac{4}{3} dr^3}} \\ x_w &= \frac{\frac{r_w^2}{2} - \frac{qt}{2\pi h_w \phi R}}{\sqrt{\frac{4}{3} dr_w^3}} \end{aligned} \right. \dots\dots\dots (4.45)$$

For a given time, x_w is a constant, thus, if $\operatorname{erfc}(x)$ is a constant then S_o becomes a constant too. Observation of $\operatorname{erfc}(x)$ as shown in Figure 4.26, we can see that $\operatorname{erfc}(x) = 2$ when $x \leq -2$ and $\operatorname{erfc}(x) = 0$ when $x \geq 2$. This observation indicates that, $S_o = \text{constant}$ when $x \leq -2$ and $S_o = 0$ when $x \geq 2$. Therefore, r_{f1} and r_{f2} are the solutions of the following equation:

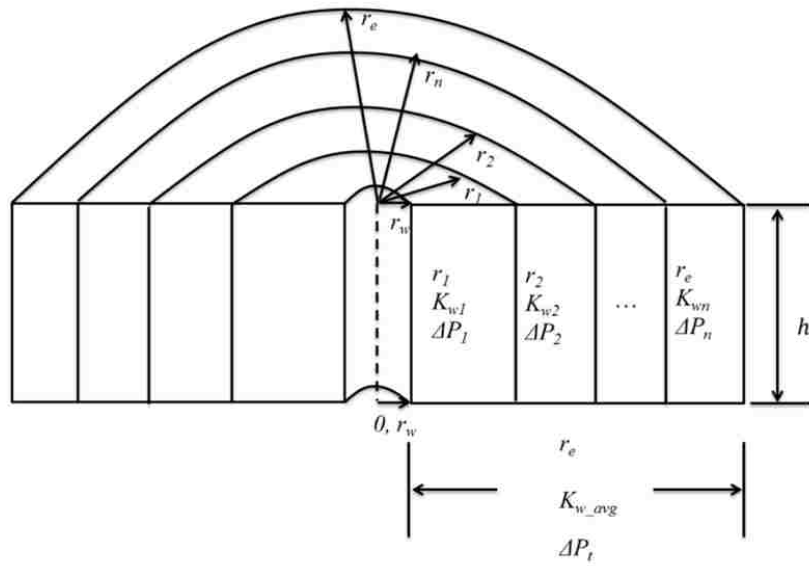


Figure 4.27. Local and average water permeability over the aquifer

For the oil front zone, the average oil saturation is:

$$S_{o_avg} = \frac{2 \int_{r_{f1}}^{r_{f2}} r S_o(r) dr}{r_{f2}^2 - r_{f1}^2} \dots\dots\dots (4.48)$$

Where, S_{o_avg} is the average oil saturation in the oil front zone, fraction; and $S_o(r)$ is the function of oil saturation distribution. By considering relative permeability relationship, $K_{rw} = \varphi(S_o)$, we can compute average relative permeability of the oil advancement front (from r_{f1} to r_{f2}) as:

$$K_{rw_avg} = \frac{\ln \frac{r_{f2}}{r_{f1}}}{\int_{r_{f1}}^{r_{f2}} \frac{dr}{r K_w(r)}} \dots\dots\dots (4.49)$$

Where, $K_w(r)$ is the local water permeability which is a function of oil saturation:

$$K_w(r) = \varphi[S_o(r)] \dots\dots\dots (4.50)$$

For oily water flowing through the aquifer, the change of permeability and pressure drop could be discretely depicted as shown in Figure 4.27. In such case, we may compute a

series of permeabilities in the rock sections as Equation 4.51 if the pressure drop in each radial section can be measured:

$$K_{wi} = K \times K_{rw}(r_i) = \frac{10^6 q \mu_w \ln \frac{r_{i+1}}{r_i}}{2\pi h_w \Delta p_i} \dots\dots\dots (4.51)$$

Or the average permeability as:

$$K_{w_avg} = \frac{\ln \frac{r_e}{r_w}}{\sum_{i=1}^n \frac{\ln \frac{r_{i+1}}{r_i}}{K_{wi}}} = \frac{10^6 q \mu_w \ln \frac{r_e}{r_w}}{2\pi h_w} \frac{1}{\sum_{i=1}^n \Delta p_i} \dots\dots\dots (4.52)$$

Where, r_w and r_e are the radii of well and aquifer, m; K_{wi} is the water permeability in a radial section from r_i to r_{i+1} , D; Δp_i is the pressure drop in a radial section from r_i to r_{i+1} , kpa; K_{w_avg} is the average water permeability over the rock section, D; i is the subsection index.

The same to injectivity decline in linear flow, we use the relative permeability concept to express water injectivity (Schramm, 1992):

$$I_w = \frac{q_w}{\Delta p} = \frac{2 \cdot 10^{-6} \pi h_w K_w}{\mu_w \ln \frac{r_e}{r_w}} = \frac{2 \cdot 10^{-6} \pi h_w K K_{rw}}{\mu_w \ln \frac{r_e}{r_w}} \dots\dots\dots (4.53)$$

Where, I_w is the water injectivity index, m³/s/kpa; q_w is the water injection rate, m³/s; Δp is the pressure drop through the rock, kpa; K_w is the effective water permeability, D; K is the absolute permeability of the core, D; K_{rw} is the relative permeability to water, fraction; r_e is the radius of aquifer, m. As only K_{rw} changes during the injection process, the water injectivity decline as a function of time can be calculated from Equation 4.54 (Saripalli, et al., 2000):

$$I_D = \frac{I_{w_t}}{I_{w_0}} = \frac{K_{w_t}}{K_{w_0}} = \frac{K_{rw_t}}{K_{rw_0}} \dots\dots\dots (4.54)$$

Where, I_D is the dimensionless injectivity decline index, and subscripts 0 and t denote initial and instant values, respectively. Relative permeability values can be obtained in various ways. If core data is not available, Corey's function might approximate the relative permeability to water at different oil saturations (Brooks and Corey, 1966) as:

$$\begin{cases} K_{rw} = K_{rw}^* \left(\frac{1-S_o-S_{wc}}{1-S_{wc}-S_{or}} \right)^{n_w} \\ K_{ro} = K_{ro}^* \left(\frac{S_o-S_{or}}{1-S_{wc}-S_{or}} \right)^{n_o} \end{cases} \dots\dots\dots(4.55)$$

Where, K_{rw}^* is the water relative permeability at residual oil saturation, fraction; K_{ro}^* is the oil relative permeability at connate water saturation, fraction; S_{wc} is the connate water saturation, fraction; S_{or} is the residual oil saturation, fraction; n_w and n_o are the exponents for water and oil relative permeabilities, respectively, dimensionless. Thus, once the oil saturation is determined, the injectivity decline can be calculated.

As no experimental data could be found in literature about oily water injection under radial flow conditions, we use the rock and fluid properties from linear flow model shown in Table 4.2 (Soo and Radke, 1984a) to illustrate an injection process in a “similar” laboratory radial flow model. We assume injecting water at 0.67 cm³/s flow rate with 5000 ppm oil concentration into a radial model with 1 cm height, 0.5 cm inner radius and 5 cm outer radius. The oil-in-water concentration change with radial distance is shown in Figure 4.28. Also, a plot of spatial distribution of oil saturation in the model is Figure 4.29.

We used numerical simulator to verify these computations. The simulation results in Figure 4.30 indicate a reasonably good match with Figure 4.29. Based on the oil saturation distribution, we calculate water permeability reduction at different radii and times (Figure 4.31), and the overall injectivity decline of the “radial model” is compared with the

numerical simulation results in Figure 4.32. The good match of the plots in Figure 4.32 confirms predicted quality of the analytical model.

Table 4.2. Parameters used in ADA and simulation models

Parameter	Value	Unit
Water injection rate (q)	0.67	cm^3/s
Absolute permeability (K)	1.15	D
Porosity (ϕ)	0.34	<i>fraction</i>
Well radius (r_w)	0.5	cm
Rock radius (r_e)	5	cm
Core height (h_w)	1	cm
Oil density (ρ_o)	860	kg/m^3
Water viscosity (μ_w)	1	cp
Oil viscosity (μ_o)	1.50	cp
Water relative permeability exponent (n_w)	15	<i>dimensionless</i>
Oil relative permeability exponent (n_o)	3	<i>dimensionless</i>
Water relative permeability at S_{or} (K_{rw}^*)	1	<i>dimensionless</i>
Oil relative permeability at S_{wc} (K_{ro}^*)	1	<i>dimensionless</i>
Connate water saturation (S_{wc})	0	<i>fraction</i>
Residual oil saturation (S_{or})	0	<i>fraction</i>
Oil concentration (C_0)	5000	ppm
Size ratio (N_d)	0.071~0.152	<i>dimensionless</i>
Equilibrium oil saturation (S_{oe})	0.02~0.08	<i>fraction</i>
Oil water interfacial tension (σ_{ow})	50	$dyne/cm$
Critical capillary number (N_{Ca}^*)	10^{-4}	<i>dimensionless</i>
Bump rate constant (λ)	5	<i>dimensionless</i>
Adsorptive constant (β)	2~7	<i>dimensionless</i>
Dispersivity (d)	0.2~2	cm

The results of our virtual experiment with the “radial model” built using the Soo and Radke data reveal existence of a frontal zone with sharp drop of oil saturation that defines two regions in radial flow: damaged region with equilibrium oil saturation and undamaged region without oil as shown in Figure 4.29. In the near-well region, all injected oil

accumulates first, thus resulting in rapid initial drop of the well's injectivity shown in Figure 4.32. Later, oil adsorption in the rock away from the well does not affect injectivity that tends to become stable as shown also in Figure 4.32. This phenomenon has been found in many wells with produced water re-injection, and the half-life of these injectors is significant shorter than those injecting clean water (Paige, et al., 1995; Palsson, et al., 2003; Bai, et al., 2009). Very similar observations have also been made in fines migration experiments in radial flow (Liu and Civan, 1994).

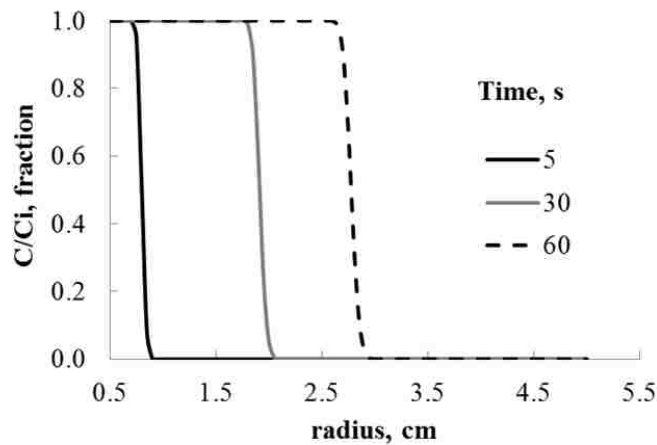


Figure 4.28. Calculated oil concentration vs. radius in “radial model” ($d_o = 2.1 \mu m$)

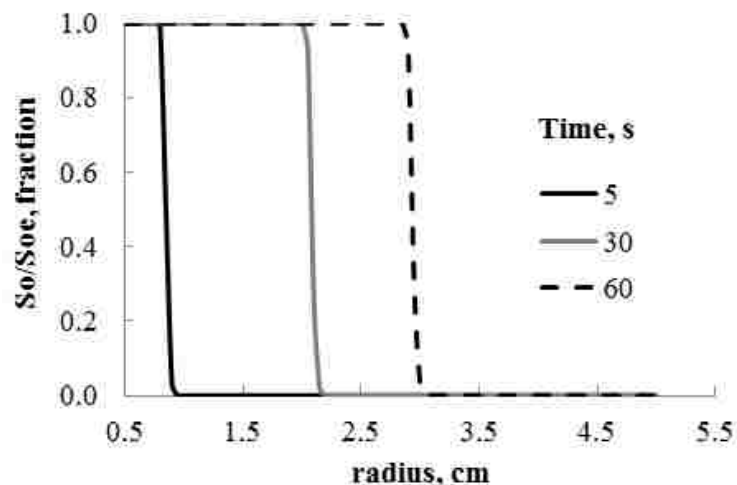


Figure 4.29. Calculated distribution of oil saturation in “radial model” ($d_o = 2.1 \mu m$)

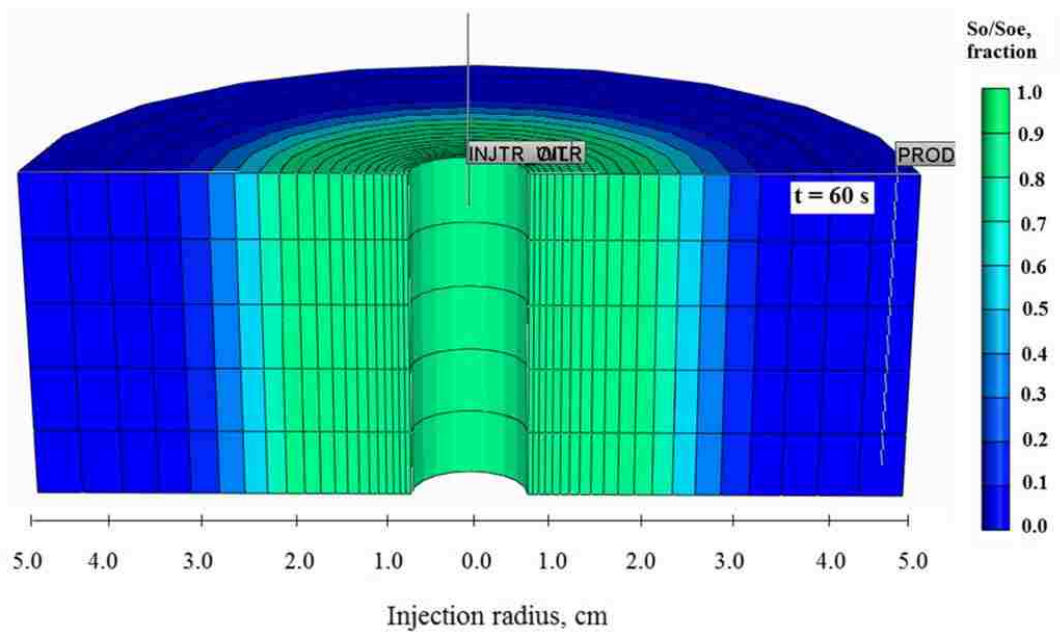


Figure 4.30. Spatial distribution of oil saturation in “radial model” from simulator ($d_o = 2.1 \mu m$; $t = 60 s$)

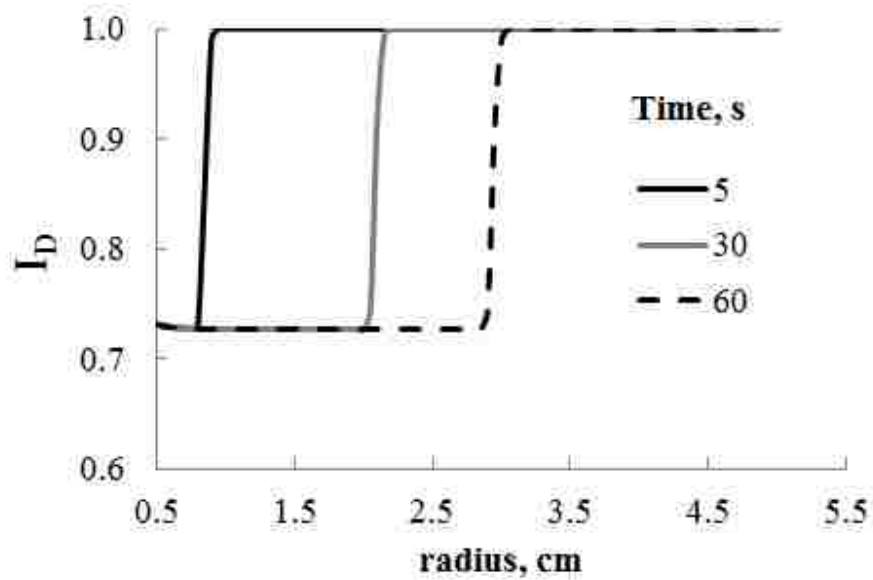


Figure 4.31. Calculated distribution of permeability in “radial model” at different times ($d_o = 2.1 \mu m$)

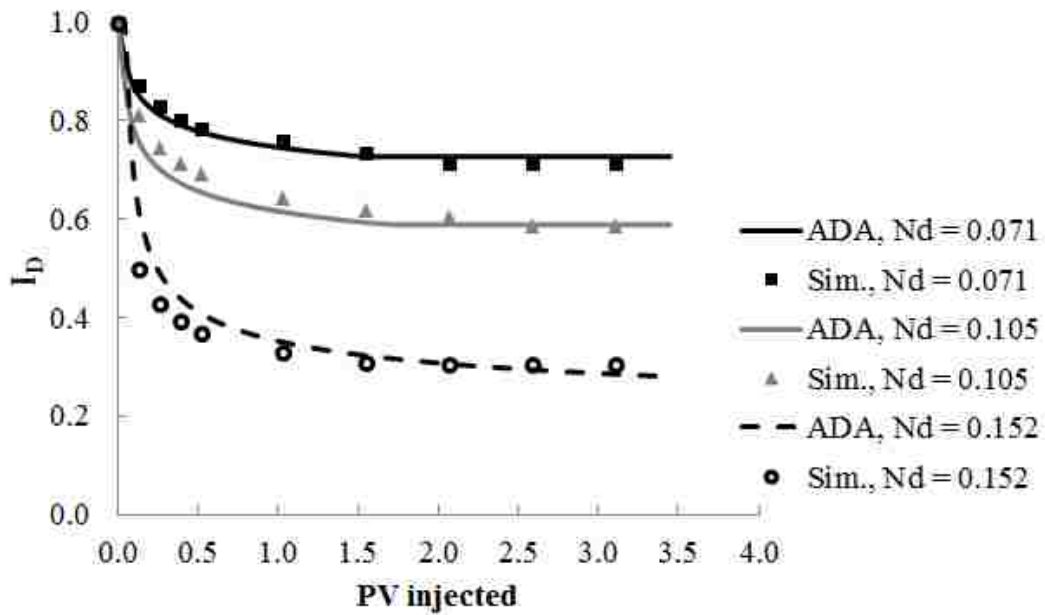


Figure 4.32. Comparison of calculated and simulated injectivity decline of the “radial model”

4.3.2 Application of Buckley-Leverett Theory to Injectivity Decline

Following the fractional flow theory proposed by Buckley and Leverett in 1942, numerous models have been developed to simulate the process of multiphase flow in porous media (Yortsos and Fokas, 1983). To date, the theory has been widely used to predict the performance of waterflooding and enhanced oil recovery (EOR) processes (Pope, 1980; Wu, et al., 1993; Zhou and Rossen, 1995; Rossen, et al., 2011; Kootiani and Samsuri, 2012; Ling, 2012). The fractional flow approach considers concurrent flow of the two phases - oil and water, by describing separately the flowing behavior of each phase. Essentially, oily water flow through porous media belongs to this category, which indicates that Buckley-Leverett theory should be applicable to the oily water injection to the aquifer (Devereux, 1974; Schmidt, et al., 1984).

Oily water flow comprises oil droplets carried by continuous water flow. As described previously, some droplets are adsorbed (trapped) in the rock pores while other droplets get

deformed and squeezed through the pore throats. The combined effect of adsorption and capillary resistance in constricted pores makes the oil phase move slower than the aqueous phase causing an overall permeability reduction. Schmidt, et al. (1984) found that injectivity decline caused by oil droplets invasion could be predicted using Buckley-Leverett approach based on the equilibrium oil saturation and relative permeability curves, however, they did not provide formulas to calculate the transient injectivity reduction during the injection. Devereux (1974a) modified the Buckley-Leverett theory by including a “retardation factor” to consider the capillary resistance effect. He proposed a mathematical model to calculate water injectivity decline caused by oil contamination, where he presented a numerical solution for the case of constant-pressure flow. The model, was verified with experimental data, analytically describes time-dependent water permeability reduction in linear flow.

We follow the premise but consider oil droplets retardation by permanent retention inside the rock that makes the bulk water flow faster than the advancement of the oil front. We also assume the instant oil capture in the rock and the primary water drainage mechanism constrained by the maximum (equilibrium) value of oil saturation $S_{o_max} = S_{oe}$. The saturation represents the “invaded” rock region while in the “uninvaded” region $S_o \equiv 0$. Also, in analytical modeling, we assume constant injection rate.

In most conditions, Buckley-Leverett theory is applied in reservoirs with residual oil saturation. However, in our case, there is no residual oil in aquifer before oily water is injected and we use the concept of “equilibrium oil saturation” instead of residual oil saturation in modeling. Thus, it is necessary to distinguish the two concepts first.

Residual and Equilibrium Oil Saturations

Residual oil saturation can be defined as the remaining oil saturation in the reservoir after waterflooding and it is usually considered as immobile with water displacement (Chang and Maerefat, 1986). In waterflooding with clean water, there is no oil component in the injection water and water displaces oil in the pores until reaches the residual oil saturation. Many methods have been developed to measure the residual oil saturation, including core analysis, well logging, backflow tracer test and so on (Chang and Maerefat, 1986). Generally, the residual oil saturation varies from 0.1 to 0.5 based on reservoir properties and measurement methods used (Owolabi and Watson, 1993; Jadhunandan and Morrow, 1995; Element, et al., 2000; Hirasaki, et al., 2005; Chen, et al., 2006). Physically, Residual oil saturation is a “snap-off and bypassing” phenomena – oil is left in larger pores because water surrounds those pores either through surrounding tubes filling with water or if the tubes have corners, water may move along the corners and as capillary pressure is lowered, water fills the corners to the point where they “snap-off” completely filling the tubes.

Based on the definition of residual oil saturation, the value is zero for rocks from aquifer as there is no oil in place, initially (Pentland, et al., 2008; Spiteri, et al., 2008). When oily water is injected to a water-wet aquifer, oil droplets displace water in pores which is known as a primary drainage process (Valvante and Blunt, 2004). As described previously, when an oil droplet encounters a pore of throat size smaller than its own diameter, it needs to deform and squeeze through before the water behind it flowing through the throat. Thus, oil droplets suffer a capillary resistance force in constricted pores, which makes the oleic phase move slower than water, however, the velocity is not zero because more oil droplets are injected with water and enter the pores continuously, i.e. the oil relative permeability is small

but not zero as shown in Figure 4.33 (Valvante and Blunt, 2004). Logarithmic scale is usually used to demonstrate the small oil relative permeability as shown in Figure 4.33(b) (Oak, et al., 1990; Braun and Holland, 1995; DiCarlo, et al., 2000; Valvante, 2004; Spiteri, et al., 2008). Corey's function shown in Equation 4.55, provides a convenient way to predict relative permeability curves despite the small value of oil relative permeability at low oil saturation as shown in Figure 4.34.

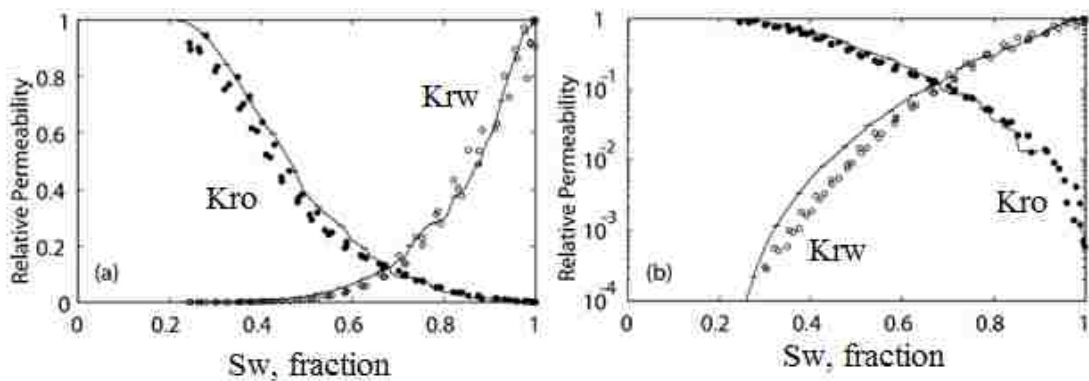


Figure 4.33. Relative permeability curves in primary drainage process for Berea sandstone (Valvante and Blunt, 2004)

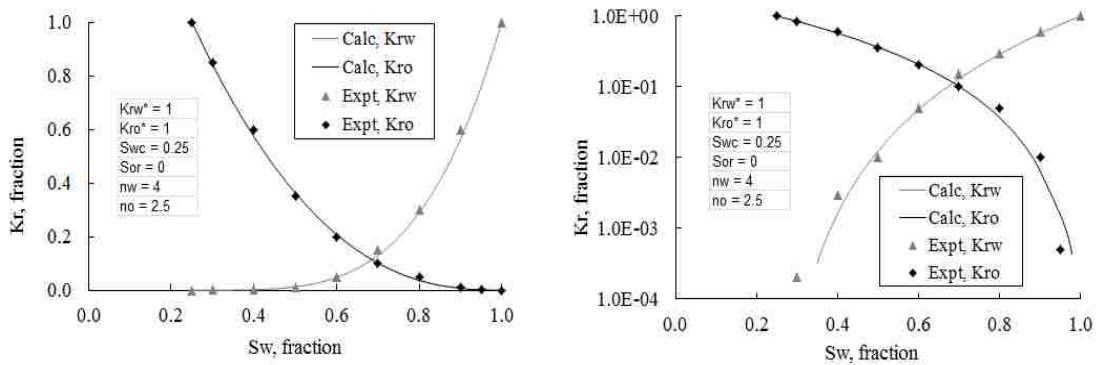


Figure 4.34. Prediction of relative permeability curves by Corey's correlation for Berea sandstone

Because of capillary resistance, oil flows slower than water which leads to oil saturation buildup in the formation and advance with the injection goes on. The equilibrium oil saturation during the injection process is a function of droplet to pore throat size ratio and

capillary number, and it is different from the residual oil saturation described above. Various experiments have shown that, the equilibrium oil saturation increases with droplet to pore throat size ratio in low capillary number region (Schmidt, et al., 1984; Soo and Radke, 1984a, b, 1986; Soo, et al., 1986; Buret, et al., 2008, 2010). If we consider the aquifer rock as a bundle of capillary tubes with different sizes (Holmes, 2002; Abdallah, et al., 2007; Civan, 2007), then the physical reason can be explained as a “filtration” process, which is described as follows:

Initially, there is no oil in the aquifer and all capillary tubes are open to water flow. Assuming the rock is composed of a bundle of capillary tubes with different diameters, $d_1 < d_2 < \dots < d_5$, as shown in Figure 4.35, when oil droplets are injected with water, the minimum resistances they need to overcome are the threshold capillary pressure shown in Equation 4.56 to enter the tubes and the flowing resistance shown in Equation 4.57 to make the droplets flow through these tubes.

$$p_{c_e} = 4 * 10^{-6} \sigma_{ow} \text{Cos}\theta \left(\frac{1}{d_t} - \frac{1}{d_o} \right) \dots\dots\dots (4.56)$$

$$p_c = \frac{4 * 10^{-6} \sigma_{ow} \text{Cos}\theta}{d_t} \dots\dots\dots (4.57)$$

Where, p_{c_e} is the threshold pressure for an oil droplet with diameter d_o to enter a capillary tube with diameter d_t , kpa; σ_{ow} is the oil water interfacial tension, dyne/cm; θ is the contact angle, degree; d_t and d_o are the diameters of a capillary tube and oil droplet, m; p_c is the capillary resistance on an droplet when it flows through a capillary tube, kpa. Thus, oil droplets suffer various capillary forces related to the droplet and tube diameters, the smaller tube size or greater droplet diameter, the higher the capillary pressure will be, $p_{c5} < p_{c4} < \dots < p_{c1}$ is valid for the capillary tubes shown in Figure 4.35. As a result, higher size ratio leads to greater equilibrium oil saturation when the viscous force generated

by water injection is constant as shown in Figure 4.36 (Cartmill and Dickey, 1969; Schmidt, et al., 1984; Soo, et al., 1986; Buret, et al., 2010).

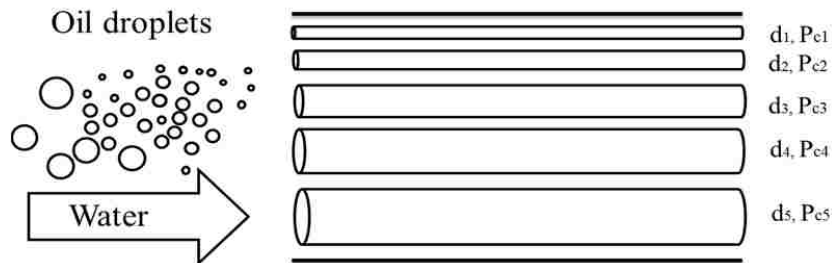
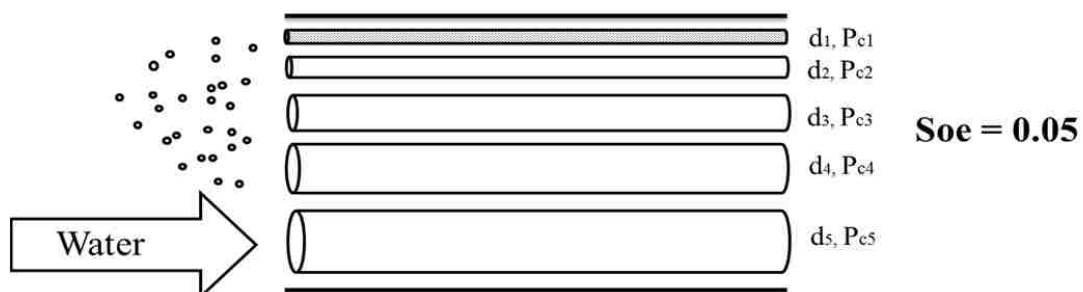


Figure 4.35. Injection water with oil droplets to a section in an aquifer without residual oil

Based on the above mechanisms, the reason of water injectivity decline in oily water injection can be explained as: during primary drainage, the oil droplets plug narrow regions in the pore space and block the flow paths for water: the bigger the droplets, the more flow paths are blocked, which leads to higher equilibrium oil saturation in the rock. When a droplet blocks a pore throat, the injection pressure needs to be increased to generate higher viscous force for overcoming the capillary resistance to make the oil droplet deform and squeeze through the pore throat. As oil droplets are continuously injected to the rock, more and more oil droplets are pushed into the pore space. As a result, the oil saturation increases and higher injection pressure is required to maintain the injection rate, which leads to significant water injectivity decline (Soo and Radke, 1986; Bennion, et al., 1998; Geosphere, 2006; Spiteri, et al., 2008).



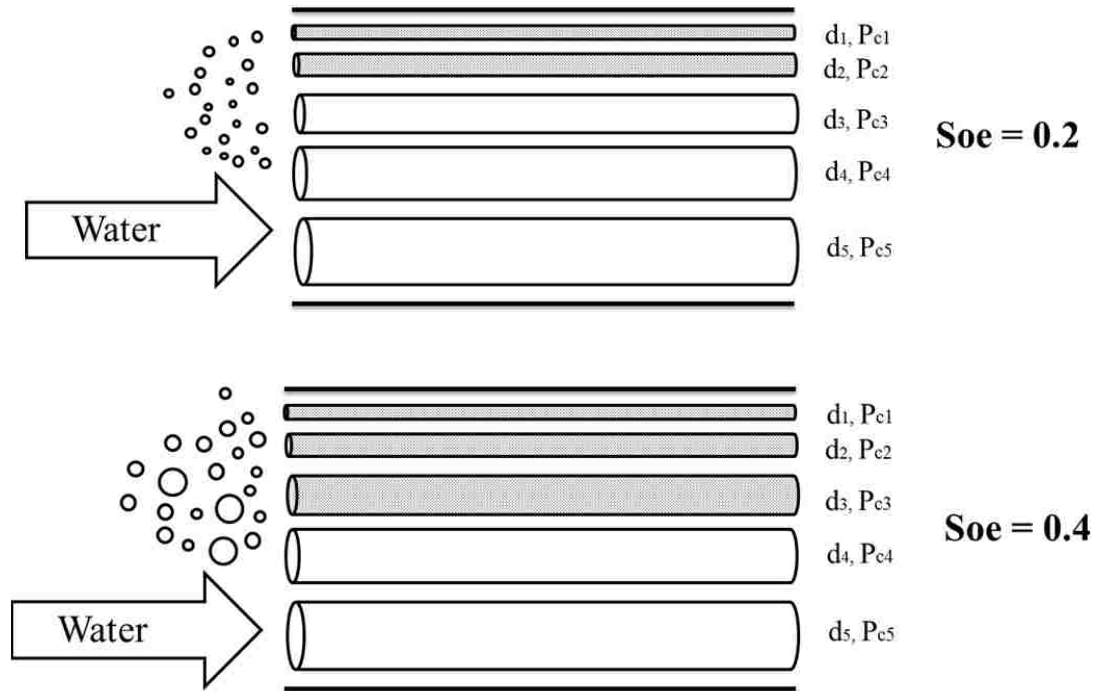


Figure 4.36. Equilibrium oil saturations for oil droplets with different sizes

Buckley-Leverett Solution in Linear Flow

Similar to ADA model, the porous medium is assumed to be initially saturated only with water, a low-concentration stable emulsion of oil in water is then injected into the rock from one end. To describe capture and retardation effect of oil droplets mentioned above, we follow Devereux (1974a) and assume two regions in the core during the emulsion injection process - shown in Figure 4.37. This assumption makes the derivation of explicit analytical solutions for injectivity decline easier as the standard Buckley-Leverett solution needs to be solved graphically. Oil front moves at a superficial velocity of u_o and water flows at a superficial velocity of u_w in the rock after the oily water is injected from the inlet. At time t , oil front advances to the position x_f (oil saturation front) and only water flows beyond this position, because oil front moves slower than water due to the retardation/capture effect. Using the average oil droplet and pore throat sizes, the region between inlet and position x_f

is called “invaded region” with constant oil saturation determined by droplet to pore throat size ratio and capillary number as described in the ADA model section. The region between position x_f and exit end of the core is called “uninvaded region” where only water exists. Thus, a sharp interface is assumed to divide the two regions, which is reasonable based on the results from ADA model.

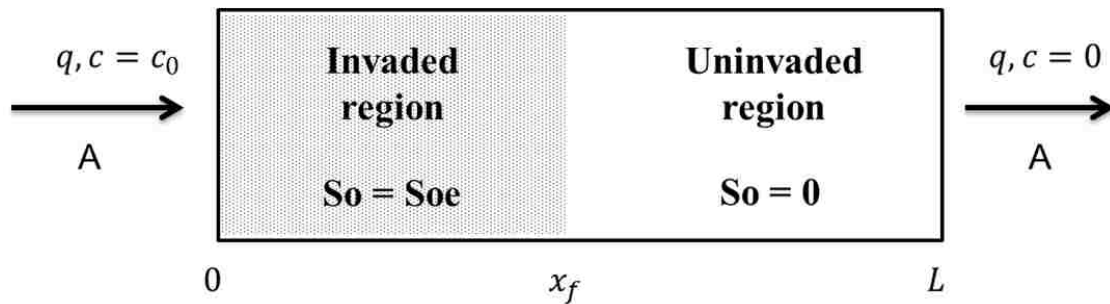


Figure 4.37. Schematic of oil droplets retardation in linear flow

To provide for retardation/retention effects but still consider fractional flow concept we need to assume that equilibrium saturation of oil captured in the rock allows oil past flow as discussed above. Thus, to apply Buckley-Leverett theory in the oily water injection process, the following assumptions in addition to those in the ADA model are presumed to be valid (Devereux, 1974; Schmidt, et al., 1984):

1. There are two regions separated by a sharp interface in the core during oily water injection;
2. Oil droplets are captured instantly by the rock in the oil front;
3. Both oil and water flow in the invaded region;
4. The viscosity of oily water is equal to that of clean water due to the low oil concentration;

5. The oil saturation in the invaded region is at the equilibrium value and zero at the uninvaded region.

Based on the above assumptions, we can write the Darcy's Law for each phase as follows:

In the invaded region:

$$q_w = \frac{10^{-6}AKK_{rw}}{\mu_w} \left(\frac{p_0 - p_{x_f}}{x_f} \right) \dots\dots\dots(4.58)$$

$$q_o = \frac{10^{-6}AKK_{ro}}{\mu_o} \left(\frac{p_0 - p_{x_f}}{x_f} \right) \dots\dots\dots(4.59)$$

Where, q_w and q_o are the water and oil flow rates, respectively, m³/s; A is the cross-section area of the core, m²; K is the absolute permeability, D; K_{rw} and K_{ro} are the relative permeabilities for water and oil at the equilibrium oil saturation, respectively, fraction; μ_w and μ_o are the water and oil viscosities, respectively, cp; p_0 is the injection pressure at the inlet, kpa; p_{x_f} is the pressure at the oil saturation front, kpa.

In the uninvaded region:

$$q = \frac{10^{-6}AK}{\mu_w} \left(\frac{p_{x_f} - p_L}{L - x_f} \right) \dots\dots\dots(4.60)$$

For the whole core:

$$q = \frac{10^{-6}AK_{wt}}{\mu_w} \left(\frac{p_0 - p_L}{L} \right) \dots\dots\dots(4.61)$$

Where, q is the total flow rates, m³/s; L is the length of the core, m; K_{wt} is the effective water permeability in the core at time t , D.

In core-flooding experiments $p_L = 0$ and the expressions for p_{x_f} and K_{wt} from Equations 4.60 and 4.61 becomes:

$$p_{x_f} = \frac{10^6 q \mu_w (L - x_f)}{AK} \dots\dots\dots (4.62)$$

$$K_{wt} = \frac{10^6 q \mu_w L}{Ap_0} \dots\dots\dots (4.63)$$

From material balance, the total flow rate is the summation of oil and water flow rates, which is expressed by:

$$q = q_w + q_o \dots\dots\dots (4.64)$$

Substitute Equations 4.58, 4.59 and 4.60 to 4.64, we get the pressure relationship in the invaded region as:

$$p_0 = p_{x_f} \left[1 + \frac{x_f}{\mu_w (L - x_f) \left(\frac{K_{rw}}{\mu_w} + \frac{K_{ro}}{\mu_o} \right)} \right] \dots\dots\dots (4.65)$$

The p_{x_f} can be eliminated from Equation 4.65 by substituting Equation 4.62:

$$p_0 = \frac{10^6 q \mu_w (L - x_f)}{AK} + \frac{10^6 q x_f}{AK \left(\frac{K_{rw}}{\mu_w} + \frac{K_{ro}}{\mu_o} \right)} \dots\dots\dots (4.66)$$

By substituting Equation 4.66 to Equation 4.63, we get the expression for the effective water permeability in the core at time t , K_{wt} as:

$$K_{wt} = \frac{K}{\left(1 - \frac{x_f}{L} \right) + \frac{x_f}{\mu_w L \left(\frac{K_{rw}}{\mu_w} + \frac{K_{ro}}{\mu_o} \right)}} \dots\dots\dots (4.67)$$

Based on the definition of water injectivity decline in ADA modeling section, shown in Equation 4.54, we get the explicit expression of the core injectivity decline as:

$$I_D = \frac{1}{\left(1 - \frac{x_f}{L} \right) + \frac{x_f}{\mu_w L \left(\frac{K_{rw}}{\mu_w} + \frac{K_{ro}}{\mu_o} \right)}} \dots\dots\dots (4.68)$$

Where, K_{rw} and K_{ro} can be calculated from Corey's correlation shown in Equation 4.55.

Based on material balance, the position of oil saturation front can be calculated as follows:

$$x_f = \begin{cases} \frac{qtC_0}{A\phi S_{oe}}, & \frac{qtC_0}{A\phi S_{oe}} \leq L \\ L, & \frac{qtC_0}{A\phi S_{oe}} \geq L \end{cases} \dots\dots\dots(4.69)$$

Where, C_0 is the oil concentration in the injection water, volume fraction; ϕ is the porosity of the rock, fraction; S_{oe} is the equilibrium oil saturation in the core, fraction. Using the experimental data from Soo and Radke (1984a) and parameters such as relative permeability curves, equilibrium oil saturation etc. used in ADA model, the Buckley-Leverett solution successfully matched the experimental results as shown in Figure 4.38.

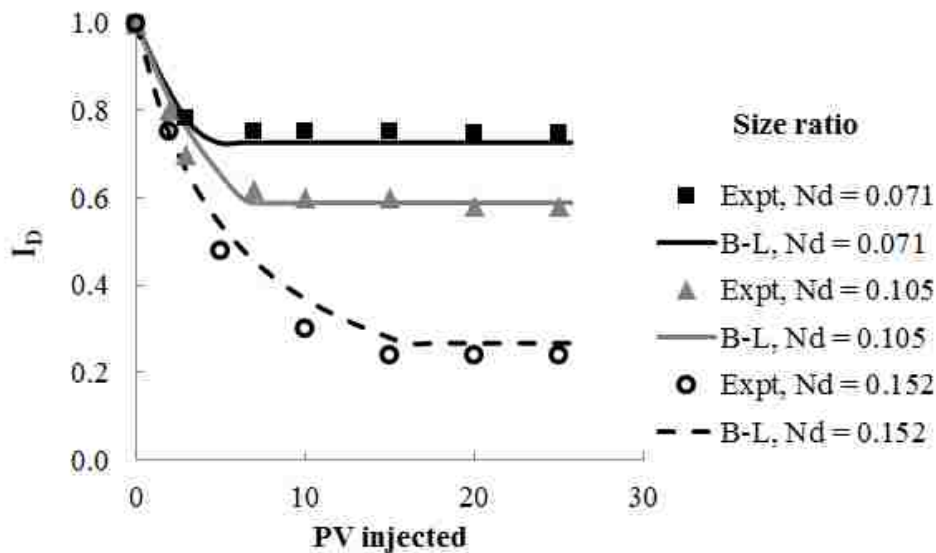


Figure 4.38. Injectivity decline prediction using Buckley-Leverett solution for different size ratio – data from Soo and Radke (1984a)

Buckley-Leverett Solution in Radial Flow

The concept of Buckley-Leverett approach to linear flow of oily water discussed above, is used here to model injection well - shown in Figure 4.39. As the two fluids flow radially outwards into the aquifer, interstitial velocity and capillary number decrease rapidly with radial distance as shown in Figure 4.40, where an injection well with 10-ft completion length and 0.3-ft well radius injected at 1,000 bpd to a formation with 0.3 porosity. As equilibrium oil saturation is a function of capillary number as shown in Equation 4.18

(Schlumberger, 2007), a variable oil saturation profile may develop in a small near-well zone as shown Figure 4.41 from r_w to r_{oe} .

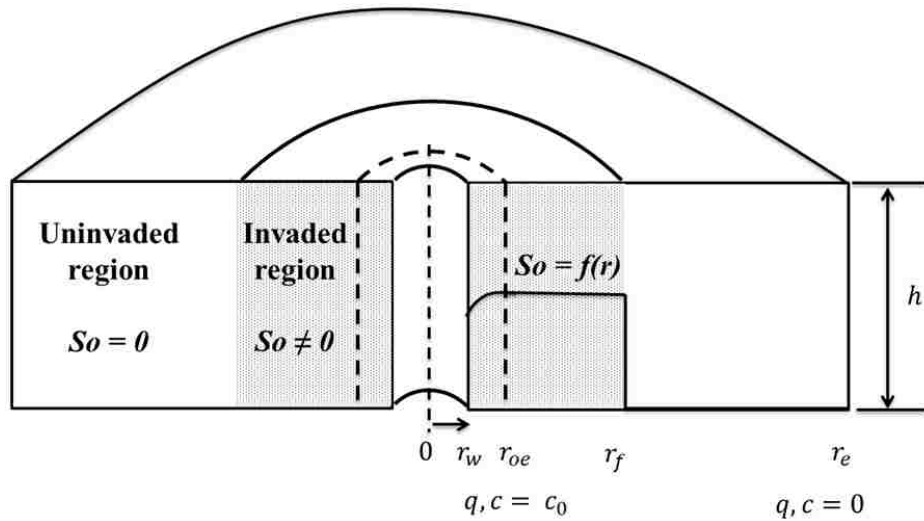


Figure 4.39. Schematics radial invasion of oil for oily water injection

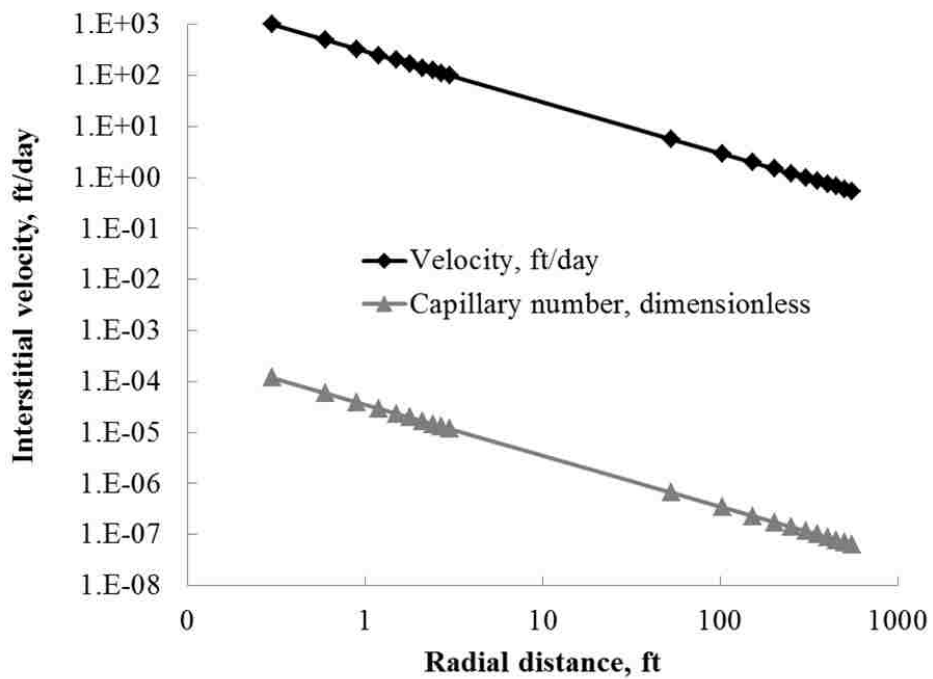


Figure 4.40. Interstitial velocity and capillary number decrease with radial distance from well

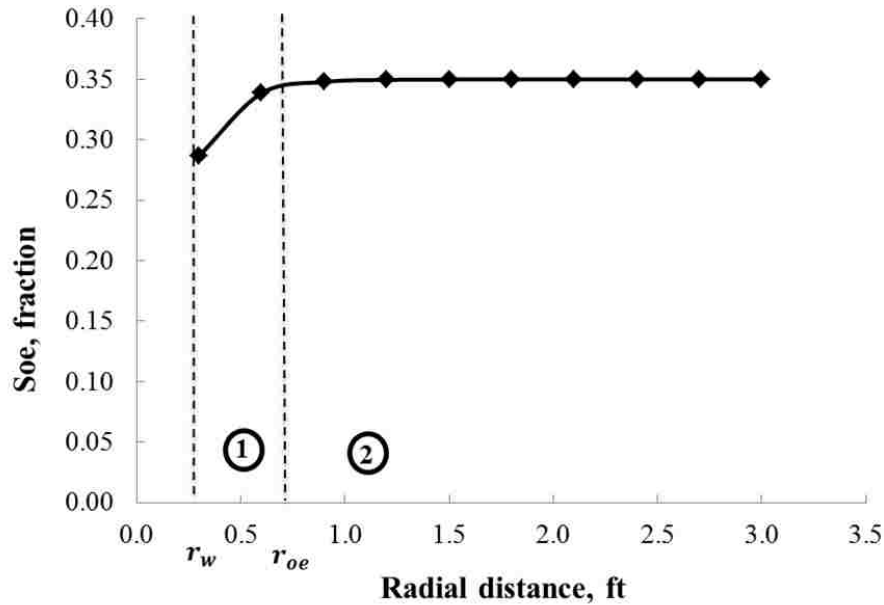


Figure 4.41. Schematic of equilibrium oil saturation distribution profile in radial flow

Outside this zone, oil saturation is constant since the capillary number falls below the critical value (Reppert and Idol, 2001). Similar phenomenon has been observed in waterflooding that, oil saturation near the injectors is below residual oil saturation but remains high far from the injection wells (Sinha, et al., 2004). It is possible to increase the capillary number within the first few feet around the injection well by increasing the water rate, which is high enough to displace the captured oil. However, to displace oil beyond about one to two feet, the flow rate would have to be higher than is practically achievable (Bennion, et al., 1999; Reppert and Idol, 2001).

From the case of linear flow, we know that the injectivity decline can be derived from the Darcy's Law for each phase. The same principle is applied here for the radial flow as shown in Figure 4.39. The first 4 assumptions in linear flow are valid for radial flow and also the pressure at the outer boundary of the aquifer is constant, i.e. $p_{r_e} = \text{constant}$.

Darcy's Law for each phase in the two regions is expressed as follows:

In the invaded region:

$$q_w = \frac{2 \times 10^{-6} \pi h_w K K_{rw}}{\mu_w \ln \frac{r_f}{r_w}} (p_{r_w} - p_{r_f}) \dots\dots\dots (4.70)$$

$$q_o = \frac{2 \times 10^{-6} \pi h_w K K_{ro}}{\mu_o \ln \frac{r_f}{r_w}} (p_{r_w} - p_{r_f}) \dots\dots\dots (4.71)$$

In the uninvaded region:

$$q = \frac{2 \times 10^{-6} \pi h_w K}{\mu_w \ln \frac{r_e}{r_f}} (p_{r_f} - p_{r_e}) \dots\dots\dots (4.72)$$

For the whole aquifer:

$$q = \frac{2 \times 10^{-6} \pi h_w k_{wt}}{\mu_w \ln \frac{r_e}{r_w}} (p_{r_w} - p_{r_e}) \dots\dots\dots (4.73)$$

Where, h_w is the aquifer thickness, m; r_w is the well radius, m; r_f is the position of oil saturation front, m; r_e is the radius of aquifer, m; P_{r_w} is the injection pressure at the wellbore, kpa; P_{r_f} is the pressure at the oil saturation front, kpa; P_{r_e} is the pressure at the outer boundary of the aquifer, kpa.

From Equation 4.73, the effective water permeability of the aquifer for constant injection rate is defined as:

$$K_{wt} = \frac{10^6 q \mu_w \ln \frac{r_e}{r_w}}{2 \pi h_w (p_{r_w} - p_{r_e})} \dots\dots\dots (4.74)$$

From material balance, the total flow rate is the summation of oil and water flow rates, which is expressed by Equation 4.64 Substitute Equations 4.70 and 4.71 into 4.72, we get the pressure relationship in the invaded region as:

$$p_{r_w} = p_{r_f} + \frac{(p_{r_f} - p_{r_e}) \ln \frac{r_f}{r_w}}{\mu_w \left(\frac{K_{rw}}{\mu_w} + \frac{K_{ro}}{\mu_o} \right) \ln \frac{r_e}{r_f}} \dots\dots\dots (4.75)$$

Substitute Equations 4.72 and 4.73 into 4.75, we can get the relationship between P_{r_w} and P_{r_e} as:

$$p_{r_w} - p_{r_e} = \frac{10^6 q \mu_w \ln \frac{r_e}{r_f}}{2\pi h_w K} + \frac{10^6 q \ln \frac{r_f}{r_w}}{2\pi h_w K \left(\frac{K_{rw}}{\mu_w} + \frac{K_{ro}}{\mu_o} \right)} \dots\dots\dots (4.76)$$

Substitute Equation 4.76 into Equation 4.74, the injectivity decline can be expressed as:

$$I_D = \frac{1}{\frac{\ln \frac{r_e}{r_f}}{\ln \frac{r_f}{r_w}} + \frac{\mu_w \left(\frac{K_{rw}}{\mu_w} + \frac{K_{ro}}{\mu_o} \right) \ln \frac{r_e}{r_w}}{\ln \frac{r_f}{r_w}}} \dots\dots\dots (4.77)$$

Based on material balance, there is a relationship between oil saturation front position and total oil injected:

$$\int_{r_w}^{r_f} 2\pi h r \phi S_{oe} dr = qtC_o \dots\dots\dots (4.78)$$

Solve Equations 4.78 and 4.18, we can get the expression of oil saturation front position as:

$$\frac{r_f^2 - r_w^2}{2} - \frac{1}{\delta^2} [(\delta r_f - 1) \exp(\delta r_f) - (\delta r_w - 1) \exp(\delta r_w)] = \frac{qtC_o}{2\pi h_w \phi S_{oe}^*} \dots\dots (4.79)$$

$$\delta = \frac{-\lambda N_{Ca}^* 2\pi h_w \phi \sigma_{ow}}{q \mu_w} \dots\dots\dots (4.80)$$

Where, δ is an expression used to simplify Equation 4.79, 1/m; S_{oe}^* is the maximum equilibrium oil saturation under low capillary number condition, which is determined by routine core analysis, dimensionless; λ is empirical constant experimentally determined from bump rate tests, dimensionless; σ_{ow} is oil water interfacial tension, dyne/cm; N_{Ca}^* is the critical capillary number that the equilibrium oil saturation begins to decrease, dimensionless. Equation 4.79 is a strong non-linear function which is difficult to write out the explicit solution for r_f , however, it can be solved easily by a graphic method.

Practically, $(\delta r_f - 1) \exp(\delta r_f) / \delta^2$ is close to zero as δ is a large negative value as q is very small due to its unit: m^3/s , and r_f increases with time, thus this term in Equation 4.79 could be ignored. Then, the oil front position can be explicitly expressed as:

$$r_f \cong \sqrt{r_w^2 + \frac{2(\delta r_w - 1) \exp(\delta r_w)}{\delta^2} + \frac{qtC_0}{\pi h_w \phi S_{\delta e}}} \dots\dots\dots (4.81)$$

Figure 4.42 shows the water injectivity decline for different oil droplet sizes in radial flow using the same data as in Figure 4.38. Similar to situation in linear flow, higher size ratio leads to more injectivity damage. The water injectivity declines more rapidly in radial flow than in linear flow, especially in the beginning of injection.

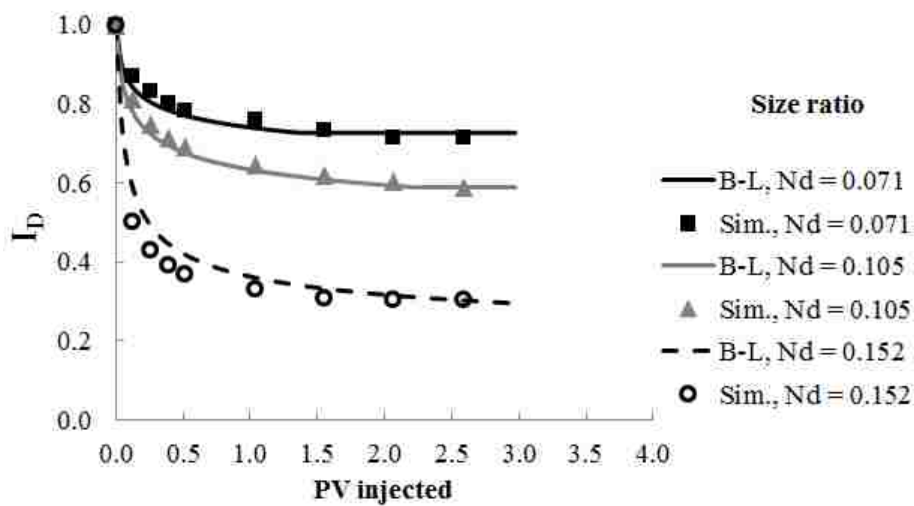


Figure 4.42. Water injectivity decline for different size ratio in radial flow

4.3.3 Comparison of ADA and Buckley-Leverett Models

So far, two water injectivity decline models (ADA and B-L) have been developed for linear and radial flows in this study. Both of the models are derived from material balance principle and widely accepted theories in petroleum engineering. They successfully match the experimental and simulation results. Their commonality and difference is compared in this section.

In mechanisms, both ADA and B-L models consider transient water permeability reduction by assuming oil saturation advancement in the rock. However, in the ADA concept, there is only one flow stream of oily water, while the B-L approach considers two flow streams: water and oil. When describing the injectivity decline process, the two models use the principle of relative permeability. Both models obey material balance. The ADA model considers mass balance of oil removed and retained in the o/w mixture to track oil content in the water. In contrast, B-L computes balance of cumulative volumes of the fluids to determine position of oil front. Moreover, the concept of oil transport differs in the models. In ADA, oil is being dragged by water and captured in rock out of the water stream until reach the equilibrium oil saturation. In the B-L model, oil flows due pressure gradient in the ever expanding “invaded” region with constant oil saturation and piston-like front.

Figure 4.43 and Figure 4.44 show the comparison of results from ADA and B-L models for the linear injection into a core reported by Soo and Radke (1984a), and the “simulated” model - described above. It is clear that, both models give similar results that generally match - especially in the radial flow. In linear flow, water permeability declines somewhat faster for ADA model than for the B-L model before stabilization. This is because ADA model considers time-dependent oil saturation due oil concentration change in contrast to the instant oil trapping in the B-L model. The disparity becomes negligible in radial flow, as the oil front computed from the ADA model becomes as sharp as the assumed one in the B-L model. Thus, the two models yield almost identical results in radial flow.

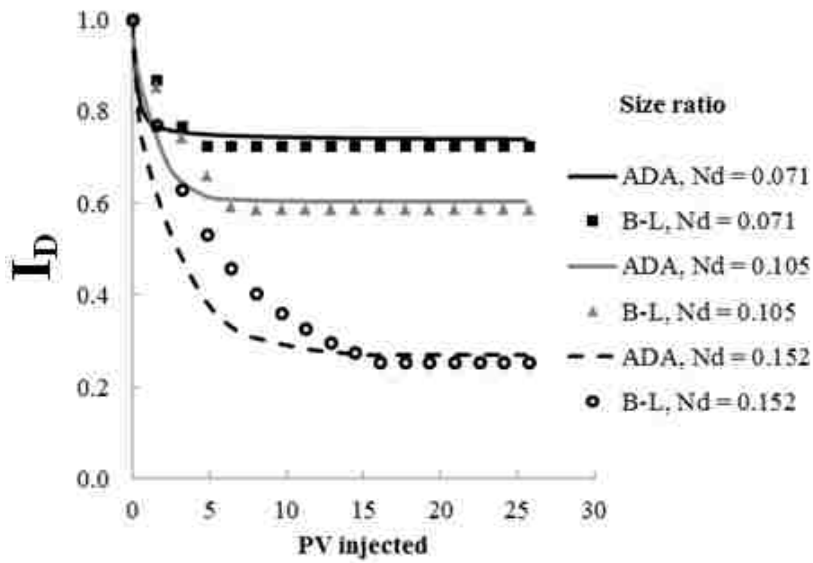


Figure 4.43. Comparison of results from ADA and B-L models in linear flow

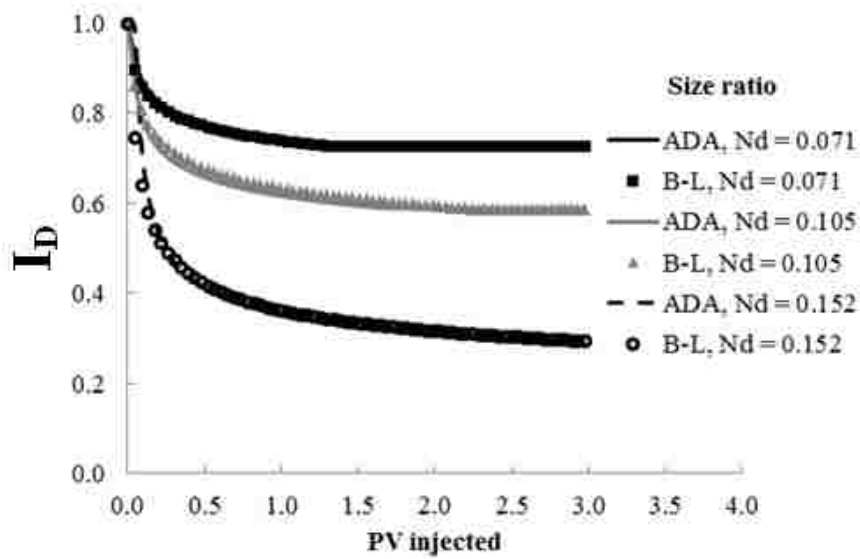


Figure 4.44. Comparison of results from ADA and B-L models in radial flow

Due to the large volume of water produced with oil and gas, most injection wells are operated at high rates for the purposes of produced water disposal and reservoir pressure maintenance. Thus, high quality formation is a premise to attain injection objectives, especially in cases where reservoir conditions dictate that the wells not be fractured (Paige, et al., 1995; Sharma, et al., 2000). To further compare the ADA and B-L models, we use an

aquifer with Bentheimer sandstone as shown in Table 4.3. The rock properties and relative permeability curves shown in Figure 4.45 are reported by Patzek (2001).

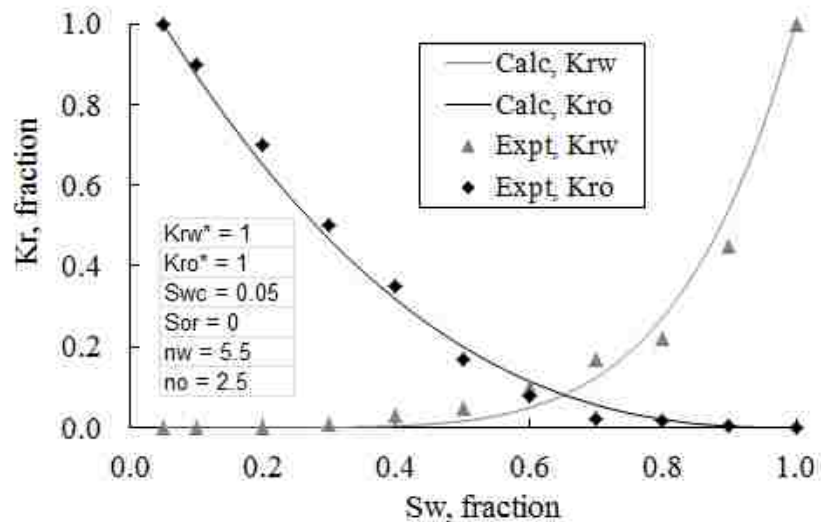


Figure 4.45. Primary drainage relative permeability curves for Bentheimer sandstone - data from Patzek (2001)

Figure 4.46 shows the injectivity decline development at different injection rates. It is clear that, injectivity declines fast at the beginning of injection and then levels off with the continuing of injection. This phenomenon has been observed in field cases of downhole oil/water separation (DOWS) and produced water re-injection (PWRI).

The separation of fluids in a DOWS is not complete and some oil, from 50 to 500 ppm, is carried along with the water for injection (Veil, et al., 1999). From the field trails of this technology, injectivity decline was found to be a main problem that hampers its performance, many wells lost injectivity in some degree (Veil and Quinn, 2004). However, the severity of decline strongly relates to the injection formation, for example, a well in East Texas lost 60% of the injectivity in just 3 days with injection rate 2000 ~ 3000 bpd, while some wells could operate continuously for 18 months without a problem (Veil, et al., 1999; Veil and Layne, 2001; Veil and Quinn, 2004). PWRI cases also showed that, instant injectivity damage might

happen when raw produced water is injected to the formation and then stabilizes with the injection continues (Hsi, et al. 1990; Paige, et al., 1995; Palsson, et al., 2003; Bai, et al., 2009).

Table 4.3. Parameters used in ADA and B-L models comparison

Parameter	Value	Unit	Value	Unit
Water injection rate (q)	1000~5000	<i>bpd</i>	0.00184~0.0092	m^3/s
Absolute permeability (K)	5149	<i>md</i>	5.149	<i>D</i>
Porosity (ϕ)	0.234	<i>fraction</i>	0.234	<i>fraction</i>
Well radius (r_w)	0.292	<i>ft</i>	0.089002	<i>m</i>
Aquifer radius (r_e)	1000	<i>ft</i>	304.8	<i>m</i>
Aquifer depth (H_a)	5000	<i>ft</i>	1524	<i>m</i>
Aquifer thickness (h_w)	15	<i>ft</i>	4.572	<i>m</i>
Aquifer outer boundary pressure (p_{r_e})	2165	<i>psi</i>	14927	<i>kpa</i>
Aquifer fracture pressure (p_f)	3665	<i>psi</i>	25268	<i>kpa</i>
Oil density (ρ_o)	53.7	<i>lbm/ft³</i>	860	<i>kg/m³</i>
Water viscosity (μ_w)	1	<i>cp</i>	1	<i>cp</i>
Oil viscosity (μ_o)	1.40	<i>cp</i>	1.40	<i>cp</i>
Water relative permeability exponent (n_w)	5.5	<i>dimensionless</i>	5.5	<i>dimensionless</i>
Oil relative permeability exponent (n_o)	2.5	<i>dimensionless</i>	2.5	<i>dimensionless</i>
Connate water saturation (S_{wc})	0.05	<i>fraction</i>	0.05	<i>fraction</i>
Residual oil saturation (S_{or})	0	<i>fraction</i>	0	<i>fraction</i>
Oil concentration (C_o)	500	<i>ppm</i>	500	<i>ppm</i>
Equilibrium oil saturation (S_{oe})	0.08	<i>fraction</i>	0.08	<i>fraction</i>
Oil water interfacial tension (σ_{ow})	35	<i>dyne/cm</i>	35	<i>dyne/cm</i>
Critical capillary number (N_{ca}^*)	10^{-4}	<i>dimensionless</i>	10^{-4}	<i>dimensionless</i>
Bump rate constant (λ)	5	<i>dimensionless</i>	5	<i>dimensionless</i>
Size ratio (N_d)	0.152	<i>dimensionless</i>	0.152	<i>dimensionless</i>
Adsorptive constant (β)	58	<i>dimensionless</i>	58	<i>dimensionless</i>
Dispersivity (d)	0.00066	<i>ft</i>	0.0002	<i>m</i>

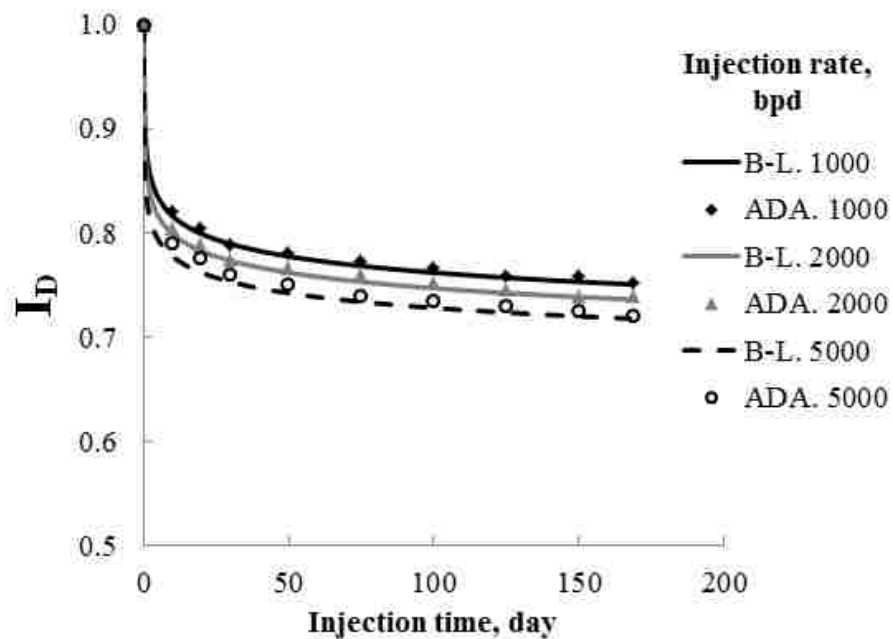


Figure 4.46. Prediction of water injectivity decline development using B-L and ADA models at different injection rates

From Equations 4.51 and 4.52 we can see that, a thin layer with low permeability in the near well region can significantly impact the average permeability of the whole aquifer and causes severe injectivity decline. It also indicates that, fast formation damage would occur even for wells operated at moderate injection rate with low oil concentration. Due to the radial expanding of injection fluids, oil accumulates quickly in the near well zone and slowly with the increase of injection radius. As a result, water relative permeability reduces following the speed of oil invasion. Per Darcy's Law, injection pressure in the near well region will increase faster and be higher than locations far away. Figure 4.47 and Figure 4.48 confirm this deduction by both B-L and ADA models, which also show the good agreement between the two models.

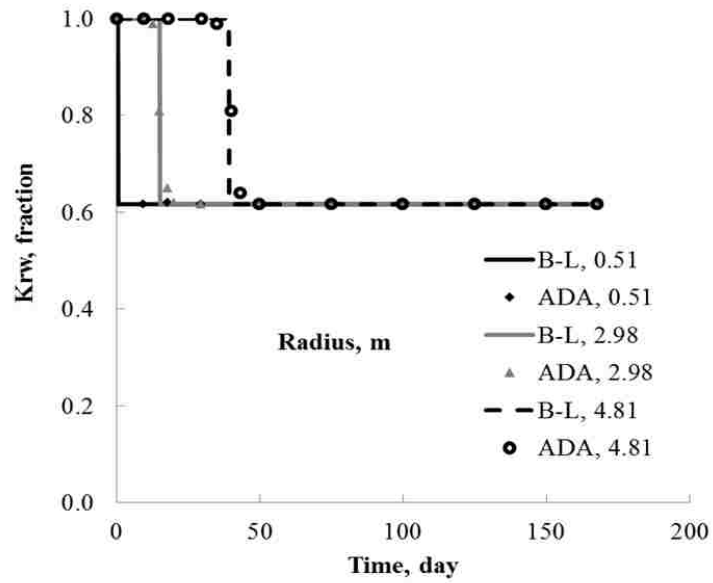


Figure 4.47. Prediction of water relative permeability in different radii using B-L and ADA models ($q_w = 2000$ bpd)

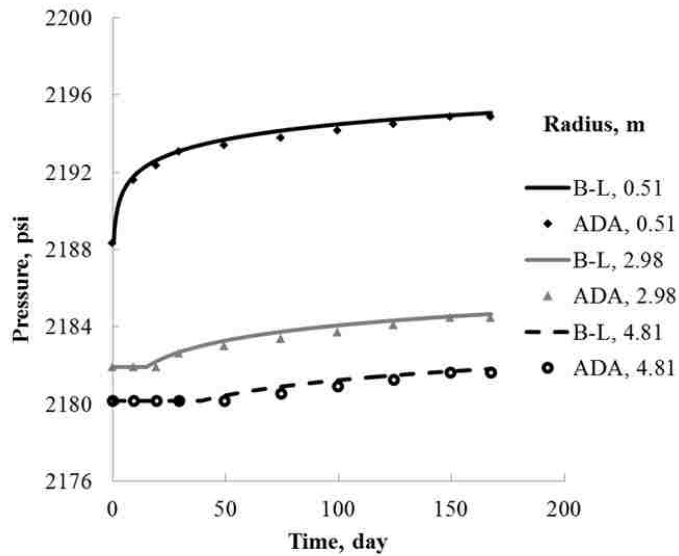


Figure 4.48. Prediction of pressure in different radii using B-L and ADA models ($q_w = 2000$ bpd)

4.4 Summary

Although water injectivity decline caused by solid particles are widely studied, there are only few models of injectivity damage due oily water – particularly with very small oil

content. This study introduces two analytical models explaining injectivity decline caused by spatial advancement of water permeability damage over time in both linear and radial geometries. The first model is derived from the mass balance of oil phase while considering the effects of oil droplets transport and capture due combined effects of advection, dispersion and adsorption (ADA), while the second model is based on the well-known Buckley-Leverett (B-L) theory, both models are coupled with the two phase relative permeability relationship to represent the injectivity decline. The study leads to the following conclusions:

1. The proposed models are verified using published experiments showing good match and replicating reported observations. The decline of water injectivity is mainly caused by oil retention in the formation and follows the two phase relative permeability relationship. Both models can be used to predict the formation damage respect to time and distance;
2. The ADA model can be calibrated by matching results from standard laboratory injection with oil-contaminated water and rock cores. The match can be improved with relative permeability and bump rate testing;
3. Oily water injection to an aquifer follows the primary drainage process, both oil and water flow during the injection and the process can be described by Buckley-Leverett theory;
4. The models replicate experimental observation that very small oil content in injected water does not reduce the ultimate damage but merely delays the development of oil saturation in the rock;
5. The models reproduce the oil droplet to pore size ratio effect on injectivity damage. The effect is represented by the correlation of equilibrium oil saturation

and oil droplet to pore size ratio. Oil saturation reaches equilibrium condition faster for large oil droplets;

6. Oil saturation advances in radial flow with a sharp interface and large oil droplets are captured faster leading to higher equilibrium oil saturation, which results in severer water permeability damage;
7. The study demonstrates rock wettability effect by showing that injectivity damage with oily water is more severe in water wet formation than in oil wet rocks. The wettability effect is implicit in the model through the fractional flow relationship;
8. Injectivity decline due oily water injection is predominantly controlled by equilibrium oil saturation and water relative permeability curve, higher equilibrium oil saturation leads to more decline;
9. The effect of injection rate on injectivity damage is included in the model through the correlation of capillary number and equilibrium oil saturation. The rate has little effect when the capillary number is less than 10^{-4} , however, it can significantly reduce the equilibrium oil saturation when it becomes greater than 10^{-4} ;
10. High injection rate helps injectivity improvement in linear flow as the flow velocity is constant over the core while it may cause more damage in radial flow as the flow velocity (capillary number) decreases rapidly with injection radius and more oil is injected to the formation.

CHAPTER 5. SCREENING RESERVOIR AQUIFER FOR DWL WATER INJECTION

Two analytical models have been developed to predict injectivity damage caused by oily water injection based on oil droplets transport in porous media and Buckley-Leverett theory. This chapter intends to convert the formation damage to a skin factor, which can be used to evaluate the performance of injection wells, assess the formations for oily water injection and screen formation candidates for DWL.

5.1 Representing Injectivity Decline by Skin Factor

The concept of skin factor describes the effects of formation permeability damage or stimulation around the wellbore. Usually, a skin region is represented as a zone with altered permeability in the formation near the wellbore. In this study, we use a radial composite model to describe the water permeability reduction effect in the near wellbore region, which leads to a formula of injectivity with a skin factor (White, 2010):

$$I_w = \frac{2 \cdot 10^{-6} \pi h_w K}{\mu_w \left(\ln \frac{r_e}{r_w} + S \right)} \dots\dots\dots (5.1)$$

In a certain time t , the water permeability is assumed to be altered from the original value K_{wi} to the skin permeability K_{ws} in a region from well radius r_w to the outer boundary of damaged zone r_s . Based on the correlation proposed by Hawkins (1956), the skin factor can be expressed as:

$$S = \left(\frac{K_{wi}}{K_{ws}} - 1 \right) \ln \frac{r_s}{r_w} \dots\dots\dots (5.2)$$

When the formation is damaged by oil, K_{ws} is smaller than K_{wi} and r_s increases with injection. Thus, skin factor is mostly positive during the injection if the formation is not

fractured (Civan, 2007). From the results of previous sections, we know that the oil saturation front moves in the aquifer with a sharp interface. We assume the radius of skin zone is equal to the position of oil saturation front determined either from B-L model or ADA model. As water permeability is a continuous function of skin zone radius, the skin permeability can be calculated using Equation 4.52 as:

$$K_{ws}(t) = \frac{\ln \frac{r_s(t)}{r_w}}{\int_{r_w}^{r_s} \frac{dr}{r K_w(r)}} = \frac{\ln \frac{r_s(t)}{r_w}}{\sum_{i=1}^n \frac{\ln \frac{r_{i+1}}{r_i}}{K_{wi}}} = \frac{10^6 q \mu_w \ln \frac{r_s(t)}{r_w}}{2 \pi h_w \sum_{i=1}^n \Delta p_i} \dots\dots\dots (5.3)$$

Where, K_{wi} is the effective water permeability in each subsection from r_i to r_{i+1} and it can be calculated by Equation 4.51, Δp_i is the pressure drop in each subsection if measurable, kpa; $r_s(t)$ is the radius of oil invaded zone at time t , it is equal to the oil front position using B-L model as shown in Equation 4.81 or using ADA model as shown in Equation 4.47, m. Notice that the oil saturation front is not strictly vertical in ADA model as shown in Figure 4.25. Due to the small difference between r_{f1} and r_{f2} , we use their average as the radius of the skin zone. Thus, the time dependent skin zone radius can be determined using one of the following expressions:

$$\begin{cases} r_s(t)_{BL} = \sqrt{r_w^2 + \frac{2(\delta r_w - 1) \exp(\delta r_w)}{\delta^2} + \frac{qtC_0}{\pi h_w \phi S_{oe}^*}} \\ r_s(t)_{ADA} = \frac{r_{f1} + r_{f2}}{2} = \frac{a^2 + b^2}{2} \end{cases} \dots\dots\dots (5.4)$$

Where, a and b can be calculated from the following equation:

$$\begin{cases} a^4 + 4Ba^3 - E = 0 \\ b^4 - 4Bb^3 - E = 0 \end{cases} \dots\dots\dots (5.5)$$

Where, $a = \sqrt{r_{f1}}$, $b = \sqrt{r_{f2}}$, $B = \sqrt{4/(3d)}$, $E = qt/(\pi h_w \phi R)$.

Figure 5.1 and Figure 5.2 show the radii of skin zone computed from two models using data in Table 4.2 and Table 4.3, respectively, which indicate that the results are almost identical due to sharp interface in the oil saturation front. The reason is that, with increase of radius in the aquifer, the flow velocity decreases and the volume of clean sand increases fast, which make the dispersive effect smaller and adsorptive effect stronger as more sites are available for oil trapping (Hoopes and Harleman, 1967; Schmidt, et al., 1984). The dispersive effect becomes strong when the injection rate is high which makes the oil saturation front less sharp. The front advances in the aquifer with continuing of injection as more oil is injected.

Some difference may exist between the skin zone radii computed from ADA and B-L models as we use the middle point of r_{f1} and r_{f2} as the radius of skin zone in ADA model. However, the difference is small: only 4% after injecting at 5,000 bpd for 1,700 days. Usually, wells for PWRI are stimulated several times a year to remove the skin (Sharma, et al., 2000). Also, the difference is negligible in skin factor computation as shown in Figure 5.3, because it is proportional to “ $\ln[r_s(t)/r_w]$ ” as shown in Equation 5.7. Since the two models give similar results, we use B-L model to determine skin zone radius in the following study for its simplicity comparing to the ADA model. By including the skin factor, the pressure drop required to maintain constant injection rate is:

$$\Delta p_t = \frac{10^6 q \mu_w}{2\pi h_w K} \left[\ln \frac{r_e}{r_w} + S(t) \right] \dots\dots\dots (5.6)$$

Where, for variable skin:

$$S(t) = \left[\frac{K_{wi}}{K_{ws}(t)} - 1 \right] \ln \frac{r_s(t)}{r_w} \dots\dots\dots (5.7)$$

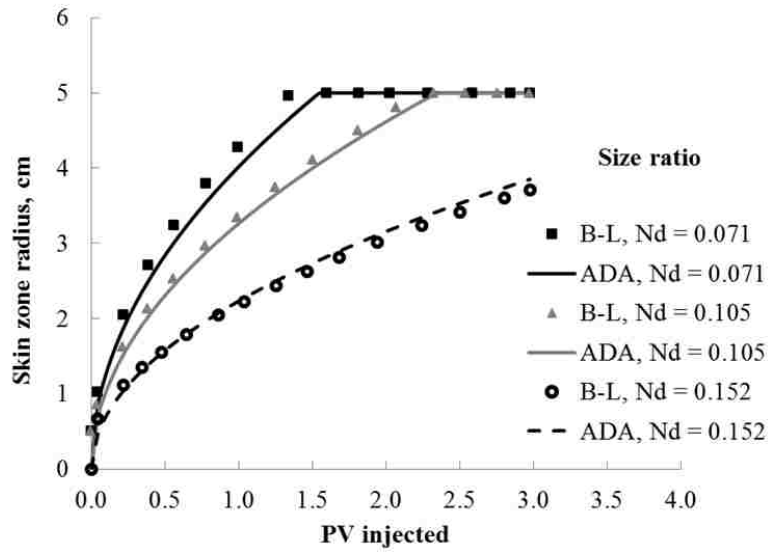


Figure 5.1. Comparison of skin zone radius between B-L and ADA models

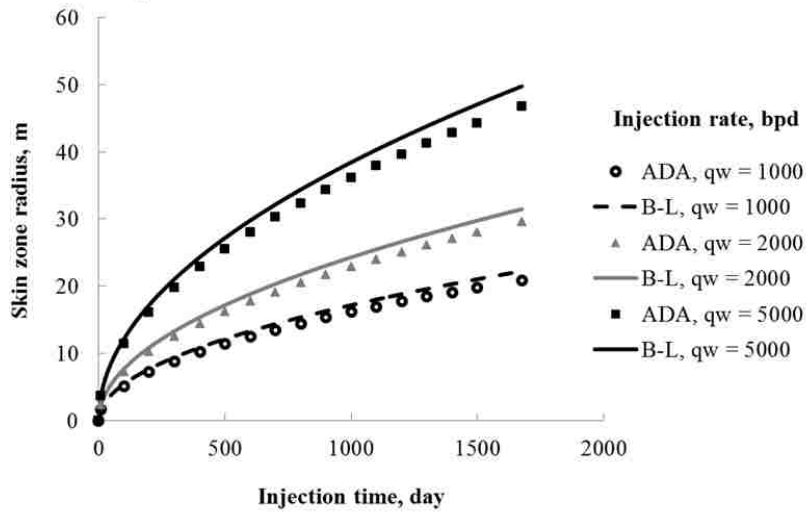


Figure 5.2. Comparison of skin zone radius between B-L and ADA models for different injection rates

Before injection, there is no skin in the aquifer, i.e. $S = 0$, which leads to the following expression of injectivity decline based on its definition:

$$I_D = \frac{\frac{q_w}{\Delta P_t}}{\frac{q_w}{\Delta P_0}} = \frac{\ln \frac{r_e}{r_w}}{\ln \frac{r_e}{r_w} + S(t)} \dots\dots\dots (5.8)$$

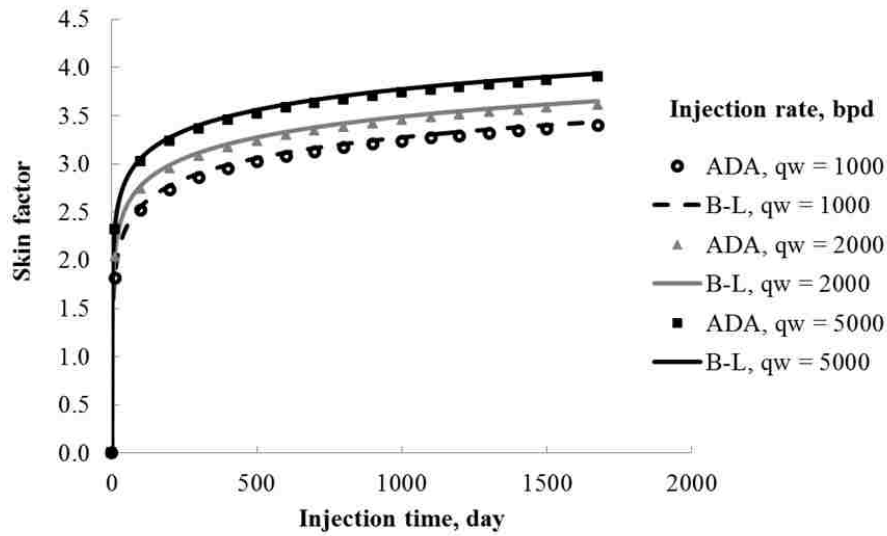


Figure 5.3. Comparison of skin factor between B-L and ADA models for different injection rates

Figure 5.4 shows the development of skin factor computed from Equation 5.7 during injection for different size ratio. It is clear that skin increases fast in the beginning of injection due to the quick increase of damaged zone in this period. Also, higher size ratio leads to greater skin. This is because the capillary number decreases rapidly in radial flow which means capillary force is greater than viscous force in this flow geometry. Based on droplet capture mechanisms, there will be more oil retention for big oil droplets in the low capillary number flow region. Figure 5.5 shows that injectivity decline can be satisfactorily represented by the variable skin model.

5.2 Formation Assessment for Oily Water Injection

For many situations, water needs to be injected to thin formations for the purposes of produced water disposal, waterflooding and so on (Russell, 1952; Haggerty and Seyler, 1997; Bennion, et al., 2000; Lee, et al., 2003; Veil and Quinn, 2009). Usually, injection pressure is a limitation for an injection well.

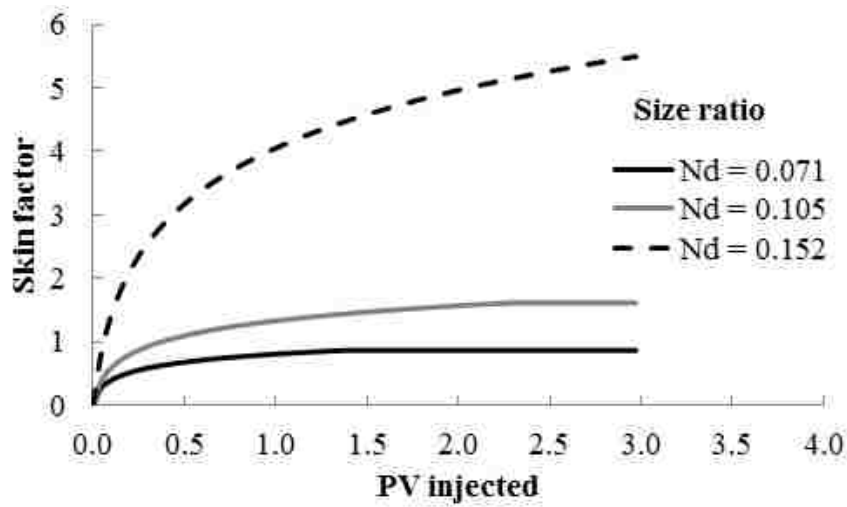


Figure 5.4. Development of skin factor during injection for different size ratios

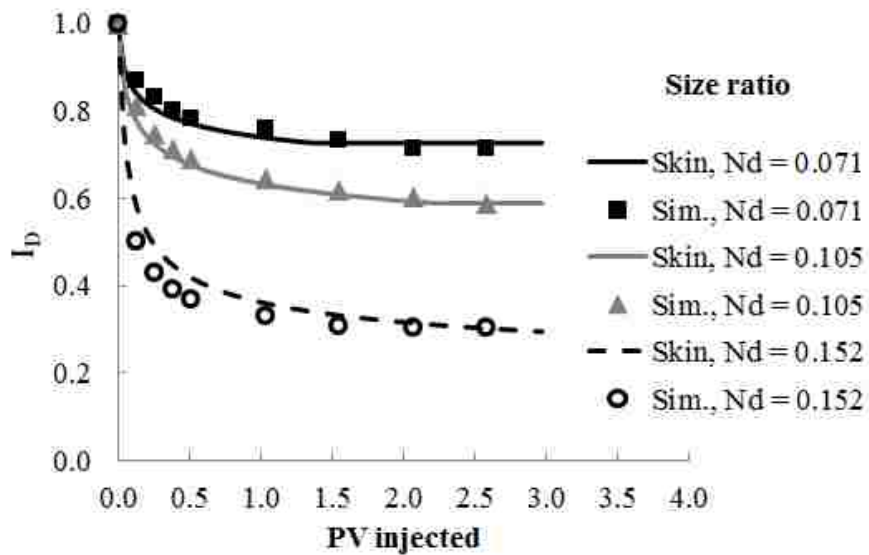


Figure 5.5. Injectivity decline with variable skin

According to Underground Injection Control (UIC) regulations, injection pressure at the wellhead shall not exceed a maximum which shall be calculated so as to assure that the pressure during injection does not initiate new fractures or propagate existing fractures in the confining zone adjacent to the underground sources of drinking water (USDW's) (Herman, 1988). For wells used for waterflooding or water coning control, such as DOWS and DWL, fracture should also be avoided to prevent the direct connection between injection and

production completions (Veil and Layne, 2001; Furtado, et al., 2005). From Equation 5.6, the injection pressure in the well can be easily determined as follows:

$$p_{r_w} = p_{r_e} + \frac{10^6 q \mu_w}{2\pi h_w K} \left[\ln \frac{r_e}{r_w} + S(t) \right] \dots\dots\dots(5.9)$$

Equations 5.7 and 5.9 provide a convenient way to evaluate the relationship between injection rate, pressure and time while considering injectivity decline effect. Skin factor is mostly positive and it can increase to a large value when the water permeability in the damaged zone is very small (Civan, 2007). This is possible when the disposal zone is water wet and injected water contains big oil droplets. Although the skin factor only depends on the amount of water permeability alteration in the damaged zone, the injection pressure depends on many fluid and rock properties as shown in Equation 5.9. For example, a well can inject to a damaged formation ($S \approx 200$) at 10,000 bpd without stimulation due to the high absolute permeability of the formation ($K \approx 10$ D) (White, 2010), while another well in Gulf of Mexico, with lower skin ($S = 46$), needs frequent stimulation to maintain the injection rate at 7,000 bpd because of the moderate formation permeability ($K \approx 1$ D) (Sharma, et al., 2000). Thus, it is important to select a right formation to carry out injection to meet the target.

Here, we try to develop a procedure to assess formations for a given target of oily water injection when the formation is fully penetrated, i.e. whether the formation can sustain the injection rate for a certain period of time without fracturing the formation and how frequent the stimulation should be to maintain the injection rate.

Step 1: Determine the fracture pressure of the formation;

Usually, the fracture pressure can be determined from a step-rate test. If the test data is not available, the following equation can be used to estimate the maximum bottomhole pressure without causing a fracture (Herman, 1988):

$$p_f = p_{r_w_{max}} = 16.58H_a \dots\dots\dots(5.10)$$

Where, p_f is the fracture pressure, kpa; H_a is the depth of the aquifer, m.

Step 2: Predict skin development with injection using Equations 5.3, 5.4 and 5.7;

Step 3: Compute the injection pressure using Equation 5.9. When the bottomhole pressure reaches the fracture pressure, stop injection and stimulate the formation to remove the skin.

We use the hypothetical aquifer with Bentheimer sandstone as shown in Table 4.3 to demonstrate the application of the skin model: a water injection well with radius 0.292 ft located in the center of an aquifer with radius 1000 ft, injecting water with 500 ppm oil contamination from 1000 to 5000 bpd, the skin and injection pressure are computed.

Figure 5.6 illustrates the development of skin factor with time, which clearly shows that skin factor increases quickly in the first 10 days and then grows gradually for all three injection rates. Obviously, higher injection rate leads to greater skin. The reason is that, when oil concentration is the same, higher injection rate means more oil is injected to the aquifer which leads to thicker damaged zone. Therefore, the value of skin factor becomes high based on Equation 5.2. According to the increase of skin factor, the injectivity decline for different injection rates is shown in Figure 4.46. The injectivity loses about 20% in the first several days for all three cases and then decreases slowly. This phenomenon was also observed by other researchers in a numerical study (Liu and Civan, 1994).

Based on the given properties of the well-aquifer system, the dynamic increase of injection pressure can be determined as shown in Figure 5.7. It can be found that, although the injectivity decline is severe in this aquifer, high injection rate is still achievable without

causing fracture in the formation. For example, the injection pressure is about 2270 psi which is below the fracture pressure of 3665 psi, when water is injected at 5000 bpd for 5 months.

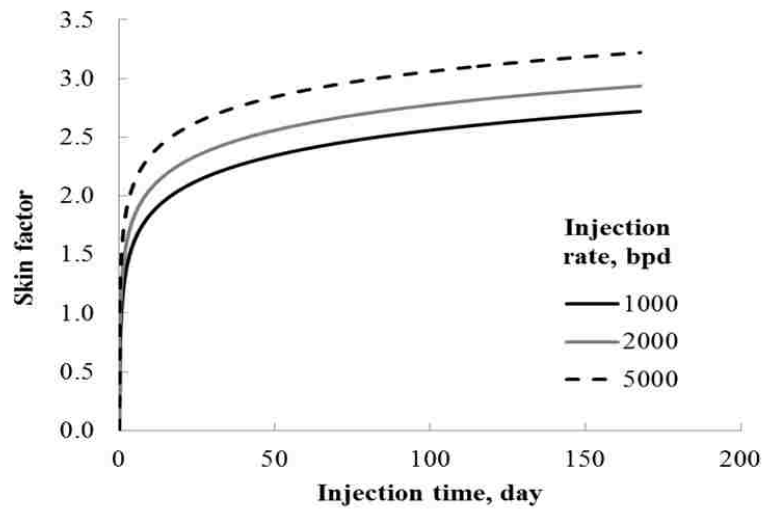


Figure 5.6. Skin develops with time for different injection rates in Bentheimer sandstone

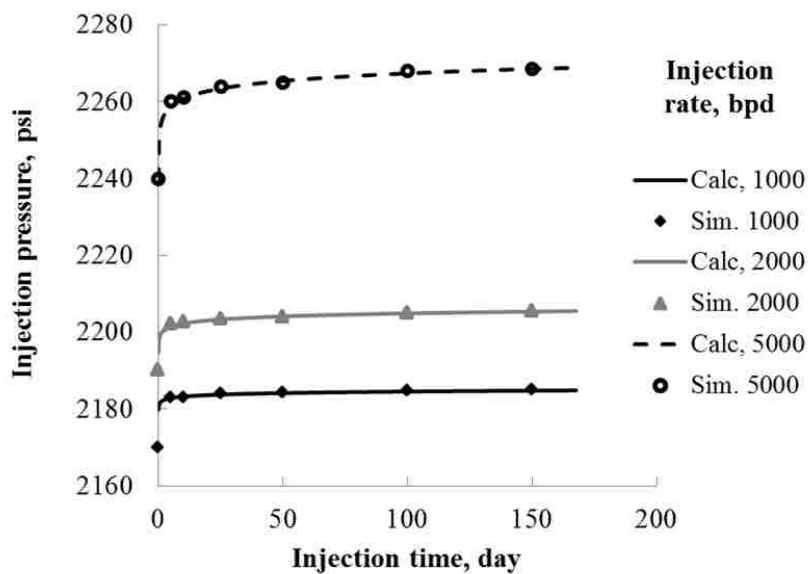


Figure 5.7. Injection pressure increases with time for different injection rates in Bentheimer sandstone

For another case, we use the fluids and rock properties from Entrada formation in New Mexico, which are shown in Table 5.1. The skin and injection pressure developments are

shown in Figure 5.8 and Figure 5.9, respectively, which are similar to those in Bentheimer sandstone. Although the skin factor is less than 2.5 when water is injected at 5000 bpd as shown in Figure 5.8, the injection pressure reaches to the fracture pressure in 5 days as shown in Figure 5.9, due to the low absolute permeability and water-wet characteristic of the formation ($n_w = 4$).

Table 5.1. Fluids and rock properties of Entrada Formation

Parameter	Value	Unit	Value	Unit
Water injection rate (q)	1000~5000	<i>bpd</i>	0.00184~0.0092	m^3/s
Absolute permeability (K)	256	<i>md</i>	0.256	<i>D</i>
Porosity (ϕ)	0.212	<i>fraction</i>	0.212	<i>fraction</i>
Well radius (r_w)	0.292	<i>ft</i>	0.089002	<i>m</i>
Aquifer radius (r_e)	1000	<i>ft</i>	304.8	<i>m</i>
Aquifer depth (H_a)	5914	<i>ft</i>	1797	<i>m</i>
Aquifer thickness (h_w)	15	<i>ft</i>	4.572	<i>m</i>
Aquifer outer boundary pressure (p_{r_e})	2560	<i>psi</i>	17656	<i>kpa</i>
Aquifer fracture pressure (p_f)	4335	<i>psi</i>	29888	<i>kpa</i>
Oil density (ρ_o)	53.7	<i>lbm/ft³</i>	860	<i>kg/m³</i>
Water viscosity (μ_w)	1	<i>cp</i>	1	<i>cp</i>
Oil viscosity (μ_o)	6.11	<i>cp</i>	6.11	<i>cp</i>
Water relative permeability exponent (n_w)	4	<i>dimensionless</i>	4	<i>dimensionless</i>
Oil relative permeability exponent (n_o)	4.5	<i>dimensionless</i>	4.5	<i>dimensionless</i>
Connate water saturation (S_{wc})	0.068	<i>fraction</i>	0.068	<i>fraction</i>
Residual oil saturation (S_{or})	0	<i>fraction</i>	0	<i>fraction</i>
Oil concentration (C_0)	500	<i>ppm</i>	500	<i>ppm</i>
Equilibrium oil saturation (S_{oe})	0.08	<i>fraction</i>	0.08	<i>fraction</i>
Oil water interfacial tension (σ_{ow})	35	<i>dyne/cm</i>	35	<i>dyne/cm</i>
Critical capillary number (N_{ca}^*)	10^{-4}	<i>dimensionless</i>	10^{-4}	<i>dimensionless</i>
Bump rate constant (λ)	5	<i>dimensionless</i>	5	<i>dimensionless</i>
Size ratio (N_d)	0.152	<i>dimensionless</i>	0.152	<i>dimensionless</i>

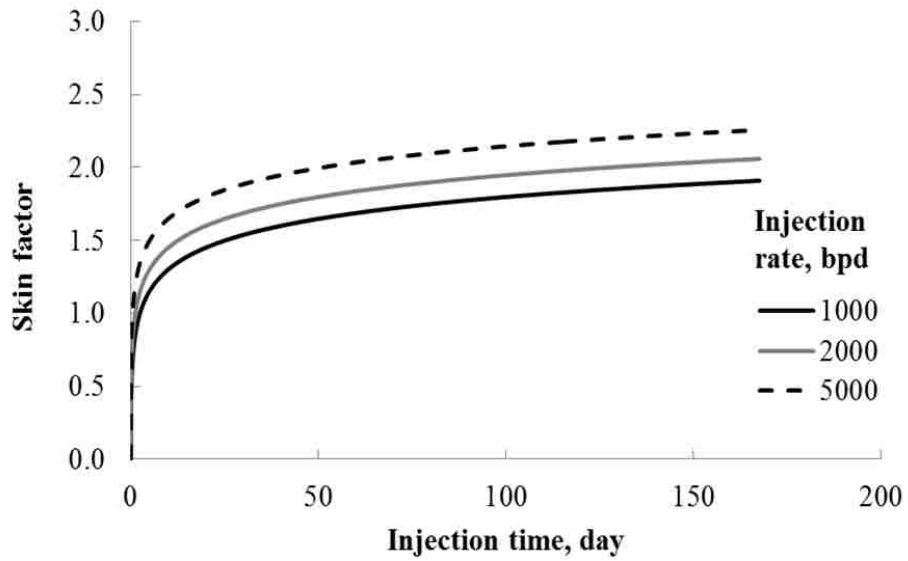


Figure 5.8. Skin develops with time for different injection rates in Entrada formation

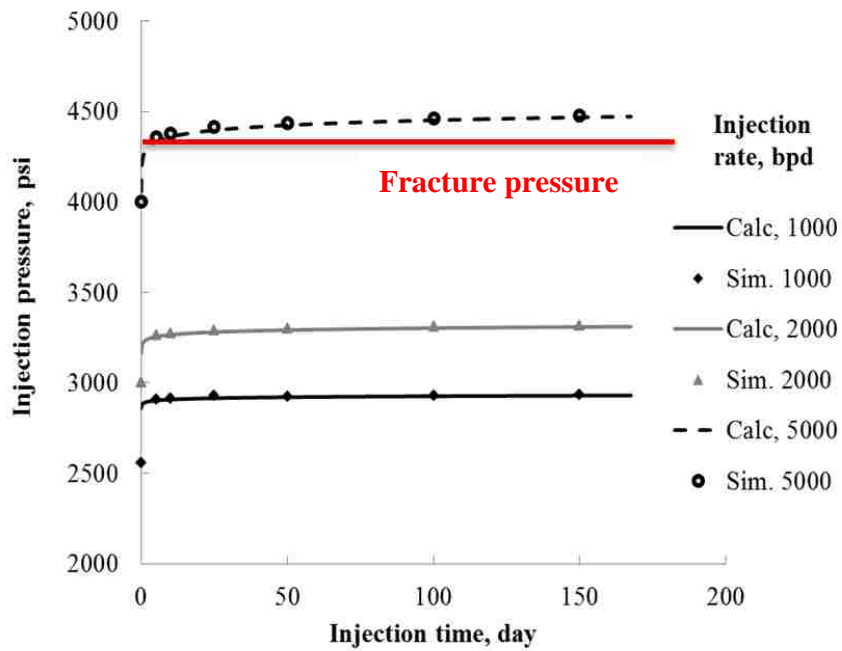


Figure 5.9. Injection pressure increases with time for different injection rates in Entrada formation

If we changed the rock wettability to oil-wet ($n_w = 2$) and kept the other parameters the same, then both skin factor and injection pressure would decrease as shown in Figure

5.10 and Figure 5.11, respectively. It is clear that skin factor is reduced significantly in oil-wet formation as water becomes easier to flow, which leads to the decreasing of injection pressure when the injection rate is constant. The water injection rate can be maintained at 5000 bpd without fracturing the formation after changing the wettability.

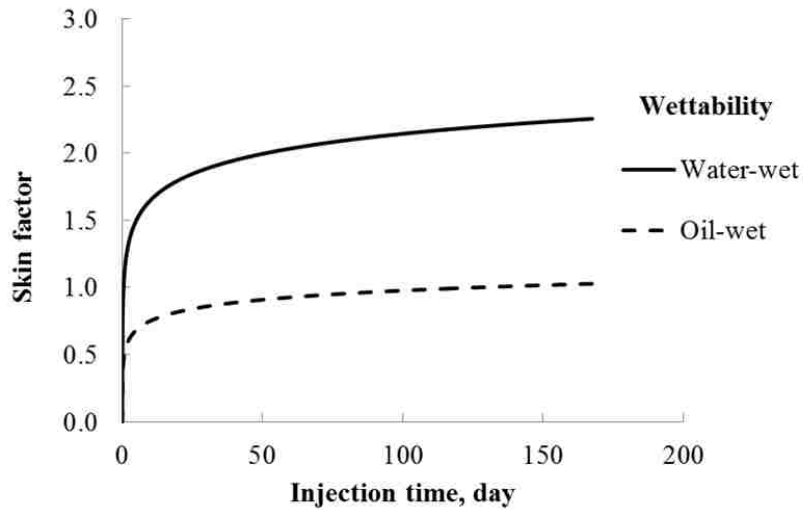


Figure 5.10. Conceptual effect of wettability change on skin damage in Entrada ($q_w = 5000$ bpd)

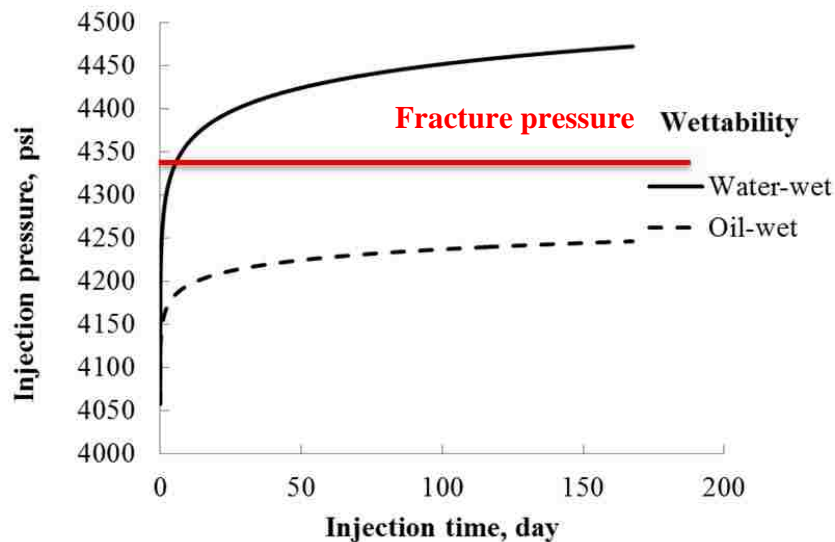


Figure 5.11. Conceptual effect of wettability change on injection pressure in Entrada ($q_w = 5000$ bpd)

From the above cases, we can see that oily water injection is possible when the target formation is carefully selected (Abou-Sayed, et al., 2007). Both absolute and relative permeabilities are critical for the injection operations. For example, the absolute permeability in the Bentheimer sandstone aquifer is high (5149 md), there is still about 1545 md permeability available for water injection even if 70% of the injectivity is lost and skin reaches to 20. But for Entrada formation, only 1.5 skin factor would fracture the formation when the injection rate is 5000 bpd. Unlike solid particle caused formation damage, there is an equilibrium oil saturation in the aquifer, when the oil saturation reaches this value it will be stable and water injectivity is stabilized. Therefore, oil-wet formations are more favorable for oily water injection due to the high water relative permeability for a given equilibrium oil saturation, which has been confirmed by both the laboratory research and field tests (Wang, et al., 2010; Ju, et al., 2012).

5.3 Including Partial Penetration Effect in Formation Assessment

In the above cases, the aquifers are assumed to be fully penetrated. However, in many cases, wells are partially completed in aquifers, which restrict the flow and increase the injection pressure inside the wells. The skin factor caused by the partial penetration has been widely studied and many correlations have been developed (Gui, et al., 2008). Papatzacos (1987) provided one of the most popular correlations to calculate this skin factor which has been used for many years. The well-reservoir system used in his model is shown in Figure 5.12 and the skin factor correlation is:

$$S_{pp} = \left(\frac{1}{h_{pD}} - 1 \right) \ln \frac{\pi}{2r_D} + \frac{1}{h_{pD}} \ln \left[\frac{h_{pD}}{2 + h_{pD}} \left(\frac{A-1}{B-1} \right)^{1/2} \right] \dots\dots\dots (5.11)$$

Where,

$$r_D = (r_w / h_w)(k_v / k_h)^{1/2} \dots\dots\dots (5.12)$$

$$h_{wD} = h_{wi} / h_w \dots\dots\dots (5.13)$$

$$h_{1D} = h_1 / h_w \dots\dots\dots (5.14)$$

$$A = 1 / (h_{1D} + h_{wD} / 4) \dots\dots\dots (5.15)$$

$$B = 1 / (h_{1D} + 3h_{wD} / 4) \dots\dots\dots (5.16)$$

Where, S_{pp} is the skin factor caused by partial penetration, dimensionless; h_1 is the distance from oil water contact to the penetration top, m.

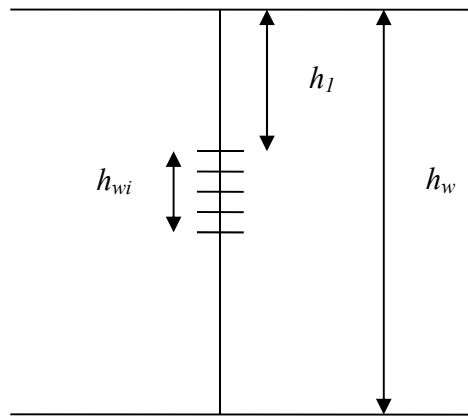


Figure 5.12. Partial penetration of a well

As the partial penetration skin does not change with time, the injection pressure can be calculated by including it in Equation 5.9 as:

$$p_{r_w} = p_{r_e} + \frac{10^6 q \mu_w}{2\pi h_w K} \left[\ln \frac{r_e}{r_w} + S_{pp} + S(t) \right] \dots\dots\dots (5.17)$$

Apply the same formation assessment procedure, the calculated injection pressure was compared to simulation results to verify the analytical model. Using data in Table 4.3 and

Table 5.1, assume $h_w = 15$ ft, $h_1 = 9$ ft and $h_{wi} = 6$ ft, the injection pressure at different rates in the two hypothetical aquifers are shown in Figure 5.13 and Figure 5.14, respectively.

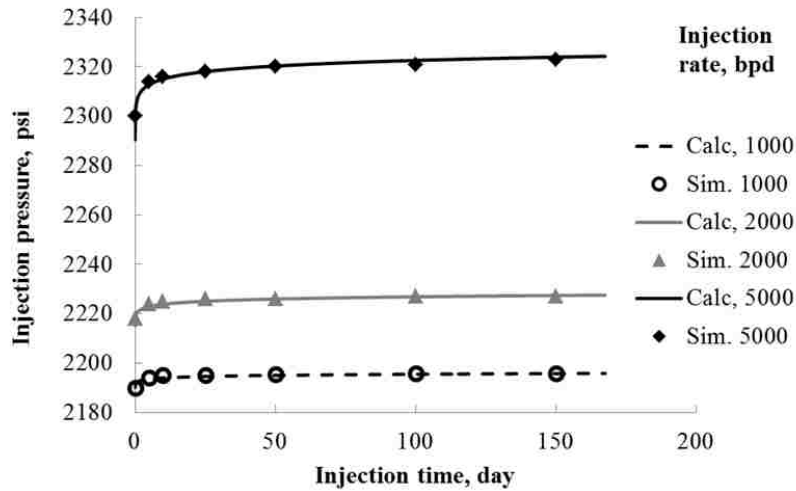


Figure 5.13. Injection pressure increases with time for different injection rates in Bentheimer sandstone for partial penetrated well

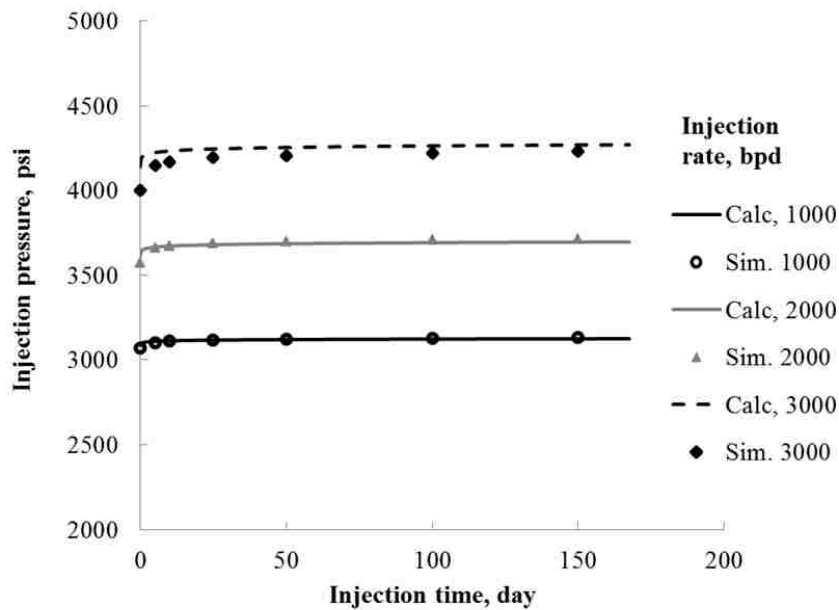


Figure 5.14. Injection pressure increases with time for different injection rates in Entrada formation for partial penetrated well

Comparing to the fully penetrated wells, the partial penetrated wells need significantly high injection pressure to inject the same amount of water. To avoid fracturing the formation, the maximum injection rate for short completion is much less than that for long completion. For example, if an aquifer has properties shown in Table 5.1, the maximum injection rate for a fully penetrated well is about 4300 bpd and only 3000 bpd for a 1/3 penetrated well. Thus, full penetration is recommended when a water injection well is completed in a thin formation.

5.4 Formation Screening for DWL Considering Injectivity Decline

For DWL, the aquifer should be thick enough to install the water looping system and the water injection completion has to be partially penetrated. Also, as the drainage water is injected back to the aquifer without treatment, the oil droplets might be contained in the water. According to the experimental work of Engelsvoll (2011), the average oil droplet size at the outlet of centrifugal pump varies between 10 to 30 microns for different pump heads and flow rates. The pore throat size of the injection formation can be estimated by Katz-Thompson correlation as (Katz and Thompson, 1986; Nelson, 2009):

$$d_{pt} = \sqrt{\frac{K}{4.48\phi^2}} \dots\dots\dots(5.18)$$

Where, d_{pt} is the pore throat size, μm ; K is the absolute permeability of the rock, md; ϕ is the porosity, fraction.

When the oil droplet and pore throat sizes are known, the equilibrium oil saturation can be determined by Equation 4.15 and Figure 4.5. The following criteria are set to screen the formation candidates for DWL:

1. The formation can tolerate oily water injection, i.e. oily water can be injected at a target rate without causing fracture in a certain period;

2. The formation stimulation cycle (time needed for the injection pressure rises from the initial value to the formation fracture pressure) is long enough to make the well profitable.

Similar to formation assessment for oily water injection, the following procedure is used to evaluate whether a formation is suitable for DWL when there are oil droplets in the injection water:

Step 1: Determine the fracture pressure of the formation;

Step 2: Determine the partial penetration skin using Equation 5.11;

Step 3: Predict skin development with injection using Equations 5.3, 5.4 and 5.7;

Step 4: Compute the injection pressure using Equation 5.17. When the bottomhole pressure reaches the fracture pressure, stop injection and stimulate the formation to reduce the skin.

The Nebo-Hemphill field in North Louisiana is a bottom-water-drive reservoir with active water coning. To control this problem, DWS technology was used and good results were reported (Swisher and Wojtanowicz, 1995). However, due to the strong water coning, large amount of water needs to be drained and lifted to the surface in order to reduce water cut in the top completion. Since there is a thick aquifer with high permeability under the oil zone as shown in Table 5.2, DWL might be an option to produce oil with minimum produced water.

Assume two 12-ft completions are perforated 8 and 50 ft below the OWC to drain and inject water, the maximum water rate with complete oil/water separation at the top 1/2 of the water drainage completion is about 2700 bpd according to Equation 3.30, which indicates

that a trace of oil might enter the injection water when the drainage rate is greater than this value.

Table 5.2. Field data of Nebo-Hemphill field

Parameter	Value	Unit	Value	Unit
Water injection rate (q)	2000~5000	<i>bpd</i>	0.00368~ 0.0092	m^3/s
Absolute permeability (K)	3500	<i>md</i>	3.5	<i>D</i>
Porosity (ϕ)	0.3	<i>fraction</i>	0.3	<i>fraction</i>
Well radius (r_w)	0.292	<i>ft</i>	0.089002	<i>m</i>
Oil zone thickness (h_o)	18	<i>ft</i>	5.486	<i>m</i>
Aquifer radius (r_e)	850	<i>ft</i>	259	<i>m</i>
Aquifer depth (H_a)	2000	<i>ft</i>	607.6	<i>m</i>
Aquifer thickness (h_w)	64	<i>ft</i>	19.5	<i>m</i>
Drainage completion length (h_{wd})	12	<i>ft</i>	3.66	<i>m</i>
Injection completion length (h_{wi})	12	<i>ft</i>	3.66	<i>m</i>
Aquifer outer boundary pressure (p_{r_e})	866	<i>psi</i>	5971	<i>kpa</i>
Aquifer fracture pressure (p_f)	1466	<i>psi</i>	10108	<i>kpa</i>
Oil density (ρ_o)	58.058	<i>lbm/ft³</i>	930	<i>kg/m³</i>
Water viscosity (μ_w)	1	<i>cp</i>	1	<i>cp</i>
Oil viscosity (μ_o)	17	<i>cp</i>	17	<i>cp</i>
Water relative permeability exponent (n_w)	7	<i>dimensionless</i>	7	<i>dimensionless</i>
Oil relative permeability exponent (n_o)	4	<i>dimensionless</i>	4	<i>dimensionless</i>
Connate water saturation in aquifer (S_{wc})	0.2	<i>fraction</i>	0.2	<i>fraction</i>
Residual oil saturation in aquifer (S_{or})	0	<i>fraction</i>	0	<i>fraction</i>
Oil concentration (C_o)	500	<i>ppm</i>	500	<i>ppm</i>
Equilibrium oil saturation (S_{oe}^*)	0.29	<i>fraction</i>	0.29	<i>fraction</i>
Oil water interfacial tension (σ_{ow})	30	<i>dyne/cm</i>	30	<i>dyne/cm</i>
Critical capillary number (N_{Ca}^*)	10^{-4}	<i>dimensionless</i>	10^{-4}	<i>dimensionless</i>
Bump rate constant (λ)	5	<i>dimensionless</i>	5	<i>dimensionless</i>
Size ratio (N_d)	0.4	<i>dimensionless</i>	0.4	<i>dimensionless</i>

If the injection water contains 500 ppm oil and is injected from 2000 to 5000 bpd, then the injection pressure can be shown in Figure 5.15. It is clear that oily water can be safely injected to the aquifer without fracturing the formation even if the injection rate reaches to 5000 bpd, and the formation does not need to be stimulated for a long time due to the high absolute permeability. Thus, this reservoir is a good candidate for DWL.

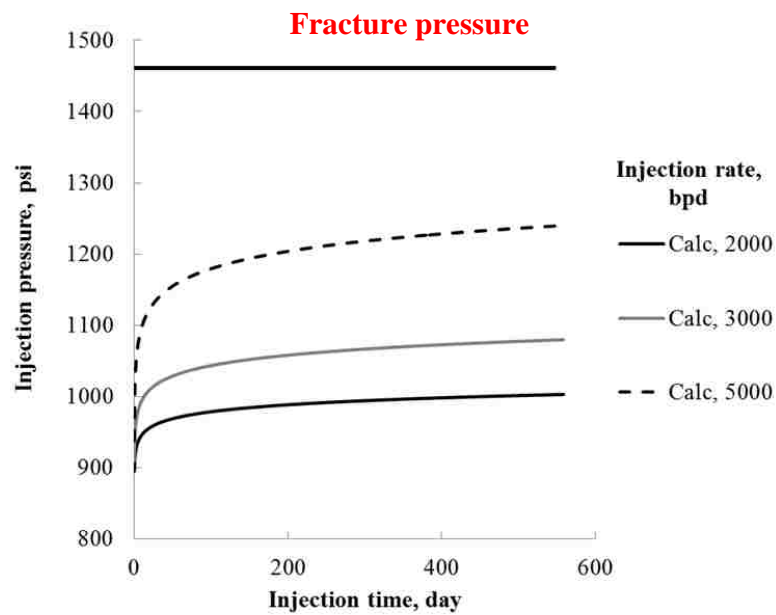


Figure 5.15. Formation screening for different injection rates in Nebo-Hemphill field

The M field is a shallow heavy oil field with thick bottom water located in the west coast of Africa. The fluid and rock properties of the field are shown in Table 5.3. The sand in the field is well-sorted as shown in Figure 5.16. Due to the high oil viscosity and thick aquifer, water coning is severe in this field and DWL might be used to control the problem. Assume a 20-ft water drainage completion and an injection completion with same length are perforated 10 and 100 ft below the OWC, the maximum water drainage rate with complete oil/water separation at the top 1/3 of the water drainage completion is about 4500 bpd. However, it is still possible that a trace of oil enters the injection water.

Table 5.3. Field data of M field

Parameter	Value	Unit	Value	Unit
Water injection rate (q)	2000~7000	<i>bpd</i>	0.00368~ 0.01288	m^3/s
Absolute permeability (K)	1218	<i>md</i>	1.218	<i>D</i>
Porosity (ϕ)	0.28	<i>fraction</i>	0.28	<i>fraction</i>
Well radius (r_w)	0.292	<i>ft</i>	0.089002	<i>m</i>
Oil zone thickness (h_o)	65.6	<i>ft</i>	20	<i>m</i>
Aquifer radius (r_e)	1000	<i>ft</i>	304.8	<i>m</i>
Aquifer depth (H_a)	1345	<i>ft</i>	410	<i>m</i>
Aquifer thickness (h_w)	295	<i>ft</i>	90	<i>m</i>
Drainage completion length (h_{wd})	20	<i>ft</i>	6	<i>m</i>
Injection completion length (h_{wi})	20	<i>ft</i>	6	<i>m</i>
Aquifer outer boundary pressure (p_{r_e})	582.5	<i>psi</i>	4016	<i>kpa</i>
Aquifer fracture pressure (p_f)	986	<i>psi</i>	6798	<i>kpa</i>
Oil density (ρ_o)	58.68	<i>lbm/ft³</i>	940	<i>kg/m³</i>
Water viscosity (μ_w)	0.7	<i>cp</i>	0.7	<i>cp</i>
Oil viscosity (μ_o)	230	<i>cp</i>	230	<i>cp</i>
Water relative permeability exponent (n_w)	7	<i>dimensionless</i>	7	<i>dimensionless</i>
Oil relative permeability exponent (n_o)	5	<i>dimensionless</i>	5	<i>dimensionless</i>
Connate water saturation (S_{wc})	0.224	<i>fraction</i>	0.224	<i>fraction</i>
Residual oil saturation (S_{or})	0	<i>fraction</i>	0	<i>fraction</i>
Oil concentration (C_o)	500	<i>ppm</i>	500	<i>ppm</i>
Equilibrium oil saturation (S_{oe}^*)	0.34	<i>fraction</i>	0.34	<i>fraction</i>
Oil water interfacial tension (σ_{ow})	50	<i>dyne/cm</i>	50	<i>dyne/cm</i>
Critical capillary number (N_{Ca}^*)	10^{-4}	<i>dimensionless</i>	10^{-4}	<i>dimensionless</i>
Bump rate constant (λ)	5	<i>dimensionless</i>	5	<i>dimensionless</i>
Size ratio (N_d)	0.5	<i>dimensionless</i>	0.5	<i>dimensionless</i>

The injection pressure can be shown in Figure 5.17 if water is injected from 2000 to 7000 bpd with 500 ppm oil. It is obvious that water can be injected safely below 5000 bpd without stimulation for more than 500 days. When the injection rate increases to 6000 bpd, the formation needs to be stimulated at 280 days and the stimulation cycle reduces to 75 days

if the injection rate increases to 7000 bpd. Due to the shallow depth of the reservoir, the water drainage-injection rate may not be achievable to 6000 bpd, which means the formation will not be fractured for a long time even if water is injected at the maximum rate. Thus DWL can be used to control water coning in this field.

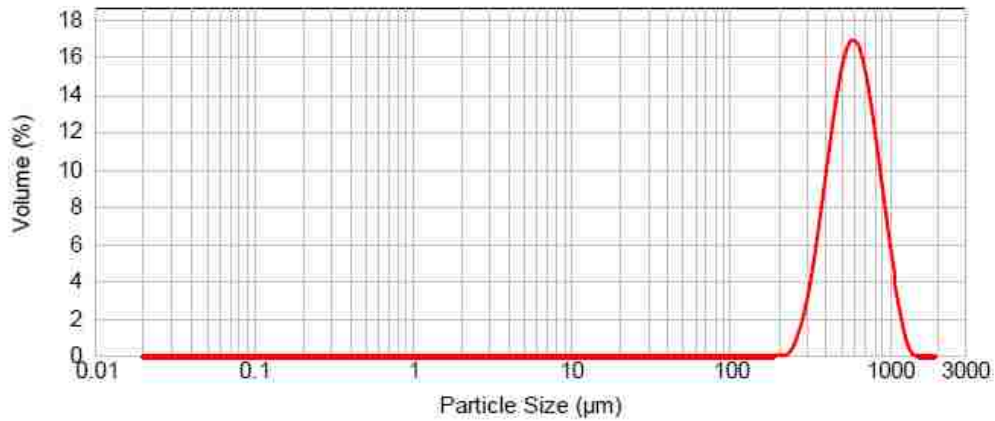


Figure 5.16. Particle size distribution of the core sample from M field

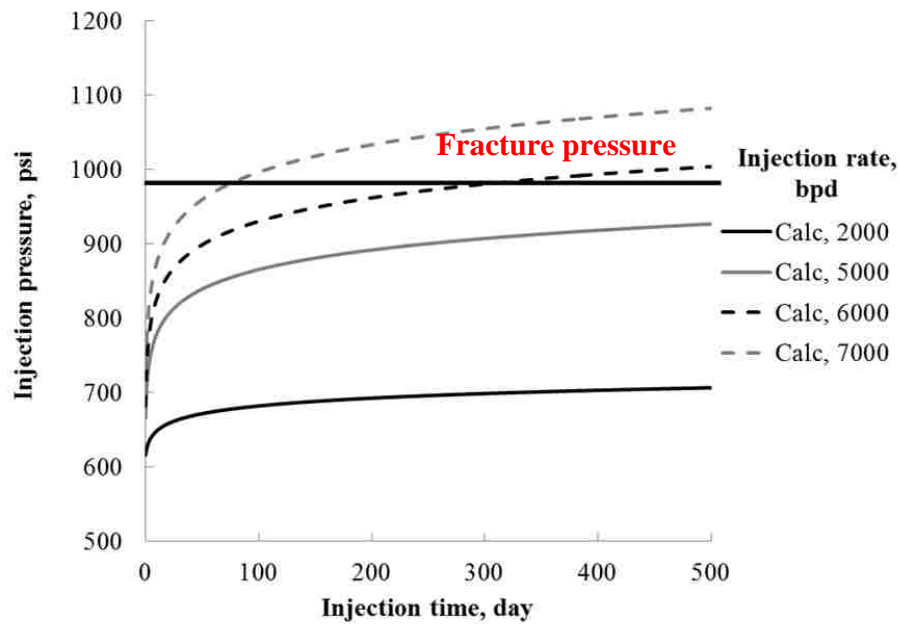


Figure 5.17. Formation screening for different injection rates in M field

5.5 Discussion

From Chapter 4 we know that, oil droplets can damage the injectivity by straining and interception captures. Straining capture happens when the oil droplet size is greater than the pore throat size causing a quick pressure increase on the injection face due to the Jamin effect, which is explained in Chapter 4. If the initial oily water injection rate is q_1 with injection pressure p_1 as shown in Figure 5.18, the injection pressure will increase to p_2 when pores are plugged by oil droplets and injection rate will reduce to q_2 . If p_2 is greater than the capillary resistance then oil droplets will be deformed and squeezed through the rock, as a result, injection pressure reduces and injection rate increases again, which means there will be a dynamic pressure change between p_1 and p_2 in the injection process. When there are a large number of oil droplets in the injection water, the oil droplets may soon plug all the pores on the injection surface and the injection pressure increases to the maximum value which makes the injection rate reduce to zero. Thus, large amount of big oil droplets will cause DWL lose function and should be avoided.

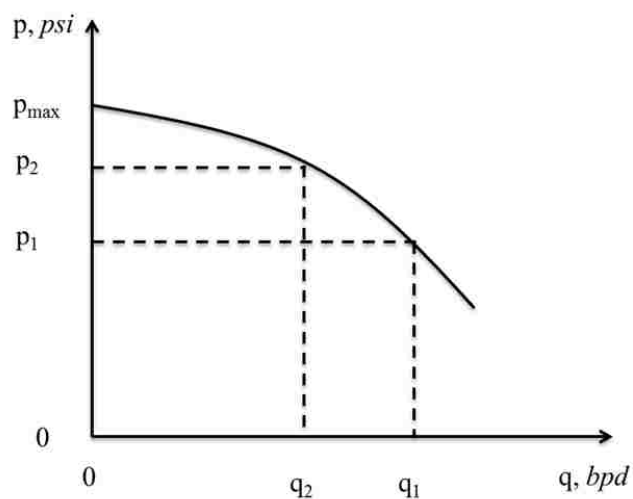


Figure 5.18. Schematic of flow rate - pressure relationship in centrifugal pump

5.6 Summary

The distributed water permeability damage caused by oily water injection and flow restriction due partial penetration were converted to skin factors, which could represent the dynamic growth of formation damage during the oily water injection process. The dynamic skin model provides a convenient way to predict injection pressure, assess formations for oily water injection and screen candidates for DWL. Based on the study, we can get the following conclusions:

1. The injectivity decline is caused by the growth of water permeability damaged zone in the formation, the process can be represented by a dynamic skin factor;
2. A thin damaged layer around the well can impair the overall injectivity, thus, water permeability damage is immediate and develops fast even for extremely small oil concentration in the injection water;
3. Partial penetration restricts the flow from well to the formation, which increases the overall skin factor and injection pressure, thus, full penetration is recommended for thin formations;
4. Formations with high initial permeability and weak water wettability are favorable for oily water injection and DWL.

CHAPTER 6. DIMENSIONAL ANALYSIS OF DWL FEASIBILITY

Feasibility assessment of ideal DWL requires numerical and analytical calculations that involve more than 20 dimensional parameters (reservoir-aquifer properties, rock-fluid properties, well configurations and operational parameters). It is difficult to consider combinations of so many parameters, so dimensionless scaling groups should be determined for DWL system. The approach known as dimensional scaling has been widely used in the petroleum engineering research and design studies (Croes and Schwarz, 1955; Rapoport, 1955; Geertsma, et al, 1956; Craig, et al, 1957; Perkins and Collins, 1960; Carpenter, 1962; Van Daalen and Van Domselaar, 1972; Shook, et al, 1992; Gharbi, et al, 1998; Novakovic, 2002; Hernandez and Wojtanowicz, 2007).

In general, two methods may be used to define dimensionless scaling groups: (1) dimensional analysis (DA), which gives dimensionless groups from primary dimensions of the physical system; (2) inspectional analysis (IA), which derives dimensionless groups from the differential equations that govern the process. The difference and relationship between these two methods have been discussed in Chapter 2. In this Chapter, dimensionless groups will be derived using IA for DWL. The completeness and independence of the groups will be tested using two real reservoir databases with properties of more than 700 reservoirs in the US. Dimensionless correlations will be developed using the derived scaling groups to screen the reservoir candidates that are suitable for installing DWL. Finally, the model will be tested with real field data.

This chapter (sections 6.1 to 6.3) previously appeared as “Jin, L. et al. Scaling Analysis of Wells with Downhole Water Loop Completion for Bottomwater Control. *Journal of Canadian Petroleum Technology*, Vol. 49, No. 11, Nov. 2010.” It is reprinted by permission of Society of Petroleum Engineers provided by Copyright Clearance Center.

6.1 DWL Performance Modeling

In the following sections, we use the IA method to define dimensionless scaling groups for DWL wells in 5 clear steps as:

1. Formulation of all governing equations together with the initial and boundary conditions;
2. Transformation to dimensionless space by defining scale and transformation factors;
3. Primary elimination and secondary substitution;
4. Redundancy elimination;
5. Completeness validation.

By doing so, we will also learn the reason for inconsistency between dimensionless scaling groups derived by different authors.

6.1.1 Governing Equations of DWL

DWL well schematics used for derivation of the dimensionless scaling groups are shown in Figure 6.1 and Figure 6.2. The well produces oil from the top of the oil zone – away from OWC. Water is drained from below OWC and is injected back to the same aquifer. Several researchers proposed flow equations for systems similar to DWL (Meyer and Garder, 1954; Carpenter, et al, 1962; Nielsen and Tek, 1963; Bear, 1972; Mattax and Dalton, 1990; Shook, et al, 1992; Novakovic, 2002).

In this study, the DWL system is described by Equations 6.1 through 6.19 based on the immiscible displacement equations (Mattax and Dalton, 1990; Shook, et al, 1992; Novakovic, 2002). The governing equations in a two-dimensional cylindrical system (r, z), are:

Continuity equation:

$$\phi \frac{\partial S_w}{\partial t} + \frac{1}{r} \frac{\partial(ru_{wr})}{\partial r} + \frac{\partial u_{wz}}{\partial z} = 0 \dots\dots\dots(6.1)$$

$$\frac{1}{r} \frac{\partial(ru_{wr} + ru_{or})}{\partial r} + \frac{\partial(u_{wz} + u_{oz})}{\partial z} = 0 \dots\dots\dots(6.2)$$

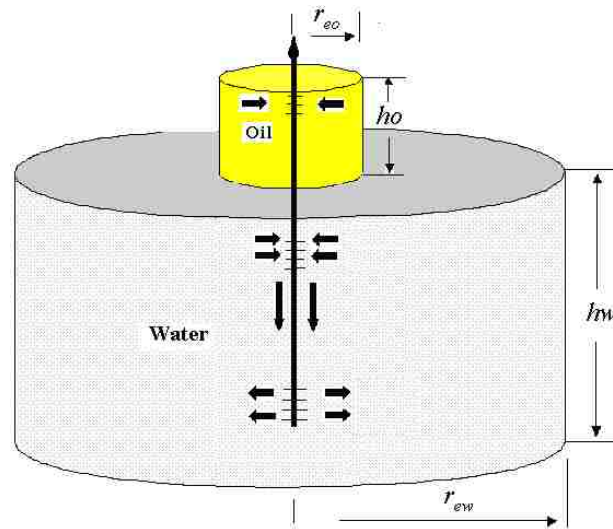


Figure 6.1. Schematic of DWL installation in bottom water drive reservoir

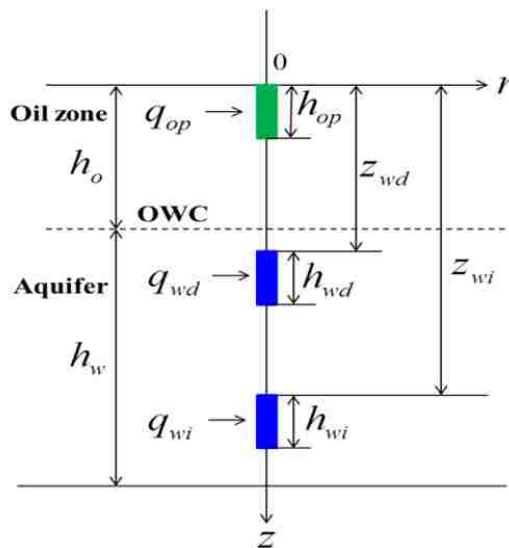


Figure 6.2. Cross-section of DWL installation and its dimensions

$$u_{wr} = -k_r \lambda_w \left(\frac{\partial p_w}{\partial r} \right) \dots\dots\dots (6.3)$$

$$u_{or} = -k_r \lambda_o \left(\frac{\partial p_o}{\partial r} \right) \dots\dots\dots (6.4)$$

$$u_{wz} = -k_z \lambda_w \left(\frac{\partial p_w}{\partial z} + \rho_w g \right) \dots\dots\dots (6.5)$$

$$u_{oz} = -k_z \lambda_o \left(\frac{\partial p_o}{\partial z} + \rho_o g \right) \dots\dots\dots (6.6)$$

$$p_o - p_w = \sigma \sqrt{\frac{\phi}{k_z}} J(S_w) = \Delta \rho g z \dots\dots\dots (6.7)$$

Initial conditions:

$$S_w = S_{wc} \quad \text{at } t = 0, 0 < z < h_o \dots\dots\dots (6.8)$$

$$S_w = 1 \quad \text{at } t = 0, h_o < z < h_o + h_w \dots\dots\dots (6.9)$$

Boundary conditions:

$$u_{wz} = 0, \quad \text{at } z = 0, \forall r, t \dots\dots\dots (6.10)$$

$$u_{oz} = 0, \quad \text{at } z = 0, \forall r, t \dots\dots\dots (6.11)$$

$$u_{wz} = 0, \quad \text{at } z = h_o + h_w, \forall r, t \dots\dots\dots (6.12)$$

$$u_{oz} = 0, \quad \text{at } z = h_o + h_w, \forall r, t \dots\dots\dots (6.13)$$

$$u_{wr} = 0, \quad \text{at } r = r_{ew}, \quad h_o < z < h_o + h_w, \forall t \dots\dots\dots (6.14)$$

$$u_{or} = 0, \quad \text{at } r = r_{eo}, \quad 0 < z < h_o, \forall t \dots\dots\dots (6.15)$$

$$q_{op} = 2\pi r_{well} \int_0^{h_{op}} u_{or} dz, \quad \text{at } r = r_{well}, t > 0 \dots\dots\dots (6.16)$$

$$q_{wd} = 2\pi r_{well} \int_{z_{wd}}^{z_{wd}+h_{wd}} u_{wr} dz, \text{ at } r = r_{well}, t > 0 \dots\dots\dots(6.17)$$

$$q_{wi} = -2\pi r_{well} \int_{z_{wi}}^{z_{wi}+h_{wi}} u_{wr} dz, \text{ at } r = r_{well}, t > 0 \dots\dots\dots(6.18)$$

$$q_{wi} = -q_{wd}, \text{ at } r = r_{well}, t > 0 \dots\dots\dots(6.19)$$

In the above equations, the reservoir fluids and the pore space are assumed to be incompressible, and the initial reservoir pressure is known. Equations 6.8 and 6.9 are the initial conditions, Equations 6.10 to 6.15 are no-flow conditions at the outer boundaries, Equations 6.16 to 6.19 give the inner boundary (well inflow) conditions.

6.1.2 Inspectional Analysis Procedure

In the above equations, there are 17 parameters ($\phi, S_{wc}, \lambda_w, \lambda_o, \rho_w, \rho_o, \sigma_{ow}, r_w, k_r, k_z, h_o, h_w, h_{op}, h_{wd}, h_{wi}, z_{wd}, z_{wi}$) influencing 10 dependent variables ($S_w, p_w, p_o, u_{wr}, u_{or}, u_{wz}, u_{oz}, q_{op}, q_{wd}, q_{wi}$) in dimensional space. In order to get dimensionless scaling groups, the equations should be transformed to dimensionless space as follows.

1. Transformation to dimensionless space (Initial Substitution)

Dimensionless variables are defined using linear combinations as:

$$\begin{aligned} r &= r_1^* \cdot r_D + r_2^* & u_{oz} &= u_{oz1}^* \cdot u_{ozD} + u_{oz2}^* \\ z &= z_1^* \cdot z_D + z_2^* & u_{wz} &= u_{wz1}^* \cdot u_{wzD} + u_{wz2}^* \\ t &= t_1^* \cdot t_D + t_2^* & p_w &= p_{w1}^* \cdot p_{wD} + p_{w2}^* \\ u_{wr} &= u_{wr1}^* \cdot u_{wrD} + u_{wr2}^* & p_o &= p_{o1}^* \cdot p_{oD} + p_{o2}^* \\ u_{or} &= u_{or1}^* \cdot u_{orD} + u_{or2}^* & S_w &= S_{w1}^* \cdot S_{wD} + S_{w2}^* \end{aligned}$$

The quantities with an asterisk “*” are called scale factors. Subscripts “1” and “2” indicate the multiplicative and additive scale factors, respectively. Dimensionless variables are those with a subscript “D”. Defining the scale factors is somewhat subjective. It has been done, here, by following other work (Shook, et al, 1992). Substituting the above transformations into Equations 6.1 to 6.19, then all of these equations can be transformed to dimensionless space. Take Equation 6.1 as an example, it can be transformed to Equation 6.20 as:

$$\begin{aligned} & \frac{\phi S_{w1}^*}{t_1^*} \cdot \frac{\partial S_{wD}}{\partial t_D} + \frac{u_{wr1}^*}{(r_1^* r_D + r_2^*)} \cdot \frac{\partial(r_D u_{wrD})}{\partial r_D} + \frac{u_{wr2}^*}{(r_1^* r_D + r_2^*)} + \dots \\ & + \frac{r_2^* u_{wr1}^*}{r_1^* (r_1^* r_D + r_2^*)} \cdot \frac{\partial u_{wrD}}{\partial r_D} + \frac{u_{wz1}^*}{z_1^*} \cdot \frac{\partial u_{wzD}}{\partial z_D} = 0 \end{aligned} \dots\dots\dots(6.20)$$

Similarly, all other equations have been transformed to dimensionless space. This step is called initial substitution.

2. Primary elimination and secondary substitution

After the initial substitution, we need to choose a scaling direction. It can be either “r” or “z” direction. “z” direction is chosen in this study for the ease of analyzing completion locations. Then, we rearrange these equations in dimensionless space and write them in dimensionless form. Take Equation 6.20 as an example, it can be rearranged to become Equation 6.21 as:

$$\begin{aligned} & \frac{\partial S_{wD}}{\partial t_D} + \frac{\boxed{1}}{\phi S_{w1}^* r_1^*} \cdot \frac{1}{r_D} \cdot \frac{\partial(r_D u_{wrD})}{\partial r_D} + \frac{\boxed{2}}{\phi S_{w1}^* r_1^*} + \dots \\ & + \frac{\boxed{3}}{\phi S_{w1}^* r_1^{*2}} \cdot \frac{1}{r_D} \cdot \frac{\partial u_{wrD}}{\partial r_D} + \frac{\boxed{4}}{\phi S_{w1}^* z_1^*} \cdot \frac{\partial u_{wzD}}{\partial z_D} = 0 \end{aligned} \dots\dots\dots(6.21)$$

After rearrangement, the equation becomes fully dimensionless, and four dimensionless groups are defined as shown by the rectangles in Equation 6.21. The form of dimensionless equation should be the same as the initial dimensional equation. So, groups (1) and (4) should have value of “1”, while the groups (2) and (3) value should be “0”. If we use the same approach to all other equations in the dimensionless space, a total of 110 dimensionless groups can be obtained --- 34 of them are set to be “1” and 45 are “0”. The remaining 31 groups cannot be assigned any values at this stage. The detailed derivation is shown in Appendix C.1. This process is called primary elimination, which can be done simply by observing the forms of equations. From the dimensionless groups with values “1” and “0”, we can get the transformation factors to address the remaining 31 groups:

$$\begin{aligned}
 r_2^* &= z_2^* = t_2^* = S_{w2}^* = 0 & p_{w2}^* &= p_{o2}^* = 0 \\
 u_{wr2}^* &= u_{or2}^* = u_{wz2}^* = u_{oz2}^* = 0 & u_{wr1}^* &= u_{or1}^* = \frac{q_{op}}{2\pi r_{well} h_o} \\
 u_{wz1}^* &= u_{oz1}^* = \frac{q_{op}}{2\pi r_{well}^2} & p_{w1}^* &= p_{o1}^* = \frac{q_{op}}{2\pi k_r \lambda_w h_o} \\
 p_{wD} &= \frac{2\pi p_w k_r \lambda_w h_o}{q_{op}} & p_{oD} &= \frac{2\pi p_o k_r \lambda_w h_o}{q_{op}} \\
 r_1^* &= r_{well} & r_D &= \frac{r}{r_{well}} \\
 z_1^* &= h_o & z_D &= \frac{z}{h_o} \\
 t_1^* &= \frac{\phi S_{1r} r_w}{u_{wr1}^*} & t_D &= \frac{t q_{op}}{2\pi \phi h_o S_{wr} r_{well}^2} \\
 S_{w1}^* &= S_{wC} & S_{wD} &= \frac{S_w}{S_{wC}}
 \end{aligned}$$

The use of transformation factors defines 15 groups with remaining 16 groups not yet defined. However, these remaining dimensionless groups are no longer arbitrary. They are:

$$\begin{aligned}
 \pi_1 &= \frac{2\pi k_z \lambda_w \rho_w g r_{well}^2}{q_{op}} & \pi_6 &= \frac{k_z r_{well}^2}{k_r h_o^2} & \pi_{11} &= \frac{z_{wi}}{h_o} \\
 \pi_2 &= \frac{2\pi k_z \lambda_o \rho_o g r_{well}^2}{q_{op}} & \pi_7 &= \frac{\lambda_o}{\lambda_w} & \pi_{12} &= \frac{h_{wi}}{h_o} \\
 \pi_3 &= \frac{2\pi k_r \lambda_w \Delta \rho g h_o^2}{q_{op}} & \pi_8 &= \frac{h_w}{h_o} & \pi_{13} &= \frac{h_{op}}{h_o} \\
 \pi_4 &= \frac{2\pi k_r \lambda_w h_o \sigma}{q_{op}} \sqrt{\frac{\phi}{k_z}} & \pi_9 &= \frac{z_{wd}}{h_o} & \pi_{14} &= \frac{q_{wd}}{q_{op}} \\
 \pi_5 &= \frac{k_z \lambda_o r_{well}^2}{k_r \lambda_w h_o^2} & \pi_{10} &= \frac{h_{wd}}{h_o} & \pi_{15} &= \frac{r_{ew}}{r_{well}} \\
 \pi_{16} &= \frac{r_{eo}}{r_{well}}
 \end{aligned}$$

3. Redundancy elimination

With the remaining 16 groups defined, the flow equations in dimensionless space become completely dimensionless. However, the groups are not all independent. It is easy to see that all these 16 dimensionless groups are multiplicative, hence they can be transformed to a system of linear equations if logarithms are taken (Shook, et al, 1992; Novakovic, 2002). The elements of the coefficient matrix in Figure 6.3 are exponents of the parameters found in the 16 dimensionless groups. According to linear algebra theory, the number and formats of independent dimensionless groups can be arrived at by determining the rank of the 16×23 coefficient matrix (Shook, et al, 1992).

Five dimensionless groups, above, are clearly identical to those published by other authors (Geertsma, et al, 1956; Henley, et al, 1961; Shook, et al, 1992; Novakovic, 2002; Hernandez and Wojtanowicz, 2007): Well penetration (H_p); Dimensionless well ratio (N_w); Mobility ratio (M); Aquifer strength (R_w); and, Density number (N_ρ). Also, the other two numbers, Gravity (or buoyancy) number (N_b), and Capillary number (N_v) have similar format to those published that – by themselves – have not been consistently identical and have varied with different authors. Moreover, Drainage area number (R_o) is similar to the well spacing number published by Henley, et al, 1961, and Hernandez, 2007, since these authors also used a single-well radial model in their studies.

The remaining six dimensionless groups are new. They include: Production-to-drainage rate ratio (N_q), two Water zone penetration ratios (H_d) and (H_i), two Completion location numbers (Z_d) and (R_i), and the Aquifer thickness number (N_h). Five of the groups describe the DWL well completion geometry and the (N_q) group - DWL operation.

Physical meaning of the dimensionless groups can be discerned from their format or their derivation; The N_b group scales the ratio of buoyancy to pressure drawdown resulting from water drainage; The N_v group scales the ratio of capillary pressure to buoyancy; The N_w group represents reservoir anisotropy and well radius; The density number, (N_ρ) stands for the density contrast of oil and water; The N_q group relates oil production and water drainage rates; The M group is the well-known mobility ratio.

The remaining groups describe geometrical properties of the reservoir-well system: The (R_o) group gives the size of the oil zone – a measure of the well’s drainage area; The two groups (N_h), and (R_w) relate aquifer size to the size of oil pay zone - a measure of the aquifer strength; The three groups H_p , H_d , H_i embody the effects of partial penetration by each of the

three well completions; The Z_d group represents the position of water drainage completion within the water zone. Finally, the (R_i) group stands for the drainage-injection (D/I) spacing – a vertical distance between the drainage and injection completions and key parameter of DWL system design (Jin and Wojtanowicz, 2010a, b, c).

4. Dimensionless model of DWL well system

The equations describing DWL systems in dimensionless space are:

Dimensionless continuity equation:

$$\frac{\partial S_{wD}}{\partial t_D} + \frac{1}{r_D} \cdot \frac{\partial(r_D u_{wrD})}{\partial r_D} + \frac{\partial u_{wzD}}{\partial z_D} = 0 \dots\dots\dots(6.22)$$

$$\frac{1}{r_D} \cdot \frac{\partial(r_D u_{wrD} + r_D u_{orD})}{\partial r_D} + \frac{\partial(u_{wzD} + u_{ozD})}{\partial z_D} = 0 \dots\dots\dots(6.23)$$

$$u_{wrD} = -\frac{\partial p_{wD}}{\partial r_D} \dots\dots\dots(6.24)$$

$$u_{orD} = -\pi_6 \frac{\partial p_{oD}}{\partial r_D} \dots\dots\dots(6.25)$$

$$u_{wzD} = -\pi_3^2 \frac{\partial p_{wD}}{\partial z_D} - \frac{\pi_1 \pi_4}{\pi_5} \dots\dots\dots(6.26)$$

$$u_{ozD} = -\pi_6 \pi_3^2 \frac{\partial p_{oD}}{\partial z_D} - \frac{\pi_1 (\pi_4 - 1) \pi_6}{\pi_5} \dots\dots\dots(6.27)$$

$$p_{oD} - p_{wD} = \frac{\pi_1 \pi_2}{\pi_3 \pi_5} J(S_{wD}) = \frac{\pi_1}{\pi_5 \pi_3^2} (1 - z_D) \dots\dots\dots(6.28)$$

Dimensionless initial conditions:

$$S_{wD} = S_{wc}, \text{ at } t_D = 0, 0 < z_D < 1 \dots\dots\dots(6.29)$$

$$S_{wD} = 1, \text{ at } t_D = 0, 1 < z_D < 1 + \pi_8 \dots\dots\dots(6.30)$$

Dimensionless boundary conditions:

$$u_{wzD} = 0, \text{ at } z_D = 0, \forall r_D, t_D \dots\dots\dots (6.31)$$

$$u_{ozD} = 0, \text{ at } z_D = 0, \forall r_D, t_D \dots\dots\dots (6.32)$$

$$u_{wzD} = 0, \text{ at } z_D = 1 + \pi_8, \forall r_D, t_D \dots\dots\dots (6.33)$$

$$u_{ozD} = 0, \text{ at } z_D = 1 + \pi_8, \forall r_D, t_D \dots\dots\dots (6.34)$$

$$u_{wrD} = 0, \text{ at } r_D = \pi_{13}\pi_{14}, 1 < z_D < 1 + \pi_8, \forall t_D \dots\dots\dots (6.35)$$

$$u_{orD} = 0, \text{ at } r_D = \pi_{14}, 0 < z_D < 1, \forall t_D \dots\dots\dots (6.36)$$

$$1 = \int_0^{\pi_9} u_{orD} dz_D, \text{ at } r_D = 1, t_D > 0 \dots\dots\dots (6.37)$$

$$\frac{1}{\pi_5} = \int_{\pi_7\pi_8}^{\pi_8(\pi_7+\pi_{11})} u_{wrD} dz_D, \text{ at } r_D = 1, t_D > 0 \dots\dots\dots (6.38)$$

$$-\frac{1}{\pi_5} = \int_{\pi_7\pi_8\pi_{10}}^{\pi_8(\pi_7+\pi_{12})} u_{wrD} dz_D, \text{ at } r_D = 1, t_D > 0 \dots\dots\dots (6.39)$$

6.2 Verification of DWL Dimensionless Groups with Field Databases

A total of 14 dimensionless scaling groups have been defined, which transform all the equations from dimensional space to dimensionless space. In theory, these groups completely describe DWL systems, i.e. their inter-relations are not changed by varying the system's physical properties. As pointed out by Shook, et al., (1992), validating the dimensionless groups is unnecessary because the derivation presented above is evidently complete in itself. However, validating provides an additional independent check and gives insight into which groups are important to the process.

Two databases with real reservoir properties are used in the validation process: Tertiary Oil Recovery Information System (TORIS) and US Heavy Oil Database (USHOD). TORIS is an extensive field- and reservoir-level database used for technical and economical evaluation of tertiary recovery potential of specific crude oil reservoirs. It contains more than 2,540 oil reservoirs, which account for over 64% of the original oil-in-place estimated to exist in discovered crude oil reservoirs in the U.S. A part of TORIS is accessible to public, which contains 192 oil reservoirs including formation and fluids properties (Sharma, 2008). The USHOD is a database constructed by National Institute for Petroleum and Energy Research (NIPER) with the commission from U.S. DOE. NIPER analyzed about 1,025 reservoirs containing heavy oil and built the database with 500+ reservoirs in March 1996. The database is currently accessible to public. As only a few wells have been drilled into the bottom aquifers, information about aquifer properties is limited and there is no reservoir database with detailed aquifer properties could be found. Elkins (1959) reported the thicknesses of oil zone and aquifer from 23 wells, which indicated that there is no relationship between them. Thus, a population of “synthetic” bottom water systems have been created using real oil reservoirs case data with the aquifer thicknesses randomly assigned to each case.

6.2.1 Completeness Validation of the Groups

To demonstrate the completeness, we study the DWL well model response (output) to various combinations of physical parameters while keeping the dimensionless group values constant.

In the testing we varied the physical properties in dimensional space while held the values of dimensionless groups constant. Eight combinations (cases) with wide range of

dimensional property values within real range were considered as shown in Table 6.1, while the values of dimensionless groups are constant for all 8 cases as shown in Table 6.2. It is hypothesized that the relationship of independent dimensionless quantities such as water cut and movable oil recovery would not change for different systems as long as the systems are similar, i.e. have the same values of all dimensionless groups.

Table 6.1. Dimensional properties used in completeness validation

Case Parameters	1	2	3	4	5	6	7	8
k_r, md	3500	1410.9	917.6	435.48	215.3	111	92	75
H_{o_2}, ft	18	28.13	34.88	50.63	72	100	112.67	126.58
H_{w_2}, ft	64	100	124	180	256	355.5	400	450
μ_{o_2}, cp	17	1.7	34	5.1	8.5	6.8	11.9	3.4
μ_{w_2}, cp	1	1.5	0.5	2	0.25	1.25	0.75	3.4
$\rho_{o_2}, lbm/ft^3$	58.058	58.058	55	55	58.058	52	55	53
$\rho_{w_2}, lbm/ft^3$	65.72	65.72	62.28	62.28	65.72	58.86	62.28	60.00
r_{w_2}, ft	0.292	0.292	0.2995	0.2995	0.292	0.3085	0.2995	0.3054
Z_{wd_2}, ft	20.5	32	39.68	57.6	81.92	113.6	128	144
Z_{wi_2}, ft	70.5	110.1	136.5	198.14	281.8	390.784	440.32	495.4
h_{op_2}, ft	10	15.75	19.53	28.35	40.32	56	63.1	70.4
h_{wi_2}, ft	5	7.8	9.7	14	20	27.8	31	35.1
h_{wd_2}, ft	5	7.8	9.7	14	20	27.8	31	35.1

Table 6.2. Dimensionless values used in completeness validation

Dimensionless Group	Value	Dimensionless Group	Value
N_b	5400	N_h	3.556
N_v	0.014	H_p	0.556
N_w	0.028	R_i	3.44
N_p	8.577	H_d	0.078
N_d	0.020	H_i	0.078
M	12.234	R_w	5882
Z_d	0.320	R_o	2913

Results in Figure 6.4 show that water cut develops differently for the 8 cases in dimensional space while the curves become virtually identical in dimensionless space as shown in Figure 6.5, as they have the same values of dimensionless groups. The results indicate that the dimensionless groups fully describe similarity of DWL systems.

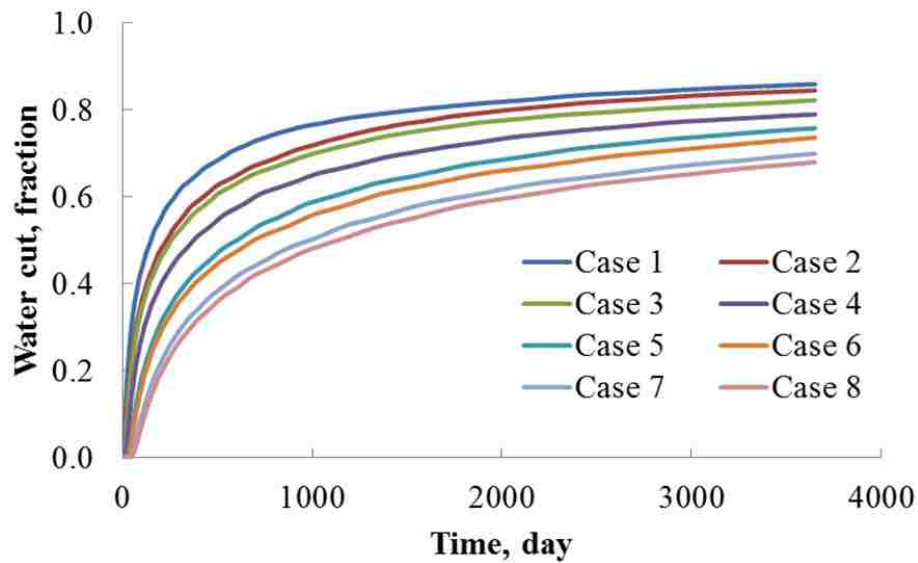


Figure 6.4. Water cut development of different cases in dimensional space

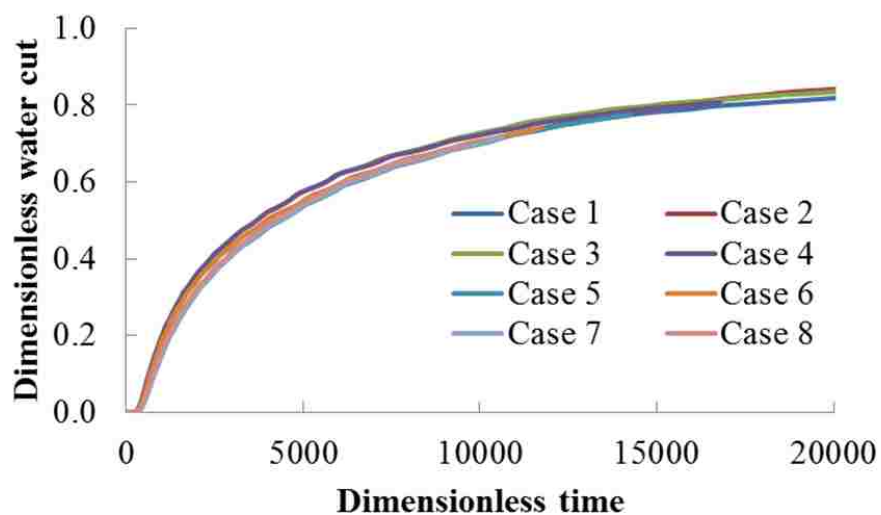


Figure 6.5. Water cut development of different cases in dimensionless space

6.2.2 Independence Testing of the Groups

Close observation of the dimensionless groups shows that, many of them include operating parameters such as “ q_{wd} ” and “ q_{op} ”, design parameters as “ r_{well} , h_{op} , z_{wd} , h_{wd} , h_{wi} ” and so on, these parameters can vary individually in a wide range based on design and operating conditions, thus dimensionless groups including these parameters are inherently independent to each other if no mandatory constraints put on them. Thus, only the following groups need to be tested:

$$N_b = \frac{2\pi k_z \lambda_w \Delta \rho g r_{well}^2}{q_{wd}} \quad N_v = \frac{\sigma \sqrt{k_r \phi}}{k_z \Delta \rho g r_{well}}$$

$$N_\rho = \frac{\rho_w}{\Delta \rho} \quad M = \frac{\lambda_o}{\lambda_w} = \frac{\mu_o k_{rw}}{\mu_w k_{ro}}$$

We used Pearson's product moment correlation coefficient (γ_p) and cross plots of two groups to test the independence between these groups. The value of γ_p changes in range from -1 to 1 with 0 indicating no association and -1 (or 1) indicating strong relationship as shown in Figure 6.6. Figure 6.7 clearly shows the interrelationship between the investigated dimensionless groups. The values of γ_p fall between -0.1 and 0.1, which means there are no clear correlations between these groups and thus they are independent from each other.

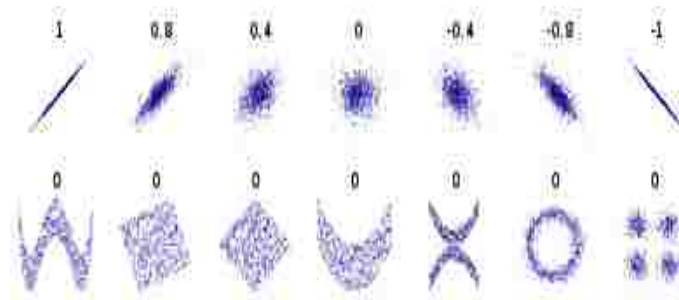


Figure 6.6. Examples of scatter diagrams with different values of γ_p

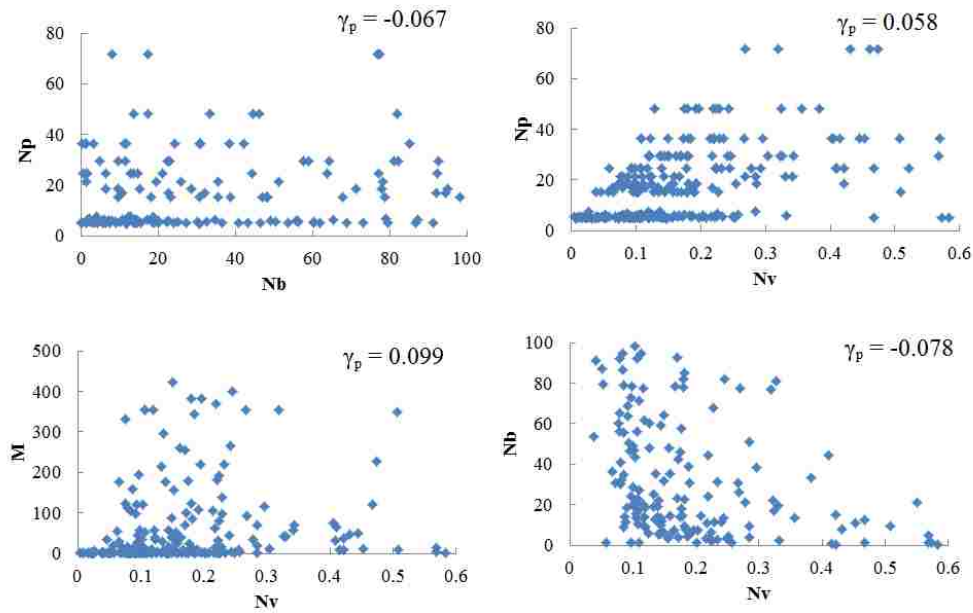


Figure 6.7. Cross plots and γ_p between dimensionless groups

6.3 Relevance of Dimensionless Groups

Although DWL systems are theoretically described by fourteen dimensionless groups, the number could be reduced by disregarding the groups with small significance in explaining DWL system performance. For example, some previous studies have shown irrelevance of the well drainage group, R_o , since water coning is a local phenomenon, while other studies revealed irrelevance of the density and capillary effects that did not affect the sweep efficiency of bottom water drive reservoirs over the range of conditions normally encountered in the field (Henley, et al, 1961 and Hernandez, 2007). Typically, the relevance of dimensionless groups is found through a rigorous sensitivity study using designed series of experiments and statistical analysis. However, 14 groups will lead to a large amount of simulation runs if all of them are considered in different levels (Hernandez, 2007). In this study, we firstly qualify the relevance of the dimensionless groups by testing their effect on oil recovery to remove the groups that are irrelevant in the water coning control component

of DWL. Then a rigorous sensitivity analysis is carried out to identify the most important groups in the whole DWL process.

The cluster of dimensionless groups could be divided into three subsets: DWL well design, DWL well operation, and the reservoir/fluid properties. The DWL design groups are N_w , Z_d , H_p , R_i , H_d , and H_i ; They control the position and size of three well completions. The two DWL well operation groups are N_b and N_q , as they are related to the oil production and water “looping” rates and can be controlled by operators. The reservoir/fluid property groups are N_v , N_ρ , M , N_h , R_w and R_o and constitute intrinsic properties of the reservoir and fluid systems. Values of these groups are systemic and cannot be controlled.

Based on the results of Henley, et al, (1961) and Hernandez (2007), N_w , N_v and N_ρ can be ignored in numerical experiments as they are unimportant in water coning problems. Also R_o is negligible as the possible practical range of values for the well radius is quite small and the drainage area effect is included in R_w . Thus, the following groups are selected and qualified using commercial reservoir simulator: H_p , H_d , H_i , Z_d , R_i , N_b , N_q , $(N_h * R_w^2)$ and M . Note that testing these 9 groups is equivalent to evaluation of 30 physical parameters they represent. In a single series of simulation runs, we would fix the values of seven groups and change the other two groups to monitor resulting values of the recovery factor. A typical approach for the simulations shown in Figure 6.8 is to set the values of H_d , H_i , Z_d , R_i , N_b , N_q , and $(N_h * R_w^2)$ using Case 1 in Table 6.3, and to change the values of H_p and M (from 0.167 to 1.0, and from 0.7 to 21.5, respectively). Table 6.3 represents typical range and levels of the dimensionless groups.

Figure 6.8 shows no effect of oil zone penetration for low mobility ratio and some reduction of recovery for higher M values. Figure 6.9 to Figure 6.11 clearly demonstrate

practically no effect of the water loop completions' position (below OWC) and lengths on the oil recovery (as long as their vertical spacing is constant).

Table 6.3. Dimensionless values used in the relevance testing

Group Case	H_p	H_d	H_i	Z_d	R_i	N_b	N_q	$N_h * R_w^2$	M
1	0.167~1.0	0.078	0.078	0.391	1.964	1175	0.017	2902	0.7~21.5
2	0.500	0.078~0.39	0.078	0.313	1.964	1175	0.017	2902	0.7~21.5
3	0.500	0.078	0.078~0.39	0.313	1.964	1175	0.017	2902	0.7~21.5
4	0.333	0.078	0.078	0.31~0.75	2.321	822	0.013	2902	0.7~21.5
5	0.333	0.078	0.078	0.313	1.0~2.7	822	0.013	2902	0.7~21.5
6	0.667	0.078	0.078	0.313	2.321	548~8222	0.013	2902	0.7~21.5
7	0.333	0.078	0.078	0.313	1.964	548	0.01~0.15	2902	0.7~21.5
8	0.667	0.078	0.078	0.313	1.964	1175	0.0365	3.5~2902	0.7~21.5

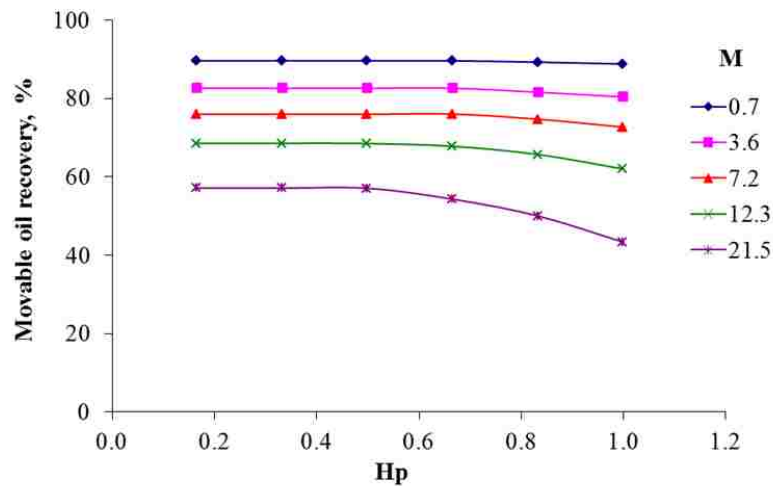


Figure 6.8. Movable oil recovery as a function of H_p for various M --- case 1

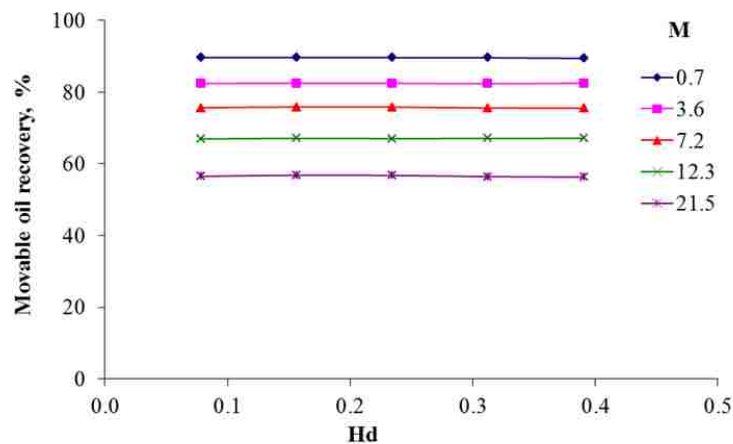


Figure 6.9. Movable oil recovery as a function of H_d for various M --- case 2

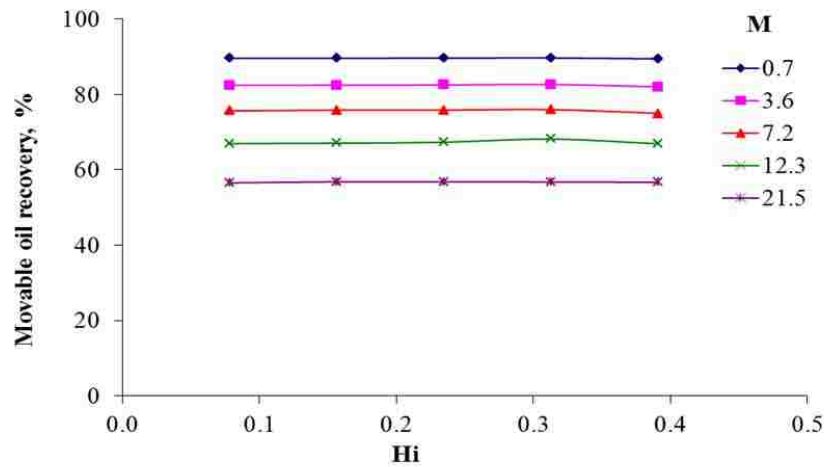


Figure 6.10. Movable oil recovery as a function of H_i for various M --- case 3

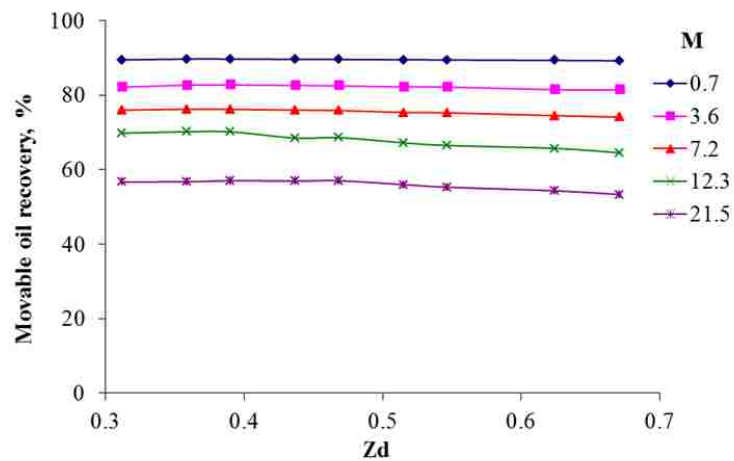


Figure 6.11. Movable oil recovery as a function of Z_d for various M --- case 4

As shown in Figure 6.12, the R_i group (the injection-to drainage depths ratio) appears to be the key design parameter for a DWL system that – if too small – could significantly reduce oil recovery. By combining some dimensionless groups, we can get the dimensionless D/I spacing ratio as: $H_{D/I} = Z_d * (R_i - 1)$, which is the ratio of distance between the two completions to the thickness of the aquifer. It is clear from Figure 6.13 that there is a critical D/I spacing ratio for a DWL system, which is usually around 0.3. This value is identical to our previous findings (Jin and Wojtanowicz, 2010a, b; Jin, et al, 2010).

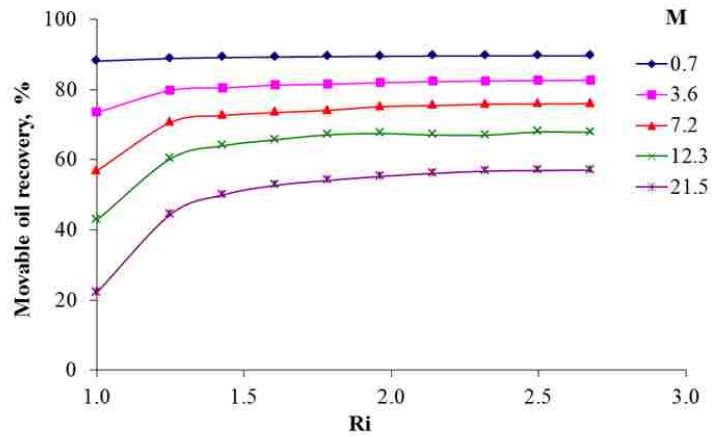


Figure 6.12. Movable oil recovery as a function of R_i for various M --- case 5

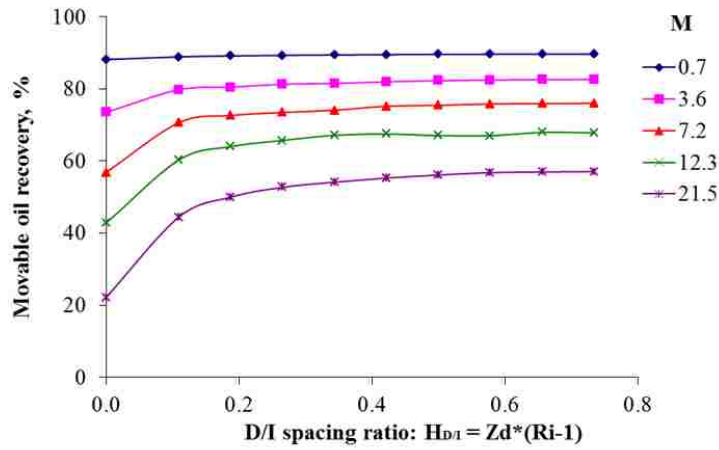


Figure 6.13. Movable oil recovery as a function of D/I spacing ratio for various M --- case 5

Figure 6.14 shows the recovery effect of the N_b group that is inversely proportional to the water “looping” (drainage-injection) rate. It is clear that increased looping rates would stimulate recovery – particularly for the systems with high mobility ratios, as water coning is controlled and bypassed oil is reduced. The finding is further confirmed by the plots in Figure 6.15 showing better recovery for smaller values of the oil-to-water rate ratio group, N_q . Since maximizing oil rate is always desirable, the practical approach would be to increase the water looping rate.

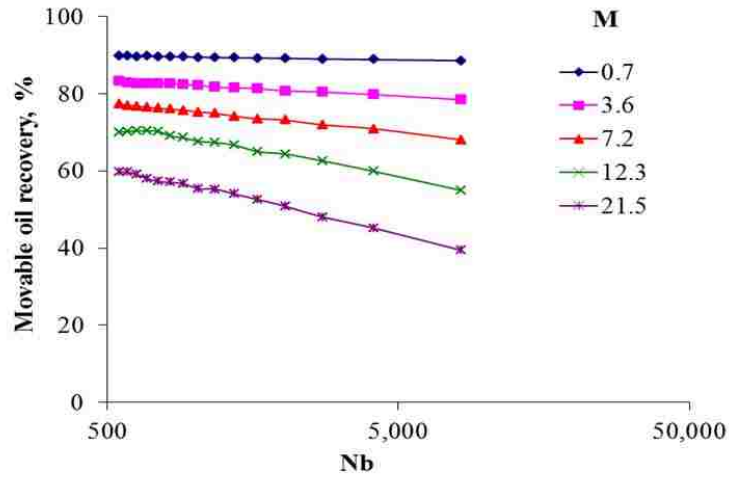


Figure 6.14. Movable oil recovery as a function of N_b for various M --- case 6

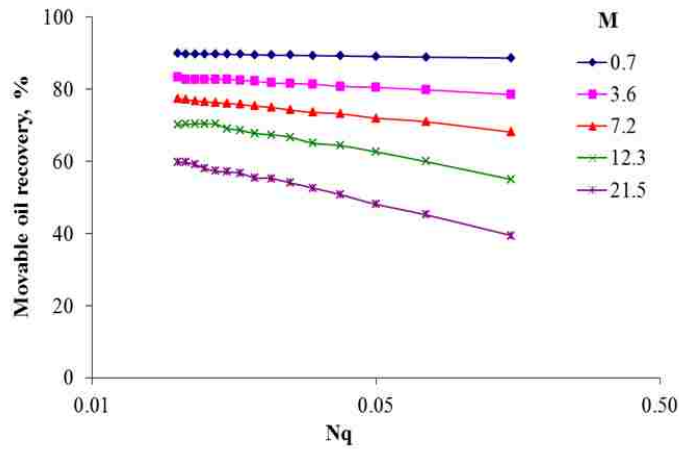


Figure 6.15. Movable oil recovery as a function of N_q for various M --- case 7

In the bottom-water-drive reservoirs, the aquifer strength –expressed as a ratio of the aquifer to the oil zone volumes (Hernandez, 2007) - becomes a combination of two dimensionless groups: $V_{w/o} = V_w/V_o = N_h * R_w^2$. This new group appears to be important to the (primary) oil recovery efficiency as clearly depicted in Figure 6.16. In the water-drive systems, the aquifer pressure depletion is the prime reason for small primary recovery. Although DWL returns the drained water to the aquifer, pressure decline is still unavoidable due depletion of the oil payzone.

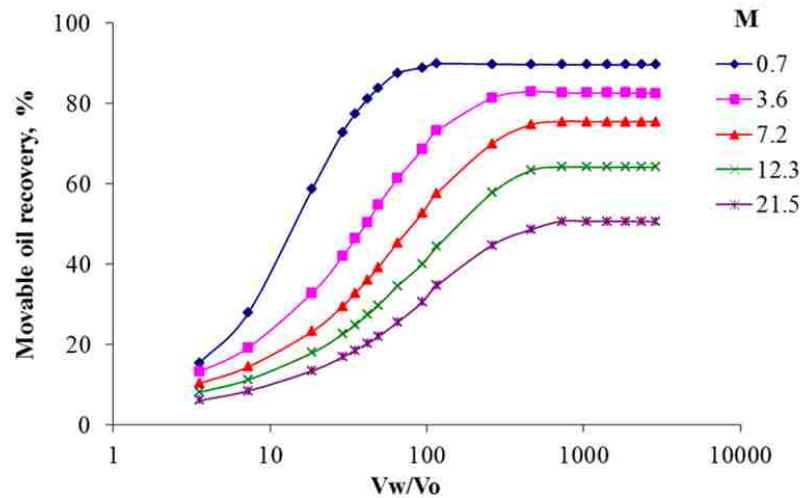


Figure 6.16. Movable oil recovery as a function of V_w/V_o for various M --- case 8

In view of the results, the number of DWL scaling groups can be reduced from fourteen to seven relevant dimensionless groups: $H_{D/I}$ (or R_i), N_q , N_b , H_p , $V_{w/o}$ ($=N_h * R_w^2$) and M . The first three groups uniquely represent the DWL systems and describe locations of the water drainage and injection completions, D/I spacing and water looping rate effect.

6.4 Dimensionless Model of DWL Performance

The seven dimensionless groups described above are used to scale recovery performance of DWL serving as the basis for the screening model, which is used to produce a quick look at the oil recovery potential of a reservoir if it is developed by DWL. To create such a model, experimental results are needed to serve as the inputs and outputs of the model. Numerical simulation is used to generate the results for analysis.

6.4.1 Experimental Design

Generally, two-level factorial designs (2LD) and space-filling Latin hypercube sampling (LHS) designs can be used for statistical analysis when the parameters are linearly distributed (Aslett, et al., 1998). Multilevel designs are needed to capture the accurate

response of a model if the parameter distribution is nonlinear. In reservoir engineering, the response of an oil or gas simulation model is always nonlinear, so designs must consider factors at more than two levels, not just high and low values as in two-level factorial designs (Box, et al., 1978). Three-level factorial designs (3LD) assign each factor its minimum, center-point or maximum value in all possible combinations with other factors, which are more accurate than the two-level factorial designs (Hernandez, 2007). However, multilevel designs increase the computational burden as they need more simulations to fit the greater number of model parameters. In this study, three-level factorial designs for 7 dimensionless groups need 3^7 (2187) simulations, which are time-consuming to carry out.

Experimental design is a well-known technique to maximize the information gained from each experiment and to statistically evaluate the significance of each input variable (Myers, 1971). It attempts to minimize the number of runs while capturing all of the desired effects for each variable. The Box-Behnken design (BBD) is such a method which was proposed by Box and Behnken by modifying three-level factorial designs in 1960. BBD keeps the advantages of three-level factorial designs while significantly reducing the number of experiments. Figure 6.17 shows the configuration of BBD for three factors, which requires 13 experiments comparing 27 for three-level full factorial design (White, et al., 2001; Ferreira, et al., 2007).

The number of experiments needed in BBD can be calculated as follows:

$$N_{BBD} = 2n(n - 1) + C_0 \dots\dots\dots (6.40)$$

Where, N_{BBD} is the total experiments in BBD; n is the number of variables; C_0 is the center-point number. The experimental savings of BBD are significant comparing to 2LD (2^n) and 3LD (3^n) with the increasing number of experimental factors (n). In this study, BBD is

used to design the simulation experiments, which requires 62 simulation runs for 7 dimensionless groups.

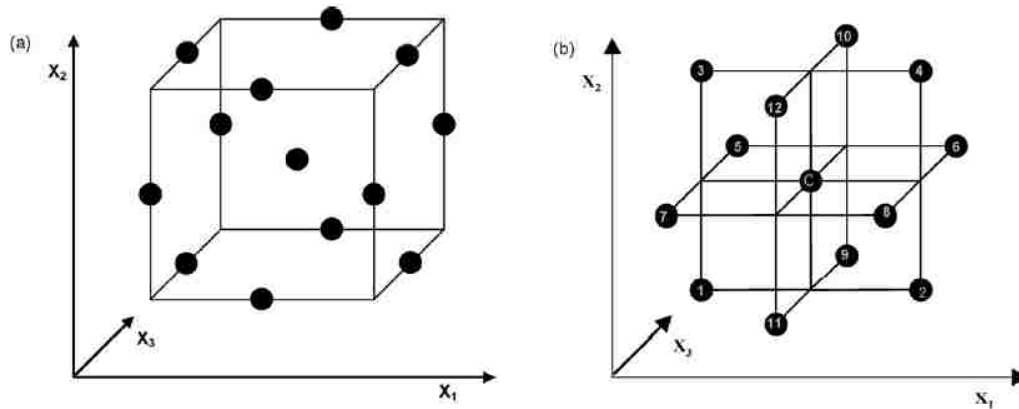


Figure 6.17. Pictorial representation of a 3-factor Box-Behnken experimental design (Ferreira, et al., 2007)

The BBD requires three levels: low, intermediate and high, which are coded as -1, 0 and +1, for each factor to capture quadratic effects. Thus, it is necessary to determine high, low and intermediate values for each of the 7 groups. This is done by investigating bottom water reservoir systems in literature and calculating group values. Based on reservoir properties taken from sources such as the National Petroleum Council (NPC), the Society of Petroleum Engineers (SPE) and the US Geological Survey (USGS), Hernandez (2007) generated a reservoir database to study the oil bypassing problem in edge-water and bottom-water drive reservoirs. The probability distributions of individual properties were obtained from Monte Carlo Simulations (10,000 passes), which could represent most possible reservoir situations, and it is confirmed by comparing the database to TORIS and USHOD. Based on the reservoir properties in these databases, the values of each dimensionless group can be summarized as shown in Table 6.4.

Table 6.4. Values for dimensionless groups

Group Level	$H_{D/I}$	N_q	N_b	H_p	N_h	R_w	M
Low	0	0.01	15	0.1	1	3	0.25
Intermediate	0.5	0.055	500	0.5	2	10	2.6
High	0.8	1	1245	1.0	5	100	100

6.4.2 DWL Performance Model

The purpose of the screening model is to produce a quick look at the movable oil recovery from a reservoir to see whether it could be developed with DWL technology. Since there is no analytical model available for recovery of DWL, a response surface method (RSM) is used to generate such a screening model based on simulation results. The following criteria are used in simulation (Hernandez, 2007):

1. Well's production is controlled by the top and bottom rates, which means the well is operated at constant top and bottom rates all the time;
2. Movable oil recovery is terminated when the water cut in the top completion reaches 98% or the average reservoir pressure falls below the minimum bottom-hole pressure (Hernandez, 2007).

The response surface method is a collection of mathematical and statistical techniques for empirical model building and it is widely applied to generate regression model that fits the true response surface of the objective function where several inputs influence the output. First (linear) and second order (quadratic) models are frequently used in engineering applications for process or product optimizations (Myers and Montgomery, 1995). A quadratic response surface model is (Wood, 2006, 2008):

$$y = \beta_0 + \sum_{i=1}^n \beta_i x_i + \sum_{i<j} \sum_{j=2}^n \beta_{ij} x_i x_j + \sum_{i=1}^n \beta_{ii} x_i^2 \dots\dots\dots(6.41)$$

Where, y is the objective function; x is the independent variable; β is the regression coefficient; i and j are the variable index; n is the total number of independent variables.

$\sum_{i=1}^n \beta_i x_i$ and $\sum_{i=1}^n \beta_{ii} x_i^2$ represent the linear and quadratic effects of the variables, respectively,

while the interaction effects between variables are expressed by $\sum_{i<j} \sum_{j=2}^n \beta_{ij} x_i x_j$. In this study,

the objective function is the movable oil recovery and the independent variables are the selected seven dimensionless groups. Based on the simulation results from BBD, the regression coefficients of Equation 6.41 are shown in Table 6.5.

Table 6.5. Regression coefficients for movable oil recovery

Dimensionless group	Symbol	Coefficient	Dimensionless group	Symbol	Coefficient
$H_{D/I}$	β_1	15.18	$N_q * R_w$	β_{26}	0.13
N_q	β_2	153.77	$N_q * M$	β_{27}	- 0.09
N_b	β_3	- 0.02	$N_b * N_b$	β_{33}	0.00002
H_p	β_4	3.86	$N_b * H_p$	β_{34}	- 0.01
N_h	β_5	15.40	$N_b * N_h$	β_{35}	- 0.00086
R_w	β_6	5.86	$N_b * R_w$	β_{36}	0.0001
M	β_7	- 4.00	$N_b * M$	β_{37}	- 0.00013
$H_{D/I} * H_{D/I}$	β_{11}	- 4.84	$H_p * H_p$	β_{44}	- 11.11
$H_{D/I} * N_q$	β_{12}	- 15.50	$H_p * N_h$	β_{45}	1.95
$H_{D/I} * N_b$	β_{13}	- 0.01	$H_p * R_w$	β_{46}	- 0.04
$H_{D/I} * H_p$	β_{14}	6.00	$H_p * M$	β_{47}	0.25
$H_{D/I} * N_h$	β_{15}	1.90	$N_h * N_h$	β_{55}	- 1.94
$H_{D/I} * R_w$	β_{16}	- 0.10	$N_h * R_w$	β_{56}	- 0.03
$H_{D/I} * M$	β_{17}	- 0.05	$N_h * M$	β_{57}	- 0.01
$N_q * N_q$	β_{22}	- 151.09	$R_w * R_w$	β_{66}	- 0.05
$N_q * N_b$	β_{23}	- 0.0041	$R_w * M$	β_{67}	- 0.00253
$N_q * H_p$	β_{24}	18.58	$M * M$	β_{77}	0.03
$N_q * N_h$	β_{25}	- 4.15	Intercept	β_0	16.10

Figure 6.18 is a crossplot of the predicted and simulated values of movable oil recovery for reservoir conditions shown in Table 6.4 when water cut reaches 98% or pressure drawdown drops to zero and the simulation run stops because of lack of pressure support from the aquifer. Due to the widely distributed reservoir/aquifer properties, well design and operational parameters used in simulation, the movable oil recovery varies widely from 0.1% to 99%, however, the regression model successfully matched the results with R-squared value at 0.9164 within extreme values that are merely theoretical. The results indicate, however, that the reservoir screening model in Equation 6.41 with coefficients in Table 6.5 can be used to estimate the movable oil recovery.

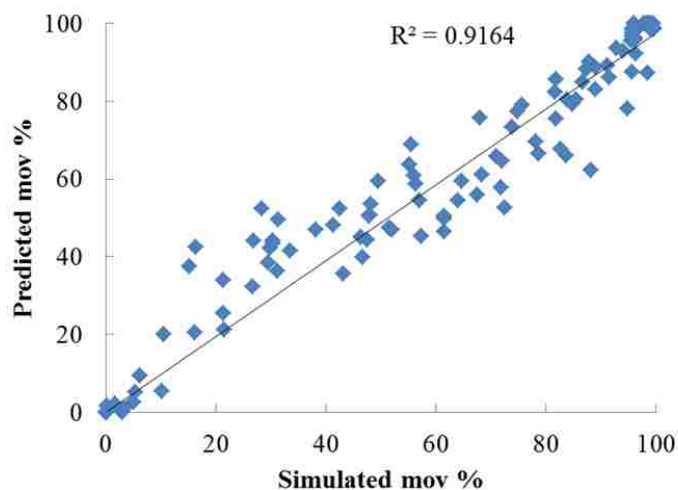


Figure 6.18. Crossplot of movable oil recovery from simulations and regression model

6.5 Model Simplification

The Equation 6.41 with 36 regression coefficients is not practical and can be further reduced by removing unimportant items. Usually, the interaction effects between groups are not important for a quadratic response surface model, which means these items could be dropped from the model (Afonja, 2013). The simplified regression coefficients are shown in Table 6.6 and the movable oil recovery prediction is shown in Figure 6.19. It is clear that, the

simplified model maintains the accuracy and can effectively replace the model with 36 coefficients.

$$\begin{aligned}
 MRF_{DWL} = & 16.10 - 4M + 5.86R_w + 15.4N_h + 3.86H_p - 0.02N_b + \dots \\
 & +153.77N_q + 15.18H_{D/I} + 0.03M^2 - 0.05R_w^2 - 1.94N_h^2 - \dots \\
 & -11.11H_p^2 + 0.00002N_b^2 - 151.09N_q^2 - 4.84H_{D/I}^2 \dots \dots \dots (6.42)
 \end{aligned}$$

Table 6.6. Simplified regression coefficients for movable oil recovery

Dimensionless group	Symbol	Coefficient	Dimensionless group	Symbol	Coefficient
$H_{D/I}$	β_1	15.18	$H_{D/I} * H_{D/I}$	β_{11}	- 4.84
N_q	β_2	153.77	$N_q * N_q$	β_{22}	- 151.09
N_b	β_3	- 0.02	$N_b * N_b$	β_{33}	0.00002
H_p	β_4	3.86	$H_p * H_p$	β_{44}	- 11.11
N_h	β_5	15.40	$N_h * N_h$	β_{55}	- 1.94
R_w	β_6	5.86	$R_w * R_w$	β_{66}	- 0.05
M	β_7	- 4.00	$M * M$	β_{77}	0.03
Intercept	β_0	16.10			

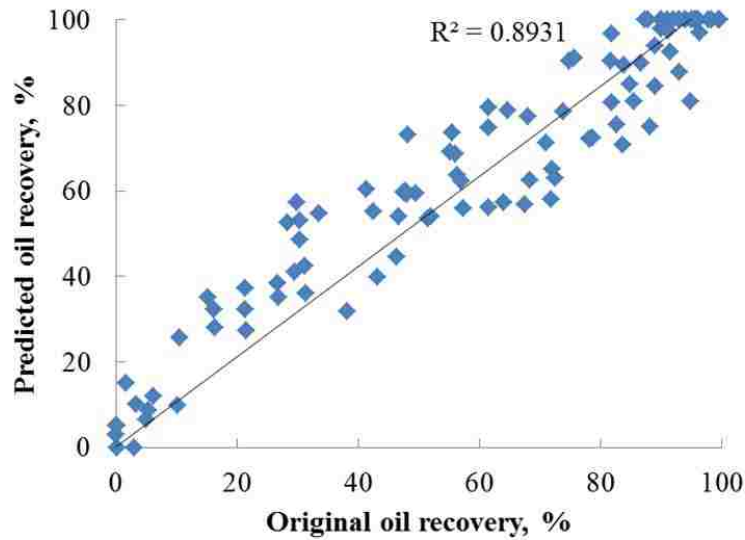


Figure 6.19. Crossplot of movable oil recovery from simulations and simplified regression model

The relative effect of the seven dimensionless groups on movable oil recovery can be determined by analysis of variance (ANOVA), as shown in Figure 6.20. From the figure, we can see that the most important groups affecting movable oil recovery are mobility ratio (M) and aquifer strength (R_w). The mobility ratio is a measure of the oil and water viscosity contrast that controls flow of oil and water in the reservoir and the shape of oil water contact. Although the aquifer strength plays little effect on the shape of oil water interface, it is the main energy source to support reservoir pressure which drives oil to the well (Hernandez, 2007). It is difficult to maintain the target production rate when there is a lack of pressure support in the reservoir.

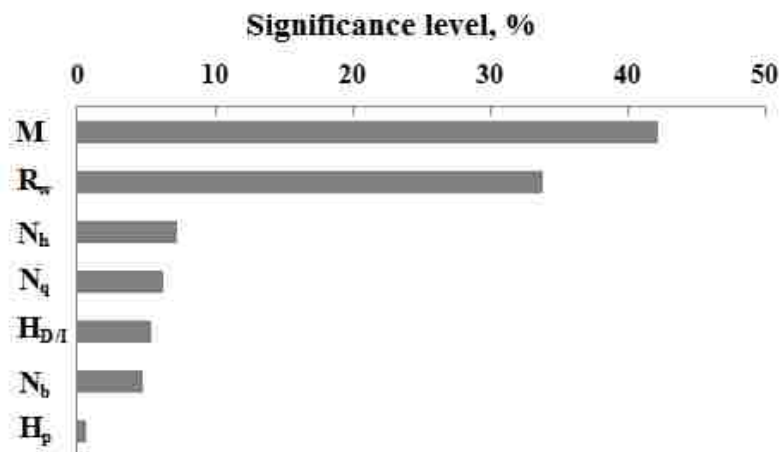


Figure 6.20. Effects of dimensionless groups on movable oil recovery

Unlike oil production in conventional well, the following groups are important for the performance of DWL: N_h , N_q , $H_{D/I}$ and N_b , which represent the effects of aquifer thickness, production-to-drainage rate ratio, D/I spacing and buoyancy-to-viscous force ratio. These groups are closely related to the DWL design and operations: larger D/I spacing is favorable to DWL as it minimizes the pressure interference from the water injection completion and requires sufficiently thick aquifer; higher water drainage rate reduces water cut at the top well completion and leads to lower values of N_h and N_q . These four groups have nearly 24% effect

on the movable oil recovery of DWL. As water coning is mainly controlled by design and operation of bottom completions, the effect of top completion length becomes minimum comparing to other groups.

The mathematical model in Equation 6.42 includes effects of reservoir and operational parameters which could be on the expected performance of a DWL well. The model could also be used to assess whether a reservoir is suitable for DWL. Equation 6.42 describes additive contributions of the reservoir properties and well parameters as:

$$MRF_{DWL} = RC_{MRF} + OP_{MRF} + WD_{MRF} \dots\dots\dots(6.43)$$

Figure 6.20 shows that reservoir properties (M , R_w and N_h) are the most important groups for DWL. Thus, the RC_{MRF} component of Equation 6.42 can be used for reservoir candidate screening as shown in Equation 6.44:

$$MRF_{DWL} = 16.10 - 4M + 5.86R_w + 15.4N_h + \dots + 0.03M^2 - 0.05R_w^2 - 1.94N_h^2 \dots\dots\dots(6.44)$$

Where, MRF is the movable oil recovery factor; RC_{MRF} is the controbution of reservoir properties and OP_{MRF} and WD_{MRF} are the contributions of DWL well's operational and design parameters, respectively.

6.6 Comparative Assessment of DWL Feasibility

Summarizing our study, we identify the following factors (limitations) to be considered for deciding on DWL feasibility for a reservoir: aquifer thickness, injectivity decline and recovery factor. A decision algorithm is shown in Figure 6.21.

A detailed reservoir-well assessment procedure includes the following steps:

Step 1: Ensure the aquifer is thick enough to install the water loop system and oil can be separated from the drainage water. Assume the water drainage completion is operated at

the maximum rate, the critical D/I spacing can be determined by Equation 6.45 and the aquifer should be 20% thicker than this value in order to install the two completions (Jin, 2009a);

$$h_{diC} = \sqrt{\frac{\frac{h'_{wo} q_{wd} B_w h'_o}{MB_o h'_w} \left(\ln \left(\frac{r'_e}{r'_w} \right) + S_{pp-wi} \right)}{\left[\ln \left(\frac{r'_e}{r'_w} \right) + S_{pp-op} \right] \frac{\partial q_{opC}}{\partial h_{di}}} - \frac{\sqrt{0.003066 h'_{wo} k_o h'_o h'_{wo} (\gamma_w - \gamma_o)}}{\sqrt{\mu_o B_o \left[\ln \left(\frac{r'_e}{r'_w} \right) + S_{pp-op} \right] \frac{\partial q_{opC}}{\partial h_{di}}}} - h_{wo}} \quad \dots \dots \dots (6.45)$$

$0 < h_{diC} < 0.8h_w$

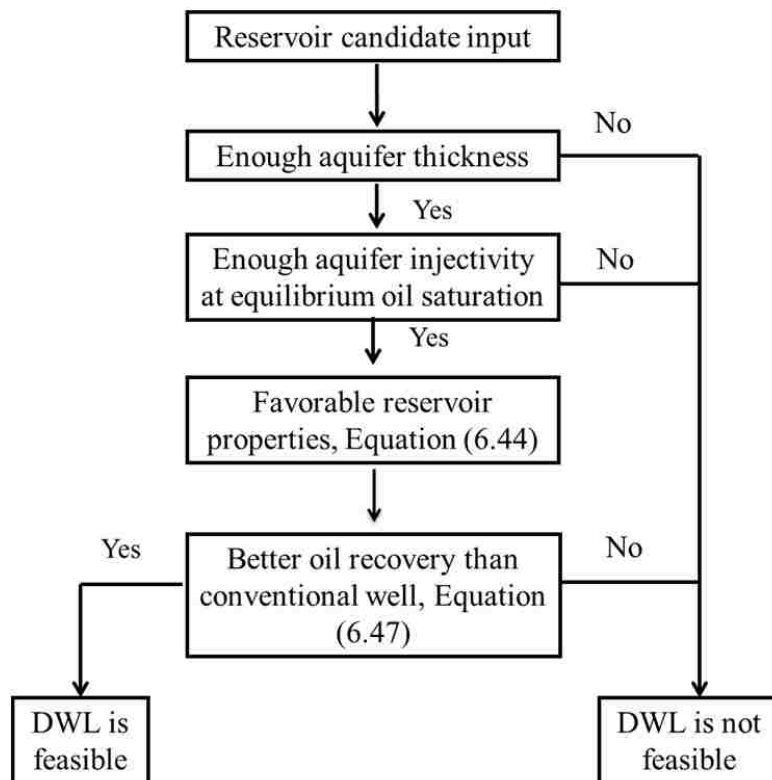


Figure 6.21. Procedure of feasibility assessment for DWL

Step 2: Evaluate injectivity of the aquifer to make sure that oily water can be injected at the target rate without fracturing the formation. If the top completion is operated at a certain rate, the maximum water drainage rate without oil breakthrough can be calculated from Equation 6.46. Water injection pressure at this rate should not be greater than the formation fracture pressure for a sufficient long time when injectivity decline is considered;

$$q_{wd_max} = \frac{q_{top} MB_o h_w'}{B_w h_o'} \frac{\ln\left(\frac{r_e'}{r_w'}\right) + S_{pp_op}}{\left[(1 - D_{di}) \ln\left(\frac{r_e'}{r_w'}\right) + S_{pp_wd} - D_{di} S_{pp_wi} \right]} + \frac{0.003066 k_w h_w' (\gamma_w - \gamma_o)}{\mu_w B_w} \frac{\left[h_{wo}' - h_o' + h_{op}' - D_{di} h_{wo}' \right]}{\left[(1 - D_{di}) \ln\left(\frac{r_e'}{r_w'}\right) + S_{pp_wd} - D_{di} S_{pp_wi} \right]} \dots\dots\dots (6.46)$$

Step 3: Rate the best candidates for DWL using Equation 6.44;

Step 4: Estimate and compare the movable oil recovery from conventional and DWL wells produced at the same top rate until water cut reaches 98%, or the aquifer support is lost. The movable oil recovery for conventional wells can be estimated from Equation 6.47 (Hernandez, 2007). DWL should be able to control water coning and reduce bypassed oil.

$$MRF_{conv} = 73.82 + 1.04W_{sp} - 0.87M - 0.0278W_{sp}^2 - \dots - 0.0095W_{sp}M + 0.00066M^2 \dots\dots\dots (6.47)$$

Where, $W_{sp} = \frac{r_{eo}\sqrt{K_v/K_h}}{h_o}$, it represents the well spacing or drainage area of a well.

Six real reservoirs from different oilfields are used in this study to demonstrate the DWL feasibility assessment procedure (Elkins, 1959; Kuo and DesBrisay, 1983; Swisher and Wojtanowicz, 1995; Kartoredjo, et al., 2006). The reservoir properties are shown in Table 6.7. Their values represent a wide range of real reservoir systems with bottom water drive.

Table 6.7. Reservoir properties of different oilfields

Field Parameter	M	Nebo- Hemphill	NB	Tambaredjo	South Huayari	Fosterton
H_o, ft	65.6	18	50	24	45	28
H_w, ft	295	64	75	8	100	27
k, md	1218	3500	900	5000	37	100
$\phi, fraction$	0.28	0.3	0.33	0.35	0.164	0.2
μ_o, cp	230	17	75	600	1.1	14
μ_w, cp	0.7	1	0.8	0.7	1	1
$\rho_o, lbm/ft^3$	58.68	58.058	58.8	59.4	53.68	58.05
$\rho_w, lbm/ft^3$	64.0	64.0	65.2	66.5	68.52	64.5
$S_{wc}, fraction$	0.224	0.2	0.22	0.23	0.288	0.21
$S_{or}, fraction$	0.285	0.275	0.15	0.25	0.367	0.25
r_{eo}, ft	500	550	550	372	1053	800
r_{ew}, ft	10000	8500	13000	5000	20000	10000

The Tambaredjo oilfield has only 8 ft bottom water which is not enough for two completions and it requires a 65 ft aquifer for the Fosterton oilfield, where only 27 ft is available. Thus, these two oilfields are dropped in step 1 as they don't have sufficiently thick aquifers.

Production rate is usually controlled for reservoirs with bottom water to prevent fast water coning. For the six cases under this study, only South Huayari oilfield has production rates from 2000 to 6000 bpd due to the low oil viscosity and high reservoir pressure, while all the others have rates less than 500 bpd. However, the South Huayari oilfield does not have good injectivity due to the low absolute permeability. The injection pressure would reach the formation fracture pressure after 10 days of production when water was injected at 4000 bpd. Thus, this oilfield is eliminated in step 2.

Thick aquifer, good permeability and high oil viscosity make the remaining three reservoirs good candidates for DWL. Using the "Favorable Reservoir Properties" criterion, Equation 6.44, we can rate the best candidates for DWL as shown in Table 6.8. Using

Equations 6.42 and 6.47, the movable oil recovery can be estimated for DWL and conventional wells, respectively, as shown in Table 6.8. It is clear that, DWL can improve oil recovery from 2 to 13% comparing to conventional well, which means DWL is feasible in these reservoirs. The 4-step assessment procedure provides a convenient way to screen reservoir candidates for DWL.

Table 6.8. Movable oil recovery estimation for different wells

Field \ Well	MRF, %	Conv.	DWL	Improvement	Favorable reservoir for DWL
M		59	68	9	Yes
Nebo-Hemphill		31	44	13	Yes
NB		26	28	2	Yes

6.7 Summary

In this chapter, we applied a systematic procedure of the inspectional analysis method to derive 14 dimensionless scaling groups for DWL wells in the bottom-water-drive reservoirs. 7 groups were found to be important in oil recovery process by experimental design and sensitivity analysis. These groups could be used to predict oil recovery and screen right reservoir candidate for DWL. Additional analysis of the groups leads to the following conclusions:

In this chapter, we applied a systematic procedure of the inspectional analysis method to derive 14 dimensionless scaling groups for DWL wells in the bottom-water-drive reservoirs. 7 groups were found to be important in oil recovery process by experimental design and sensitivity analysis. These groups could be used to predict oil recovery and screen right reservoir candidate for DWL. Additional analysis of the groups leads to the following conclusions:

1. All the dimensionless groups have physical meaning. Of the 14 groups total, six groups control DWL well design, two groups - well operation, and the remaining six groups describe the reservoir and fluid properties;
2. Completeness testing of the water cut and movable oil recovery show that their response does not change for different well-reservoir systems having the same values of other dimensionless groups, which means the dimensionless groups can fully describe the DWL system;
3. Independent testing was carried out using two real reservoir databases with more than 700 reservoirs with both light and heavy oil properties. The results show that there are no clear correlations between the groups, which indicates the dimensionless groups are independent to each other;
4. A series of simulation testing was carried out to study the effect of each dimensionless group on movable oil recovery, which indicates that only seven groups are important for DWL to produce oil from bottom-water-drive reservoirs;
5. Based on the results of Box-Behnken design, a simple dimensionless correlation has been generated to predict the movable oil recovery of DWL in various reservoirs using response surface method;
6. A general algorithm including practical limitations and recovery performance was developed to assess the feasibility of DWL in different reservoirs. Real reservoirs were used to demonstrate the screening procedure.

CHAPTER 7. CONCLUSIONS AND RECOMMENDATIONS

7.1 Conclusions

Feasibility of DWL well technology has been studied by considering physical limitations of the multi-functional wells with a downhole water sink (DWS) component for water coning control and an injection component for subsurface water disposal. The main findings of the study are summarized as follows:

1. The main limitation of DWL stems from the under-drained oil entering the drainage water. Although very small (up to 1.5%) oil contamination may cause severe formation damage around the injection completion and make the system ineffective. To avoid oil being injected to the aquifer, the maximum water drainage rate and minimum length of water looping section have been determined;
2. The maximum water drainage rate was investigated experimentally by observing oil separation in the counter-current flow conditions that represent the flow of oil and water in DWL well. The results show that, separation of large oil droplets requires water velocity below a critical value of about 0.33 ft/s (0.1 m/s). Mechanistic and drift-flux models were derived in this work - can be used to predict the critical water velocity from oil droplet terminal velocity determined experimentally for a given crude oil;
3. Parametric study shows that, oil-water interfacial tension is the most important factor in the counter-current separation process, as it controls the oil droplet size. Oil and water viscosities are also important and contribute more than 10% in determining the critical water velocity. As the water viscosity is almost constant,

the oil viscosity effect is difficult to explain physically. One explanation stems from the interdependence between viscosity and interfacial tension;

4. At initial stage of DWL well operation, oil under-drainage is likely to occur. Sage DWL well design requires longer well drainage section and larger well size to ensure oil separation and prevent oil entering the water disposal zone;
5. Some oil may not be completely separated from the water and get injected into the aquifer causing injectivity damage. To assess the water injectivity decline, an analytical model of oil transport and capture (ADA model) is developed for linear flow and coupled with results from two-phase relative permeability “bump-rate” testing. The model - verified using published data from core flooding experiments - correctly predicts the oil saturation progress and confirms experimental observation that a very small oil content in injected water does not reduce the ultimate damage but merely delays its development;
6. The results show that the ultimate injectivity damage is controlled by the equilibrium oil saturation. Based on published experimental results, a correlation of the equilibrium oil saturation and the oil droplet-to-pore size ratio has been derived. Large oil droplets lead to high equilibrium oil saturation resulting in fast injectivity decline, even for low injection rates;
7. The effect of injection rate on injectivity damage was included in the ADA model by correlating capillary number and equilibrium oil saturation. The damage is not affected by rate for capillary number below 10^{-4} . However, significant improvement of injectivity occurs for capillary number greater than 10^{-4} in linear flow;

8. By including the two phase relative permeability relationship in the model, the effect of formation wettability could be evaluated. It was found that injectivity damage with oily water is more severe in water wet formation than in oil wet rocks;
9. Based on the same damage mechanisms and oil droplet transport principle in linear flow, a radial flow model was built to evaluate the formation damage for real wells. Both analytical and simulation results show almost frontal advancement of equilibrium oil saturation with a sharp interface at the oil-free zone;
10. In radial flow, high injection rate does not help to improve injectivity as the flow velocity (and capillary number) decrease rapidly with radial distance. Thus, a thin damaged layer around the well with equilibrium oil saturation can impair the overall injectivity. In the result, in real wells water permeability damage is immediate even for extremely small oil content in the injection water. The damage is entirely controlled by equilibrium oil saturation;
11. Since oily water injection to an aquifer follows the primary drainage process, both oil and water flow during the injection and the process could be described by Buckley-Leverett fluid displacement theory. Based on the theory, two analytical models were derived based on the theory for injectivity decline in linear and radial flows. The results from B-L models closely match those from the ADA models;
12. The radially-distributed water permeability damage was mathematically converted to time-dependent skin factor. A combination of high oil droplet-to-

pore size ratio, high injection rate and water-wet rock contribute to high value of skin factor, which reduces water injectivity. The results show that formations with highly-permeable less water-wet aquifers are the best candidates for DWL;

13. Dimensional (inspectional) analysis of DWL well-reservoir system identifies 14 dimensionless scaling groups. Six groups represent parameters of DWL well design, two groups - well operation variables, and the remaining six groups describe the reservoir and fluid properties;
14. Independence and completeness testing dimensionless of the groups has been performed using large population (over 700) of actual reservoirs with randomly-assigned bottom aquifers. The results show that only seven dimensionless groups significantly explain variation of the movable oil recovery with DWL;
15. Sensitivity analysis of the seven significant groups shows that the mobility ratio (M), aquifer strength (R_w) and aquifer thickness ratio (N_h) are not only the most significant (of the seven total) but also they uniquely represent the reservoir-aquifer system - the reservoir flow conductivity and the flow drive energy of the aquifer. The remaining four groups representing DWL design and operations contribute only 24 percent of the movable oil recovery variation;
16. A simple dimensionless multivariable regression model was developed using the response surface method and the Box-Behnken design procedure to predict the movable oil recovery of DWL in various reservoirs. Part of the model representing the reservoir-aquifer system effect can be used for screening of the best reservoir candidates for DWL;

17. Combing the practical limitations and recovery performance of DWL, a general algorithm was developed to assess the feasibility of DWL for different reservoirs. Real reservoirs were used to demonstrate the screening procedure. The algorithm provides a quick and convenient way to rate the feasible reservoir candidates for DWL technology.

7.2 Recommendations

As DWL is still in a conceptual modeling stage, there is lack of some experimental and theoretical data to evaluate its actual performance. Particularly, more work is needed on the following issues:

1. A pilot field test would provide real production data and better understanding of the system shortcomings;
2. Needed are laboratory bump rate tests data on the aquifer rock samples and statistical data relating pore and droplet size to ultimate oil saturation in oil and water wet rocks. Also, droplet size measurement for different crude oils at the outlet of submersible centrifugal pumps should be carried out, as they are essential for DWL well feasibility assessment;
3. More study is needed to determine a well that would provide effective removal and lifting of the under-drained oil separated from water in the drainage section of the well. The three options presented in this work are merely conceptual ideas rather than real solutions;
4. Analytical models for DWL performance such as water breakthrough time, water cut development and oil recovery should be developed to better understand and assess the feasibility of DWL in various conditions;

5. More work on dimensionless analysis of DWL is recommended, groups including oil/water separation, formation damage skin and reservoir heterogeneity need to be integrated in the model, also their significance should be evaluated;
6. The DWL principle should be also studied for application in multi-lateral wells comprising a water-disposal vertical/horizontal well section.

NOMENCLATURE

ΔL	length of the core, [L]
Δp	pressure drop through the core, [M/LT ²]
$\Delta \rho$	density difference, [M/L ³]
μ_o	oil viscosity, [M/LT]
μ_w	water viscosity, [M/LT]
A	area, [L ²]
C	oil droplet size coefficient (Chapter 3), [dimensionless]
C	mass concentration of oil in the water (Chapters 4 and 5), [M/L ³]
C_a	capillary number, [dimensionless]
C_D	drag coefficient, [dimensionless]
C_o	drift-flux profile parameter, [dimensionless]
d	well diameter or dispersivity, [L]
D	dispersive coefficient, [L ² /T]
d_o	oil droplet diameter, [L]
F_B	buoyancy force, [ML/T ²]
F_D	drag force, [ML/T ²]
F_G	gravity force, [ML/T ²]
f_o	oil volume fraction, [fraction]
g	gravitational constant, [L/T ²]
h	completion thickness, [L]
h_o	oil zone thickness, [L]
h_{op}	length of top perforation, [L]
h_{sep}	oil separation section length, [L]
h_w	aquifer thickness, [L]
h_{wd}	water drainage completion length, [L]
h_{wi}	length of water injection perforation, [L]
I_w	water injectivity index, [L ⁴ T/M]
K	absolute permeability of the core, [L ²]
K_x	local permeability at time t , [L ²]
K_0	initial permeability, [L ²]
K_r	horizontal permeability, [L ²]
K_{rw}	relative permeability to water, [fraction]
K_{rw}^*	relative permeability to water at residual oil saturation, [fraction]
K_{ro}	relative permeability to oil, [fraction]
K_{ro}^*	relative permeability to oil at connate water saturation, [fraction]
K_w	effective water permeability, [L ²]
kz	vertical permeability, [L ²]
L_i	length of a subsection, [L]
L_t	total length of the core section investigated, [L]

M	mobility ratio, [dimensionless]
m	dimensionless viscosity number exponent or mass, [dimensionless]
n	drift-flux exponent, [dimensionless]
N_{Ca}	capillary number, [dimensionless]
N_{Ca}^*	critical capillary number, [dimensionless]
N_d	droplet to pore throat size ratio, [dimensionless]
n_w	exponent for water relative permeability, [dimensionless]
p	pressure, [M/LT ²]
q	injection rate, [L ³ /T]
q_{op}	oil production rate, [L ³ /T]
q_{oC}	critical oil production rate, [L ³ /T]
q_{sep}	water separation rate, [L ³ /T]
q_w	water rate, [L ³ /T]
q_{wd}	water drainage rate, [L ³ /T]
q_{wi}	water injection rate, [L ³ /T]
r	radial distance from well axis, [L]
Re_d	oil droplet Reynolds number, [dimensionless]
r_{eo}	oil zone radius, [L]
r_{ew}	aquifer radius, [L]
r_f	oil front position, [L]
r_s	skin zone radius, [L]
r_{well}	well radius, [L]
S	skin factor, [dimensionless]
$S_{o\ m}$	mass oil saturation, [M/L ³]
$S_{oe\ m}$	equilibrium mass oil saturation, [M/L ³]
S_{oe}	equilibrium volume oil saturation, [fraction]
S_{oe}^*	equilibrium volume oil saturation at low capillary number, [fraction]
$S_{o\ avg}$	average oil saturation, [fraction]
S_{or}	residual oil saturation, [fraction]
S_{wc}	connate water saturation, [fraction]
t	time, [T]
u	velocity, [L/T]
u_d	drift velocity for $u_w=0$, [L/T]
u_m	average superficial mixture velocity, [L/T]
u_o	in-situ oil droplet velocity, [L/T]
u_w	in-situ water velocity, [L/T]
u_{wr}	relative water velocity, [L/T]
v_{wC}	critical in-situ water velocity, [L/T]
W_e	Weber number, [dimensionless]
$W_{e,cr}$	critical Weber number, [dimensionless]
x	location at direction, [L]
z	vertical distance below top of oil zone, [L]

z_{wd}	position of water drainage completion below the top of oil zone, [L]
z_{wi}	position of water injection completion below the top of oil zone, [L]
α	adsorptive coefficient, [1/T]
β	parameters related to oil adsorption process, [dimensionless]
λ	mobility or constant in oil droplets departure process, [M/LT]
μ	viscosity, [M/LT]
μ_D	dimensionless viscosity group, [dimensionless]
π	dimensionless group, [dimensionless]
ρ	density, [M/L ³]
ρ_w	water density, [M/L ³]
σ_{ow}	oil-water interfacial tension, [M/T ²]
σ	local retention, [fraction]
\square	porosity, [fraction]

Subscripts

0	initial, $t = 0$
1	multiplicative scale factor
2	additive scale factor
avg	average
B	buoyancy
C_a	capillary
D	dimensionless or drag force
d	oil droplet or drift
d	droplet
D	decline
in	inlet
o	oil
oe	equilibrium oil saturation
or	residual oil
out	outlet
ow	oil and water
ow	oil water
pt	pore throat
r	radial (horizontal) direction
t	time t
w	water
wc	connate water
x	x direction or location
y	y direction
z	z direction

REFERENCES

- Abdallah, W. et al. Fundamentals of Wettability. *Oilfield Review*, Summer, 2007.
- Abou-Sayed, A.S. et al, A Mechanistic Model for Formation Damage and Fracture Propagation During Water Injection, *SPE 94606, Proceedings of SPE European Formation Damage Conference, Scheveningen, Netherland, May 25-27, 2005.*
- Abou-Sayed, A.S, et al. Produced Water Management Strategy and Water Injection Best Practices: Design, Performance, and Monitoring. *SPE Production & Operations, Vol. 22, No. 1, Feb. 2007.*
- Afonja, G. I. Development of a Framework for Scaling Surfactant Enhanced CO₂ Flooding from Laboratory Scale to Field Implementation. *Ph.D dissertation of Louisiana State University, Baton Rouge, LA, Aug. 2013.*
- Alhoni, M. A. et al. Application of Downhole Oil-Water Separation: A Feasibility Study. *SPE 80485, Proceedings of SPE Asia Pacific Oil and Gas Conference and Exhibition, Jakarta, Indonesia, Apr. 15–17, 2003.*
- Alkaya, B. Drift-Flux Models for Multiphase Flow in Wells. *MS Report of Stanford University, Stanford, CA, Sep. 2002.*
- Al-Riyamy, K and Sharma, M.M. Filtration Properties of Oil-in-Water Emulsions Containing Solids. *SPE 73769, Proceedings of International Symposium and Exhibition on Formation Damage Control, Lafayette, LA, Feb. 20-21, 2002.*
- Alvarado, D.A. and Marsden, S.S. Jr. Flow of Oil-in-Water Emulsions through Tubes and Porous Media. *SPE Journal, Vol. 19, No. 6, Dec. 1979.*
- Ambrose, A.W. Analysis of Oil-field Water Problems. *AIME, Vo. 65, p. 245-268, 1921.*
- Angeli, P. and Hewitt, G. F. Drop Size Distributions in Horizontal Oil-Water Dispersed Flows. *Chemical Engineering Science, Vol. 55, 2000.*
- API. Overview of Exploration and Production Waste Volumes and Waste Management Practices in the United States. *Prepared by ICF Consulting for the American Petroleum Institute, Washington, DC, May. 2000.*
- Argonne National Laboratory and Arthur Langhus Layne – LLC. Analysis of Data from a Downhole Oil/Water Separator Field Trial in East Texas. *Report for the U.S. Department of Energy National Petroleum Technology Office, Feb. 2001.*
- Arntzen, R. Gravity Separator Revamping. *Thesis of Dr. Ing., Norwegian University of Science and Technology, Trondheim, Norway, Mar. 2001.*

- Arya, A, et al. Dispersion and Reservoir Heterogeneity. *SPE Reservoir Engineering*, Vol. 3, No. 1, Feb. 1988.
- Aslett, R., et al. Circuit Optimization via Sequential Computer Experiments: Design of an Output Buffer. *Journal of the Royal Statistical Society, Series C (Applied Statistics)*, Vol. 47, No. 1, 1998.
- Augier, F. et al. Slip Velocity and Drag Law in a Liquid-Liquid Homogeneous Dispersed Flow. *AIChE Journal*, Vol. 49, No. 9, Sep. 2003.
- Auset, M and Keller, A. Pore-scale Visualization of Colloid Straining and Filtration in Saturated Porous Media Using Micromodels. *Water Resources Research*, Vol. 42, 2006.
- Bai, M., et al. An Alternative Method for Predicting Injectivity Decline in Produced Water Re-Injection. *SPE 120829, Proceedings of 8th European Formation Damage Conference, Scheveningen, The Netherlands, May. 27-29, 2009.*
- Balasubramaniam, R. et al. Two Phase Flow Modeling: Summary of Flow Regimes and Pressure Drop Correlations in Reduced and Partial Gravity. *NASA/CR-2006-214085, Report for National Aeronautics and Space Administration, Jan. 2006.*
- Barkman, J.H. and Davidson, D.H. Measuring Water Quality and Predicting Well Impairment. *JPT*, 865-873, 1972.
- Barton, D.R. An experimental investigation into the mixture stability of crude oil and brine within the Weeks Island Strategic Petroleum Reserve. *MS Thesis of Louisiana State University, Baton Rouge, LA, 1990.*
- Bear, J. Dynamics of Fluids in Porous Media. *Elsevier Publishing Co., Inc. p. 665–727, New York, 1972.*
- Bennion, D.B. et al. Injection Water Quality - A Key Factor to Successful Waterflooding. *Journal of Canadian Petroleum Technology*, Vol. 37, No. 6, Jun. 1998.
- Bennion, D.B., et al. Remediation of Water and Hydrocarbon Phase Trapping Problems in Low Permeability Gas Reservoirs. *Journal of Canadian Petroleum Technology*, Vol. 38, No. 8, Aug. 1999.
- Bennion, D. B., et al. Water Quality Considerations Resulting in the Impaired Injectivity of Water Injection and Disposal Wells. *CIPC 2000-067, Proceedings of Canadian International Petroleum Conference, Calgary, AB, Jun. 4 - 8, 2000.*
- Bennion, D.B., et al. Water Quality Considerations Resulting in the Impaired Injectivity of Water Injection and Disposal Wells. *Journal of Canadian Petroleum Technology*, Vol. 40, No. 6, Jun. 2001.

- Bird, R. B. et al. *Transport Phenomena*. J. Wiley, New York, 2007.
- Bowers, B.E. et al. Development of a Downhole Oil/Water Separation and Reinjection System for Offshore Application. *SPE Production & Facilities*, Vol. 15, No. 2, May. 2000.
- Box, G.E.P. and Behnken, D.W. Some New Three Level Designs for the Study of Quantitative Variables. *Technometrics*, Vol. 2, No. 4, Nov. 1960.
- Box, G.E.P., et al. *Statistics for Experimenters: An Introduction to Design, Data Analysis, and Model Building*. John Wiley & Sons. New York City, 1978.
- Braun, E.M. and Holland, R.F. Relative Permeability Hysteresis: Laboratory Measurements and a Conceptual Model. *SPE Reservoir Engineering*, Vol. 10, No. 3, Aug. 1995.
- Brauner, N. Multiphase fluid flow and pressure drop: liquid-liquid two-phase flow. *Heat Exchanger Design Updates*, Vol. 5, Begell House Inc, New York, NY, 1998.
- Brauner, N. Modeling and Control of Two-Phase Phenomena: Liquid-Liquid Two-Phase Flow Systems. Ed. V Bertola, CISM Center, Udine, Italy, 2002.
- Brigham, W.E. Mixing Equations in Short Laboratory Cores. *SPE Journal*, Vol. 14, No. 1, Feb. 1974.
- Brooks, R.H and Corey, A.T. Properties of Porous Media Affecting Fluid Flow. *Journal of the Irrigation and Drainage Division*, Vol. 92, No. 2, Jun. 1966.
- Buckingham, E. On Physically Similar Systems; Illustrations of the Use of Dimensional Equations. *Phys. Rev.*, vol. 4, Iss. 4, Oct. 1914.
- Buret, S, et al. Emulsion Deposition in Porous Media: Impact on Well Injectivity. *SPE 113821, Proceedings of Europec/EAGE Conference and Exhibition, Rome, Italy, Jun. 9-12, 2008*.
- Buret, S, et al. Water Quality and Well Injectivity: Do Residual Oil-in-Water Emulsions Matter? *SPE Journal*, Vol. 15, No. 2, Jun. 2010.
- Carpenter, C. W., et al. A Verification of Waterflood Scaling in Heterogeneous Communicating Flow Models. *Soc. Pet. Eng. J.* Vol. 2, No. 1, 1962.
- Carslaw, H. S. and Jaeger, J. C. *Conduction of Heat in Solids*. 2nd Edition, Oxford, Clarendon Press, 1959.
- Cartmill, J.C. and Dickey, P.A. Flow of a Disperse Emulsion of Crude Oil in Water in Porous Media. *SPE 2481, proceedings of Fall Meeting of the Society of Petroleum Engineers of AIME, Denver, CO, Sep. 28 - Oct. 1, 1969*.

- Chang, M.M. and Maerefat, N.L. State-of-the-art Report Summarizing Techniques to Determine Residual Oil Saturation and Recommendations on the Requirements for Residual Oil Saturation Research and Development. *Technical report for National Inst. for Petroleum and Energy Research, Bartlesville, OK, May. 1986.*
- Chen, C.S. Analytical and Approximate Solutions to Radial Dispersion from an Injection Well to a Geological Unit with Simultaneous Diffusion into Adjacent Strata. *Water Resources Research. Vol. 21, No. 8, Aug. 1985.*
- Chen, J., et al. NMR Wettability Indices: Effect of OBM on Wettability and NMR Responses. *Journal of Petroleum Science and Engineering, Vol. 52, 2006.*
- Christophe, F., et al. Conceptual Design Framework Supported by Dimensional Analysis and System Modeling. *Estonian Journal of Engineering, Vol. 14, 2008.*
- Chün, N. M. Mining a Massive Reservoir Engineering Database for Determinants of Recovery Efficiency. *Report AES/PE/12-02 for Section for Petroleum Engineering, Delft University of Technology, Delft, The Netherlands, Jan. 2012.*
- Civan, F. Reservoir Formation Damage: Fundamentals, Modeling, Assessment, and Mitigation. *2nd edition, Gulf Professional Publishing, 2007.*
- Clift, R. et al. Bubbles, Drops and Particles. *Academic Press, New York, 1978.*
- CMG. STARS User's Guide – Version 2011. *Computer Modelling Group Ltd, Calgary, Canada, 2011.*
- Coats, K.H and Smith, B.D. Dead-End Pore Volume and Dispersion in Porous Media. *SPE Journal, Vol. 4, No. 1, Mar. 1964.*
- Cosse, R. Basics of Reservoir Engineering: Oil and Gas Field Development Techniques. *Editions Technip, Paris, France, 1993.*
- Craig, F. F., et al. A Laboratory Study of Gravity Segregation in Frontal Drives. *Trans. AIME, Vol. 210, 1957.*
- Croes, G. A., Schwarz, N. Dimensionally Scaled Experiments and the Theories on the Water-Drive Process. *Trans. AIME, Vol. 204, 1955.*
- Detienne, J.L, et al. A Simulator for Produced Water Re-injection in Thermally Fractured Wells. *SPE 95021, Proceedings of SPE European Formation Damage Conference, Scheveningen, The Netherlands, May. 25-27, 2005.*
- Detienne, J.L, et al. Produced Water Re-injection on A Low Permeability Carbonaceous Reservoir. *SPE 78482, Proceedings of Abu Dhabi International Petroleum Exhibition and Conference, Abu Dhabi, United Arab Emirates, Oct. 13-16, 2002.*

- Devereux, O.F. Emulsion Flow in Porous Solids: I. A Flow Model. *The Chemical Engineering Journal*, Vol. 7, Iss. 2, 1974a.
- Devereux, O.F. Emulsion Flow in Porous Solids: II. Experiments with A Crude Oil-in-water Emulsion in Porous Sandstone. *The Chemical Engineering Journal*, Vol. 7, Iss. 2, 1974b.
- DiCarlo, D.A., et al. Three-Phase Relative Permeability of Water-Wet, Oil-Wet and Mixed-Wet Sandpacks. *SPE Journal*, Vol. 5, No. 1, Mar. 2000.
- Duan, S. Progressive Water-oil Transition Zone Due to Transverse Mixing near Wells. *Ph.D Dissertation, Louisiana State University, Baton Rouge, LA, Aug. 2009.*
- Eastwood, C. D., et al. The Breakup of Immiscible Fluids in Turbulent Flows. *J. Fluid Mech.* Vol. 502, 2004.
- Element, D.J., et al. Comparison of Polymer and Waterflood Residual Oil Saturations. *Report for the IEA Collaborative Project on Enhanced Oil Recovery, 21st International Workshop and Symposium, Edinburgh, UK, Sep. 2000.*
- Elkins, L. F. Fosterton Field – An Unusual Problem of Bottom Water Coning and Volumetric Water Invasion Efficiency. *Petroleum Transactions, AIME, Vol. 216, 1959.*
- Engelsvoll, O. J. Throttle Valves and Pumps Affects Oil-water Separation. *Report for TEKNA Produced Water Management, Stavanger, Jan. 19-20, 2011.*
- Ferreira, S.L.C., et al. Box-Behnken Design: an Alternative for the Optimization of Analytical Methods. *Analytica Chimica Acta*, Vol. 597, Iss. 2, 2007.
- Fitnawan, E.A.Y. et al. Inclined Gravity Downhole Oil-Water Separator: Using Laboratory Experimental Results for Predicting the Impact of Its Application in High Rate Production Wells. *SPE 119939, Proceedings of Asia Pacific Oil and Gas Conference & Exhibition, Jakarta, Indonesia, Aug. 4-6, 2009.*
- Fleming, P.D. and Mansoori, J. An Accurate Numerical Technique for Solution of Convection-Diffusion Equations without Numerical Dispersion. *SPE Reservoir Engineering*, Vol. 2, No. 3, Aug. 1987.
- Flores, J.G., et al. Characterization of Oil–Water Flow Patterns in Vertical and Deviated Wells. *SPE Prod. & Facilities*, Vol. 14, No. 2, May. 1999.
- Friedman, B.M.C and Friedman, C.R. Terminal Velocity of Canola Oil, Hexane, and Gasoline Drops Rising in Water due to Buoyancy. *International Journal of Scientific & Engineering Research*, Vol. 2, Iss. 12, Dec. 2011.
- Foster, W.R. A Low-Tension Waterflooding Process. *JPT*, Feb. 1973.

- Furtado, C.J.A., et al. Produced Water Reinjection in Petrobras Fields: Challenges and Perspectives. *SPE 94705, Proceedings of SPE Latin American and Caribbean Petroleum Engineering Conference, Rio de Janeiro, Brazil, Jun. 20-23, 2005.*
- Furtado, C.J.A. et al. Evaluation of Different Models for Injectivity Decline Prediction. *SPE 108055, Proceedings of the Latin American & Caribbean Petroleum Engineering Conference, Buenos Aires, Argentina, Apr. 15-18, 2007.*
- Geankoplis, C.J. Transport Processes and Unit Operations. *Prentice-Hall International, Inc. 3rd Edition, Massachusetts, Mar. 1993.*
- Geertsma, J., Croes, G. A., Schwarz, N. Theory of Dimensionally Scaled Models of Petroleum Reservoirs. *Trans., AIME, Vol. 207, 1956.*
- Geosphere, Inc. Maximum Allowable Concentration, Residual Saturation, and Free-Product Mobility Technical Background Document and Recommendations. *Report for Alaska Statement of Cooperation Working Group, Sep. 2006.*
- Gelhar, L.W. and Collins, M.A. General Analysis of Longitudinal Dispersion in Nonuniform Flow. *Water Resources Research. Vol. 7, No. 6, Dec. 1971.*
- Gharbi, R, et al. Scaling Miscible Fluid Displacements in Porous Media. *Energy Fuels, Vol. 12, No. 4, 1998.*
- Ghiaasiaan, S.M., et al. Hydrodynamic Characteristics of Counter-Current Two-Phase Flow in Vertical and Inclined Channels: Effect of Liquid Properties. *Int. J. Multiphase Flow, Vol. 23, 1997.*
- Gibbings, J.C. Dimensional Analysis. *Springer-Verlag London Limited, London, 2011.*
- Gokcal, B. et al. Effects of High Oil Viscosity on Drift Velocity for Horizontal and Upward Inclined Pipes. *SPE Projects, Facilities & Construction, Vol. 4, No. 2, Jun. 2009.*
- Gokcal, B. et al. Effects of High Oil Viscosity on Oil/Gas Flow Behavior in Horizontal Pipes. *SPE Projects, Facilities & Construction, Jun. 2008.*
- Grattoni, C.A., et al. Dimensionless Groups for Three-Phase Gravity Drainage Flow in Porous Media. *Journal of Petroleum Science and Engineering, Vol. 29, 2001.*
- Gunning, J., et al. Coning in Dual Completed Systems. *Journal of Petroleum Science and Engineering, Vol. 23, Iss. 1, May. 1999.*
- Gupta, S.P and Greenkorn, R.A. Determination of Dispersion and Nonlinear Adsorption Parameters for Flow in Porous Media. *Water Resource Research, Vol. 10, No. 4, 1974.*

- Haggerty, D. J. and Seyler, B. Investigation of Formation Damage from Mud Cleanout Acids and Injection Waters in Aux Vases Sandstone Reservoirs. *ISGS IL Petroleum Series No. 152, 1997.*
- Hahn, K. Solving Cubic and Quartic Polynomials. *Karl's Calculus Tutor, July, 2005.*
- Harmathy, T. Z. Velocity of Large Drops and Bubbles in Media of Infinite or Restricted Extent. *AIChE Journal, Vol. 6, Iss. 2, Jun. 1960.*
- Hasan, A.R. and Kabir, C.S. A New Model for Two-Phase Oil/Water Flow: Production Log Interpretation and Tubular Calculations. *SPE Production Engineering, Vol. 5, No. 2, May. 1990.*
- Hasan, A.R. and Kabir, C.S. A Simplified Model for Oil/Water Flow in Vertical and Deviated Wellbores. *SPE Production & Facilities, Vol. 14, No. 1, Feb. 1999.*
- Hawkins, M. F. A Note on the Skin Effect. *Journal of Petroleum Technology, Vol. 8, No. 12, Dec. 1956.*
- Hayashi, K. et al. Terminal Velocity of A Taylor Drop in A Vertical Pipe. *International Journal of Multiphase Flow, Vol. 37, 2011.*
- Henley D., et al. A Scale-Model Study of Bottom-Water Drives. *Journal of Petroleum Technology, Vol. 13, No. 1, Jan. 1961.*
- Herman, M. E. Mathematical Evaluation of Operating Parameters Identified in a Class II Brine Disposal Well Permit Application. *Report to US EPA, 1988.*
- Hernandez, J.C. Oil Bypassing by Water Invasion to Wells Mechanisms and Remediation, *Ph.D dissertation, Louisiana State University, Baton Rouge, 2007.*
- Hernandez, J.C. and Wojtanowicz, A.K. Prediction of Oil Bypassing in Bottom Water Systems Using Dimensionless Groups. *CIPC 2007-064. Canadian International Petroleum Conference. Calgary, Alberta, Canada, June 12 – 14, 2007.*
- Hilfer, R. and Øren, P. E. Dimensional Analysis of Pore Scale and Field Scale Immiscible Displacement. *Transport in Porous Media, Vol. 22, Iss. 1, Jan. 1996.*
- Hinze, J. O. Fundamentals of the Hydrodynamic Mechanism of Splitting in Dispersion Processes. *AIChE Journal, Vol. 1, No. 3, 1955.*
- Hirasaki, G.J., et al. Surfactant Based Enhanced Oil Recovery and Foam Mobility Control. *2nd Annual Technical Report for DE-FC26-03NT15406, Jul. 2005.*
- Hirasaki, G.J., et al. Surfactant Based Enhanced Oil Recovery and Foam Mobility Control. *Technical Report to DOE, DE-FC26-03NT15406, Jul. 2006.*

- Holmes, M. Capillary Pressure and Relative Permeability Petrophysical Reservoir Models. *Digital Formation, Inc. Denver, CO, May. 2002.*
- Hoopes, J.A. and Harleman, D.R.F. Dispersion in Radial Flow from a Recharge Well. *Journal of Geophysical Research, Vol. 72, No. 14, Jul. 1967.*
- Hsi, C.D., et al. Prudhoe Bay Field, Alaska, Waterflood Injection Water Quality and Remedial Treatment Study. *SPE 20689, Proceedings of SPE Annual Technical Conference and Exhibition, New Orleans, LA, Sep. 23-26, 1990.*
- Hsieh, P.A. A New Formula for the Analytical Solution of the Radial Dispersion Problem. *Water Resources Research. Vol. 22, No. 11, Oct. 1986.*
- Huang, D.D, et al. An Improved Model for Relative Permeability and Capillary Pressure Incorporating Wettability. *SCA-9718, Proceedings of SCA International Symposium, Calgary, Canada, Sep. 7-10, 1997.*
- Hull, L.C. and Karen, N.K. Dispersion in Fracture Networks. *Proceedings of Eighth Workshop Geothermal Reservoir Engineering, Stanford University, Stanford, CA, Dec. 1982.*
- Hustedt, B, et al. Induced Fracturing in Reservoir Simulations: Application of a New Coupled Simulator to a Water Flooding Field Example. *SPE Reservoir Evaluation & Engineering, Vol. 11, No. 3, Jun. 2008.*
- Idowu, N.A. Pore-Scale Modeling: Stochastic Network Generation and Modeling of Rate Effects in Waterflooding. *Ph.D Dissertation, Imperial College, London, Jul. 2009.*
- Ishii, M. One-Dimensional Drift-Flux Model and Constitutive Equations for Relative Motion Between Phases in Various Two-Phase Flow Regimes. *Argonne National Lab Report, Argonne, IL, Oct. 1977.*
- Jadhunandan, P.P. and Morrow, N.R. Effect of Wettability on Waterflood Recovery for Crude-Oil/Brine/Rock Systems. *SPE Reservoir Engineering, Vol. 10, No. 1, Feb. 1995.*
- Janssen, P.H. et al. Laboratory Study Investigating Emulsion Formation in the Near-Wellbore Region of a High Water-Cut Oil Well. *SPE Journal, Vol. 6, No. 1, Mar. 2001.*
- Janssen, J. M. H. and Meijer, H. E. H. Droplet Breakup Mechanisms: Stepwise Equilibrium versus Transient Dispersion. *Journal of Rheology, Vol. 37, Iss. 4, 1993.*
- Jha, R.K, et al. Effect of Diffusion on Dispersion. *SPE Journal, Vol. 16, No. 1, Mar. 2011.*
- Jin, L. and Wojtanowicz, A.K. Analytical Assessment of Water-free Production in Oil Wells with Downhole Water Loop for Coning Control. *SPE 141470, Proceedings of SPE Production and Operations Symposium, Oklahoma City, OK, Mar. 27-29, 2011a.*

- Jin, L. and Wojtanowicz, A.K. Coning Control and Recovery Improvement Using In-Situ Water Drainage/Injection in Bottom/Water/Drive Reservoir. *SPE 129663, Proceedings of SPE Improved Oil Recovery Symposium, Tulsa, OK, Apr. 24-28, 2010d.*
- Jin, L. and Wojtanowicz, A.K. Minimum Produced Water from Oil Wells with Water-Coning Control and Water-Loop Installations. *SPE 143715, Proceedings of SPE Americas E&P Health, Safety, Security, and Environmental Conference, Houston, TX, Mar. 21-23, 2011b.*
- Jin, L. and Wojtanowicz, A.K. Performance Analysis of Wells with Downhole Water Loop Installation for Water Coning Control. *Journal of Canadian Petroleum Technology, Vol. 49, No. 6, Jun. 2010a.*
- Jin, L. Downhole Water Loop (DWL) Well Completion for Water Coning Control --- Theoretical Analysis. *MS Thesis, Louisiana State University, Baton Rouge, LA, Dec. 2009a.*
- Jin, L. et al. An Analytical Model for Water Coning Control Installation in Reservoir with Bottom Water. *CIPC 2009-098, Proceedings of Canadian International Petroleum Conference, Calgary, Alberta, Jun. 16 - 18, 2009c.*
- Jin, L. et al. An Analytical Model for Water Coning Control Installation in Reservoir With Bottomwater. *Journal of Canadian Petroleum Technology, Vol. 49, No. 5, May. 2010b.*
- Jin, L. et al. Scaling Analysis of Wells with Downhole Water Loop Completion for Bottomwater Control. *Journal of Canadian Petroleum Technology, Vol. 49, No. 11, Nov. 2010c.*
- Johnson, S.J, et al. An Overview of Oil and Grease Determination in Produced Water. *SPE 35877, Proceedings of SPE Health, Safety and Environment in Oil and Gas Exploration and Production Conference, New Orleans, LA, Jun. 9-12, 1996.*
- Johnston, A.J. An Investigation into Stratified Co- and Countercurrent Two-Phase Flow. *SPEPE, Vol. 3, No. 3, Aug. 1988a.*
- Johnston, A.J. Controlling Effects in Countercurrent Two-Phase Flow. *SPEPE, Vol. 3, No. 3, Aug. 1988b.*
- Joseph, D. D. Rise Velocity of a Spherical Cap Bubble. *J. Fluid Mech, Vol. 488, 2003.*
- Ju, B, et al. Improving Water injectivity and Enhancing Oil Recovery by Wettability Control Using Nanopowders. *Journal of Petroleum Science and Engineering, Vol. 86-87, May. 2012.*

- Jurgawczynski, M. Predicting Absolute and Relative Permeabilities of Carbonate Rocks Using Image Analysis and Effective Medium Theory. *Ph.D Dissertation, Imperial College, London, Feb. 2007.*
- Karabelas, A.J. Droplet Size Spectra Generated in Turbulent Pipe Flow of Dilute Liquid /Liquid Dispersions. *AIChE Journal, Vol. 24, No. 2, Mar. 1978.*
- Kartoredjo, H., et al. Heavy Oil Development and Reservoir Management Challenges in Producing Onshore Shallow Reservoirs in Suriname. *SPE 104068, Proceedings of First International Oil Conference and Exhibition in Mexico, Cancun, Mexico Aug. 31 - Sep. 2, 2006.*
- Katz, A. J. and Thompson, A. H. Quantitative Prediction of Permeability in Porous Rock. *Physical Review B, Vol. 34, No. 11, Dec. 1986.*
- Khatib, Z. and Verbeek, P. Water to Value - Produced Water Management for Sustainable Field Development of Mature and Green Fields. *SPE 73853, Proceedings of SPE International Conference on Health, Safety and Environment in Oil and Gas Exploration and Production, Kuala Lumpur, Malaysia, Mar. 20-22, 2002.*
- Khatib, Z. Produced Water Management: Is it a Future Legacy or a Business Opportunity for Field Development. *IPTC 11624, Proceedings of the International Petroleum Technology Conference, Dubai, U.A.E., Dec. 4-6, 2007.*
- Kim, H.Y., et al. Flow Pattern and Flow Characteristics for Counter-current Two-phase Flow in a Vertical Round Tube with Wire-coil Inserts. *Int. J. Multiphase Flow, Vol. 27, 2001.*
- King, R.W and Adegbesan, K.O. Resolution of the Principal Formation Damage Mechanisms Causing Injectivity and Productivity Impairment in the Pembina Cardium Reservoir. *SPE 38870, Proceedings of SPE Annual Technical Conference and Exhibition, San Antonio, TX, Oct. 5-8, 1997.*
- Kjos, T. et al. Down-Hole Water-Oil Separation and Water Reinjection through Well Branches, *SPE 030518, Proceedings of SPE Annual Meeting held in Dallas, Texas, October 22-25, 1995.*
- Klee, A. J. and Treybal, R. E. Rate of Rise or Fall of Liquid Drops. *AIChE J. Vol. 2, Iss. 4, Dec. 1956.*
- Kocurek Industries. Core Samples for Research. *Hard Rock Division, available at <http://www.kocurekindustries.com/>, 2013.*
- Kootiani, R.C. and Samsuri, A.B. Analysis Fraction Flow of Water versus Cumulative Oil Recoveries Using Buckley Leverett Method. *World Academy of Science, Engineering and Technology, Vol. 72, 2012.*

- Krummel, A.T., et al. Visualizing Multiphase Flow and Trapped Fluid Configurations in a Model Three-Dimensional Porous Medium. *AICHE Journal*, 2013.
- Kuo, C. T. and DesBrisay, C. L. A Simplified Method for Water Coning Predictions. *SPE 12067, Proceedings of the 58th ATCE, San Francisco, Oct. 5–8, 1983.*
- Kurimoto, R. et al. Terminal Velocity of A Single Drop in A Vertical Pipe in Clean and Fully-Contaminated Systems. *ICMF2010, Paper No. 4.2.3, Proceedings of the 7th International Conference on Multiphase Flow, 2010.*
- Kwok, W., et al. Dispersion in Consolidated Sandstone with Radial Flow. *Transport in Porous Media, Vol. 19, Iss. 1, Apr. 1995.*
- Lake, L.W. Enhanced Oil Recovery. *Prentice Hall, New Jersey, 1989.*
- Lee, J., et al. Pressure Transient Testing. *SPE Textbook Series, Vol. 9, Richardson, TX, 2003.*
- Lee, R., et al. Strategies for Produced Water Handling in New Mexico. *Proceedings of Ground Water Protection Council Produced Water Conference, Colorado Springs, CO, Oct. 16-17, 2002.*
- Levich, V. G. Physicochemical Hydrodynamics. *Englewood Cliffs, Prentice-Hall, N.J. 1962.*
- Licht, W. and Narasimhamurty, G. S. R. Rate of Fall of Single Liquid Droplets. *AICHE J. Vol. 1, No. 3, Sept. 1955.*
- Ling, K. Fractional Flow in Radial Flow System - A Study for Peripheral Waterflood. *SPE 152129, Proceedings of SPE Latin America and Caribbean Petroleum Engineering Conference, Mexico City, Mexico, Apr. 16-18, 2012.*
- Liu, X. and Civan, F. Formation Damage and Skin Factor Due to Filter Cake Formation and Fines Migration in the Near-Wellbore Region. *SPE 27364, Proceedings of the SPE Formation Damage Control Symposium, Lafayette, LA, Feb. 7-10, 1994.*
- Lyman, W.J, et al. Handbook of Chemical Property Estimation Methods. *McGraw-Hill Book Co, 1982.*
- Mandal, T. K. et al. Motion of Taylor Bubbles and Taylor Drops in Liquid-Liquid Systems. *Ind. Eng. Chem. Res. Vol. 47, 2008.*
- Marino, M.A. Distribution of Contaminants in Porous Media Flow. *Water Resources Research, Vol. 10, No. 5, Oct. 1974.*
- Mattax C. and Dalton, R.: Reservoir Simulation. *SPE Monograph Vol. 13, Richardson, Texas, 1990.*

- Matthews, C.M. et al. Application of Downhole Oil/Water Separation Systems in the Alliance Field. *SPE 35817, Proceedings of the 3rd International Conference on Health, Safety & Environment in Oil & Gas Exploration and Production, New Orleans, LA, Jun. 9-12, 1996.*
- McAuliffe, C.D. Oil-in-Water Emulsions and Their Flow Properties in Porous Media. *Journal of Petroleum Technology, Vol. 25, No. 6, Jun. 1973(a).*
- McAuliffe, C.D. Crude-Oil-Water Emulsions to Improve Fluid Flow in an Oil Reservoir. *Journal of Petroleum Technology, Vol. 25, No. 6, Jun. 1973(b).*
- McCoy, T.E. and Kelkar, B.G. Investigation of Radial Dispersion-capacitance System in Porous Media, *Water Resources Research. Vol. 26, No. 1, Jan. 1990.*
- McKee, S and Swailes, D. On the Derivation of the Langmuir Isotherm for Adsorption Kinetics. *J. Phys. A Math. Gen. 24, L207, 1991.*
- Mendez, P.F. and Ordóñez, F. Scaling Laws from Statistical Data and Dimensional Analysis. *Journal of Applied Mechanics, Vol. 72, Sep. 2005.*
- Meyer, H.I. and Garder, A.O. Mechanics of Two Immiscible Fluids in Porous Media. *Journal of Applied Physics, Vol. 25, Iss. 11, Nov. 1954.*
- Mishra, B. K. and Sharma, M. M. Measurement of Pore Size Distributions from Capillary Pressure Curves. *AIChE Journal, Vol. 34, Iss. 4, Apr. 1988.*
- Moghadasi, J, et al. Theoretical and Experimental Study of Particle Movement and Deposition in Porous Media during Water Injection. *Journal of Petroleum Science and Engineering, Vol. 43, Iss. 3-4, Aug. 2004.*
- Montgomery, D. C. and Runger, G. C. Applied Statistics and Probability for Engineers. *John Wiley & Sons, New York, NY, Mar. 22, 2010.*
- Morrow, N.R., et al. Measurement and Correlation of Conditions for Entrapment and Mobilization of Residual Oil. *Final Report for U.S. DOE Project, Oct. 1981.*
- Morrow, N.R., et al. Entrapment and Mobilization of Residual Oil in Bead Packs. *SPE Reservoir Engineering, Aug. 1988.*
- Mousaviraad, S.M. Intermediate Mechanics of Fluids. *Lecture Notes of College of Engineering, The University of Iowa, 2010.*
- Munson, B.R., et al. Fundamentals of Fluid Mechanics. *6th Edition, John Wiley & Sons, Inc., R. R. Donnelley/Jefferson City, 2009.*

- Muskat, M. and Wyckoff, R.D. An Approximate Theory of Water Coning in Oil Production. *Trans. AIME, Vol. 114, 1934.*
- Muskat, M. and Wyckoff, R.D. An Approximate Theory of Water-coning in Oil Production. *Trans. AIME, Vo. 114, 1935.*
- Myers, R.H. Response Surface Methodology. *Allyn and Bacon, Boston, 1971.*
- Myers, R.H. and Montgomery, C.D. Response Surface Methodology: Process and Product Optimization Using Designed Experiments. *John Wiley and Sons, New York, 1995.*
- Nelson, P. H. Pore-throat Sizes in Sandstones, Tight Sandstones, and Shales. *AAPG Bulletin, Vol. 93, No. 3, Mar. 2009.*
- Ng, K.M., et al. Visualization of Blob Mechanics in Flow through Porous Media. *Chemical Engineering Science, Vol. 33, Iss. 8, 1978.*
- Nielsen, R. L. and Tek, M. R. Evaluation of Scale-Up Laws for Two-Phase Flow through Porous Media. *Soc. Pet. Eng. J. Vol. 3, No. 2, Jun. 1963.*
- Novakovic, D. Numerical Reservoir Characterization Using Dimensionless Scale Numbers with Application in Upscaling. *Ph.D Dissertation, Louisiana State University, August, 2002.*
- Oak, M.J. et al. Three-Phase Relative Permeability of Berea Sandstone. *Journal of Petroleum Technology, Vol. 42, No. 8, Aug. 1990.*
- Offeringa, J., van der Poel, C. Displacement of Oil from Porous Media by Miscible Liquids. *JPT, Vol. 5, No. 12 Dec. 1954.*
- Ogunsina, O.O. and Wiggins, M.L. A Review of Downhole Separation Technology. *SPE 94276, Proceedings of SPE Production and Operations Symposium, Oklahoma City, OK, Apr. 17 – 19, 2005.*
- Ohen, H.A, et al. A Systematic Laboratory Core and Fluid Analysis Program for the Design of a Cost Effective Treatment and Cleanup Guidelines for a Produced Water Disposal Scheme. *SPE 35369, Proceedings of SPE/DOE Improved Oil Recovery Symposium, Tulsa, OK, Apr. 21-24, 1996.*
- Ould-amer, Y., et al. Attenuation of water coning using dual completion technology. *Journal of Petroleum Science and Engineering, Vol. 45, Iss. 1-2, Nov. 2004.*
- Ouyang, L.B. A Mechanistic Model Based Approach to Evaluate Oil/Water Slip at Horizontal or Highly-Deviated Wells. *SPE 63262, Proceedings of SPE Annual Technical Conference and Exhibition, Dallas, TX, Oct. 1-4, 2000.*

- Ouyang, L.B. Modeling Oil–Water Countercurrent Flow in Deviated Wells Using Mechanistic and Simplified Approaches. *Petroleum Science and Technology*, Vol. 21, Nos. 7&8, 2003a.
- Ouyang, L.B. Prediction of the Occurrence of Oil–Water Countercurrent Flow in Deviated Wells. *Petroleum Science and Technology*, Vol. 21, Nos. 7&8, 2003b.
- Owolabi, O.O. and Watson, R.W. Effects of Rock-Pore Characteristics on Oil Recovery at Breakthrough and Ultimate Oil Recovery in Water-Wet Sandstones. *SPE 26935, Proceedings of SPE Eastern Regional Meeting, Pittsburgh, PA, Nov. 2-4, 1993.*
- Paige, R.W., et al. Optimising Water Injection Performance. *SPE 29774, Proceedings of Middle East Oil Show, Bahrain, Mar. 11-14, 1995.*
- Palsson, B. et al. The Water Injection Process A Technical and Economic Integrated Approach. *Trans IChemE, Vol. 81, Part A, Mar. 2003.*
- Pang, S and Sharma, M.M. A Model for Predicting Injectivity Decline in Water-Injection Wells. *SPE Formation Evaluation, Vol. 12, No. 3, Sept. 1997.*
- Patzek, T.W. Verification of a Complete Pore Network Simulator of Drainage and Imbibition. *SPE Journal, Vol. 6, No. 2, Jun. 2001.*
- Peachey, B.R., et al. Downhole Oil/Water Separation Moves into High Gear. *Journal of Canadian Petroleum Technology, Vol. 37, No. 7, Jul. 1998.*
- Pentland, C.H., et al. Measurement of Non-Wetting Phase Trapping in Sand Packs. *SPE 115697, Proceedings of SPE Annual Technical Conference and Exhibition, Denver, CO, Sep. 21–24, 2008.*
- Perkins, F. M. and Collins, R. E. Scaling Laws for Laboratory Flow Models of Oil Reservoirs. *JPT, Vol. 12, No. 8, Aug. 1960.*
- Perkins, T.K. and Johnston, O.C. A Review of Diffusion and Dispersion in Porous Media. *SPE Journal, Vol. 3, No. 1, Mar. 1963.*
- Perkins, T.K. and Johnston, O.C. A Study of Immiscible Fingering in Linear Models. *SPE Journal, Vol. 9, No. 1, Mar. 1969.*
- Perron, A. et al. An Experimental Investigation of the Motion of Single bubbles under a Slightly Inclined Surface. *International Journal of Multiphase Flow, Vol. 32, 2006a.*
- Perron, A.L. et al. Motion of Single Bubbles Moving under a Slightly Inclined Surface through Stationary Liquids. *International Journal of Multiphase Flow, Vol. 32, 2006b.*

- Peters, E.J. and Ham, J.D. A Novel Approach to Modeling Unstable EOR Displacements. *Quarterly Report for OSTI, Sep. 1993.*
- Pope, G. A. The Application of Fractional Flow Theory to Enhanced Oil Recovery. *SPE Journal, Vol. 20, No. 3, Jun. 1980.*
- Rai, K. Screening Model for Surfactant-Polymer Flooding Using Dimensionless Groups. *MS Thesis of the University of Texas at Austin, Austin, TX, Dec. 2008.*
- Ramakrishnan, T.S. and Wasan, D.T. The Relative Permeability Function for Two-Phase Flow in Porous Media: Effect of Capillary Number. *SPE 12693, Proceedings of SPE Enhanced Oil Recovery Symposium, Tulsa, OK, Apr. 15-18, 1984.*
- Rapoport, L. A. and Leas, W. J. Properties of Linear Waterfloods. *Trans. AIME, Vol. 198, pp. 139-148, 1953.*
- Rapoport, L. A. Scaling Laws for Use in Design and Operation of Water-Oil Flow Model. *Trans. AIME, Vol. 204, 1955.*
- Rege, S.D. and Fogler, H.S. A Network Model for Deep Bed Filtration of Solid Particles and Emulsion Drops. *AIChE Journal, Vol. 34, No. 11, Nov. 1988.*
- Reppert, T.R. and Idol, K.W. Method to Reduce Water Saturation in Near-Well Region. *US Patent 6227296 B1, May. 2001.*
- Rhee, C.H, et al. Removal of Oil and Grease in Oil Processing Wastewater. *Report for Sanitation District of Los Angeles County, 1989.*
- Rivera, R.M., et al. Water Separation from Wellstream in Inclined Separation Tube with Distributed Tapping. *SPE Projects, Facilities & Construction, Vol. 3, No. 1, Mar. 2008.*
- Romero, M.I, et al. Experiments and Network Model of Flow of Oil-water Emulsion in Porous Media. *Phys. Rev. E 84, 2011.*
- Russell, J. E. Application of Water Injection to the Reddin Unit Field. *Monroe G. Cheney Memorial Volume: Geological Contributions, 1952.*
- Rossen, W.R., et al. Fractional Flow Theory Applicable to Non-Newtonian Behavior in EOR Processes. *Transport in Porous Media, Vol. 89, Iss. 2, Sep. 2011.*
- Rousseau, D, et al. Injectivity Decline from Produced-Water Reinjection: New Insights on In-Depth Particle-Deposition Mechanisms. *SPE Production & Operations, Vol. 23, No. 4, Nov. 2008.*
- Ruark, A.E. Inspectional Analysis: A Method Which Supplements Dimensional Analysis. *J. Elisha Mitchell Sci. Soc., Vol. 51, 1935.*

- Saxena, J. Hazard Assessment of Chemicals. *Vol. 7. Hemisphere Publishing Corporation, New York, 1990.*
- Saylor, J. R. and Bounds, G. D. Experimental Study of the Role of the Weber and Capillary Numbers on Mesler Entrainment. *AIChE Journal, Vol. 58, Iss. 12, Feb. 23, 2012.*
- Saripalli, K.P, et al. Modeling Injection Well Performance during Deep-well Injection of Liquid Wastes. *Journal of Hydrology, Vol. 227, Iss. 1–4, Jan. 31, 2000.*
- Satter, A, et al. Chemical Transport in Porous Media with Dispersion and Rate-Controlled Adsorption. *SPE Journal, Vol. 20, No. 3, Jun. 1980.*
- Schlumberger. Eclipse Technical Description. *Feb. 2007.*
- Schlumberger: Oilfield Review: Water Control. *Vol. 12, Iss. 1, Mar. 1, 2000.*
- Schmidt, D.P, et al. Linear Oil Displacement by the Emulsion Entrapment Process. *SPE Journal, Vol. 24, No. 3, Jun. 1984.*
- Schramm, L.L. Emulsions: Fundamentals and Applications in the Petroleum Industry. *American Chemical Society, Vol. 231, May. 1992.*
- Seright, R.S. et al. A Strategy for Attacking Excess Water Production. *SPE Production & Facilities Vo. 18, No. 3, p. 158-169, Aug. 2003.*
- Sharma, A. Classification of Hydrocarbon Recovery Factor Based on Reservoir Databases. *Thesis, University of Texas at Austin, Austin, TX, Aug. 2008.*
- Sharma, M.M., et al. Injectivity Decline in Water-Injection Wells: An Offshore Gulf of Mexico Case Study. *SPE Production & Facilities, Vol. 15, No. 1, Feb. 2000.*
- Sheng, J. J. Modern Chemical Enhanced Oil Recovery: Theory and Practice. *Gulf Professional Publishing, Elsevier, 2011.*
- Shi, H. et al. Drift-Flux Modeling of Two-Phase Flow in Wellbores. *SPE Journal, Vol. 10, No. 1, Mar. 2005a.*
- Shi, H. et al. Drift-Flux Parameters for Three-Phase Steady-State Flow in Wellbores. *SPE Journal, Vol. 10, No. 2, Jun. 2005b.*
- Shirman E.L. An Analytical Model of 3-D Flow Near a Limited-Entry Wellbore in Multilayered Heterogeneous Strata - Theory and Applications, *Master Thesis, Louisiana State University, Baton Rouge, LA, Aug. 1995.*
- Shmakov, S.L. A Universal Method of Solving Quartic Equations. *International Journal of Pure and Applied Mathematics, Vol. 71, No. 2, 2011.*

- Shook, M., et al. Scaling Immiscible Flow Through Permeable Media by Inspectional Analysis. *In Situ*, Vol. 16, No. 3, 1992.
- Sinha, R., et al. Simulation of Natural and Partitioning Interwell Tracers to Calculate Saturation and Swept Volumes in Oil Reservoirs. *SPE 89458, Proceedings of SPE/DOE Symposium on Improved Oil Recovery, Tulsa, OK, Apr. 17-21, 2004.*
- Shosho, C. E. and Ryan, M. E. An Experimental Study of the Motion of Long Bubbles in Inclined Tubes. *Chemical Engineering Science*, Vol. 56, 2001.
- Sleicher, C.A. Maximum Stable Drop Size in Turbulent Flow. *AIChE Journal*, Vol, 8, No. 4, Sep. 1962.
- Sonin, A. The Physical Basis of Dimensional Analysis. *Department of Mechanical Engineering, MIT, Cambridge, 1997.*
- Soo, H, et al. A Filtration Model for The Flow of Dilute Stable Emulsions in Porous Media—II. Parameter Evaluation and Estimation. *Chemical Engineering Science*, Vol. 41, Iss. 2, 1986.
- Soo, H. and Radke, C.J. A Filtration Model for The Flow of Dilute Stable Emulsions in Porous Media—I. Theory. *Chemical Engineering Science*, Vol. 41, Iss. 2, 1986.
- Soo, H. and Radke, C.J. The Flow Mechanism of Dilute, Stable Emulsions In Porous Media. *Ind. Eng. Chem. Fundamen*, Vol. 23, Iss. 3, 1984a.
- Soo, H. and Radke, C.J. Velocity Effects in Emulsion Flow through Porous Media. *Journal of Colloid and Interface Science*, Vol. 102, Iss. 2, Dec. 1984b.
- Spiteri, E.J., et al. A New Model of Trapping and Relative Permeability Hysteresis for All Wettability Characteristics. *SPE Journal*, Vol. 13, No. 3, Sep. 2008.
- Spielman, L.A. and Su, Y.P. Coalescence of Oil-in-Water Suspensions by Flow through Porous Media. *Ind. Eng. Chem., Fundam.*, Vol. 16, No. 2, 1977.
- Stuebinger, L. et al. Dual Injection and Lifting Systems: Rod Pumps. *SPE 38790, Proceedings of SPE Annual Technical Conference and Exhibition, San Antonio, TX, Oct. 5-8, 1997.*
- Stuebinger, L.A. and Elphinstone, G.M. Multipurpose Wells: Downhole Oil/Water Separation in the Future. *SPE Production & Facilities*, Vol. 15, No. 3, Aug. 2000.
- Swisher, M.D. and Wojtanowicz, A.K. New Dual Completion Method Eliminates Bottom Water Coning. *SPE 30697, Proceedings of the SPE ATCE, Dallas, TX, Oct. 22– 25, 1995.*

- Syunyaev, R.Z, et al. Adsorption of Petroleum Asphaltenes onto Reservoir Rock Sands Studied by Near-Infrared (NIR) Spectroscopy. *Energy & Fuels*, Vol. 23, 2009.
- Tang, D.H. and Babu, D.K. Analytical Solution of a Velocity Dependent Dispersion Problem. *Water Resources Research*. Vol. 15, No. 6, Dec. 1979.
- Tang, D.H.E. and Peaceman, D.W. New Analytical and Numerical Solutions for the Radial Convection-Dispersion Problem. *SPE Reservoir Engineering*, Vol. 2, No. 3, Aug. 1987.
- Trivedi, J. and Babadagli, T. Scaling Miscible Displacement in Fractured Porous Media Using Dimensionless Groups. *Journal of Petroleum Science and Engineering*, Vol. 61, 2008.
- Valvante, P.H. and Blunt, M.J. Predictive Pore-Scale Modelling of Two-Phase Flow in Mixed Wet Media. *Water Resources Research*, Vol. 40, Iss. 7, Jul. 2004.
- Valvante, P.H. Predictive Pore-Scale Modeling of Multiphase Flow. *Ph.D dissertation of Imperial College London, London, UK, 2004.*
- Van Daalen, F. and Van Domselaar, H. R. Scaled Fluid-Flow Models with Geometry Differing from that of Prototype. *SPEJ*, Vol. 12, No. 3, Jun. 1972.
- Van den Broek, W. M. G. T., et al. Downhole Dehydration vs. Reduction of Oil Droplet Break-Up. *SPE 66542, Proceedings of SPE/EPA/DOE Exploration and Production Environmental Conference, San Antonio, TX, Feb. 26-28, 2001.*
- Van der Zande, M. J., et al. Size of Oil Droplets under High-Water-Cut Conditions. *SPE 67250, Proceedings of SPE Production and Operations Symposium. Oklahoma City, OK, Mar. 24-27, 2001.*
- Van Genuchten, M.Th. and Wierenga, P.J. Solute Dispersion Coefficients and Retardation Factors. in: Klute, A. *Methods of Soil Analysis. Part 1. Physical and Mineralogical Methods. 2nd Edition, American Society of Agronomy, Madison, WI, 1986.*
- Vaz, A.S.L. et al. Effects of Residual Oil on Reinjection of Produced Water. *SPE 100341, Proceedings of the SPE Europec/EAGE Annual Conference and Exhibition, Vienna, Austria, Jun. 12-15, 2006.*
- Veil, J.A. and Clark, C.E. Produced Water Volumes and Management Practices in the United States. *Report for U.S. DOE, National Energy Technology Laboratory, Sept. 2009.*
- Veil, J.A. and Layne, A.L. Analysis of Data from a Downhole Oil/Water Separator Field Trial in East Texas. *Report for U.S. DOE, Feb. 2001.*

- Veil, J.A. and Quinn, J.J. Downhole Separation Technology Performance: Relationship to Geologic Conditions. *Report for U.S. DOE, National Energy Technology Laboratory, Nov. 2004.*
- Veil, J. A. and Quinn, J. J. Water Issues Relating to Heavy Oil Production. *SPE 120630, Proceedings of SPE Americas E&P Environmental and Safety Conference, San Antonio, TX, Mar. 23-25, 2009.*
- Veil, J.A. et al. Feasibility Evaluation of Downhole Oil/Water Separator (DOWS) Technology. *Report for U.S. DOE, National Energy Technology Laboratory, Jan. 1999.*
- Verbeek, P.H.J. et al. Downhole Separator Produces Less Water and More Oil. *SPE 50617, Proceedings of European Petroleum Conference, The Hague, Netherlands, Oct. 20-22, 1998.*
- Wallis, G.B. One-dimensional Two-phase Flow. *McGraw-Hill, Inc. New York, 1969.*
- Wang, K.L., et al. Research of Improving Water Injection Effect by Using Active SiO₂ Nano-Powder in the Low-Permeability Oilfield. *Advanced Materials Research, Vol. 92, Jan. 2010.*
- Wegener, M. et al. Terminal and Transient Drop Rise Velocity of Single Toluene Droplets in Water. *AIChE Journal, Vol. 56, No. 1, Jan. 2010.*
- Wojtanowicz, A.K. and Xu, H. A New Method to Minimize Oil well Production Water Cut Using A Downhole Water Loop, *CIM 92-13, Proceedings of the 43rd Annual Technical Meeting of the Petroleum Society of CIM, Calgary, Canada, June, 1992.*
- Wojtanowicz, A.K., et al. Oil Well Coning Control Using Dual Completion with Tailpipe Water Sink. *SPE 21654, Production Operation Symposium, Oklahoma, Apr. 7 –9, 1991.*
- Wood, D.J. Creating A Quick Screening Model for CO₂ Flooding and Storage in Gulf Coast Reservoirs Using Dimensionless Groups. *MS Thesis of the University of Texas at Austin, Austin, TX, Aug. 2006.*
- Wood, D.J., et al. A Screening Model for CO₂ Flooding and Storage in Gulf Coast Reservoirs Based on Dimensionless Groups. *SPE Reservoir Evaluation & Engineering, Vol. 11, No. 3, Jun. 2008.*
- Wu, Y.S. et al. Buckley-Leverett Flow in Composite Porous Media. *SPE Advanced Technology Series, Vol. 1, No. 2, Jul. 1993.*
- White, C.D. Reservoir Dynamics. *Class Notes distributed in Louisiana State University, Baton Rouge, LA, Feb. 2010.*

- White, C. D., et al. Identifying and Estimating Significant Geologic Parameters with Experimental Design. *SPE Journal*, Vol. 6, No. 3, Sep. 2001.
- Wygol, R. J. Construction of Models that Simulate Oil Reservoirs. *SPEJ*, Vol. 3, No. 4, Dec. 1963.
- Xu, Z, et al. Mathematically Modeling Fixed-bed Adsorption in Aqueous Systems. *Journal of Zhejiang University SCIENCE A*, Vol.14 No.3, 2013.
- Yadava, R.R., et al. One-dimensional Dispersion in Unsteady Flow in An Adsorbing Porous Medium: An Analytical Solution. *Hydrological Processes*, Vol. 4, 1990.
- Yortsos, Y.C. and Fokas, A.S. An Analytical Solution for Linear Waterflood Including the Effects of Capillary Pressure. *SPE Journal*, Vol. 23, No. 1, Feb. 1983.
- Zhang, N.S., et al. An Experimental Investigation of the Formation Damage Caused by Produced Oily Water Injection. *SPE 26702, Proceedings of the Offshore Europe, Aberdeen, United Kingdom, Sept. 7-10, 1993.*
- Zhou, Z.H. and Rossen, W.R. Applying Fractional-flow Theory to Foam Processes at the limiting capillary pressure. *SPE Advanced Technology Series*, Vol. 3, No. 1, Mar. 1995.
- Zuber, N and Findlay, J.A. Average Volumetric Concentration in Two-Phase Flow Systems. *Trans of ASME Ser C Journal of Heat Transfer*, Vol. 87, Iss. 4, 1965.
- Zukoski, E. E. Influence of Viscosity, Surface Tension, and Inclination Angle on Motion of Long Bubbles in Closed Tubes. *J. Fluid Meek*. Vol. 25, Part 4, 1966.

APPENDIX A: SOLUTION DERIVATION FOR ADA MODEL IN LINEAR FLOW

This section presents the derivation process of a solution for the ADA model in linear flow developed in Chapter 4. The governing equation, initial and boundary conditions are shown in the following equations:

$$D \frac{\partial^2 C}{\partial x^2} - u \frac{\partial C}{\partial x} = \frac{\partial C}{\partial t} + \frac{(1-\phi) \partial S_{o_m}}{\phi \partial t} \dots\dots\dots (A.1)$$

$$S_{o_m} = C = 0 \quad \text{at } t = 0, x > 0 \dots\dots\dots (A.2)$$

$$C = C_0 \quad \text{at } t > 0, x = 0 \dots\dots\dots (A.3)$$

$$S_{o_m} = C = 0 \quad \text{at } t > 0, x \rightarrow \infty \dots\dots\dots (A.4)$$

When the oil concentration is low, i.e. the value of C is small, linear adsorption is valid and could be used to solve Equation A.1 analytically (Marino, 1974; Satter, et al., 1980; Yadava, et al., 1990):

$$S_{o_m} = \beta C \dots\dots\dots (A.5)$$

Substitute Equations A.5 into A.1, we can eliminate the variable S_{o_m} in the governing equation and simplify it to:

$$D \frac{\partial^2 C}{\partial x^2} - u \frac{\partial C}{\partial x} = R \frac{\partial C}{\partial t} \dots\dots\dots (A.6)$$

$$R = 1 + \frac{\beta(1-\phi)}{\phi} \dots\dots\dots (A.7)$$

Where, R is an expression used to simplify Equation A.6, dimensionless, which is also called retention factor - represents the interaction between oil droplets and rock. Its higher value means more oil droplets contact to the grains and are captured faster, which leads to higher oil saturation in the pore space (Gupta and Greenkorn, 1974; Rege and Fogler, 1988).

Rearrange Equation A.6, we get the following expression:

$$A \frac{\partial^2 C}{\partial x^2} - B \frac{\partial C}{\partial x} = \frac{\partial C}{\partial t} \dots\dots\dots (A.8)$$

Where, $A = D/R, B = u/R$.

In order to solve the partial differential equation A.8, we need to transform it to an ordinary equation first by introducing a new function C^* , which is a function of x and t and relates to C as:

$$C = C^* \exp\left(\frac{Bx}{2A} - \frac{B^2t}{4A}\right) \dots\dots\dots (A.9)$$

The derivatives of C with respect to x and t are:

$$\frac{\partial C}{\partial t} = \frac{\partial C^*}{\partial t} \exp\left(\frac{Bx}{2A} - \frac{B^2t}{4A}\right) - \frac{C^* B^2}{4A} \exp\left(\frac{Bx}{2A} - \frac{B^2t}{4A}\right) \dots\dots\dots (A.10)$$

$$\frac{\partial C}{\partial x} = \frac{\partial C^*}{\partial x} \exp\left(\frac{Bx}{2A} - \frac{B^2t}{4A}\right) - \frac{C^* B}{2A} \exp\left(\frac{Bx}{2A} - \frac{B^2t}{4A}\right) \dots\dots\dots (A.11)$$

$$\frac{\partial^2 C}{\partial x^2} = \frac{\partial^2 C^*}{\partial x^2} \exp\left(\frac{Bx}{2A} - \frac{B^2t}{4A}\right) + \frac{C^* B^2}{4A^2} \exp\left(\frac{Bx}{2A} - \frac{B^2t}{4A}\right) + \frac{B}{A} \frac{\partial C^*}{\partial x} \exp\left(\frac{Bx}{2A} - \frac{B^2t}{4A}\right) \dots\dots\dots (A.12)$$

Substitute Equations A.10, A.11 and A.12 into A.8, the partial differential equation is transformed to an ordinary equation as:

$$A \frac{d^2 C^*}{dx^2} = \frac{dC^*}{dt} \dots\dots\dots (A.13)$$

The initial and boundary conditions are transformed to:

$$C^* = 0 \quad \text{at } t = 0, x > 0 \dots\dots\dots (A.14)$$

$$C^* = C_0 \exp\left(\frac{B^2t}{4A}\right) \quad \text{at } t > 0, x = 0 \dots\dots\dots (A.15)$$

$$C^* = 0 \quad \text{at } t > 0, x \rightarrow \infty \dots\dots\dots (A.16)$$

Thus, the original problem with a partial differential equation A.8 has been transformed to an equilibrium problem with an ordinary differential equation A.13, which has been solved by Carslaw and Jaeger in 1959:

$$C^* = \frac{C_0}{2} e^{\frac{B^2 t}{4A}} \left[e^{-\frac{Bx}{2A}} \operatorname{erfc} \left(\frac{x}{2\sqrt{At}} - \frac{B}{2} \sqrt{\frac{t}{A}} \right) + e^{\frac{Bx}{2A}} \operatorname{erfc} \left(\frac{x}{2\sqrt{At}} + \frac{B}{2} \sqrt{\frac{t}{A}} \right) \right] \dots\dots\dots (A.17)$$

Substitute Equation A.17 into Equation A.9, we can get the following equation for C :

$$C = \frac{C_0}{2} \left[\operatorname{erfc} \left(\frac{x-Bt}{\sqrt{4At}} \right) + e^{\frac{Bx}{A}} \operatorname{erfc} \left(\frac{x+Bt}{\sqrt{4At}} \right) \right] \dots\dots\dots (A.18)$$

Because $A = D/R, B = u/R$, substitute them into Equation A.18, we get the solution for ADA model in linear flow:

$$C = \frac{C_0}{2} \left\{ \operatorname{erfc} \left(\frac{Rx-ut}{\sqrt{4DRt}} \right) + \exp \left(\frac{ux}{D} \right) \operatorname{erfc} \left(\frac{Rx+ut}{\sqrt{4DRt}} \right) \right\} \dots\dots\dots (A.19)$$

In the actual evaluation of Equation A.19, the third term “ $\exp \left(\frac{ux}{D} \right)$ ” is large while the fourth term “ $\operatorname{erfc} \left[\frac{Rx+ut}{\sqrt{4DRt}} \right]$ ” is extremely small (tens of magnitude smaller than the third term), so their product is essentially zero. (There are usually no tabulated values of the error function for the fourth term.) As a result, only the first and second terms are considered in Equation A.19 to match laboratory results under various conditions (Brigham, 1974).

The adsorbed oil saturation $S_{o,m}$ can be calculated using the simplified Equation A.20, which is also adopted by some commercial reservoir simulators such as CMG[®] (Satter, et al., 1980; McKee and Swailes, 1991; CMG, 2011):

$$S_{o,m} = \frac{\alpha S_{oe,m} C}{1+\alpha C} \dots\dots\dots (A.20)$$

By substituting Equations A.19 to A.20, we get the oil saturation distribution along the core. The final mass oil concentration in the water and oil volume saturation in the pore space can be expressed in Equation A.21.

$$\left\{ \begin{array}{l} C = \frac{C_0}{2} \operatorname{erfc} \left(\frac{Rx-ut}{\sqrt{4DRt}} \right) \\ S_o = \frac{S_{o,m}}{\rho_o} = \frac{\alpha S_{oe,m} C_0 \operatorname{erfc} \left(\frac{Rx-ut}{\sqrt{4DRt}} \right)}{\rho_o [2 + \alpha C_0 \operatorname{erfc} \left(\frac{Rx-ut}{\sqrt{4DRt}} \right)]} \end{array} \right. \dots\dots\dots (A.21)$$

Satter, et al. (1980) proposed an analytical solution to Equation A.1 considering flow through porous media with linear adsorption as shown in Equation A.5. The solution for the effluent concentration is given by:

$$C = \frac{C_0}{2} \operatorname{erfc} \left(\frac{1 - \frac{I}{\theta}}{2 \sqrt{\frac{I\lambda}{\theta L}}} \right) - C_0 \sqrt{\frac{I\lambda}{\pi\theta L}} \frac{\exp \left[-\frac{\theta L (1 - \frac{I}{\theta})^2}{4 I\lambda} \right]}{1 + \frac{I}{\theta}} \cdot \left[1 - 6 \frac{\frac{I}{\theta}}{1 + \frac{I}{\theta}} - \frac{2 \left(\frac{I}{\theta} \right)^2}{\left(1 + \frac{I}{\theta} \right)^2} \right] \dots \dots \dots (\text{A.22})$$

$$\theta = 1 + \frac{\rho_r(1-\phi)\beta}{\phi} \dots \dots \dots (\text{A.23})$$

$$I = \frac{qt}{AL\phi} \dots \dots \dots (\text{A.24})$$

$$\lambda = \frac{D}{u} \dots \dots \dots (\text{A.25})$$

To verify the solution of this study, the results of Equations A.21 and A.22 are compared using data in Table A.1 (Satter, et al., 1980). Figure A.1 shows that two analytical solutions give the same results, however, the solution developed in this study is much simpler than the one proposed by Satter, et al. (1980).

Table A.1. Parameters for analytical solutions comparison

Parameter	Value		Unit
	Case 1	Case 2	
Core length (L)	0.5	0.5	m
Core diameter (d)	0.01	0.01	m
Porosity (ϕ)	0.2	0.2	<i>fraction</i>
Grain density (ρ_r)	2650	2650	kg/m^3
Injection rate (q)	$4.58 \cdot 10^{-11}$	$4.58 \cdot 10^{-11}$	m^3/s
Oil concentration (c_o)	10	10	kg/m^3
Dispersive coefficient (D)	$1.465 \cdot 10^{-8}$	$1.465 \cdot 10^{-8}$	m^2/s
Adsorptive constant (β)	0	0.1325	<i>dimensionless</i>

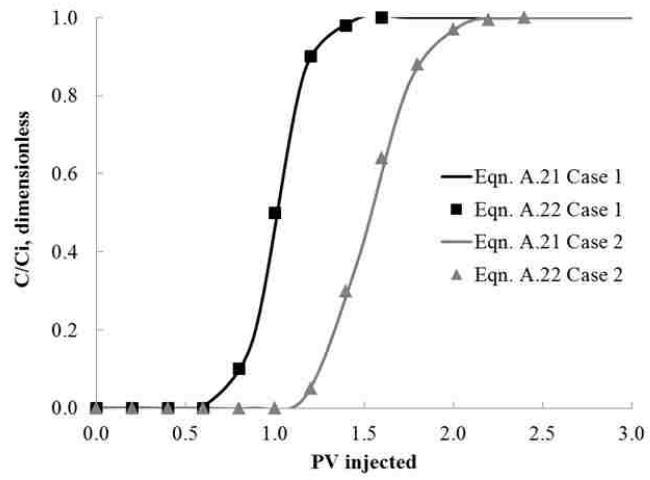


Figure A.1. Comparison of results between analytical solutions

APPENDIX B: SOLUTION DERIVATION FOR ADA MODEL IN RADIAL FLOW

B.1 Solution of Oil Saturation for ADA Radial Model

This section presents the derivation process of a solution for the ADA model in radial flow described in Chapter 4. The governing equation, initial and boundary conditions are shown in the following equations:

$$\frac{\partial C}{\partial t} + v \frac{\partial C}{\partial r} = dv \frac{\partial^2 C}{\partial r^2} \dots\dots\dots (B.1)$$

$$S_{o_m} = C = 0 \quad \text{at } t = 0, r > r_w \dots\dots\dots (B.2)$$

$$C = C_0 \quad \text{at } t > 0, r = r_w \dots\dots\dots (B.3)$$

$$S_{o_m} = C = 0 \quad \text{at } t > 0, r \rightarrow \infty \dots\dots\dots (B.4)$$

Where, v is the interstitial velocity with retention factor, m/s:

$$v = \frac{q}{2\pi h\phi Rr} \dots\dots\dots (B.5)$$

It is clear that v decreases fast with r from Equation B.5, and also the dispersivity d in Equation B.1 is a very small value. Thus, the influence of dispersion, expressed by the right-hand side term of Equation B.1, becomes small comparing to the local advective effect as the fluids move away from the well (Hoopes and Harleman, 1967; Tang and Babu, 1979). Equation B.1 is simplified to the following expression:

$$\frac{\partial C}{\partial t} + v \frac{\partial C}{\partial r} \approx 0 \dots\dots\dots (B.6)$$

Based on Equation B.6, the first and second derivatives of C with respect to r can be expressed as (Bear, 1972, pp. 635~638):

$$\frac{\partial C}{\partial r} \approx -\frac{1}{v} \frac{\partial C}{\partial t} \dots\dots\dots (B.7)$$

$$\frac{\partial^2 C}{\partial r^2} \approx \frac{1}{v^2} \frac{\partial^2 C}{\partial t^2} \dots\dots\dots (B.8)$$

Substitute Equations B.8 into B.1, the governing equation becomes:

$$\frac{\partial C}{\partial t} + v \frac{\partial C}{\partial r} = \frac{d}{v} \frac{\partial^2 C}{\partial t^2} \dots\dots\dots (B.9)$$

As v is a function of injection radius, it is necessary reduce the variables in the equation by introducing a constant A as shown in Equation B.10:

$$A = \frac{q}{2\pi h_w \phi R} \dots\dots\dots (B.10)$$

Substitute Equations B.10 into B.9, the governing equation can be written as:

$$\frac{\partial C}{\partial t} + \frac{A}{r} \frac{\partial C}{\partial r} = \frac{dr}{A} \frac{\partial^2 C}{\partial t^2} \dots\dots\dots (B.11)$$

The next step is to convert this partial differential equation to an ordinary equation. As new function of r and t is introduced in order to achieve this purpose:

$$\varepsilon = \frac{\frac{r^2}{2} - At}{\sqrt{\frac{4}{3} dr^3}} \dots\dots\dots (B.12)$$

The derivatives of C with respect to r and t are:

$$\frac{\partial C}{\partial r} = \left(\frac{r}{4\sqrt{\frac{4}{3} dr^3}} + \frac{\frac{3}{2} At}{r\sqrt{\frac{4}{3} dr^3}} \right) \frac{dC}{d\varepsilon} \dots\dots\dots (B.13)$$

$$\frac{\partial C}{\partial t} = - \frac{A}{\sqrt{\frac{4}{3} dr^3}} \frac{dC}{d\varepsilon} \dots\dots\dots (B.14)$$

$$\frac{\partial^2 C}{\partial t^2} = \frac{A^2}{\frac{4}{3} dr^3} \frac{d^2 C}{d\varepsilon^2} \dots\dots\dots (B.15)$$

Substitute Equations B.13, B.14 and B.15 into B.11, the partial differential equation is converted to the following ordinary equation:

$$\frac{d^2 C}{d\varepsilon^2} + 2\varepsilon \frac{dC}{d\varepsilon} = 0 \dots\dots\dots (B.16)$$

The initial and boundary conditions become:

$$C = C_0 \quad \text{at } t > 0, \varepsilon = \frac{r_w^2 - At}{\sqrt{\frac{4}{3}dr_w^3}} \dots\dots\dots (B.17)$$

$$C = 0 \quad \text{at } t > 0, \varepsilon \rightarrow \infty \dots\dots\dots (B.18)$$

Equation B.16 can be further simplified by assuming:

$$C' = \frac{dC}{d\varepsilon} \dots\dots\dots (B.19)$$

Substitute Equations B.19 into B.16, we get the following expression:

$$\frac{dC'}{d\varepsilon} + 2\varepsilon C' = 0 \dots\dots\dots (B.20)$$

Solve Equations B.19 and B.20, we get the general expression of C :

$$C = C_1 \int \exp(-\varepsilon^2) d\varepsilon + C_2 \dots\dots\dots (B.21)$$

Based on Equation B.18 and the definition of error function as shown in Equation B.22, the general solution of C becomes Equation B.23:

$$\text{erf}(\varepsilon) = \frac{2}{\sqrt{\pi}} \int_0^\varepsilon \exp(-\varepsilon^2) d\varepsilon \dots\dots\dots (B.22)$$

$$C = C_1 \text{erf}(\varepsilon) + C_2 \dots\dots\dots (B.23)$$

Substitute Equations B.17 and B.18 into B.23, we get the approximate solution for the ADA model in radial flow when the well radius is neglectable comparing to the size of aquifer:

$$C = \frac{C_0 \text{erfc}\left(\frac{r_w^2 - qt}{2 \frac{2\pi h_w \phi R}{\sqrt{\frac{4}{3}dr_w^3}}}\right)}{\text{erfc}\left(\frac{r_w^2 - qt}{2 \frac{2\pi h_w \phi R}{\sqrt{\frac{4}{3}dr_w^3}}}\right)} \dots\dots\dots (B.24)$$

Where, $\text{erfc}()$ is the complementary error function which is equal to $1 - \text{erf}()$.

The same adsorption relationship is used here as in the linear flow. The time and radius dependent oil volume saturation in the aquifer can be expressed as:

$$S_o = \frac{\alpha S_{oe} C_0 \operatorname{erfc}\left(\frac{r^2 - \frac{qt}{2\pi h_w \phi R}}{\sqrt{\frac{4}{3} dr^3}}\right)}{\rho_o \left[\operatorname{erfc}\left(\frac{r_w^2 - \frac{qt}{2\pi h_w \phi R}}{\sqrt{\frac{4}{3} dr_w^3}}\right) + \alpha C_0 \operatorname{erfc}\left(\frac{r^2 - \frac{qt}{2\pi h_w \phi R}}{\sqrt{\frac{4}{3} dr^3}}\right) \right]} \dots\dots\dots (B.25)$$

B.2 Solution of Oil Saturation Front Positions

This section presents the solution derivation process of oil saturation positions for ADA model in radial flow developed in Chapter 5. The oil front positions r_{f1} and r_{f2} in ADA model could be determined by solving the following equation:

$$\begin{cases} r_{f1}^2 = \frac{qt}{\pi h_w \phi R} - 4\sqrt{\frac{4}{3} dr_{f1}^3} \\ r_{f2}^2 = \frac{qt}{\pi h_w \phi R} + 4\sqrt{\frac{4}{3} dr_{f2}^3} \end{cases} \dots\dots\dots (B.26)$$

There are two solutions for each r_f from the above equation, however, only the positive one is valid since the oil saturation position is always greater than zero. Equation B.26 could be solved by decomposing it to three individual parts as:

$$\begin{cases} Y_1 = r_f^2 \\ Y_2 = \frac{qt}{\pi h_w \phi R} + 4\sqrt{\frac{4}{3} dr_f^3} \\ Y_3 = \frac{qt}{\pi h_w \phi R} - 4\sqrt{\frac{4}{3} dr_f^3} \end{cases} \dots\dots\dots (B.27)$$

Using Equation B.27, r_{f1} and r_{f2} can be determined graphically as shown in Figure B.1. Due to the small difference between r_{f1} and r_{f2} , we use their average as the radius of the skin zone as:

$$r_s(t)_{ADA} = \frac{r_{f1} + r_{f2}}{2} = \frac{a^2 + b^2}{2} \dots\dots\dots (B.28)$$

Where, a and b can be calculated from the following quartic equation:

$$\begin{cases} a^4 + 4Ba^3 - E = 0 \\ b^4 - 4Bb^3 - E = 0 \end{cases} \dots\dots\dots (B.29)$$

Where, $a = \sqrt{r_{f1}}$, $b = \sqrt{r_{f2}}$, $B = \sqrt{4d/3}$, $E = qt/(\pi h_w \phi R)$. Although there are four solutions for a or b in Equation B.29, only the real positive one is valid as r_f is sole and positive as shown in Figure B.1. The quartic equation can be solved using the following steps as discussed by Hahn (2005) and Shmakov (2011):

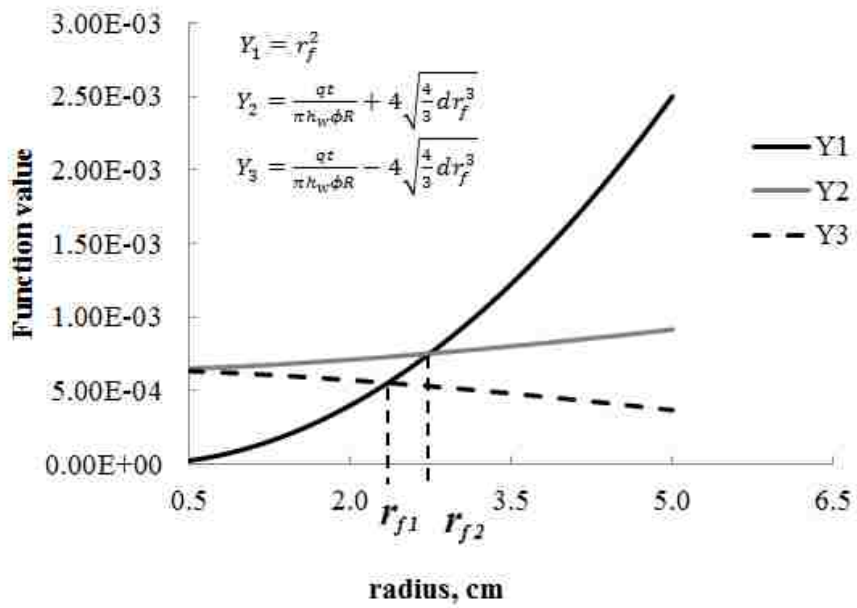


Figure B.1. Graphically determination of oil saturation front positions in ADA model

Step 1: Assume $a = u - B$ and substitute it into “ $a^4 + 4Ba^3 - E = 0$ ” to eliminate a^3 as:

$$u^4 + a'u^2 + b'u + c' = 0 \dots\dots\dots (B.30)$$

Where, $a' = -6B^2$, $b' = 8B^3$, $c' = -3B^4 - E$.

Step 2: Express Equation B.30 as the product of quadratics as:

$$(u^2 + \alpha u + \beta)(u^2 - \alpha u + \delta) = 0 \dots\dots\dots (B.31)$$

Where, $\alpha = \sqrt{z}$, $\beta = 0.5(a' + \alpha^2 - b'/\alpha)$, $\delta = 0.5(a' + \alpha^2 + b'/\alpha)$ and z is the real positive solution of the following equation:

$$z^3 + 2a'z^2 + (a'^2 - 4c')z - b'^2 = 0 \dots\dots\dots (B.32)$$

Step 3: Substitute α , β and δ into Equation B.31 and solve the two quadratics, there will be two complex solutions, one real positive solution and one real negative solution, keep the real positive one as u_1 , and the oil saturation front position is: $a = u_1 - B$;

Step 4: Repeat steps 1 to 3 for equation “ $b^4 - 4Bb^3 - E = 0$ ” by assuming “ $b = u + B$ ” and get another oil saturation front position: $b = u_2 + B$;

Step 5: The radius of skin zone can be determined from Equation B.28.

APPENDIX C: DERIVATION OF DIMENSIONLESS GROUPS FOR DWL

This section presents the derivation process of dimensionless groups for DWL in a homogeneous anisotropic system as shown in Figure 6.1.

C.1 Governing Equations

When oil and water flow to DWL, the governing equations in a two-dimensional cylindrical system (r, z) , are:

Continuity equation:

$$\phi \frac{\partial S_w}{\partial t} + \frac{1}{r} \frac{\partial (ru_{wr})}{\partial r} + \frac{\partial u_{wz}}{\partial z} = 0 \dots\dots\dots (C.1)$$

$$\frac{1}{r} \frac{\partial (ru_{wr} + ru_{or})}{\partial r} + \frac{\partial (u_{wz} + u_{oz})}{\partial z} = 0 \dots\dots\dots (C.2)$$

$$u_{wr} = -k_r \lambda_w \left(\frac{\partial p_w}{\partial r} \right) \dots\dots\dots (C.3)$$

$$u_{or} = -k_r \lambda_o \left(\frac{\partial p_o}{\partial r} \right) \dots\dots\dots (C.4)$$

$$u_{wz} = -k_z \lambda_w \left(\frac{\partial p_w}{\partial z} + \rho_w g \right) \dots\dots\dots (C.5)$$

$$u_{oz} = -k_z \lambda_o \left(\frac{\partial p_o}{\partial z} + \rho_o g \right) \dots\dots\dots (C.6)$$

$$p_o - p_w = \sigma \sqrt{\frac{\phi}{k_z}} J(S_w) = \Delta \rho g z \dots\dots\dots (C.7)$$

Initial conditions:

$$S_w = S_{wc} \quad \text{at } t = 0, 0 < z < h_o \dots\dots\dots (C.8)$$

$$S_w = 1 \quad \text{at } t = 0, h_o < z < h_o + h_w \dots\dots\dots (C.9)$$

Boundary conditions:

$$u_{wz} = 0, \text{ at } z = 0, \forall r, t \dots\dots\dots (C.10)$$

$$u_{oz} = 0, \text{ at } z = 0, \forall r, t \dots\dots\dots (C.11)$$

$$u_{wz} = 0, \text{ at } z = h_o + h_w, \forall r, t \dots\dots\dots (C.12)$$

$$u_{oz} = 0, \text{ at } z = h_o + h_w, \forall r, t \dots\dots\dots (C.13)$$

$$u_{wr} = 0, \text{ at } r = r_{ew}, h_o < z < h_o + h_w, \forall t \dots\dots\dots (C.14)$$

$$u_{or} = 0, \text{ at } r = r_{eo}, 0 < z < h_o, \forall t \dots\dots\dots (C.15)$$

$$q_{op} = 2\pi r_{well} \int_0^{h_{op}} u_{or} dz, \text{ at } r = r_{well}, t > 0 \dots\dots\dots (C.16)$$

$$q_{wd} = 2\pi r_{well} \int_{z_{wd}}^{z_{wd}+h_{wd}} u_{wr} dz, \text{ at } r = r_{well}, t > 0 \dots\dots\dots (C.17)$$

$$q_{wi} = -2\pi r_{well} \int_{z_{wi}}^{z_{wi}+h_{wi}} u_{wr} dz, \text{ at } r = r_{well}, t > 0 \dots\dots\dots (C.18)$$

$$q_{wi} = -q_{wd}, \text{ at } r = r_{well}, t > 0 \dots\dots\dots (C.19)$$

C.2 Transformation to Dimensionless Space

In order to transform the above equations from dimensional to dimensionless space, the following dimensionless variables are defined using linear combination:

$$\begin{aligned} r &= r_1^* \cdot r_D + r_2^* & u_{oz} &= u_{oz1}^* \cdot u_{ozD} + u_{oz2}^* \\ z &= z_1^* \cdot z_D + z_2^* & u_{wz} &= u_{wz1}^* \cdot u_{wzD} + u_{wz2}^* \\ t &= t_1^* \cdot t_D + t_2^* & p_w &= p_{w1}^* \cdot p_{wD} + p_{w2}^* \\ u_{wr} &= u_{wr1}^* \cdot u_{wrD} + u_{wr2}^* & p_o &= p_{o1}^* \cdot p_{oD} + p_{o2}^* \end{aligned}$$

$$u_{or} = u_{or1}^* \cdot u_{orD} + u_{or2}^* \quad S_w = S_{w1}^* \cdot S_{wD} + S_{w2}^*$$

The quantities with an asterisk “*” are called scale factors. Subscripts “1” and “2” indicate the multiplicative and additive scale factors, respectively. Dimensionless variables are those with a subscript “D”. Defining the scale factors is somewhat subjective. It has been done, here, by following other work (Shook, et al, 1992). Substituting these transformations into Equations C.1 through C.19, then all of them can be transformed to dimensionless space. This step is called initial substitution. Take Equation C.1 as an example, it can be transformed to Equation C.20 as:

$$\begin{aligned} & \frac{\phi S_{w1}^*}{t_1^*} \cdot \frac{\partial S_{wD}}{\partial t_D} + \frac{u_{wr1}^*}{(r_1^* r_D + r_2^*)} \cdot \frac{\partial (r_D u_{wrD})}{\partial r_D} + \frac{u_{wr2}^*}{(r_1^* r_D + r_2^*)} + \dots \\ & + \frac{r_2^* u_{wr1}^*}{r_1^* (r_1^* r_D + r_2^*)} \cdot \frac{\partial u_{wrD}}{\partial r_D} + \frac{u_{wz1}^*}{z_1^*} \cdot \frac{\partial u_{wzD}}{\partial z_D} = 0 \end{aligned} \quad \dots \dots \dots (C.20)$$

C.3 Primary Elimination and Secondary Substitution

After the initial substitution, we need to choose a scaling direction. It can be either “r” or “z” direction. “z” direction is chosen in this study for the ease of analyzing completion locations. Then, we rearrange these equations in dimensionless space and write them in dimensionless form as follows:

$$\begin{aligned} & \frac{\partial S_{wD}}{\partial t_D} + \frac{\boxed{1}}{\phi S_{w1}^* r_1^*} \cdot \frac{u_{wr1}^* t_1^*}{r_D} \cdot \frac{\partial (r_D u_{wrD})}{\partial r_D} + \frac{\boxed{2}}{\phi S_{w1}^* r_1^*} \cdot \frac{u_{wr2}^* t_1^*}{r_D} + \dots \\ & + \frac{\boxed{3}}{\phi S_{w1}^* r_1^*} \cdot \frac{r_2^* u_{wr1}^* t_1^*}{r_D} \cdot \frac{\partial u_{wrD}}{\partial r_D} + \frac{\boxed{4}}{\phi S_{w1}^* z_1^*} \cdot \frac{u_{wz1}^* t_1^*}{z_D} \cdot \frac{\partial u_{wzD}}{\partial z_D} = 0 \end{aligned} \quad \dots \dots \dots (C.21)$$

$$\frac{\boxed{5}}{u_{oz1}^* r_1^*} \cdot \frac{1}{r_D} \cdot \frac{\partial(r_D u_{wrD})}{\partial r_D} + \frac{\boxed{6}}{u_{oz1}^* r_1^*} \cdot \frac{1}{r_D} \cdot \frac{\partial(r_D u_{orD})}{\partial r_D} + \frac{\boxed{7}}{u_{oz1}^* r_1^*} \cdot \frac{1}{r_D} + \frac{\boxed{8}}{u_{oz1}^* r_1^*} \cdot \frac{1}{r_D} + \dots \quad (C.22)$$

$$+ \frac{\boxed{9}}{u_{oz1}^* r_1^{*2}} \cdot \frac{1}{r_D} \cdot \frac{\partial u_{wrD}}{\partial r_D} + \frac{\boxed{10}}{u_{oz1}^* r_1^{*2}} \cdot \frac{1}{r_D} \cdot \frac{\partial u_{orD}}{\partial r_D} + \frac{\boxed{11}}{u_{oz1}^*} \cdot \frac{\partial u_{wzD}}{\partial z_D} + \frac{\partial u_{ozD}}{\partial z_D} = 0$$

$$u_{wrD} = \frac{\boxed{12}}{u_{wr1}^* r_1^*} \cdot \frac{\partial p_{wD}}{\partial r_D} - \frac{\boxed{13}}{u_{wr1}^*} \dots \quad (C.23)$$

$$u_{orD} = \frac{\boxed{14}}{u_{or1}^* r_1^*} \cdot \frac{\partial p_{oD}}{\partial r_D} - \frac{\boxed{15}}{u_{or1}^*} \dots \quad (C.24)$$

$$u_{wzD} = \frac{\boxed{16}}{u_{wz1}^* z_1^*} \cdot \frac{\partial p_{wD}}{\partial z_D} - \frac{\boxed{17}}{u_{wz1}^*} \cdot \frac{\partial p_{oD}}{\partial z_D} - \frac{\boxed{18}}{u_{wz1}^*} \dots \quad (C.25)$$

$$u_{ozD} = \frac{\boxed{19}}{u_{oz1}^* z_1^*} \cdot \frac{\partial p_{oD}}{\partial z_D} - \frac{\boxed{20}}{u_{oz1}^*} \cdot \frac{\partial p_{wD}}{\partial z_D} - \frac{\boxed{21}}{u_{oz1}^*} \dots \quad (C.26)$$

$$p_{oD} - \frac{\boxed{22}}{p_{o1}^*} p_{wD} = \frac{\boxed{23}}{p_{o1}^*} \sqrt{\frac{\Phi}{k_z}} J(s_{wD}) + \frac{\boxed{24}}{p_{o1}^*} + \frac{\boxed{25}}{p_{o1}^*} \dots \quad (C.27)$$

$$p_{oD} - \frac{\boxed{26}}{p_{o1}^*} p_{wD} = \frac{\boxed{27}}{p_{o1}^*} \Delta \rho g z_1^* z_D + \frac{\boxed{28}}{p_{o1}^*} \Delta \rho g z_2^* z_D + \frac{\boxed{29}}{p_{o1}^*} + \frac{\boxed{30}}{p_{o1}^*}$$

$$s_{wD} = \frac{\boxed{31}}{s_{w1}^*} - \frac{\boxed{32}}{s_{w1}^*} \quad \text{at } t_D = -\frac{\boxed{33}}{t_1^*}, \quad -\frac{\boxed{34}}{z_1^*} < z_D < \frac{\boxed{35}}{z_1^*} - \frac{\boxed{36}}{z_1^*}, \quad \dots\dots\dots (C.28)$$

$$r_D > \frac{\boxed{37}}{r_1^*} - \frac{\boxed{38}}{r_1^*}$$

$$s_{wD} = \frac{\boxed{39}}{s_{w1}^*} - \frac{\boxed{40}}{s_{w1}^*} \quad \text{at } t_D = -\frac{\boxed{41}}{t_1^*}, \quad \frac{\boxed{42}}{z_1^*} - \frac{\boxed{43}}{z_1^*} < z_D < \frac{\boxed{44}}{z_1^*} - \frac{\boxed{45}}{z_1^*} - \frac{\boxed{46}}{z_1^*}, \quad \dots\dots\dots (C.29)$$

$$r_D > \frac{\boxed{47}}{r_1^*} - \frac{\boxed{48}}{r_1^*}$$

$$u_{wzD} = -\frac{\boxed{49}}{u_{wz1}^*} \quad \text{at } z_D = -\frac{\boxed{50}}{z_1^*}, \quad r_D > \frac{\boxed{51}}{r_1^*} - \frac{\boxed{52}}{r_1^*}, \quad \forall t_D \dots\dots\dots (C.30)$$

$$u_{ozD} = -\frac{\boxed{53}}{u_{oz1}^*} \quad \text{at } z_D = -\frac{\boxed{54}}{z_1^*}, \quad r_D > \frac{\boxed{55}}{r_1^*} - \frac{\boxed{56}}{r_1^*}, \quad \forall t_D \dots\dots\dots (C.31)$$

$$u_{wzD} = -\frac{\boxed{57}}{u_{wz1}^*} \quad \text{at } z_D = \frac{\boxed{58}}{z_1^*} + \frac{\boxed{59}}{z_1^*} - \frac{\boxed{60}}{z_1^*}, \quad \dots\dots\dots (C.32)$$

$$r_D > \frac{\boxed{61}}{r_1^*} - \frac{\boxed{62}}{r_1^*}, \quad \forall t_D$$

$$u_{ozD} = -\frac{\boxed{63} \quad u_{oz2}^*}{\boxed{63} \quad u_{oz1}^*} \quad \text{at } z_D = \frac{\boxed{64} \quad h_o}{\boxed{64} \quad z_1^*} - \frac{\boxed{65} \quad h_w}{\boxed{65} \quad z_1^*} - \frac{\boxed{66} \quad z_2^*}{\boxed{66} \quad z_1^*}, \quad \dots\dots\dots (C.33)$$

$$r_D > \frac{\boxed{67} \quad r_{well}}{\boxed{67} \quad r_1^*} - \frac{\boxed{68} \quad r_2^*}{\boxed{68} \quad r_1^*}, \quad \forall t_D$$

$$u_{wrD} = -\frac{\boxed{69} \quad u_{wr2}^*}{\boxed{69} \quad u_{wr1}^*} \quad \text{at } r_D > \frac{\boxed{70} \quad r_{ew}}{\boxed{70} \quad r_1^*} - \frac{\boxed{71} \quad r_2^*}{\boxed{71} \quad r_1^*}, \quad \dots\dots\dots (C.34)$$

$$\forall \frac{\boxed{72} \quad h_o}{\boxed{72} \quad z_1^*} - \frac{\boxed{73} \quad z_2^*}{\boxed{73} \quad z_1^*} < z_D < \frac{\boxed{74} \quad h_o}{\boxed{74} \quad z_1^*} - \frac{\boxed{75} \quad h_w}{\boxed{75} \quad z_1^*} - \frac{\boxed{76} \quad z_2^*}{\boxed{76} \quad z_1^*}, \quad t_D$$

$$u_{orD} = -\frac{\boxed{77} \quad u_{or2}^*}{\boxed{77} \quad u_{or1}^*} \quad \text{at } r_D > \frac{\boxed{78} \quad r_{eo}}{\boxed{78} \quad r_1^*} - \frac{\boxed{79} \quad r_2^*}{\boxed{79} \quad r_1^*}, \quad \dots\dots\dots (C.35)$$

$$\forall \frac{\boxed{80} \quad z_2^*}{\boxed{80} \quad z_1^*} < z_D < \frac{\boxed{81} \quad h_o}{\boxed{81} \quad z_1^*} - \frac{\boxed{82} \quad z_2^*}{\boxed{82} \quad z_1^*}, \quad t_D$$

$$\frac{\boxed{83} \quad q_{op}}{2\pi r_{well} z_1^* u_{or1}^*} = \int_{\frac{\boxed{86} \quad -z_2^*}{\boxed{86} \quad z_1^*}}^{\frac{\boxed{84} \quad h_{op}}{\boxed{84} \quad z_1^*} - \frac{\boxed{85} \quad z_2^*}{\boxed{85} \quad z_1^*}} \left(u_{orD} + \frac{\boxed{87} \quad u_{or2}^*}{\boxed{87} \quad u_{or1}^*} \right) dz_D \quad \text{at } r_D = \frac{\boxed{88} \quad r_{well}}{\boxed{88} \quad r_1^*} - \frac{\boxed{89} \quad r_2^*}{\boxed{89} \quad r_1^*}, \quad t_D > -\frac{\boxed{90} \quad t_2^*}{\boxed{90} \quad t_1^*} \quad (C.36)$$

$$\begin{array}{c}
\begin{array}{|c|c|c|} \hline 92 & 93 & 94 \\ \hline \end{array} \\
\frac{q_{wd}}{2\pi r_{well} z_1^* u_{wr1}^*} = \int_{\frac{z_{wd}^*}{z_1^*} - \frac{h_{wd}^*}{z_1^*}}^{\frac{z_2^*}{z_1^*}} \left(u_{wrD} + \frac{u_{wr2}^*}{u_{wr1}^*} \right) dz_D \quad \text{at} \quad r_D = \frac{r_{well}^*}{r_1^*} - \frac{r_2^*}{r_1^*}, \quad t_D > -\frac{t_2^*}{t_1^*} \quad (C.37) \\
\begin{array}{|c|c|c|} \hline 91 & 95 & 96 \\ \hline \end{array}
\end{array}$$

$$\begin{array}{c}
\begin{array}{|c|c|c|} \hline 102 & 103 & 104 \\ \hline \end{array} \\
\frac{q_{wd}}{2\pi r_{well} z_1^* u_{wr1}^*} = \int_{\frac{z_{wi}^*}{z_1^*} - \frac{z_2^*}{z_1^*}}^{\frac{z_2^*}{z_1^*}} \left(u_{wrD} + \frac{u_{wr2}^*}{u_{wr1}^*} \right) dz_D \quad \text{at} \quad r_D = \frac{r_{well}^*}{r_1^*} - \frac{r_2^*}{r_1^*}, \quad t_D > -\frac{t_2^*}{t_1^*} \quad (C.38) \\
\begin{array}{|c|c|c|} \hline 101 & 106 & 107 \\ \hline \end{array}
\end{array}$$

After rearrangement, the equation becomes fully dimensionless, and total of 110 dimensionless groups are defined as shown by the rectangles in Equations C.21 through C.38. The form of dimensionless equation should be the same as the initial dimensional equation. Take Equation C.21 for example, groups (1) and (4) should have value of “1”, while the groups (2) and (3) value should be “0”. If we use the same approach to all other equations in the dimensionless space, 34 of the groups are set to be “1” and 45 are “0”. The remaining 31 groups cannot be assigned any values at this stage. This process is called primary elimination, which can be done simply by observing the forms of equations. From the dimensionless groups with values “1” and “0”, we can get the transformation factors to address the remaining 31 groups. This step is called secondary substitution.

$$\begin{array}{ll}
r_2^* = z_2^* = t_2^* = S_{w2}^* = 0 & p_{w2}^* = p_{o2}^* = 0 \\
u_{wr2}^* = u_{or2}^* = u_{wz2}^* = u_{oz2}^* = 0 & u_{wr1}^* = u_{or1}^* = \frac{q_{op}}{2\pi r_{well} h_o}
\end{array}$$

$$\begin{aligned}
u_{wz1}^* = u_{oz1}^* &= \frac{q_{op}}{2\pi r_{well}^2} & p_{w1}^* = p_{o1}^* &= \frac{q_{op}}{2\pi k_r \lambda_w h_o} \\
p_{wD} &= \frac{2\pi p_w k_r \lambda_w h_o}{q_{op}} & p_{oD} &= \frac{2\pi p_o k_r \lambda_w h_o}{q_{op}} \\
r_1^* &= r_{well} & r_D &= \frac{r}{r_{well}} \\
z_1^* &= h_o & z_D &= \frac{z}{h_o} \\
t_1^* &= \frac{\phi S_{1r} r_w}{u_{wr1}^*} & t_D &= \frac{t q_{op}}{2\pi \phi h_o S_{wr} r_{well}^2} \\
S_{w1}^* &= S_{wC} & S_{wD} &= \frac{S_w}{S_{wC}}
\end{aligned}$$

The use of transformation factors defines 15 groups with remaining 16 groups not yet defined. However, these remaining dimensionless groups are no longer arbitrary. They are:

$$\begin{aligned}
\pi_1 &= \frac{2\pi k_z \lambda_w \rho_w g r_{well}^2}{q_{op}} & \pi_6 &= \frac{k_z r_{well}^2}{k_r h_o^2} & \pi_{11} &= \frac{z_{wi}}{h_o} \\
\pi_2 &= \frac{2\pi k_z \lambda_o \rho_o g r_{well}^2}{q_{op}} & \pi_7 &= \frac{\lambda_o}{\lambda_w} & \pi_{12} &= \frac{h_{wi}}{h_o} \\
\pi_3 &= \frac{2\pi k_r \lambda_w \Delta \rho g h_o^2}{q_{op}} & \pi_8 &= \frac{h_w}{h_o} & \pi_{13} &= \frac{h_{op}}{h_o} \\
\pi_4 &= \frac{2\pi k_r \lambda_w h_o \sigma}{q_{op}} \sqrt{\frac{\phi}{k_z}} & \pi_9 &= \frac{z_{wd}}{h_o} & \pi_{14} &= \frac{q_{wd}}{q_{op}} \\
\pi_5 &= \frac{k_z \lambda_o r_{well}^2}{k_r \lambda_w h_o^2} & \pi_{10} &= \frac{h_{wd}}{h_o} & \pi_{15} &= \frac{r_{ew}}{r_{well}} \\
\pi_{16} &= \frac{r_{eo}}{r_{well}}
\end{aligned}$$

C.4 Redundancy Elimination

With the remaining 16 groups defined, the flow equations in dimensionless space become completely dimensionless. However, the groups are not all independent. It is easy to see that all these 16 dimensionless groups are multiplicative, hence they can be transformed

$$\frac{\partial S_{wD}}{\partial t_D} + \frac{1}{r_D} \cdot \frac{\partial(r_D u_{wrD})}{\partial r_D} + \frac{\partial u_{wzD}}{\partial z_D} = 0 \dots\dots\dots (C.39)$$

$$\frac{1}{r_D} \cdot \frac{\partial(r_D u_{wrD} + r_D u_{orD})}{\partial r_D} + \frac{\partial(u_{wzD} + u_{ozD})}{\partial z_D} = 0 \dots\dots\dots (C.40)$$

Table C.1. Dimensionless groups for DWL in a homogeneous system

π	Expression	π	Expression	π	Expression
1	$N_b = \frac{2\pi k_z \lambda_w \Delta \rho g r_{well}^2}{q_{wd}}$	6	$M = \frac{\lambda_o}{\lambda_w}$	11	$H_d = \frac{h_{wd}}{h_w}$
2	$N_v = \frac{\sigma \sqrt{k_r \phi}}{k_z \Delta \rho g r_{well}}$	7	$Z_d = \frac{z_{wd}}{h_w}$	12	$H_i = \frac{h_{wi}}{h_w}$
3	$N_w = \frac{r_{well}}{h_{op}} \sqrt{\frac{k_z}{k_r}}$	8	$N_h = \frac{h_w}{h_o}$	13	$R_w = \frac{r_{ew}}{r_{eo}}$
4	$N_\rho = \frac{\rho_l}{\Delta \rho}$	9	$H_p = \frac{h_{op}}{h_o}$	14	$R_o = \frac{r_{eo}}{r_{well}}$
5	$N_q = \frac{q_{op}}{q_{wd}}$	10	$R_i = \frac{z_{wi}}{z_{wd}}$		

$$u_{wrD} = -\frac{\partial p_{wD}}{\partial r_D} \dots\dots\dots (C.41)$$

$$u_{orD} = -\pi_6 \frac{\partial p_{oD}}{\partial r_D} \dots\dots\dots (C.42)$$

$$u_{wzD} = -\pi_3^2 \pi_9^2 \frac{\partial p_{wD}}{\partial z_D} - \frac{\pi_1 \pi_4}{\pi_5} \dots\dots\dots (C.43)$$

$$u_{ozD} = -\pi_6 \pi_3^2 \pi_9^2 \frac{\partial p_{oD}}{\partial z_D} - \frac{\pi_1 (\pi_4 - 1) \pi_6}{\pi_5} \dots\dots\dots (C.44)$$

$$p_{oD} - p_{wD} = \frac{\pi_1 \pi_2}{\pi_3 \pi_5 \pi_9} J(S_{wD}) = \frac{\pi_1}{\pi_5 \pi_3^2 \pi_9^2} z_D \dots\dots\dots (C.45)$$

Dimensionless initial conditions:

$$S_{wD} = S_{wc}, \text{ at } t_D = 0, 0 < z_D < 1 \dots\dots\dots (C.46)$$

$$S_{wD} = 1, \text{ at } t_D = 0, 1 < z_D < 1 + \pi_8 \dots\dots\dots (C.47)$$

Dimensionless boundary conditions:

$$u_{wzD} = 0, \text{ at } z_D = 0, \forall r_D, t_D \dots\dots\dots (C.48)$$

$$u_{ozD} = 0, \text{ at } z_D = 0, \forall r_D, t_D \dots\dots\dots (C.49)$$

$$u_{wzD} = 0, \text{ at } z_D = 1 + \pi_8, \forall r_D, t_D \dots\dots\dots (C.50)$$

$$u_{ozD} = 0, \text{ at } z_D = 1 + \pi_8, \forall r_D, t_D \dots\dots\dots (C.51)$$

$$u_{wrD} = 0, \text{ at } r_D = \pi_{13}\pi_{14}, 1 < z_D < 1 + \pi_8, \forall t_D \dots\dots\dots (C.52)$$

$$u_{orD} = 0, \text{ at } r_D = \pi_{14}, 0 < z_D < 1, \forall t_D \dots\dots\dots (C.53)$$

$$1 = \int_0^{\pi_9} u_{orD} dz_D, \text{ at } r_D = 1, t_D > 0 \dots\dots\dots (C.54)$$

$$\frac{1}{\pi_5} = \int_{\pi_7\pi_8}^{\pi_8(\pi_7+\pi_{11})} u_{wrD} dz_D, \text{ at } r_D = 1, t_D > 0 \dots\dots\dots (C.55)$$

$$-\frac{1}{\pi_5} = \int_{\pi_7\pi_8\pi_{10}}^{\pi_8(\pi_7+\pi_{12})} u_{wrD} dz_D, \text{ at } r_D = 1, t_D > 0 \dots\dots\dots (C.56)$$

APPENDIX D: COPYRIGHT PERMISSIONS

D.1 Copyright Permission from Journal of Petroleum Science and Engineering

ELSEVIER LICENSE TERMS AND CONDITIONS

Oct 31, 2013

This is a License Agreement between Lu Jin ("You") and Elsevier ("Elsevier") provided by Copyright Clearance Center ("CCC"). The license consists of your order details, the terms and conditions provided by Elsevier, and the payment terms and conditions.

All payments must be made in full to CCC. For payment instructions, please see information listed at the bottom of this form.

Supplier	Elsevier Limited The Boulevard, Langford Lane Kidlington, Oxford, OX5 1GB, UK
Registered Company Number	1982084
Customer name	Lu Jin
Customer address	3550 Nicholson Dr. Apt.# 2092 BATON ROUGE, LA 70802
License number	3259571063266
License date	Oct 31, 2013
Licensed content publisher	Elsevier
Licensed content publication	Journal of Petroleum Science and Engineering
Licensed content title	Experimental and theoretical study of counter-current oil-water separation in wells with in-situ water injection
Licensed content author	L. Jin, A.K. Wojtanowicz
Licensed content date	September 2013
Licensed content volume number	109
Licensed content issue number	
Number of pages	10
Start Page	250
End Page	259
Type of Use	reuse in a thesis/dissertation

Portion	full article
Format	both print and electronic
Are you the author of this Elsevier article?	Yes
Will you be translating?	No
Order reference number	
Title of your thesis/dissertation	A FEASIBILITY STUDY OF DOWNHOLE WATER LOOP (DWL) WELL FOR WATER CONING CONTROL
Expected completion date	Nov 2013
Estimated size (number of pages)	210
Elsevier VAT number	GB 494 6272 12
Permissions price	0.00 USD
VAT/Local Sales Tax	0.0 USD / 0.0 GBP
Total	0.00 USD

D.2 Copyright Permission from Journal of Canadian Petroleum Technology

SOCIETY OF PETROLEUM ENGINEERS LICENSE TERMS AND CONDITIONS

Nov 01, 2013

This is a License Agreement between Lu Jin ("You") and Society of Petroleum Engineers ("Society of Petroleum Engineers") provided by Copyright Clearance Center ("CCC"). The license consists of your order details, the terms and conditions provided by Society of Petroleum Engineers, and the payment terms and conditions.

All payments must be made in full to CCC. For payment instructions, please see information listed at the bottom of this form.

License Number	3260420347605
License date	Nov 01, 2013
Licensed content publisher	Society of Petroleum Engineers
Licensed content publication	The Journal of Canadian Petroleum Technology
Licensed content title	Scaling Analysis of Wells With Downhole Water Loop Completion for Bottomwater Control
Licensed content author	L. Jin, A.K. Wojtanowicz, G. Afonja and W. Li, Louisiana State University
Licensed content date	November 2010

Volume number	49
Issue number	Number 11
Type of Use	Thesis/Dissertation
Requestor type	author of the original work
SPE member	yes
SPE member number	3261694
Format	print and electronic
Portion	full article
Will you be translating?	no
Distribution	5
Order reference number	
Title of your thesis / dissertation	A FEASIBILITY STUDY OF DOWNHOLE WATER LOOP (DWL) WELL FOR WATER CONING CONTROL
Expected completion date	Nov 2013
Estimated size (number of pages)	210
Total	0.00 USD

VITA

Lu Jin, son of Weiqin Jin and Huiying Qi, was born in Zhejiang, China, in March, 1982. He attended Daqing Petroleum Institute, receiving a bachelor's degree in Petroleum Engineering in 2005. After graduation, he joined China University of Petroleum as a research assistant. In 2007, he enrolled in Louisiana State University and got his master's degree in Petroleum Engineering in 2009. He continued his Ph.D study in the same university and completed summer internships with High Plains Operating Company, LLC, on projects of water cresting control in horizontal wells and water coning control in reservoir with transition zone. He anticipates receiving his Ph.D degree in Petroleum Engineering from Louisiana State University in December 2013.